



HAL
open science

Effects of the presence of recycled tire powders on the kinetics of the radical polymerization of styrene and the properties of the resulting materials

Daniela Carolina Florez Parra

► **To cite this version:**

Daniela Carolina Florez Parra. Effects of the presence of recycled tire powders on the kinetics of the radical polymerization of styrene and the properties of the resulting materials. Chemical and Process Engineering. Université de Lorraine, 2019. English. NNT : 2019LORR0347 . tel-02976726

HAL Id: tel-02976726

<https://hal.univ-lorraine.fr/tel-02976726>

Submitted on 9 Sep 2024

HAL is a multi-disciplinary open access archive for the deposit and dissemination of scientific research documents, whether they are published or not. The documents may come from teaching and research institutions in France or abroad, or from public or private research centers.

L'archive ouverte pluridisciplinaire **HAL**, est destinée au dépôt et à la diffusion de documents scientifiques de niveau recherche, publiés ou non, émanant des établissements d'enseignement et de recherche français ou étrangers, des laboratoires publics ou privés.



AVERTISSEMENT

Ce document est le fruit d'un long travail approuvé par le jury de soutenance et mis à disposition de l'ensemble de la communauté universitaire élargie.

Il est soumis à la propriété intellectuelle de l'auteur. Ceci implique une obligation de citation et de référencement lors de l'utilisation de ce document.

D'autre part, toute contrefaçon, plagiat, reproduction illicite encourt une poursuite pénale.

Contact : ddoc-theses-contact@univ-lorraine.fr

LIENS

Code de la Propriété Intellectuelle. articles L 122. 4

Code de la Propriété Intellectuelle. articles L 335.2- L 335.10

http://www.cfcopies.com/V2/leg/leg_droi.php

<http://www.culture.gouv.fr/culture/infos-pratiques/droits/protection.htm>

Effects of the presence of recycled tire powders on the kinetics of the radical polymerization of styrene and the properties of the resulting materials

Doctoral Dissertation

submitted and defended confidentially on July 4th 2019

in a partial fulfillment of the requirements for obtaining a:

PhD title from the University of Lorraine

(Specialty : Process and Product and Molecular Engineering)

by

Daniela Carolina FLOREZ PARRA

Doctoral Committee:

<i>Reviewers:</i>	<i>Prof. Philippe CASSAGNAU</i>	Université Claude Bernard Lyon1, Lyon - France
	<i>DR. Nida OTHMAN</i>	Université Claude Bernard Lyon1, Lyon - France
<i>Examiners:</i>	<i>Prof. Isabelle ROYAUD</i>	Université de Lorraine, Nancy - France
	<i>Prof. Christophe SERRA</i>	Université de Strasbourg, Strasbourg - France
<i>Supervisors:</i>	<i>Prof. Guo-Hua HU</i>	<i>Director</i> , Université de Lorraine, Nancy - France
	<i>Dr. Dimitrios MEIMAROGLOU</i>	<i>Co-director</i> , Université de Lorraine, Nancy - France

Agradecimientos

La riqueza de este trabajo de tesis se puede definir por el número de personas que conocí y el tiempo invertido en los momentos de intercambio y de charla más o menos serios. Agradezco a todos aquellos quienes, a través de su trabajo, me ayudaron a avanzar en esta investigación. Sin embargo, quisiera agradecerles aún más por ese pequeño excedente que me pudieron ofrecer y que se traduce en un saludo, una sonrisa, un café, una broma, una mano amiga, una explicación, una re-explicación y a todos esos detalles que le dan sentido al día a día.

Para comenzar, agradezco a Dimitrios a quien admiro por su empatía y por la pasión, entusiasmo y optimismo de su trabajo. Su confianza y el trabajo en equipo nos permitió avanzar a pasos de gigante e ir más allá de lo esperado. Gracias a Sandrine por haberme apoyado desde el comienzo y hasta el fin en la búsqueda de este gran desafío.

Inmensas gracias a Richard por su carisma y entusiasmo, toda su ayuda en la creación, montaje, reparación, etc., fueron indispensables para comenzar y avanzar en este trabajo. Al equipo del taller, Charly, Christian, Yann, Alain et Laurent por su ayuda imprescindible, siempre con el buen humor y amabilidad que los caracteriza. Gracias a Véronique y Laurent por sus aportes y apoyo en la difícil y última etapa de esta carrera.

Recuerdo a mis amigos David, Alvaro, Wilmar y Fabio, su amistad, apoyo y disposición fueron indispensables durante todo este tiempo. A la banda fundadora del BJC, David Ricardo, Miriam, François y Jérémy, a quienes recuerdo por su convivialidad, buen humor y empatía. Fue un verdadero placer haberlos encontrado y acompañado en la misión del BJC. También aprecio muchas otras personas que tuve la ocasión de conocer, Guillemette, Selven, Paola, Charlotte, Divyesh, Mainak, Maud.

Gracias a los amigos que siempre han hecho parte desde el comienzo de esta aventura y quienes me mostraron los encantos de su país, Max, Karin y Alice, Gabrielle, Johanna et Alex, Marie y toda la gente de la banda Rollver. A todos otros aquellos que tuve la ocasión de encontrar en el camino Edouard, Annie y Ben, Téo y Claire, Silvia.

Infinitas gracias a mi madre quien ha hecho y dado todo de su parte para que hoy yo pueda escribir estas palabras. Tu sabes que siempre has sido mi más grande inspiración y ejemplo de persistencia y resiliencia. A Tib, mi gran amor, muchas gracias por tu paciencia, confianza y tus dulces palabras llenas de motivación sin cese. A tu lado todo es posible, interesante y mucho más divertido. Gracias a mi familia tan lejos y a la familia de Tib tan cerca, me siento realmente afortunada de tenerlos a todos.

"Quien no vive para servir, no sirve para vivir"

Madre Teresa de Calcuta

Contents

1	State of the art	5
1.1	Introduction	7
1.2	Polymer composites: a brief overview	7
1.3	Challenges and opportunities of end-of-life tires recycling	8
1.3.1	General background statistical facts	8
1.3.2	What is a tire made of?	9
1.3.3	New approaches to the management of post-consumer tires	9
1.4	Ground Tire Rubber (GTR)	11
1.4.1	GTR applications	13
1.4.2	GTR in polymer composites	14
1.4.3	Modification of GTR	14
1.5	Polystyrene (PS)	18
1.5.1	General purpose polystyrene (GPPS)	19
1.5.2	High-impact polystyrene (HIPS)	19
1.6	Composites of GTR and polystyrene	20
1.6.1	Interfacial adhesion improvement by grafting polymerization	20
1.7	Motivation and objective of this work	24
2	Polymerization of styrene with GTR: a kinetic study using DSC	27
2.1	Introduction	29
2.2	Experimental	30
2.2.1	Materials and reagents	30
2.2.2	Methods	30
2.3	Results and discussion	31
2.3.1	Monitoring of the styrene-free radical polymerization.	31
2.3.2	Effects of GTR on the DSC thermograms and monomer conversion of free-radical polymerization of styrene.	31
2.3.3	Kinetics of the polymerization of styrene in the presence of GTR.	39
2.4	Conclusions	41
3	A methodology to prepare GTR-reinforced polystyrene composites	43
3.1	Introduction	45
3.2	Mechanical properties of polymer composites	45
3.2.1	Tough and brittle behavior in polymers	45
3.2.2	Main parameters influencing toughness in thermoplastic composites based on GTR	46
3.3	A novel methodology to prepare polystyrene composites with GTR.	53
3.3.1	Product specifications	53
3.3.2	Proposed methodology for product preparation	54

3.4	Materials characterization	54
3.4.1	Ground tire rubber (GTR)	54
3.4.2	Polystyrene	55
3.4.3	Reagents	57
3.5	Process definition	57
3.5.1	Compatibility improvement	57
3.5.2	Reducing particle size	63
3.6	Process proposed	68
3.6.1	Experimental conditions to be tested	68
3.7	Operating methods	68
3.7.1	Free-radical grafting polymerization of styrene onto/into GTR particles	68
3.7.2	Free-radical solution polymerization of styrene	70
3.7.3	Compounding in a twin-screw extruder	71
3.8	Evaluation	72
3.8.1	Structural assessment	73
3.8.2	Morphological characterization	76
3.8.3	Thermal characterization	77
3.8.4	Mechanical properties	78
3.9	Conclusions	83
4	A comprehensive kinetic model of styrene polymerization	85
4.1	Introduction	87
4.1.1	Styrene polymerization	87
4.1.2	Grafting polymerization of styrene onto rubber	88
4.2	Experimental	89
4.2.1	Materials and reagents	89
4.2.2	Methods	90
4.3	Styrene homopolymerization model	92
4.3.1	Model developments	92
4.3.2	Results and discussion	98
4.3.3	Conclusions	102
4.4	Styrene grafting polymerization onto GTR model	103
4.4.1	Introduction	103
4.4.2	Model developments	105
4.4.3	Conclusions	116
5	Experimental results and discussion	117
5.1	Introduction	119
5.2	Free-radical bulk polymerization of styrene in presence of GTR in a batch reactor	119
5.2.1	Influence of the GTR content on polystyrene qualities: x and GE	119
5.2.2	Morphology of the GTR-grafted-PS particles	121
5.2.3	Verifying polystyrene grafting onto GTR	123
5.2.4	Effect of GTR content on the molecular weight of free-PS	125
5.2.5	Discussion and interpretation	125
5.3	Compounding of the polystyrene grafted GTR composites in a twin-screw extruder.	128
5.3.1	Effect of a single extrusion by using screw Profile-1 on the microstructure and mechanical properties of polystyrene composites containing 30 wt% and 50 wt% of equiv-GTR	131
5.3.2	Effect of 1, 2 and 3 extrusions by using screw Profile-1 on the microstructure and mechanical properties of polystyrene composites containing 30 wt% and 50 wt% of equiv-GTR	144

5.3.3	Influence of the extruder screw configuration after 1, 2 and 3 extrusions on the microstructure and mechanical properties of polystyrene composites containing 50 wt% of equiv-GTR.	153
5.3.4	Influence of increasing the GTR content on the microstructure and tensile properties of polystyrene composites extruded 1 and 2 times.	160
5.4	Conclusions	166
6	General conclusions and perspectives	169

State of the art

Contents

1.1	Introduction	7
1.2	Polymer composites: a brief overview	7
1.3	Challenges and opportunities of end-of-life tires recycling	8
1.3.1	General background statistical facts	8
1.3.2	What is a tire made of?	9
1.3.3	New approaches to the management of post-consumer tires	9
1.4	Ground Tire Rubber (GTR)	11
1.4.1	GTR applications	13
1.4.2	GTR in polymer composites	14
1.4.3	Modification of GTR	14
1.4.3.1	Devulcanization and reclamation	15
1.4.3.2	Surface modification	17
1.5	Polystyrene (PS)	18
1.5.1	General purpose polystyrene (GPPS)	19
1.5.2	High-impact polystyrene (HIPS)	19
1.6	Composites of GTR and polystyrene	20
1.6.1	Interfacial adhesion improvement by grafting polymerization	20
1.7	Motivation and objective of this work	24

1.1 Introduction

This introductory chapter lays out the scope of this research project, of which the purpose is to fabricate a polymer composite of ground tire rubber (GTR) and polystyrene, having specific mechanical properties, namely a high-impact resistance. The incorporation of rubber particles into the polymers alters the chemical and physical properties of the latter, and their contributions can be beneficial and/or detrimental. Accordingly, the final properties of the product will be influenced by a large number of intrinsic parameters (related to the nature of the rubber and the polymer) and extrinsic parameters (related to the formulation and processing). Since it is impossible to control all the factors involved, it may be still possible to focus on those having a considerable influence. Notably among these, the miscibility between the components is one of the key parameters that governs the final mechanical properties of polymer composites.

In this context, one of the objectives of this chapter is to present the challenges and opportunities that researches around the world are facing to reduce the environmental pollution caused by mismanagement of non-biodegradable materials such as pneumatic tires. This intends to emphasize that proper recycling of end-of-life tires has become of great interest as it is a valuable source of raw materials with a wide range of cost-effective applications, such as polymer composites.

In the second half of this chapter, attention will be paid to composites made of GTR and thermoplastics. The existing methods to improve the miscibility (compatibility) between the components are listed and briefly presented. Finally, the focus is on the method used in this research to improve the interfacial adhesion between GTR and polystyrene.

1.2 Polymer composites: a brief overview

Polymer composites or filled polymers are high performance materials that have led to tremendous advances in the manufacture of components for the automotive and aeronautic industries, wind energy farms, household goods and everyday objects [1, 2]. They are made of the mixture of polymers with reinforcement agents (organic or inorganic) normally known as *fillers*, which infer better and complementary properties to the polymer. This assembly of components builds up a high value material with combined properties. Filled polymers can contain two or more components and two or more phases that retain their individual characteristics. The polymer phase consists of either a thermoset, thermoplastic, rubber polymer or a polymer blend, and is considered as the matrix or continuous phase. Fillers are typically dispersed through mechanical mixing processes into the polymer phase at high temperatures (in the molten state) [1, 3, 4].

The role of the polymer matrix is to create an interfacial bond with all components of the mixture. For example, robust interactions between the matrix and reinforcements are crucial to increase properties such as toughness and damping [4]. Fillers are in the form of fibers or particles, and their scope of application is defined considering various factors including their chemical nature (organic or inorganic), morphology (short or long fibers and flakes, spherical, cubic or irregular shaped particles) and function (stabilizers, functionalized agents, mechanical properties modifier, etc.) [3]. Typical examples of fillers for plastics are: (i) inorganics, such as glass fibers and particles, talc, nanoclays, steel; (ii) organics, as carbon fibers and nanotubes, natural polymers (e.g., cellulose and wood fibers), and (iii) synthetic polymers in general (e.g., polyamide, polyester, polyvinyl alcohol, etc.).

In general, filled composites have remarkable characteristics as low weight and thermal expansion, high specific rigidity, strength and fatigue resistance. In fact, their exceptional properties and performance arise from the synergistic matrix-reinforcements interactions and compatibility. Nowadays, it is possible to obtain a wide spectrum of properties by means of a large choice of high performance

polymeric resins and reinforcements [1, 3, 4].

1.3 Challenges and opportunities of end-of-life tires recycling

1.3.1 General background statistical facts

The industry of rubber goods and tires exhibits continuous development and growth around the world. From pencil erasers to shoes and from bicycles to aerospace, products made of rubber have found a wide variety of applications in our daily life [5–7]. The major rubber market is dominated by the transport sector and accounts for over 75% of the global production mainly intended for the manufacture of pneumatic tires [5]. The world largest tire manufacturers are established in the United States (U.S.), European Union (EU) and Japan as shown in Figure 1.1 [8].

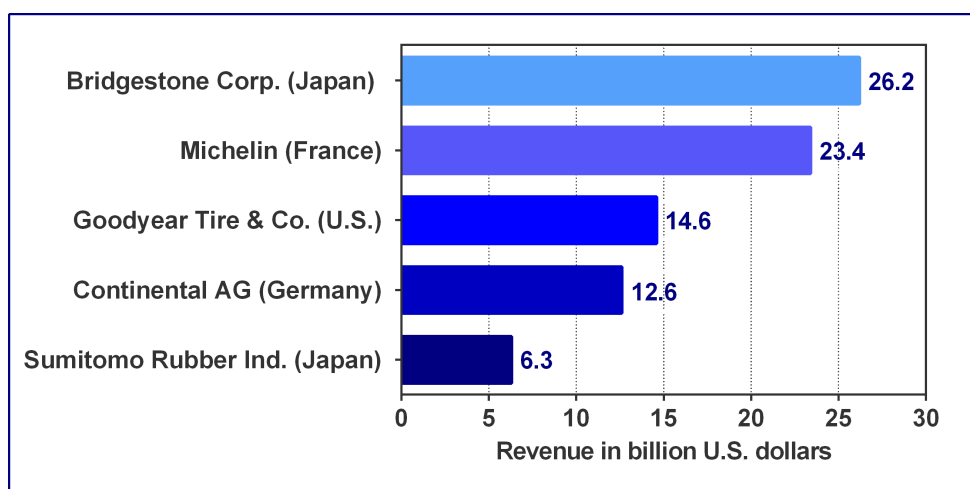


Figure 1.1 – World's largest tire manufacturers in 2017, based on tire-related sales (in billion U.S. dollars). U.S. Tire manufacturers association (2017) [9]

The automobile sector is the major contributor in the dramatic accumulation of used tires [5, 6, 10, 11]. Between 2006 and 2015, the number of passenger cars and commercial vehicles in circulation around the globe increased from 926 600 to 1282 300 thousand units [12]. As a result of this activity, the annual production of tires has reached an annual growth rate of more than 20% in the last six years [13]. In 2016, more than 285 millions of tires (light vehicles) were commercialized in the EU, representing 20% of the world market [14]. A recent study on the world tires industry [13], revealed that the worldwide demand for all-type automotive tires in 2019 is estimated to be more than 3.0 billion units of which, a third is destined to the motors trade. These statistical figures imply that vehicles and tires markets continue to develop at increasing rates. Consequently, a respective increase is observed for post-consumer tires.

At the moment that tires are dismantled from vehicles to be replaced and discarded, they generate wastes of more than 17 million tons (1.4 billion units) each year and continue to expand by 2% annually [6]. The earlier methods of disposal of post-consumer tires were based on vain land-filling and stock-piling, which led to major environmental and public health problems, related to the risk of fire with generation of toxic gases, proliferation of vectors (i.e. epidemic transmission as malaria, dengue and chikungunya) and other harmful animals (i.e. rodents and snakes). In addition, some of the chemical components and metals present in tires formulation came in landfill leaches also increase soil pollution. In fact, tires possess an engineered structure that make them difficult to reprocess and that represents a challenge for their reuse and recycling [10, 11, 15].

1.3.2 What is a tire made of?

Tires are a complex assemblage of components and properties, designed to combine high-performance with long-product lifetimes and operational capacity in a wide range of environments [15]. Therefore, post-consumer tires are considered an important source of raw materials with interesting properties. Ironically, from the technical point of view, these remarkable qualities present also an enormous obstacle to recycling and recovery [6]. Tires are essentially constructed of a textile/steel/rubber composite, whose formulation varies according to the intended application vehicle [5, 9, 15]. Figure 1.2 shows an example of materials used in tires for light vehicles and trucks, which can contain about twelve and twenty formulation components, respectively [9, 10]. In general, tires assemblies are a combination of various rubber blends, reinforcing fibers (i.e. steel cords and polymeric/textile fibers (i.e. nylon, polyester, cellulose), rubber fillers and additives. Each of these components contribute individually and collectively to the service and performance of the product [15].

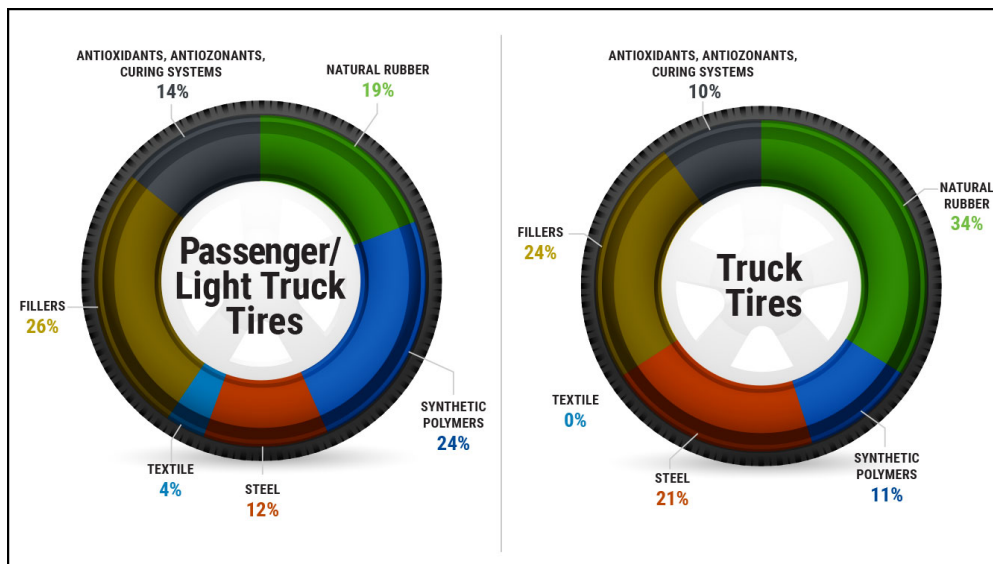


Figure 1.2 – Example of composition of passenger/light truck tires and truck tires. U.S. Tire manufacturers association (2017) [9].

The rubber composite phase makes up for about 70% to 80% of the total mass of the tire, and can be created from a large variety of high-quality natural and synthetic rubbers, reinforcing agents and additives. Among the categories of synthetic rubbers, the most commonly used elastomers are: styrene-butadiene rubber (SBR), butadiene rubber (BR) and butyl and halogenated butyl rubber (IIR) [9, 11, 15]. Addition of fillers, as carbon black, clays and amorphous silica reinforces the mechanical properties of rubbers and improves their wear and rolling resistance. Additives, such as stabilizers, antioxidants and antiozonants, are also integrated to impede degradation effects due to aging, oxidation, environmental exposure, etc. [9, 16]. Finally, the formulation is vulcanized with a curing system of sulfur and zinc agents, creating chemical bonds between elastomer chains to form a strong three-dimensional cross-linked network structure [15]. As a result, the pneumatic tire product is an elastic, insoluble, infusible and non-biodegradable composite.

1.3.3 New approaches to the management of post-consumer tires

A new approach to the management of post-consumer tires has been adopted in different regions around the globe. The largest manufacturers and importers of the tire market, such as U.S., EU, China and

Japan, have indeed changed their policies to promote a sustainable control of these wastes [17]. For example, the EU has implemented with success, since 1999, a legislative and regulatory model called *Extended Producer Responsibility* (EPR). These models assign the responsibility to the producers (manufacturers and dealers) to organize the management of the recovery and recycling of their end-of-life products [18]. As a result of the adoption of this high-efficiency model, the EU recovers almost 100% of discarded tires today. Similarly, Japan and U.S. recover approximately 90% by using alternative strategies [10, 18].

At present, the methods for waste tire utilization, generally accepted by the regulations, can be divided into two main categories depending on the condition of the worn tire [10, 11, 18]. The first category refers to partially-worn tires that can be still used on the road. They can be directly mounted to the vehicle, if there is enough remaining rubber on the tread or can be retreated before their utilization by replacing only the tread by a new one [18].

The second category concerns the end-of-life tires that are transformed for energy or material recovery.

1. **Energy recovery** is a quick and cost-effective solution that consists in combusting scrap tires as supplemental fuel in urban heating and energy plants [7, 10]. The tire-derived fuel (TDF) is mainly used in cement kilns, pulp and paper mills and industrial boilers [11, 18]. According to the U.S. Tire Manufactures Association (USTMA), the energy fuel from tires increases the boilers efficiency, and reduces cost as well as greenhouse emissions compared with coal [7].

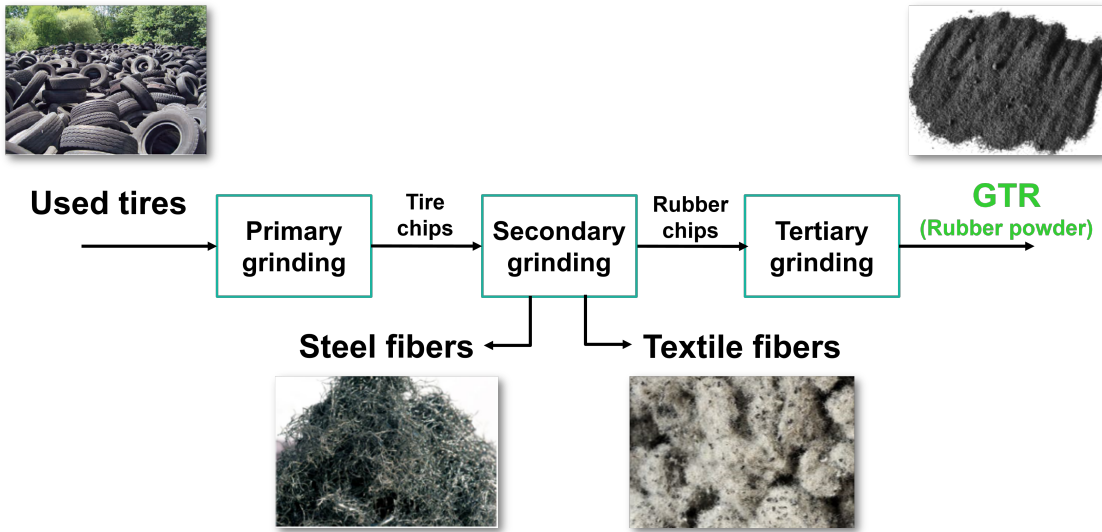


Figure 1.3 – Flow diagram process of post-consumer tires transformation for material recycling. Photos credits from Aliapur (2017-2018) [19, 20]

2. **Material recycling** resides in the reutilization of the constituent materials of tires: rubbers, steel and textiles. There are several processes to transform end-of-life tires and obtain the derived materials [18, 21]. Figure 1.3 shows a general example of the basic operations that are usually implemented. The transformation is realized through three or more consecutive mechanical grinding stages, using equipment like hammers, cracker mills, granulators, etc.

During tires transformation, the constituent components are reduced in size as follows: in a first coarse grinding step, tires are reduced first into shreds and then into smaller chips. Subsequently,

through a secondary grinding stage, steel fibers and textiles are separated out of the rubber material by means of magnets and aspiration, respectively. Finally, one or more superfine grinding steps can be performed to achieve further size reduction into crumbs, granulates or fine rubber powders, commercially called **ground tire rubber** or **GTR** [20, 21].

The products derived from tires have a high recyclability and some of the applications are mentioned here below:

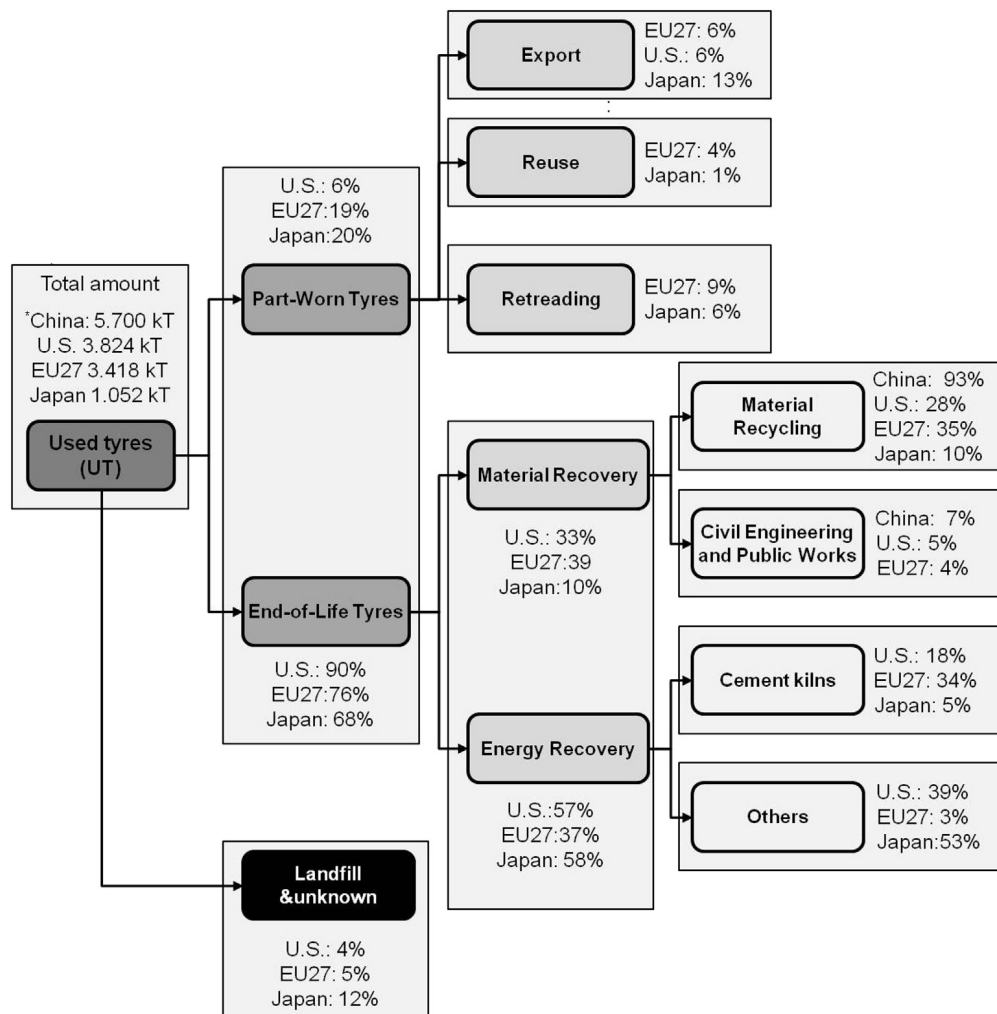
- (a) **Steel fibers recycling.** Recovered steel fibers have a high quality and their value is rather defined by the content in residual rubber (varying from 2 to 20%). This latter varies according to the efficiency of the grinding and separation processes. For instance, steel plants claim recycled fibers with low residual rubber percent (<4%) for new steel fabrication. Alternative applications include, among others, concrete reinforcement [18, 20].
- (b) **Textile fibers recycling.** Textiles present in tires for cars and heavy vehicles are only about 6% of their total weight. Nevertheless, the processing and recycling of fibers can be quite challenging, since it represents safety risks (i.e., associated to dust suspension) during separation and processing. In addition, the residual rubber content remains high. Recently, recovered textile fibers have found market opportunities in isolation products and ongoing studies are also underway to integrate them in concrete [18, 20].
- (c) **Rubber recycling.** Characteristics of the rubber material are defined by the transformation stages, equipment and operating conditions. The produced rubber can be 99% fibers-free and its composition depends on the tire's initial formulation. It is recycled as shreds, crumbs (> 20 mm), granulates (0.8 to 20 mm) or powders (10 μ - 0.8 mm). A more detailed description about recycled rubber properties and applications is presented in the following sections.

Figure 1.4 presents a flow diagram of the management of post-consumer tires along with some recycling figures by the main producers and consumers in the EU region and countries such as U.S., China and Japan [17]. As can be observed, China and U.S. are the biggest producers of wastes. The most important figures in handling wastes (up to 68%) are associated to the valorization of the end-of-life tires. Whereas the EU (27 in 2013) and China have opted for material recycling, due to the important demand of raw materials for material engineering, Japan and US partially cover their energy demand through tire-derived fuel [7, 17, 18].

The efficiency of the regulatory actions undertaken have led to a great progress in solving part of the environmental problems caused by the over-accumulation of waste tires. It has resulted in the creation of a new branch of industry and R&D, mainly managed by rubber manufacturers' associations [5, 7, 17]. These organizations are currently working on the creation of innovative methods and technologies for efficient used tires recovery and processing. They share the common vision of sustainability and for these reasons, they have engaged the mission of identifying eco-friendly solutions to find superior valorization methods with limited costs and low negative effects on the environment [7, 12, 18, 22]. Nevertheless, the commercial success of this activity is facing one big challenge, that is to deal against the inertia, in some regions, of the recycling end markets and therefore, to exploit all the ideas and projects that might involve tire derived materials [18].

1.4 Ground Tire Rubber (GTR)

Recycling of GTR is the particular interest of this research project, since it is considered a valuable component for which there are enormous potential and promising markets, as reported by the *European Tyre and Rubber Manufacturers Association* (ETRMA) [11, 18, 23]. The final composition of GTR varies



*data include only the total amount of used tyres recovered by recycling

Figure 1.4 – Flow diagram of used tires utilization in some of the most important manufacturer and trader regions and countries in the world (U.S. 2013; EU. 2010,2013; Japan 2015, China 2009-2010). Sienkiewicz et al.(2017) [17]

according to the type of tires recycled (after removing steel and textiles). Thus, it can be made up of a single type of rubber tire or more commonly, a mixture of them. Table 1.1 presents an example of GTR composition according to the tire category. Note that just over half (52% to 57%) of the components are rubbers and therefore, the contents in fillers and additives are high. In the form of crumbs, granulates or powders, GTR can be used as raw material to produce 100% recycled rubber-based products and polymer composites [11, 24].

The final morphology and some characteristics of the rubber powders are defined by the temperature at which GTR is ground. In grinding at ambient temperature, the resulting granulates have a minimum size limited to 0.3 mm with rough surfaces, irregular shapes and high superficial area (Fig. 1.5a). In contrast, in the cryogenic method, rubber is frozen at -180 °C , prior to the grinding, to obtain smaller grain sizes of several hundreds of microns. In this case, particles have sharp edges, flat surfaces and reduced superficial area (Fig. 1.5b). In the former case, for example, particles are highly irregular shaped and have a greater contact surface and bending potential when blending with other materials [11, 18].

Table 1.1 – Composition of GTR according to the tire category: passenger/light vehicles and truck tires.

	Car tires	Truck tires
Elastomers (%)	52	57
Fillers (%)	30	30
Additives (%)	16	13

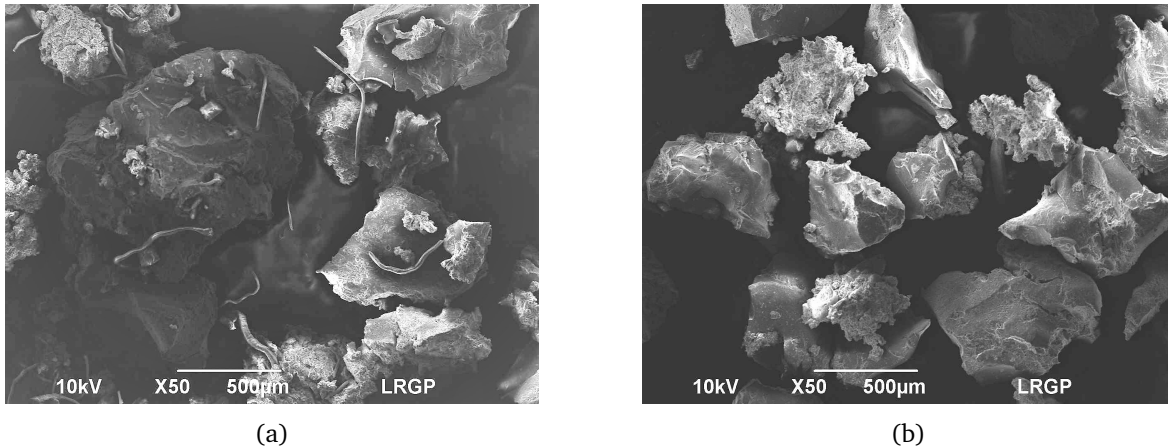


Figure 1.5 – SEM micrographs displaying differences of GTR particles morphology after mechanical grinding process at two different temperatures: (a) cryogenic and (b) environmental.

1.4.1 GTR applications

The scope of application of GTR is defined by considering its original formulation aspects, such as the filler content (e.g. carbon black and silica), crosslinks (i.e. number of sulfur bonds) and nature of the elastomers (e.g. natural and synthetic rubbers) [6, 11]. Some of the remarkable advantages of introducing GTR into other materials are improved resistance to chemical and environmental agents, higher mechanical strength and fatigue resistance [17].

Some typical applications of GTR include playgrounds and sport surfacing (e.g. athletic tracks), molded and extruded products, and cheap products in general (cable housing, floor tiles, windscreen wipers, etc.) [10, 18]. Figure 1.6 shows three examples of successful applications of GTR in the manufacture of: (a) small tires and wheels (by molding) for carts, wagons, strollers, etc. (Fig. 1.6a), (b) accessories ("sleepers") for tramway rails for noise and vibration mitigation (Fig. 1.6b), and (c) composites made of natural materials with shock-resistance properties useful for construction, design and furniture applications (Fig. 1.6c) [18, 19, 25].

The tire recycling industry is investing on R&D to develop new end-markets for tire rubber. In this way, in the recent years, a qualitative novel group of sustainable GTR-based composites have emerged [5, 17]. For example, the benefits of adding rubber into bitumen to produce "rubberized asphalt" (with 4 to 25% of GTR) include higher durability and drainage of water and noise reduction. This has been applied with success in many European countries such as Italy, Portugal and Spain. In other, rubber particles in concrete lighten the material and increase durability and performance [5, 18]. Nevertheless, despite the proved benefits for these applications, they are, in most cases, far from widespread in other European countries [18].

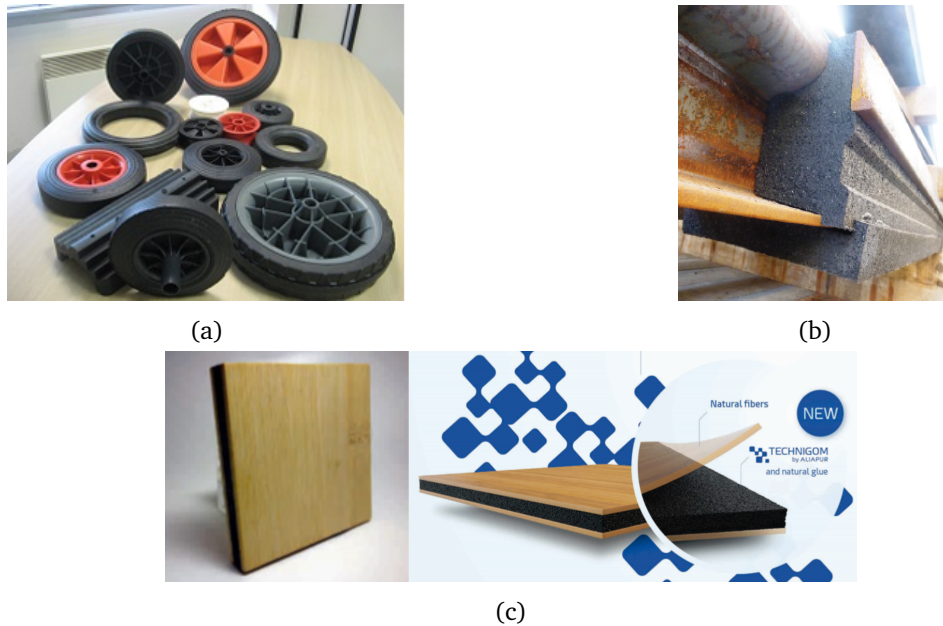


Figure 1.6 – Examples of products manufactured by using GTR. a) Small tires and wheels produced by the company Roll-Gom in France, b) sleepers adapted to the tramway rails in Bruxelles, c) Technigom composite material developed by Aliapur in France. RollGom (2018) [25], Aliapur (2017) [19]

1.4.2 GTR in polymer composites

The incorporation of GTR into fresh or recycled polymers to produce new materials has not only been considered the most straightforward recycling option offering environmental benefits, but also a promising economic alternative to reduce the current high price of composite materials [6, 10]. GTR can be blended with one or a blend of polymers, namely thermosets, thermoplastics and rubbers, with the purpose of obtaining high-performing materials [23, 26]. Since GTR is made up from a composite of elastomers rich in reinforcing agents and additives (approx. 45 % by weight, cf. Table 1.1), the GTR mixtures with pure polymers or polymer blends will be considered in this work as compounds or composite materials.

The properties of the filled polymers are determined by the formulation, the physico-chemical characteristics of the components of the mixture and the compatibility (miscibility) between them. The macromolecular nature and physico-chemical properties of the cross-linked structure of GTR and the polymers are very different, turning them into immiscible phases. As a result, a simple dispersion of GTR in a continuous polymer matrix deteriorates drastically the mechanical properties of the polymer and the effects are amplified when the GTR content is increased [10, 11]. Accordingly, to obtain a composite that would exhibit excellent combined properties (i.e., superior to those of the individual phases), the component mixture must generate synergistic rather than adverse effects. To address this matter, one or more components of the mixture have to be modified in order to make their surfaces chemically similar to each other and thus, promote their adhesion through strong physical and/or chemical interactions [10, 11, 27–29].

1.4.3 Modification of GTR

Nowadays, it is well documented that thermoplastics can be toughened with small volume fractions of rubber particles, when using appropriate methods [10, 11, 23, 30]. In addition, a common understanding has been reached to the effect that, before blending with polymers, the surface of GTR should be activated or modified to promote strong interactions with the polymer matrix. In order to do this,

one or more compatibilization techniques, presented in Figure 1.7, can be implemented [10, 11, 17]. Devulcanization, on the one hand, and surface activation on the other, are two of the most widely used techniques for GTR modification. They are performed through physical and chemical transformations. In this section, a brief description is presented of the most interesting methods in conjunction with this work to give a general idea of the progress done in this field [10, 11, 17].

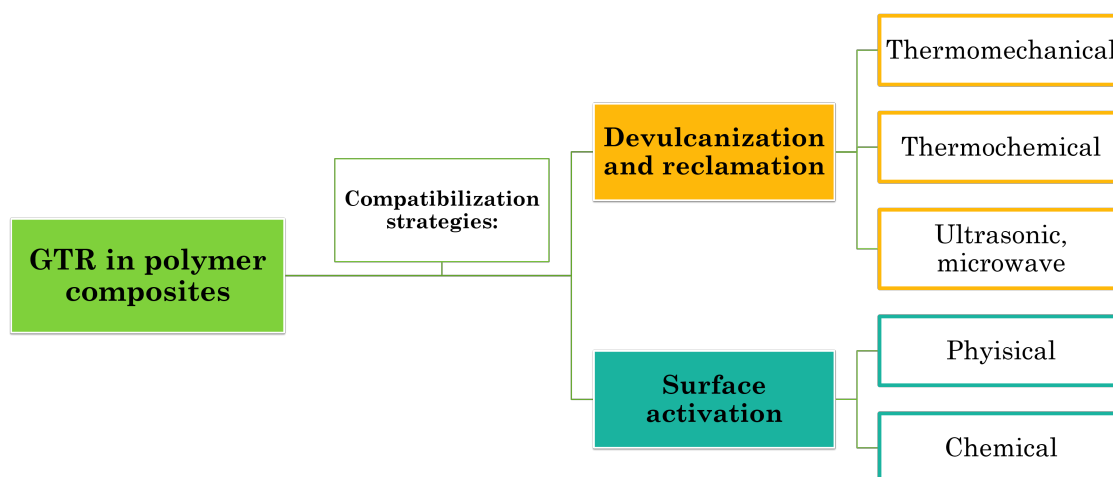


Figure 1.7 – Compatibilization strategies used for GTR modification

1.4.3.1 Devulcanization and reclamation

Devulcanization and reclamation techniques aim at restoring the GTR some plasticity and ease of processing by destroying the vulcanized-rubber structure [11, 31]. As a result, its properties become comparable to those of fresh rubbers. The difference between the two techniques is that, while the former is defined as the scission of C-S and S-S bonds, the latter involves also the cleavage of the -C-C- elastomer chains bonds, resulting in lower molecular weight fractions. Nevertheless, despite the fact that the energies required to cleave sulfur bonds -C-S-C- (273 kJ/mol), -C-S-S-C- (227 kJ/mol) and -C-S_n-C- (251 kJ/mol), are lower than the the respective energy of the -C-C- bond cleavage (348 kJ/mol), both processes occur simultaneously and to a certain extent, the scission is not selective [10, 11].

Figure 1.8 illustrates a devulcanized product. It is a mixture of a gel rubber fraction (non devulcanized) and a soluble part (devulcanized). The degree of devulcanization is generally determined by solvent extraction, in which the soluble part is removed from the insoluble gel fraction. Since the devulcanized portion helps to increase the miscibility in the polymer blends, its fraction and molecular weight must be as high as possible to reach intimate interpenetration with the polymer matrix and preserve rubber properties and processability.

At present, GTR can be devulcanized and reclaimed by several processes, of which the most commonly used ones include thermomechanical, thermochemical and ultrasound techniques [10, 11].

- **Thermomechanical treatment.** This is performed in equipment such as mills or twin-screw extruders at ambient or high temperatures [10]. The rubber crumbs are kneaded at high shear rates to provoke, under the effect of elongational stresses, the scission of bonds. The advantage of extrusion is that the efficiency of shear transmission is high and can operate continuously and at high speed. Researchers have reported that increasing operational parameters, such as temperature and screw speed, decreases both the gel fraction and crosslinking density [31, 32]. In

one study, Yazdini et al. 2011 [31], re-vulcanized a formulation prepared with devulcanized and fresh rubber (15/85 wt% ratio), and found that mechanical properties such as tensile properties, hardness and resilience were close to those of vulcanized virgin rubber.

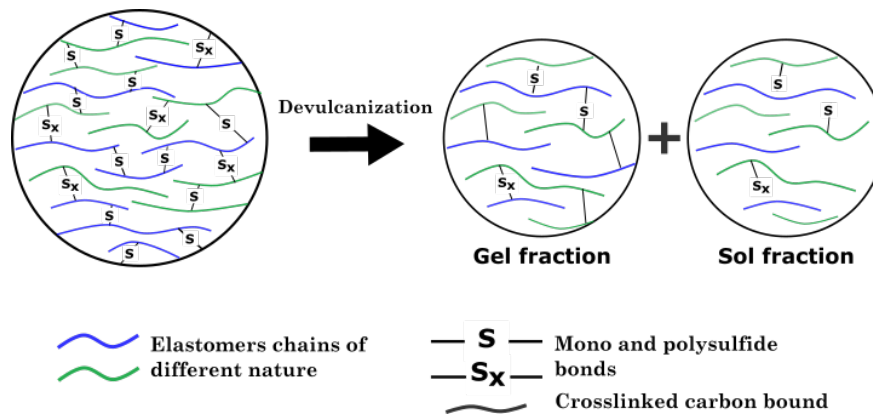


Figure 1.8 – Schematic representation of devulcanized and reclaimed GTR product.

- **Thermochemical processes.** These include the utilization of highly active chemical reclaiming agents of different nature (organic and inorganic) during mechanical treatment at elevated temperatures [11, 33]. A large number of agents has been developed. Among these, organic disulfides and related compounds (mercaptans, phenol sulfides, thiols, etc.), inorganic substances (metals, transition metal alloys) or miscellaneous chemicals (acids, organic solvents, oxides, etc.) are used. Adhikari and co-workers (2000) [33], reviewed many of the works reported in this field. Despite the efficiency of some of these methods, their main inconvenience is the utilization and subsequent need for recuperation of hazardous substances and solvents.
- **Ultrasound.** Usually, the extrusion is coupled to ultrasound, which aids to cleave the sulfuric crosslinks and double bonds of the rubber-vulcanized structure [11, 34]. The ultrasonic generator can be placed on any section of the extruder barrel or before, in or after the exit (die) [27]. Ultrasonic waves are characterized by their wavelength, frequency and amplitude. Thus, high intensity waves (e.g. frequency range from 20 to 100 kHz) produce pressure waves that induce the formation of bubbles or voids (cavities) in the bulk polymer melt (high viscosity). This phenomenon, known as cavitation, causes the creation of zones of compression (high pressure) and rarefaction (low pressure). The dramatic variation of the pressure increases the mechanical stresses into the media and consequently, the scission of the polymer chains [27, 34, 35].

Feng and Isayev 2004 [34], performed continuous ultrasonic devulcanization of unfilled butyl rubber in an extruder with two ultrasonic devices placed before the die. The amplitude of the waves was varied (5 to 10 μm) at a constant frequency (20 Hz). Authors reported that the network of the cross-linked rubber was not only devulcanized, but also partially degraded. When processing at high amplitude (10 μm), the molecular weight of the virgin rubber ($M_n = 1,7\text{E}+05$ and $M_w = 5,1\text{E}+05$ g/mol) was reduced to soluble parts having lower molecular mass ($M_n = 5,1\text{E}+04$ and $M_w = 4,2\text{E}+05$ g/mol). Despite this partial degradation, the product exhibited good processability during extrusion and its elasticity was similar to that of the fresh rubber.

Although all these techniques have proven to be useful for devulcanization and reclamation, the plasticity and reprocessing performance are restored only to a certain extent [2, 32]. In fact, chains scission takes place mainly at the surface of the rubber granulates and the vulcanized structure of the core remains. As a result, additional compatibilization strategy needs to be implemented [10].

1.4.3.2 Surface modification

The surface of GTR (devulcanized or not) can be modified using compatibilization strategies, classified as reactive and non-reactive. The former mainly focus on the chemical modification of GTR while it is blended with the second phase. The latter consists in increasing the physical interactions between the two phases (previously modified or not) via mechanical mixing at high-shear rates [11]. In both cases, the goal is to promote stronger interfacial interactions between the GTR and the rest of the components of the blend [10]. In addition, the improved adhesion also makes it possible to achieve a finer dispersion of the rubber crumbs [3]. Table 1.2, lists some of the processes that have been explored to modify the surface of GTR.

Table 1.2 – Physical and chemical methods explored to modify the surface of GTR.

Treatment	GTR modification method	Applications	References
Physical	◦ γ irradiation(with our without air)	Blends with recycled HDPE, fresh HDPE or LDPE	[36, 37]
	◦ UV-induced photografting	Blending with HDPE	[38]
	◦ Twin-screw extrusion	Blending with recycled PE	[39]
	◦ Batch mixer	Blends with PP/GTR	[40]
Chemical	◦ Chlorination to increase surface polarity	Excellent filler for polar polymers like PVC	[41, 42]
	◦ Ozonization to add functional groups	Blends with HDPE	[41, 42]
	◦ Oxidation with oxygen-containing solutions (e.g. H_2O_2 , HNO_3 , H_2SO_4)	Blends with fresh NR or HDPE	[43, 44]
	◦ Blending with compatibilizers	Blends with PE, PP, PS, NR and SBR	[40, 45] [29, 46]
	◦ Cross-linking by grafting polymerization	Grafting of MA and/or PS	[28, 47] [23, 30]

(i) Physical methods

Physical methods leading an activated GTR surface involve irradiation with gamma (γ) or ultraviolet (UV) rays, and mechanical mixing. These can be applied separately and before mixing with the polymer matrix or coupled. On the one hand, γ and UV radiation cleaves the polymer chains at the surface of GTR or in the bulk polymer, thus forming chemically active radicals. These may further react to create crosslinks and branches on polymer chains [36–38].

On the other hand, the mechanical treatment for GTR modification is performed in equipment capable of applying high-shear forces such as twin-screw extruders, two-roll mills and batch mixers. When mixing at high temperatures, the GTR is partially devulcanized, which aids to improve the miscibility with the polymer phase (in the molten state) [39, 40]. In a study carried out by Scaffaro and coworkers [39], blends of GTR with recycled PE (without GTR modification or additives), were prepared in industrial mixers and the operating parameters, such as temperature, composition and mixing speed, were optimized. The results indicated that the GTR particles were effectively devulcanized at high temperatures (about 180 °C), increasing the miscibility between both phases.

(ii) Chemical methods

Chlorination, ozonization and oxidation (with oxygen-containing solutions) are methods primarily used to create functional groups on the surface of GTR and therefore, to increase interactions with a wider variety of materials [41–43]. For example, Colomb et al., (2007) [44], treated the surface of GTR with acids like H_2SO_4 , HNO_3 and $HClO_4$, and proved that this process enhanced the capability of GTR to interact when blended with HDPE. Chemical methods also include the reactive strategy, in which rubber crumbs are chemically linked to the polymer phase. This is achieved by the addition or formation of reactive species that react with one or both phases. Sometimes the combination of physical and chemical strategies is the only way to achieve the required degree of modification.

The chemical methods can be classified into two categories as follows:

- **Compatibilization.** Chemical interactions can also be developed by the addition of compatibilizers composed of block and graft copolymers. The constituent polymers of these agents exhibit high affinity with the rubber granulates and the polymer, acting as a bridge when mixed. Maleic anhydride (MA) is, for example, one of the most commonly used vinyl monomers as compatibilizer in polymer composites [10, 37].

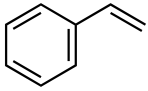
The influence of compatibilizers, such as MA-grafted styrene-ethylene-butylene-styrene (SEBS-g-MA), polypropylene-grafted-MA (PP-g-MA) and polyethylene-grafted-MA (PE-g-MA), in preparing polypropylene (PP) composites containing dispersed rubber crumbs (made of shoe sole scrap powder) was studied by Phinyocheep et al., (2002) [46]. The best results in terms of decreasing the interfacial tension between the phases were obtained with SEBS and SEBS-g-MA. In other works, Zhang et al., (2013) [45] used polystyrene-grafted-styrene-butadiene-rubber (PS-g-SBR) for compatibilization of GTR/PS mixtures. Nowadays, a large variety of compatibilizers is commercially available, but they are usually expensive [10].

- **Crosslinking.** This is a reactive technique using reactive additives such as monomers and radical initiators. This approach, which is carried out by radical polymerization in-situ, has demonstrated good results and consists in performing crosslinking reactions to graft the polymer directly on the GTR surface, leading to chemically linked interfaces [11, 48].

In recent years, this method has been widely studied and the preferred monomers for grafting are styrene, glycidyl methacrylate (GMMA), acrylic and methacrylic acids, because of their high reactivity, low cost and their ease for processing (e.g. by injection and extrusion) [11, 28, 47, 49]. Saelao and Phinyocheep (2004) [50], grafted MA onto natural rubber (NR) using benzoyl peroxide (BPO) as the radical initiator. In fact, the BPO attacks the double bonds of the NR backbone, leading to the formation of radicals to which the MA is grafted. A more detailed description of the grafting mechanism is presented below.

Polymers such as polypropylene (PP), polyethylene (PE) and polystyrene (PS) are commodity thermoplastics with remarkable properties, but poor mechanical strength at low temperatures. Thus, the incorporation of rubber granulates in these thermoplastic materials makes it possible to obtain polymer composites that combine thermoplastic and elastomer properties, commonly known as *thermoplastic elastomers* [48, 49]. For the purpose of this study, particular attention will be paid to polystyrene composites with GTR; details on the adopted blending technique are discussed in section 1.6.

1.5 Polystyrene (PS)



Styrene, $C_6H_5CH = CH_2$, is the key building block of styrenic polymers. The latter exhibit an excellent processability due to their amorphous structure, good dimensional stability and largely constant mechanical properties even up to the glass transition temperature (T_g) [51, 52].

Figure 1.9 – Styrene

1.5.1 General purpose polystyrene (GPPS)

General purpose polystyrene (GPPS), or standard PS, is the homopolymer obtained from the radical polymerization of styrene. Its backbone chain of laterally connected phenyl rings determines the high transition temperature T_g range (90 to 100 °C approx.). GPPS is a commodity plastic, transparent, gloss, rigid and brittle, widely used for food packaging, disposable dishware, injection molding products, functional and decorative/transparent applications. Due to the high reactivity of styrene with other monomers, it is commonly co-polymerized to yield copolymers with improved properties (i.e., with respect to GPPS), such as impact resistance, thermal stability, opacity, etc. [51]

1.5.2 High-impact polystyrene (HIPS)

Standard PS is commonly reinforced by combination with various rubbers to overcome brittleness and widen its scope of application. High-impact polystyrene (HIPS) is a polymer blend obtained by the incorporation of dispersed polybutadiene-based rubber (PB) particles (without fillers) into the polymer matrix [51]. As illustrated in Figure 1.10, the dispersed PB particles (black zones) contain in turn dispersed PS (clear zones) and their size varies between 1 to 5 μm . Commercial HIPS is synthesized by bulk polymerization and the volume fraction of PB particles is limited to 8 to 12%, due to the high-viscosity attained by the reaction medium. Despite its low PB content, the impact resistance of GPPS (about 2 kJ/m^2 for notched Charpy test) can be increased more than twice (4 to 15 kJ/m^2) [51, 53, 54]. HIPS opacity and translucency can be settled by varying the PB particle size. Some of the most common applications are internal/external frames in electric household and consumer electronics.



Figure 1.10 – HIPS: a) chemical structure and b) micrograph of the salami micro structure of commercial HIPS. Transmission electron micrograph, Gao et al., (2006), [54]

Nevertheless, for rubber-toughened plastics such as HIPS and others based on PB like (ABS, SBR), aging is a major problem. When molded parts are used in outdoor applications, the PB rubber-phase is photo-oxidized by sunlight, causing a drastic decrease in impact resistance. In order to overcome this problem, PB has been replaced by more stable alternative saturated rubbers like poly(ethylene-co-vinyl acetate) (EVA), poly(butyl acrylate) or ethylene-propylene-diene terpolymer (EPDM). More recently, the possibility of replacing PB by recycled rubbers is being studied.

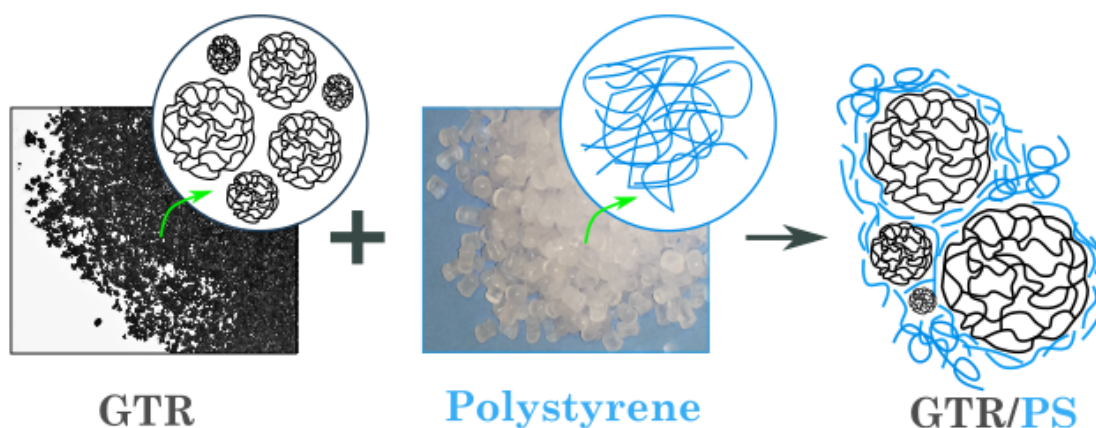


Figure 1.11 – Schematic representation of blending GTR with commercial PS.

1.6 Composites of GTR and polystyrene

As regards the composites of PS with GTR, it has been reported that the surface modification of GTR by reactive methods is the most efficient in improving the interfacial adhesion between the two phases at low costs [10, 23, 28]. Due to the high reactivity of the vinyl double bond, styrene is an excellent option to perform grafting without using additional additives or compatibilizers. In the reactive modification, polymer chains are chemically bound to the backbone of GTR by means of common peroxide initiators, like benzoyl peroxide (BPO) or dicumyl peroxide (DCP). Such initiators have the ability to attack unsaturated or saturated (i.e., via abstraction of hydrogen atoms) bonds on the rubber chains, and create macro-radicals to which the polymer chains graft through C-C bonds.[28, 47].

For example, Tuchman and Rosen (1978) [30] swollen GTR (obtained by cryogenic treatment) with a solution of styrene-BPO and pre-polymerized it before blending with PS. The polymerization led to the formation of tiny globules of PS physically trapped within the GTR structure. In another study, Pitolo and Burford (1986) [23] prepared blends of PS with cross-linked PB and SBR crumbs reinforced with carbon black (CB). Before blending, rubber crumbs were also modified by embedding them with a styrene-initiator solution and subsequent polymerization. Two initiator agents were used separately: BPO to graft covalently the PS chains to the rubber crumbs and, azobis(isobutyronitrile) (AIBN), a non-peroxide initiator, to create non grafted PS chains (free PS). Authors found that the interfacial adhesion increased by using either initiator, and suggested that the interpenetration of PS in the rubber crumbs volume was sufficient to improve the compatibility.

1.6.1 Interfacial adhesion improvement by grafting polymerization

The *interfacial adhesion* or *interfacial tension* controls the morphology of heterogeneous polymer blends. The interfacial tension is intrinsically positive and it is defined as the change in the Gibbs free energy when the interfacial area is reversibly increased. In a multicomponent system as a polymer composite, a diminution of the free Gibbs energy results in the increase of the contact area between the multiple phases. Consequently, the surface activity at the interfaces enhances as the interfacial tension decreases. This phenomenon lead to increase the degree of dispersion of fillers in polymer matrices for instance. Block and graft polymers have been reported as the most effective interfacial agents in polymer blends [3].

Two authors have mainly studied the mechanism of the kinetics of the grafting polymerization of styrene in presence of GTR particles: Coiai and coworkers (2006) and Yu (2015) [28, 55]. From their works, the global reaction can be represented schematically in Figure 1.12. The polymerization system

is composed of GTR, styrene and one or more peroxide initiators (BPO a/o DCP). A more detailed description concerning the reaction kinetics, initiators' choice, formulation and polymerization conditions (reaction time and temperature, reactor specifications, etc.), will be discussed in detail in the following chapters.

In general, the polymerization is carried out in two steps:

1. **Preparation of the polymerization system:** This is prepared by putting in contact GTR with the monomer solution, which contains styrene and peroxide initiator(s), represented as **ROOR** (soluble in the monomer). Since GTR exhibits a high affinity towards organic components, the monomer solution wets the walls of the particles and migrates to the inside, until they are saturated. Yu (2015) [55], reported that the critical threshold after which the excess of styrene remains outside the particles corresponds approx. to a styrene/GTR mass ratio of 2. This means that the monomer solution can be exclusively inside or both inside and outside the particles, depending on the formulation.
2. **Polymerization:** The reaction proceeds in significant rates when the system is brought to a given temperature (e.g. between 70 to 90 °C when using BPO as initiator). During polymerization, two main parallel and competitive reactions take place:
 - Homo-polymerization: produces free polystyrene chains, named **free-PS** (f-PS)
 - Grafting polymerization: forms grafted polystyrene chains onto GTR, called **grafted-PS** (g-PS). GTR grafted with PS is named **GTR-g-PS**

The final product, which is constituted of free-PS and GTR-g-PS is denoted **GTR-g-PS/f-PS**.

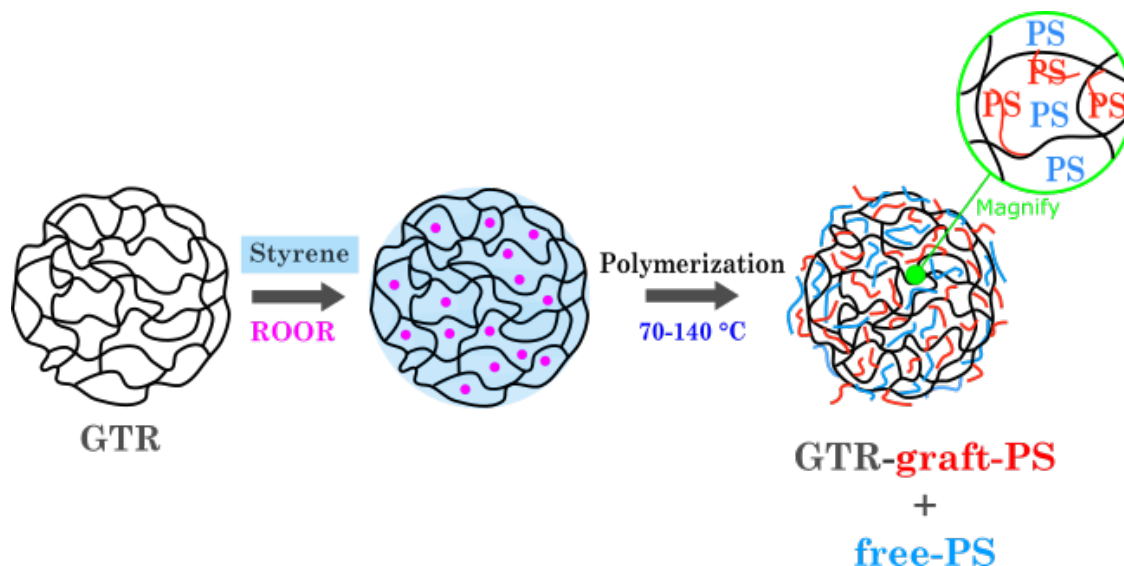


Figure 1.12 – A schematic representation of styrene polymerization in a single GTR particle.

The main objectives in GTR modification by PS grafting through free-radical polymerization consist in maximizing the qualities of the product such as i) the conversion (x) of styrene to polystyrene, and at the same time ii) the formation of grafted-PS chains, usually defined as *Grafting Efficiency* (GE) [28, 47, 55].

- **i) Monomer conversion.** The total monomer conversion, namely the transformation of styrene to free-PS and grafted-PS, can be determined by Equation (1.1). High conversion values imply an efficient polymerization and limit the loss of materials.

$$x = \frac{\text{total amount of PS formed (g)}}{\text{initial amount of styrene (g)}} \quad (1.1)$$

- **ii) Grafting efficiency.** After removing the free-PS by solvent-extraction (usually chloroform) from the polymerization product (GTR-g-PS/f-PS), GE can be calculated by Equation (1.2). A high value of GE implies that the formation of grafted-PS is favored, as well as the increase of the interfacial adhesion between GTR and PS. The competition between the two reactions will be studied in Chapter 5.

$$GE(\%) = \frac{\text{amount of grafted PS (g)}}{\text{total amount of PS formed (g)}} \cdot 100\% \quad (1.2)$$

These two indicators need to be taken into account with caution and usually in conjunction when interpreting results; for example, a high monomer conversion by itself may not be desirable when accompanied by low grafting efficiency, or a high GE may imply very low amounts of grafted PS, if combined with low monomer conversion.

According to these definitions, the overall goal is to stimulate the grafting reaction (i.e. GE) over the homo- polymerization. Nevertheless, which reaction is favored depends on several parameters related to the formulation and polymerization conditions [28, 55]. Table 1.3 shows the influence of certain parameters, such as the monomer/GTR ratio, initiator content and reaction temperature, on the above indicators, as reported in the literature [28, 55]. Reactions were initiated using BPO or DCP, or both. Each time one parameter was varied, while others were kept constant. An increase, a decrease and/or no variation in the values of these product qualities are symbolized by arrows and the conditions values are indicated in parenthesis..

Under the given polymerization conditions, GE increases for all systems by decreasing the initiator content, the monomer/GTR ratio or the reaction temperature. At the same time, the formation of grafted-PS chains prevails over free-PS chains. On the other hand, the conversion exhibits the opposite behavior in most cases and consequently, the amount of residual monomer in the product increases. The specific case of the BPO-initiated reaction with a monomer/GTR equal to 1, is an example of the optimal conditions in stimulating both polymer conversion and grafting.

In general, the grafting reaction of PS onto GTR is influenced by the following parameters:

- GTR composition
- Initial monomer/GTR ratio
- Initiator(s) type and content
- Reaction temperature and time

In the literature, efforts have been made to prepare GTR/PS composites by grafting directly PS onto GTR. Coiai et al., (2006) [28], carried out the radical polymerization of styrene in presence of GTR (10 to 30 wt% of the total weight of the sample, styrene/GTR > 2) with two different initiators, BPO or AIBN. Samples of 5 g were prepared in 25 ml glass tubes. IR analysis of the cross-section of the grafted particles GTR-g-PS revealed that the grafting took place on the external surface and inside the particle. Measurements of the final x and GE, revealed that BPO was more efficient in PS grafting ($GE = 20$ to 45%) than AIBN ($GE < 1\%$). By contrast, they found that styrene conversion in the presence of GTR with BPO was limited to below 54%, compared to 97.3% reached with AIBN or 99.6% for the pure

Table 1.3 – Influence of some polymerization parameters on styrene conversion and GE. Results adopted from [28, 55]

Initiator	Parameters			Quality indexes			Ref.
	$\left(\frac{\text{monomer}}{\text{GTR}}\right)$ (w/w)	I content (mol%) ^a	Temperature (°C)	GE	x	$\left(\frac{\text{grafted-PS}}{\text{free-PS}}\right)$	
BPO	→ (9)	↘ (1.8 to 0.2)	→ (85 °C , 24h)	↗	no trend	→	[28]
	↘ (9 to 2.3)	→ (0.2)	→ (85 °C , 24h)	↗	↘	↗	
	→ (1)	→ (0.6)	↘ (110 to 80 °C , 9h)	↗	↗	↗	[55]
DCP	→ (1)	→ (0.6)	↘ (110 to 80 °C , 9h)	↗	↘	↗	[55]
BPO & DCP	↘ (1.5 to 1)	→ (3)*		↗	↘	↗	
	↘ (5.7 to 4)	→ (1%)*	→ (Ramp 70-100 °C , 10h)	↗	↘	-	[55]
	→ (5.7)	↘ (1 to 0.2)*		↗	↘	-	
	→ (5.7)	→ (0.2)**		↘	↗	-	

* Ratio BPO/DCP=0.25 mol%.

** At constant initiator content of 0.2%, the BPO/DCP ratio was decreased from 4 to 0.25 mol%.

monomer (i.e.in absence of GTR) at the same polymerization conditions (with either BPO or AIBN).

In a similar way, Zang et al., (2012)[47] grafted styrene onto GTR using BPO as initiator agent and prepared samples of about 25 g in the bulk. Authors found that polymerization parameters such as the styrene and initiator contents, reaction time and temperature, influenced GE. Nevertheless, results of monomer conversion were not reported.

In other studies, Yu (2015) [55] performed the polymerization of styrene in the presence of GTR by using either initiator BPO or DCP or both. Variations in temperature (isothermal and non-isothermal), monomer/GTR ratio (1 to 5.7) and initiator content (0.2 to 1 mol%/mol% styrene) were studied (some of these experiments and conditions are also included in Table1.3). The reaction was performed in a stainless steel reactor of 1 L capacity and samples of 300 to 500 g were prepared. Two general conclusions were drawn from the reported results. The first is that BPO seemed to be a better initiator over DCP to increase both conversion and GE at the same polymerization conditions. Secondly, the conversion could be significantly increased (in more than 40%) to achieve conversion values above 80%, when using the mix of initiators BPO/DCP.

1.7 Motivation and objective of this work

The industry of plastics is indebted to our planet and future generations. Remediate the environmental damages caused by the million tons of non-biodegradable plastics disposed in the nature every year worldwide represents an enormous challenge and the countdown has started. Some regions have indeed changed their policies to promote a sustainable control of some of the plastic wastes generated. This is how, for example, the manufacturers and importers of the rubber tire markets have developed exemplary management models for recovery and recycling of post-consumer tires. These have led to a great progress in solving a part of the environmental problems caused by the over-accumulation of plastic wastes.

In search for durable solutions to valorize end-of-life tires, one sustainable alternative consists in taking advantage of the remarkable properties of GTR, to develop a series of new products with practical applications in everyday life. Moreover, the formulation of thermoplastic composite materials by the addition of GTR is a promising option to encourage recycling and, at the same time, to create materials with interesting mechanical properties and price.

With regard to the polystyrene composites reinforced with GTR, the issues related to the interfacial incompatibility between GTR and polystyrene have been partially overcome via the grafting polymerization strategy. In addition, certain conditions allowing to optimize the monomer conversion, more particularly, the formation of grafted polystyrene chains, have been identified. Nevertheless, little is known about the effect of GTR in the kinetics of this polymerization system and, for example, it is not clear what factors limit styrene conversion.

On the other hand, most studies have reached slight increase in the impact resistance and tensile properties of PS by adding low amounts of GTR (generally below 30 wt%). In fact, the research to date has tended to focus only on improving the interfacial adhesion between GTR and PS as the crucial factor for polystyrene toughening. Current knowledge on thermoplastic filled materials shows that toughness depends strongly on the degree of dispersion and spatial distribution of GTR in the polymer matrix. In particular, polystyrene can be effectively toughened by the addition of rubber particles of some few microns in size or by the combination of large and sub-micrometer particles. This implies a necessity to reduce the original particle size of GTR in more than two orders of magnitude. Nevertheless, this is difficult to perform by classic grinding techniques due to the high extensibility and elasticity of the vulcanized rubber particles.

The objective of this work is to develop a novel methodology to toughen brittle polymers, such as polystyrene, by using GTR as a reinforcing agent. The materials should be rich in GTR in the purpose of maximizing GTR recycling rates. This methodology combines two processes:

- free-radical grafting polymerization of styrene onto GTR by using a mix of peroxide initiators, such as BPO and DCP, in a batch reactor,
- subsequently, compounding the resulting product in a twin-screw extruder.

These consecutive processes lead to ensure the good interfacial adhesion between PS and GTR and favor fine dispersion and spatial distribution of GTR through the PS matrix.

The overall structure of this research takes the form of five chapters, including this introductory chapter.

Chapter 2 concerns the study of the free-radical bulk polymerization of styrene in the presence of GTR, by monitoring the reaction via isothermal scanning calorimetry (DSC). Two radical initiators different in nature, namely BPO and AMBN, are tested in a series of variable-composition experiments

under three different temperatures, in order to selectively address the role of the presence of GTR on the course of the polymerization reaction. The variation of the overall effective kinetic rate constant and activation energy are also calculated to quantify the effect of the addition of GTR.

The third Chapter begins by a brief review laying out the factors influencing toughness of thermo-plastic composites filled with rubber particles. Then, this presents the novel methodology proposed to toughen polystyrene by the addition of high amounts of recycled rubber particles such as GTR. The experimental procedure followed accounts for materials definition, equipment characterization, process description and definition of the optimal processing conditions.

The fourth Chapter develops the kinetic model describing the free-radical polymerization of pure styrene in a batch reactor. The model allows predicting the evolution of the total monomer conversion and that of the average molecular weights of PS during the polymerization. The parameters of the model are estimated by using literature values and data from the experiments of bulk polymerization conducted by DSC and solution polymerization in toluene. The predictive capability of the model is assessed by fitting with experimental results reported in published literature. Subsequently, this model is modified to postulate the kinetic scheme accounting the reactions occurring in the presence of GTR and the phenomena identified during the experiments performed by DSC and in the batch reactor.

The final chapter presents the physico-chemical characteristics, microstructure and mechanical properties of the obtained GTR-filled polystyrene materials. These are characterized after the PS synthesis by grafting polymerization as well as after each stage of the compounding process. The results lead to study the effect of introducing high amounts of GTR, compounding at high temperatures and changing the extruder screw configuration on the ultimate notched Charpy impact strength and tensile properties. In addition, the efficiency of the novel methodology proposed in toughening polystyrene is discussed.

On the free radical bulk polymerization of styrene in the presence of rubber particles from recycled tires. A kinetic study using DSC

Contents

2.1	Introduction	29
2.2	Experimental	30
2.2.1	Materials and reagents	30
2.2.2	Methods	30
2.3	Results and discussion	31
2.3.1	Monitoring of the styrene-free radical polymerization.	31
2.3.2	Effects of GTR on the DSC thermograms and monomer conversion of free-radical polymerization of styrene.	31
2.3.2.1	Validation of the analytical method	32
2.3.2.2	Effect of the GTR content	33
2.3.2.3	Effect of the initiator nature	36
2.3.2.4	Effect of the GTR formulation	37
2.3.2.5	Effect of the initiator content	38
2.3.3	Kinetics of the polymerization of styrene in the presence of GTR.	39
2.3.3.1	Overall kinetic rate constants and activation energies	39
2.4	Conclusions	41

2.1 Introduction

The over-accumulation of used tires has become, over the last decades, a significant ecological issue drawing the attention of scientists on a worldwide scale. Among the different routes of treatment of end-of-life tires (e.g., land-filling, energy recovery, reuse, etc.), the recycling of these tires appears as a sustainable solution offering significant benefits related to its low environmental impact and important production of secondary raw materials with high economic value [10, 22]. In this context, one method for tires recycling consists in mechanically grinding rubber-containing parts to micrometric powders, commercially called ground tire rubber (GTR). The GTR is a three-dimensional network of natural and synthetic cross-linked elastomer chains. It also contains reinforcing agents, curatives and additives [15]. It is exactly because of its elastomeric properties that GTR has found widespread applications as filler agent to reinforce polymers [11, 30].

Polystyrene (PS) is a thermoplastic commodity, widely used in several consumer products, whose mechanical properties (i.e., notably related to brittleness) can be modified by the addition of rubber into the polymer matrix, thus producing a polystyrene grade known as high-impact polystyrene [23]. Hence, several research studies have been focused on the idea of replacing fresh rubber with GTR particles in order to achieve a similar improvement on the mechanical properties of PS and to recycle used tires at the same time [30]. The main issue with this concept is that the two phases (i.e., the GTR and polystyrene matrix) display low adhesion towards one another, making it difficult to produce a homogeneous compound simply by blending them. A commonly adopted strategy to overcome this obstacle and render the two phases compatible is to graft the polymer directly onto the surface of the GTR particles via in-situ free-radical polymerization [23, 28, 56].

The presence of particulate fillers in a free-radical polymerization system may often alter, directly or indirectly, the mechanism of the reaction [57–59]. In fact, depending on their physicochemical characteristics, fillers can interact with other reactive species present in the mixture, in a series of parallel and/or competitive chemical reactions, altering the course of polymerization in terms of the monomer conversion and/or polymer chain structure. As a result, the polymerization can be either accelerated or retarded and/or inhibited solely by the presence of an additive that displays strong interactions with the initiator agent(s) and/or the monomer(s). This seems to be also the case for free-radical polymerization systems in the presence of GTR since, depending on the nature of the initiator agent, the type of the monomer and the amount and composition of GTR, an important acceleration or inhibition can be observed on the polymerization reaction. For example, Coiai et al., 2006 [28] have observed a significant decrease in the final monomer conversion of styrene, when using benzoyl-peroxide (BPO) as initiator agent, contrary to organic azo-initiators such as azobis(isobutyronitrile) (AIBN) that displayed no significant effect. In contrast, Xiong [60] demonstrated that in the presence of scrap tire rubber powder, the overall polymerization rate of acrylate monomers such as methyl methacrylate (MMA), glycidyl methacrylate (GMA) and hydroxy ethyl methacrylate (HEMA) is accelerated, if the reaction is initiated with BPO. In these studies, the observed effects were attributed to the interactions between the initiators, the monomers and several additives present in the GTR formulation, such as carbon black, the most widespread rubber tire reinforcing agent [15].

The main purpose of this chapter is to investigate the effects of the presence of GTR on the free-radical polymerization kinetics of styrene by using differential scanning calorimetry (DSC). DSC is a sensitive and precise thermal analysis technique that has proven to be a useful tool in the measuring of polymerization kinetics [57–59, 61]. In this technique, the heat flow, which is assumed to be proportional to the reaction rate evolution, is recorded during the course of the reaction. In the case of the polymerization of vinyl monomers, variations in the polymerization rate exhibit a significant exothermic heat release. Although some research has been carried out on the preparation and characterization of composites based on PS and GTR [23, 28, 30], to the best of the authors' knowledge, it is the first time that a systematic study of the kinetics of the bulk free-radical polymerization of styrene in the presence

of GTR particles is carried out using DSC, under different conditions of temperature and composition.

2.2 Experimental

2.2.1 Materials and reagents

All the reagents used, namely, styrene monomer (with a purity $\geq 99.5\%$ and stabilized with $\sim 0.005\%$ of 4-tert-butylcatechol), 2,2-Azobis(2-methylbutyronitrile) AMBN (with a purity $\geq 98\%$) and BPO (75 % remainder water), were purchased from Sigma-Aldrich and used without further purification. Commercial GTR was obtained from DeltaGom France and was used without purification, unless otherwise stated. This specific grade of GTR was derived from the recycling of end-of-life tires of different categories (light, heavy goods and agricultural vehicles, motorcycles, etc.) and is mainly constituted of a blend of styrene-butadiene rubber and natural rubber, and several additives (such as aromatic oils, organic chemicals, vulcanizing and reinforcing agents). It came in the form of powder with a mean particle size in the order of $635\ \mu\text{m}$. The purification of GTR particles, for some measurements, was carried out by extraction with chloroform during 48 hours, under permanent stirring, followed by vacuum drying until constant weight.

2.2.2 Methods

The GTR used in this study was able to absorb more than twice its weight in styrene. Thus when styrene/GTR ratio was smaller than 2, caution had to be taken to ensure uniform absorption of styrene within GTR particles. To that end, a desired amount of initiator was initially added to styrene under stirring for 15 minutes. In parallel, the required amount of GTR particles (i.e., according to the desired composition) was uniformly deposited as a thin layer on the internal surface of a cylindrical glass container. The solution of styrene and initiator was subsequently added on the layer of GTR particles. This addition took place either via a spraying process, for a ratio of GTR/styrene equal to 1, either in a dropwise manner for higher GTR/styrene ratios. Finally, the glass flask was sealed and stored at $4\ ^\circ\text{C}$ for 6 hours before measurement.

A DSC apparatus of Texas Instruments, Q2000, was used to record thermograms of the free-radical bulk polymerization of styrene, in the presence or absence of GTR. The polymerization system was placed in a hermetic aluminum pan specially adapted for containing volatile products. It was scanned in two consecutive runs. The polymerization reaction was conducted isothermally (85 to $120\ ^\circ\text{C}$) during the first scan; subsequently, it was cooled down to $50\ ^\circ\text{C}$ before a second, non-isothermal scan at $5\ ^\circ\text{C}\ \text{min}^{-1}$ from $50\ ^\circ\text{C}$ to $220\ ^\circ\text{C}$, to assure complete monomer conversion. During the scans, the polymerization temperature ($\pm 0.01\ ^\circ\text{C}$) and the heat flow ($\text{W}\ \text{g}^{-1}$) were recorded as a function of time. Before any further treatment and exploitation of the data, the recorded heat flow data were normalized with respect to the mass of styrene, ($\text{W}\ \text{g}_{\text{sty}}^{-1}$). Finally, the total sample mass was verified before and after each DSC measurement. Eventual losses in mass, recorded for certain samples, were always inferior to 2%.

On the basis of the recorded curves, the monomer conversion as a function of time can be directly determined from the heat flow by the following expression [58, 61]:

$$\frac{dx}{dt} = \frac{1}{\Delta H_T} \frac{d(\Delta H)}{dt} \quad (2.1)$$

where $d(\Delta H)$ is the instantaneous polymerization enthalpy, assigned to the corresponding area between the DSC curve and the baseline, and ΔH_T is the total enthalpy defined as the sum of the recorded enthalpies. Note that, when GTR was present in the samples, the volatile substances present in its formulation caused a burst-off of the lid of the pans during the second dynamic scan, resulting in greater mass losses. Hence, in these cases, only the first isothermal scan was carried out and the total

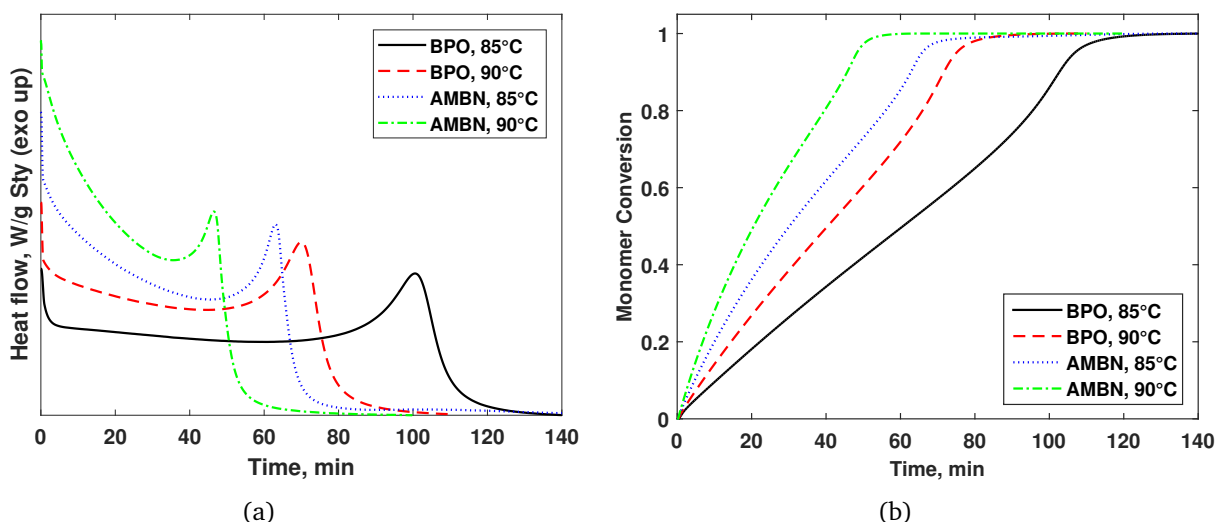


Figure 2.1 – Effect of the initiator type and temperature on a) heat flow and b) monomer conversion in function of time during isothermal free-radical bulk polymerization of styrene by using a ratio initiator to styrene of 4.6 wt%.

reaction enthalpy, recorded for the homopolymerization samples, which were also in agreement with the published literature values, was used as reference.

2.3 Results and discussion

2.3.1 Monitoring of the styrene-free radical polymerization.

The course of the isothermal free-radical bulk polymerization of styrene, in the absence of GTR, was monitored by DSC at 85 °C and 90 °C. Either BPO or AMBN was used as free radical initiator. The DSC thermograms in Figure 2.1a show the evolution of the heat flow with time for four different polymerization conditions. There is an inflection point on each of the four curves that follows the initial polymerization stage. It marks the onset of the auto-acceleration stage. In this stage, termination reactions become diffusion-controlled and a marked increase in the rate of polymerization is observed, as revealed by a sharp increase in the heat-flow release. Subsequently, at very high monomer conversion, the propagation reactions even become diffusion-controlled, resulting in a decrease in the rate of polymerization until complete monomer conversion [58, 61–63]. Figure 2.1b shows the evolution of monomer conversion as a function of time which is calculated according to Equation 2.1. The “S” shape of the curves confirms the existence of an auto-acceleration stage. Both AMBN initiated polymerizations proceed at higher reaction rates with respect to the BPO-initiated ones at the same temperatures, due to the significantly lower half-life time of AMBN at both temperatures.

The total polymerization enthalpies of styrene in the absence of GTR, calculated by numerical integration of the thermograms, are found to vary between 74 and 79 kJ/mol. These values are in agreement with those reported in the literature [64] and indicate that the monomer conversion is complete in all four cases.

2.3.2 Effects of GTR on the DSC thermograms and monomer conversion of free-radical polymerization of styrene.

GTR is a polymer network of elastomers reinforced with carbon black particles and several other additives [10, 11]. As mentioned earlier, several studies attempted to elucidate the effects of carbon black

Table 2.1 – Compositions of the tested samples.

Composition	GTR/(St+GTR) ^a (wt%)	Initiator ^b (wt%)	I/St (wt%)	I/(St+GTR) (wt%)
A	0	4.4	4.6	4.6
B	50	2.2	4.6	2.3
C	30	3.1	4.6	3.2
D	50	4.4	9.4	4.6
E	30	4.4	6.6	4.6

^a Weight/weight percentage*100% (w/w or wt%)

^b Initiator (I), either BPO or AMBN

and other additives on the course of free-radical polymerization systems in the presence of GTR [65–67]. These effects can be more or less pronounced, according to the chemical structure of the carbon black surface and to the nature of monomers and/or initiator agents. At the same time, the cross-linked structure of GTR may also have an effect on the course of the free-radical polymerization.

In an attempt to evaluate some of the aforementioned effects, a series of DSC thermograms has been produced for the free-radical polymerization of styrene in the presence of GTR, at three different temperatures (i.e. 85 °C, 90 °C and 120 °C) and for three different GTR compositions in the system (i.e., 0%, 30% and 50% wt). GTR composition is defined here as the percentage (by weight) present in the total mixture of GTR and styrene. The composition of all the tested samples is presented in Table 2.1. Regarding the initiator content (either BPO or AMBN), the composition was set as follows: a set of samples, including all three GTR compositions, were prepared keeping a constant weight ratio of initiator to styrene equal to 4.6 wt% (cf. Table 2.1, rows 1-3). In addition, another set of samples was also tested, corresponding only to the samples containing GTR, keeping this time a constant weight ratio of initiator to the total sample mass equal to 4.6 wt% (cf. Table 2.1, rows 4-5). Hence, a total of five different sample compositions (i.e., compositions A-E) was tested for each initiator agent and polymerization temperature.

2.3.2.1 Validation of the analytical method

Since, as mentioned above, there is no previously published study on the DSC investigation of the styrene polymerization in presence of GTR, an initial validation of the method was required. To this end, an assessment of the repeatability of the measurements, with respect to the polymerization enthalpy, has been carried out [68]. Then, the repeatability of the measurements was verified by measuring in duplicate the heat flow released from the polymerizing samples at the established operating conditions. Subsequently, the enthalpy was calculated as mentioned in section 2.2. Figure 2.2 shows an example of a replicated DSC thermogram, as recorded for the AMBN-initiated polymerization at 90 °C, for the sample composition B (cf. Table 2.1).

The values of the overall reaction enthalpy, as measured for the duplicate measures shown in Figure 2.2, as well as the corresponding measurements using BPO, are presented in Table 2.2. The respective average and standard deviation (σ) values are also reported in the same Table. Due to the absence of reported values on the reaction enthalpies for this system, it is impossible to validate the observed values. On the other hand, the repeatability of the measurements is clearly demonstrated. The calculated standard deviation is of the order of 3.0% and 3.8% of the mean enthalpy for the polymerization with AMBN and BPO, respectively. At the same time, when calculating the monomer conversion by using as reference the value of the polymerization in absence of GTR ($689 \text{ W/g}_{sty}^{-1}$), the corresponding

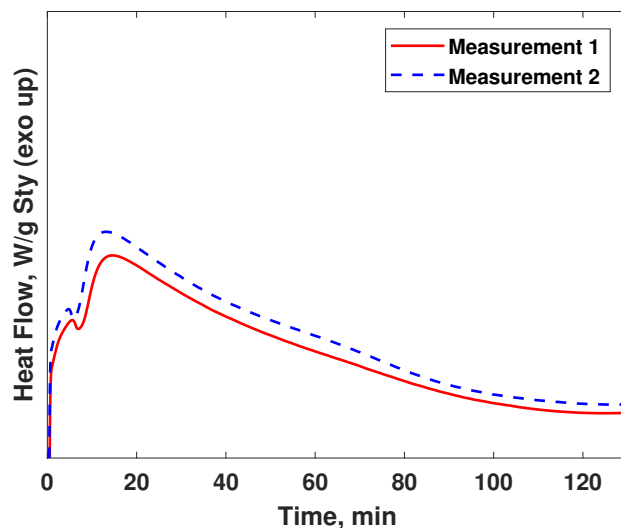


Figure 2.2 – Replicate DSC thermograms of the free-radical polymerization of styrene in presence of GTR with AMBN initiator. (50 wt% of GTR, $T = 90\text{ }^{\circ}\text{C}$; AMBN/St=4.6 wt%).

Table 2.2 – Reaction enthalpy and monomer conversion values of replicate measurements at $T = 90\text{ }^{\circ}\text{C}$ and 50 wt% of GTR.

Initiator (I) type	AMBN		BPO	
I content (wt%)	2.2		4.6	
Measurement	ΔH_T (J g^{-1})	Conversion	ΔH_T (J g^{-1})	Conversion
1	610.73	0.88	162.84	0.24
2	637.37	0.92	171.83	0.25
Mean	624.05	0.90	167.34	0.24
σ	18.84	0.02	6.36	0.01

deviation was also lower (of the order of 2.2% for AMBN and 4.16% for BPO). This initial validation of the repeatability of the measurements in presence of GTR, confirms that the overall sample preparation and measurement procedure does not introduce important uncertainties due to possible sample heterogeneity (i.e., originating from the composition of GTR) and provides a ground-level basis for the following discussions in terms of the investigated effects.

2.3.2.2 Effect of the GTR content

Figure 2.3 shows the effects of the presence of GTR on the DSC heat flow and monomer conversion of the free-radical bulk polymerization of styrene. It can be seen that the addition of GTR clearly affects both the initial rate of polymerization and the overall monomer conversion. More specifically, an increase in the GTR content shifts the maximum exothermic peak of the thermogram towards a lower polymerization time. At the same time, the ultimate monomer conversion is significantly reduced as well (cf. Fig.2.3b).

The present findings seem to be consistent with those of similar studies reported in the literature. Coiai and coworkers [28], found that the BPO-initiated polymerization of styrene in the presence of 10 wt% of GTR did not exceed 54% in monomer conversion, even after 24 hours at $85\text{ }^{\circ}\text{C}$, in contrast to the case where the GTR was absent. In the latter case, the ultimate monomer conversion reached 99.6% under the same polymerization conditions. They also observed almost a two-fold decrease in the

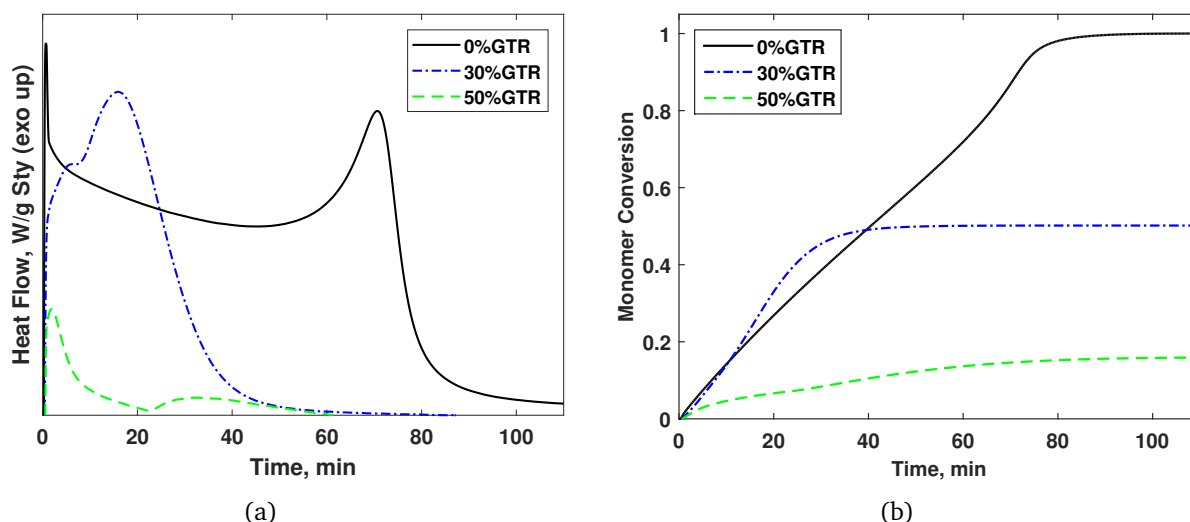


Figure 2.3 – Effect of the GTR content on the evolution of a) heat flow and b) monomer conversion, during the isothermal BPO-initiated polymerization of styrene in the presence of GTR particles. ($T=90\text{ }^{\circ}\text{C}$; ratio BPO/St=4.6 wt%).

final monomer conversion when the GTR content increased up to 30 wt%. In other studies [65, 67], carbon black significantly increased the decomposition rate of free radical initiators such as BPO. Finally, several studies have demonstrated that the peroxide-initiated polymerization of vinyl monomers was catalyzed, inhibited and/or retarded by the presence of carbon black [60, 65–67, 69, 70].

In fact, the surface of carbon black is mainly covered with oxygen-containing groups, such as carboxyl structures, phenolic or alcoholic hydroxyl, carbonyl, and quinone groups, as illustrated in Figure 2.4. At the same time, some of the carbon atoms have unsatisfied valencies, leading to a high electron transfer reactivity [71]. As a result, when the polymerization is initiated by an organic peroxide, such as BPO, the dissociated benzoyl acid radicals may react with the unpaired electrons to give rise to new surface-active sites, to which primary and growing polymer radicals compete to react. The reactivity of the newly formed radicals is not completely inert and can therefore undergo further reactions mainly with propagating chains. On the other hand, it is well known that the combination of peroxides with reducing agents is common in producing radicals at reasonable rates over a wide temperature range [63]. Therefore, when BPO gets in contact with the numerous oxide groups on the surface of carbon black, it suffers a strong redox reaction [67]. The redox decomposition reaction is favored at relatively low temperatures due to its activation energy (i.e., 40-60 kJ/mol) that is significantly lower than that of the thermal decomposition one (i.e., 120-150 kJ/mol) [63, 72].

From the above it becomes apparent that carbon black present in the composition of GTR, can produce various and sometimes even antagonistic effects within the polymerization system [65, 66, 69, 73, 74]. Besides its catalytic effect on the decomposition of peroxide initiators, it can also display an inhibitive or promoting effect on the polymerization, depending on the nature and the polarity of the participating monomer(s). Hence, peroxide-initiated polymerizations of vinyl monomers with negative e -value¹ [75], are commonly inhibited in the presence of GTR, whilst peroxide-initiated polymerizations of positive e -valued monomers are rather favored in the presence of GTR. For example, Xiong (2010) reported that in the BPO initiated-polymerization of acrylate monomers such as MMA, in the presence of 4 wt% of GTR and 0.375 mol% of BPO at only $50\text{ }^{\circ}\text{C}$, the reaction was significantly acceler-

¹ According to the Alfred and Price's Q and e scheme, the e -value is a constant characteristic value for each individual vinyl monomers that takes into account for the polarity of their double bonds; electron-rich (negative e) and electron-poor (positive e), and which influences their reactivity [75].

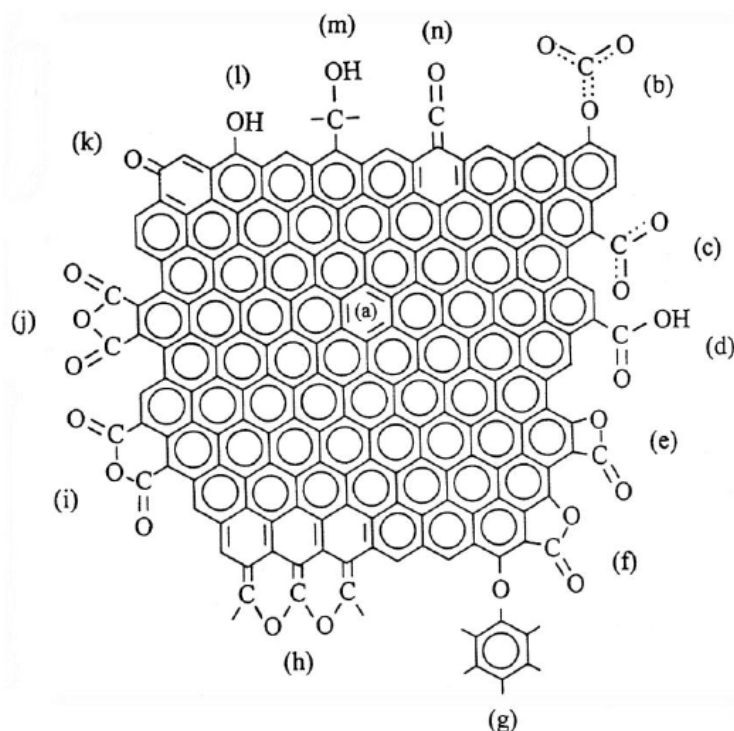


Figure 2.4 – Series of oxygen-containing groups that can be found on carbon black surfaces: (a) aromatic C=C bonds; (b to d) carboxylic groups; (e to f) lactone functions; (g) ether bridge; (h) cyclic ether; (i to j) cyclic anhydride; (k) quinone; (l) phenol; (m) alcohol; (n) ketene. Image reproduced from Radovik (2001) [71]

ated and the conversion was almost eight times higher than those of the pure monomer (i.e. in absence of GTR). In contrast, when replacing the GTR by the same rubber tire formulation (elastomer, aromatic oils, curatives and additives) but without carbon black, the reaction was moderately retarded in regard to the neat monomer polymerization under the same conditions.

Additionally, another reason that could partially contribute to the initial acceleration of the rate of polymerization is the morphological three-dimensional network of the GTR. Similar to the well-known auto-acceleration or gel-effect (or Trommsdorff effect) [76], commonly observed in certain bulk free-radical polymerization systems, the cross-linked structure of the elastomer network of GTR could also limit the mobility of long radicals, thus producing a decrease in their (apparent) termination rate.

It is the combination of some of the above effects that could explain the course of the bulk free-radical polymerization of styrene observed in Figure 2.3. When the 0 and 30 wt% of GTR polymerization systems are compared, it is noticed that the monomer conversions in the initial stage of polymerization almost superimpose. This implies that any eventual acceleration in the decomposition of BPO, induced by the carbon black of the GTR as indicated in the literature, did not display any significant effect on the rate of polymerization. Should this be the case, the initial monomer conversions for the 30 wt% GTR would have been higher than those for the 0 wt% GTR. This could be attributed to a possible parallel deactivation of part of the formed radicals (i.e., primary or short-chain radicals) on the surface of carbon black, as also indicated in the literature. Given the fact that, for the styrene polymerization system, the reported effects in the literature are antagonistic, annulling one another, it is very difficult to extract safe conclusions about the extent, or even the existence, of each effect individually. After the initial stage, the monomer conversions of the 30 wt% GTR were higher than those of the 0 wt% GTR. This could be explained by the network effect of the GTR. When the monomer conversion within the GTR network reached a certain value, the mobility of the growing polymer chains was largely reduced,

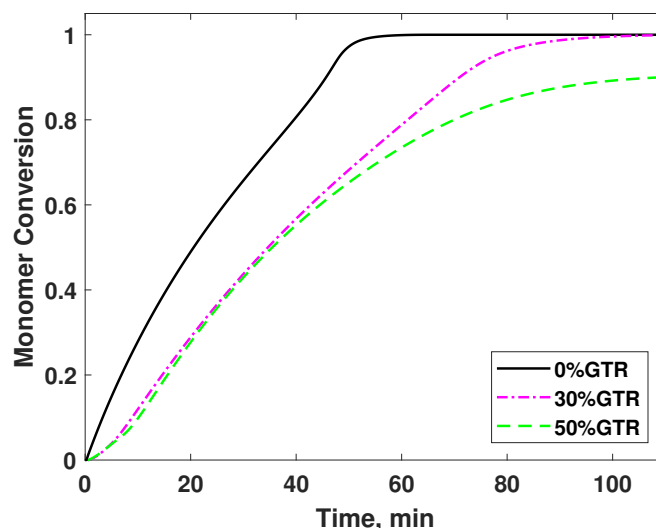


Figure 2.5 – Effect of the GTR content on the evolution of monomer conversion during the isothermal AMBN-initiated radical polymerization of styrene, in the presence of GTR. ($T=90^{\circ}\text{C}$; ratio AMBN/St=4.6 wt%).

leading to a reduced rate of termination of free radicals and an acceleration of the rate of polymerization.

The final monomer conversion of the 30 wt% was significantly lower than that of the 0 wt% GTR. This could be related purely to the inhibitive effect of the carbon black of the GTR. In fact, BPO and its primary radicals could react with the active surface (polar or functional groups) of carbon black, leading to low reactive radicals and non-reactive species, and consequently a significant inhibition of the polymerization as well as an important decrease in the ultimate monomer conversion. Finally, the inhibitive effects of the GTR on the rate of polymerization and the final monomer conversion became more significant when its content reached 50 wt%.

2.3.2.3 Effect of the initiator nature

The above effects of the GTR on the course of the polymerization of styrene were observed using BPO, a peroxide, as free radical initiator. Would those effects still exist for a different type of free radical initiator? In order to answer this question, AMBN (an azo free radical initiator) was used. Figure 2.5 shows the monomer conversion as a function of time for three different GTR contents. The DSC conditions were the same as those for BPO. Comparison between Figures 2.3a and 2.5 indicates that the effect of GTR on the evolution of the polymerization was markedly less pronounced for AMBN than for BPO. In fact, the previous acceleration effect related to the GTR network observed for BPO seems to have disappeared and its inhibitive effect was significantly reduced. The final monomer conversion reached 100% for both 0 and 30 wt% GTR, and still reached about 91% for 50 wt% of GTR.

As mentioned above, peroxides are highly reactive with the active surface of carbon black, resulting in pronounced effects on the course of peroxide-initiated polymerization. On contrast, azo compounds are less reactive towards the active surface of carbon black. Hence, regardless of the monomer e -value, polymerizations initiated by azo-compounds are only moderately retarded by the presence of GTR [69, 77]. Numerous studies reported on the differences in behavior and effects between the peroxide and azo types of free radical initiators. Ohkita et al., (1975) [66] observed that the BPO initiated radical polymerization of styrene was inhibited in presence of furnace blacks. After 10 hours of polymerization the monomer conversion was 18% in the absence of carbon black, and only 2% in the presence of 2 wt% of carbon black (0.073 wt% of BPO in the total weight of the sample). By contrast, when AIBN

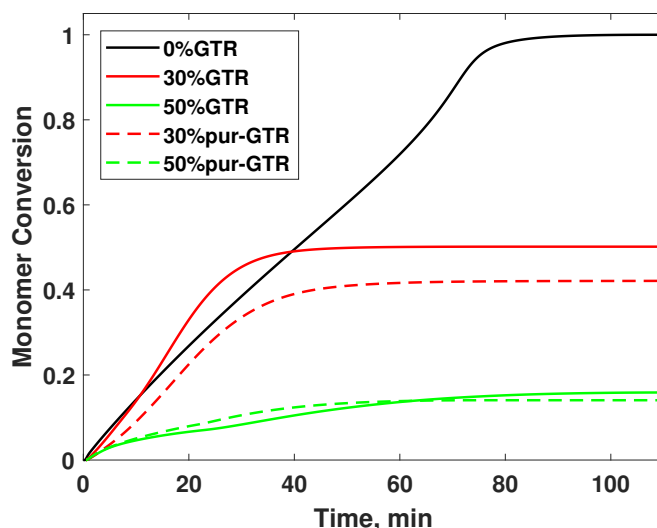


Figure 2.6 – Styrene conversion vs time in presence of 30 wt% of untreated GTR and chloroform-treated GTR (pur-GTR) at 90°C . (BPO/St=4.6 wt%).

was used as a free radical initiator, the retardation effect of carbon black was much more moderate. The monomer conversion in the presence of carbon black was only about 25% of that without carbon black. Coiai et al., 2006[28], found that in the presence of 10 wt% GTR, when BPO was used as the initiator, the monomer conversion obtained after 24 hours of polymerization at 85 °C was 54%. By simply switching the initiator to AIBN, it was 100% under the same conditions.

2.3.2.4 Effect of the GTR formulation

In addition to carbon black, GTR contains other additives which may have positive or negative effects on the rate and the extent of the polymerization. For example, antioxidants added in the formulation of tires serve to scavenge and destroy oxy radicals in order to slow-down the rubber aging process [16]. They may interact with primary and chain growing radicals. On the other hand, some of the GTR additives could also have a certain interaction with the active surface of carbon black, thus partially “masking” its effects. Unfortunately, it is once again very difficult to isolate the extent of the positive or negative contributions of each additive.

Figure 2.6 compares the effects of the presence of the as-received GTR (dashed curves) and chloroform-purified one (solid curves), on the evolution of the monomer conversion as a function of time using BPO as a free radical initiator. The inhibition effect seemed to be more pronounced in the case of the “purified” GTR, with respect to the as-received one, indicating that the additives that were extracted by chloroform had a positive effect on the rate and extent of polymerization. This can be attributed to possible interactions of the additives in the GTR formulation (i.e., the as-received GTR) with the active surface of carbon black, thus reducing the extent of interactions of the latter with the benzoyl radicals of BPO. When these additives are removed (i.e., the chloroform purified GTR), a greater number of BPO radicals and growing macroradicals are exposed to the active surface of carbon black.

It cannot be excluded that, in the case of the as-received GTR, a part of the benzoyl radicals might be deactivated by certain additives and impurities, thus resulting in a partial inhibition of the polymerization as well. Nevertheless, when additives of the GTR were removed, the net effect was a more pronounced inhibition. Similar observations have been reported in the literature. For example, Xiong (2010) [60] observed that, the promoting effect of GTR on the bulk polymerization of MMA, attributed to the interactions with the surface of carbon black, was further amplified upon purification of the GTR

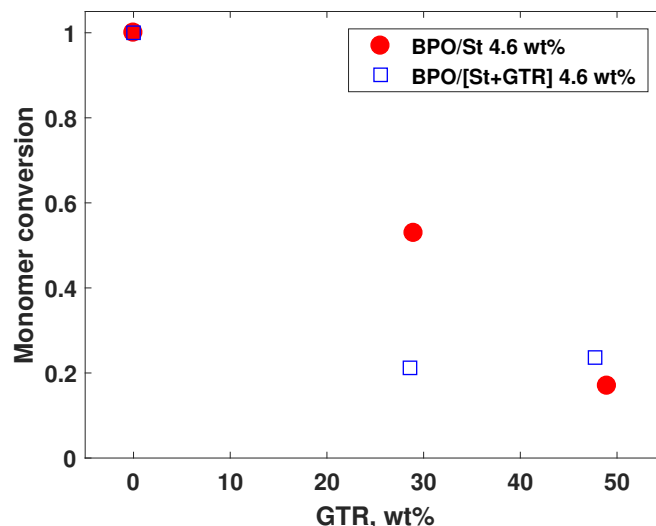


Figure 2.7 – Influence of the GTR content on the final conversion of the BPO-initiated styrene polymerization at 90 °C for two different cases: BPO/St and BPO/(St+GTR) equal to 4.6 wt%.

by methyl ethyl ketone. On the other hand, when carbon black was removed from the GTR, a significant retardation (i.e., of about 40% at 50 °C) on the monomer conversion was observed, that could be attributed to eventual interactions of the radicals with the other additives and impurities of the GTR formulation.

2.3.2.5 Effect of the initiator content

The above results were obtained at a given initiator/styrene ratio of 4.6 wt% and polymerization temperature (90 °C). Both reaction temperature and initiator content have been kept constant in order to isolate their eventual influence on the rate and extent of the polymerization from the studied effects of the GTR content, the initiator type and the GTR formulation. To assess the effect of the initiator content, additional thermograms of the polymerization have been recorded, this time for a constant ratio of the BPO over the total sample mass (GTR+styrene) equal to 4.6 wt%, in contrast to the initial measurements where the content of BPO was kept constant only with respect to the mass of styrene (c.f. Table 2.1).

Figure 2.7 shows the comparison between the final monomer conversion values, achieved under the three different GTR contents in both cases: firstly with constant BPO/styrene ratio, denoted by the filled circles (cf. Table 2.1, compositions A-C) and secondly for constant BPO/(styrene+GTR) ratio, marked with open squares (cf. Table 2.1, compositions D & E). Note that, whilst in the first case the initiator content in the total mass of the polymerization system decreases along with the monomer content, in the second case the initiator content is constant regardless of the ratio styrene/GTR. As a result, the amount of initiator present in the latter samples is higher in comparison to the respective samples of the first case. Then, as discussed previously, when the ratio BPO/styrene is constant, a monotonous decrease is observed in the final monomer conversion. On the other hand, when the ratio of BPO to total sample mass is kept constant, a rather surprising phenomenon is observed; the final monomer conversion drops very rapidly to a value around 20%, even for the 30 wt% composition in GTR, and then remains relatively invariant when increasing the GTR content to 50 wt%.

2.3.3 Kinetics of the polymerization of styrene in the presence of GTR.

2.3.3.1 Overall kinetic rate constants and activation energies

As illustrated in the previous sections, the free-radical polymerization of styrene in the presence of GTR is a system that presents a complex kinetic mechanism that has not been completely elucidated. Nevertheless, in an effort to quantify the effect of GTR on the reaction kinetics, the overall effective kinetic rate constant and activation energy of the polymerization can be calculated on the basis of the DSC data [57, 58, 78]. Accordingly, considering an oversimplified general kinetic scheme (i.e., containing only the radical initiation, propagation and termination reactions) and under the assumptions of Long-Chain Hypothesis (LCH) and Quasi Steady-State Assumption (QSSA) for the polymer radicals [79], the polymerization rate R_p will be given by:

$$R_p = -\frac{d[M]}{dt} = k_p[M\cdot][M] \quad (2.2)$$

where $[M]$ and $[M\cdot]$ denote the concentration of monomer and growing macroradicals, respectively, and k_p is the propagation rate constant. In order to further develop this expression so that it does not depend on the concentration of the radicals, which is very difficult to quantify, $[M\cdot]$ is usually replaced by an expression containing only kinetic rate constants and the concentration of the initiator agent (i.e., on the basis of the QSSA). Note however, that the form of this latter expression depends on the possible existence of inhibition phenomena, in which case the rate of the inhibition reaction R_z should also be considered, affecting the overall polymerization rate. Unfortunately, the prediction of the rate constant(s) of such inhibition reaction(s), k_z , involves difficult experimentation as the rates to be detected are very small [63]. In any case, under the assumptions of i) constant concentration for the initiator (and eventually the inhibitor(s)) and ii) invariant kinetic rate constants, one can consider the term $[M\cdot]$ as constant, thus resulting in the following expression:

$$-\ln(1-x) = kt; \quad k = k_p[M\cdot] \cong \text{const} \quad (2.3)$$

A more detailed development is presented in Appendix 1. Equation 2.3 can be implemented to estimate the overall kinetic constant, k , by plotting the linear relation $-\ln(1-x)$ versus t at constant reaction temperature. Note that Eq. 2.3 is valid only under the aforementioned assumptions and its applicability should be limited to the initial instances of the polymerization. Once the value of k has been estimated for different reaction temperatures, the overall effective activation energy E_{eff} of the polymerization can be inferred by considering an Arrhenius-type variation of k and plotting the values of $\ln(k)$ vs $1/T$. The above procedure was implemented to calculate the values of E_{eff} , under different GTR and initiator contents. An example is shown in Figure 2.8, corresponding to the curves obtained for the BPO-initiated styrene polymerization with 30 wt% of GTR. All the calculated values of E_{eff} are presented in Table 2.3.

In general, for the estimation of k and E_{eff} , the linear regression fitted well to the data in the ranges considered, as indicated also by the calculated values of the determination coefficient, R^2 . The calculated activation energy of the homopolymerization case (i.e., in the absence of GTR) was 92.7 kJ/mol ($R^2 = 0.999$) for the BPO initiator and 94.9 kJ/mol ($R^2 = 0.999$) for AMBN, which are consistent with the reported literature values [80].

Depending on the final form of Eq. (2.3) (i.e., after development of the term $[M\cdot]$, cf. Appendix 1), two extreme cases can be considered. The first corresponds to the typical case where inhibition reactions are considered negligible. In this case, the overall activation energy will be given by an expression of the form (see Appendix 1):

$$E_{eff} = E_p + 0.5(E_d - E_t) \quad (2.4)$$

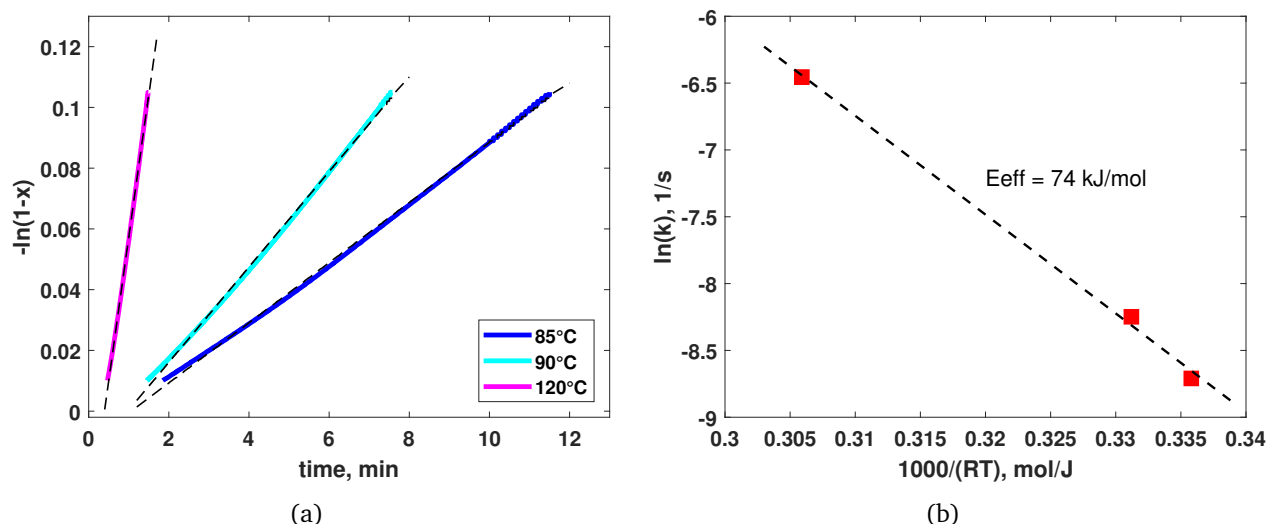


Figure 2.8 – Calculation of the a) overall kinetic constant k and b) effective activation energy E_{eff} for the BPO-initiated styrene polymerization, in the presence of GTR (30 wt%).

where the subscripts p , d and t correspond to the propagation, initiator decomposition and termination reactions, respectively. On the other hand, in the case where inhibition reactions are dominant before typical termination reactions (i.e., by combination or disproportionation), the overall activation energy will be calculated as:

$$E_{eff} = E_p + E_d - E_z \quad (2.5)$$

where E_z denotes the overall activation energy of the inhibition reactions.

Figure 2.8b and Table 2.3, show that the addition of GTR results in a decrease in the E_{eff} value for the BPO initiated polymerization. This can be attributed to the strong interactions between the peroxide initiator and the surface of carbon black that, as described earlier, may induce an accelerated redox decomposition of BPO. This would result in a decrease in the value of E_d towards activation energy values of the redox decomposition (i.e. 40-60 kJ/mol) [63]. Given the fact that this term, in the case of pure thermal homolysis, is typically in the order of 120-130 kJ/mol for BPO and AMBN [63, 72], this 2-fold to 3-fold decrease would result in a subsequent decrease of the overall value of E_{eff} (cf. Eq. (2.4) and Eq. (2.5)). It should be noted at this point that, other parallel interactions are expected to take place (e.g., inhibition and/or retardation by the additives of GTR) that might have a positive or negative influence on the value of the E_{eff} . Hence, the above explanation could only account for a part of the observed overall decrease. Nonetheless, since the interactions between BPO and the surface of carbon black are extensive in this system [65, 66], it is expected that their role will be dominant in the observed decrease of the value of E_{eff} .

On the other hand, the effect seems to be reversed in the case of AMBN, where an increase is observed on the calculated values of E_{eff} upon addition of GTR. In this case, in the absence of strong interactions between the initiator and carbon black, the observed behavior can be mainly attributed to the overall retardation effect of GTR on the course of the polymerization. This retardation, also demonstrated in Figure 2.5, is primarily caused by the various additives and impurities present in the GTR formulation. In this case, the observed increase can be partially explained considering the form of Eq. (2.5) and the fact that the contribution of the term E_d (which is in the range of 130 kJ/mol) is twice as important, with respect to the non-inhibited polymerization. On the other hand, it is certainly difficult to assess the exact contribution of the inhibition activation energy on the overall value of E_{eff} , but its combination with the increase induced by the decomposition term seems to result in the overall increasing effect of

Table 2.3 – Calculated activation energy E_{eff} values.

Composition	GTR/(St+GTR) (wt%)	E_{eff} (kJ/mol) for BPO	E_{eff} (kJ/mol) for AMBN
A	0	92.7 ($R^2=0.999$)	94.9 ($R^2=0.999$)
B	50	70.5 ($R^2=0.908$)	140.3 ($R^2=0.998$)
C	30	74.0 ($R^2=0.997$)	111.8 ($R^2=0.999$)
D	50	48.8 ($R^2=0.992$)	109.9 ($R^2=0.999$)
E	30	76.1 ($R^2=0.991$)	113.3 ($R^2=0.998$)

the value of E_{eff} . Note that, given the assumptions involved in the method used to calculate the value of E_{eff} and the complexity of the associated chemical reactions mechanism, it would be rather risky at this point to extend this discussion further than the mentioned overall trends, which would exceed as well the scope of the present work.

2.4 Conclusions

In this chapter, the aim was to assess, for the first time, the kinetics of the free-radical bulk polymerization of styrene in the presence of fine rubber particles from recycled used tires. For that purpose, the course of the reaction was monitored by DSC under different conditions in terms of temperature and composition, and two chemical initiators of different nature, BPO and AMBN. A single initiator was used instead of a mix of them in order to reduce the number of variables and thus simplify the polymerization system. The results showed that, in general, the addition of GTR displays an overall negative effect on the final extent of the reaction but, at the same, may also have a positive or negative impact on the rate of polymerization. These effects can be more or less pronounced depending on the type of initiator agent. The strongest deviations were observed for the peroxide-initiated system (i.e., with BPO), which displayed a severe inhibition that increased with the content of rubber particles and could lead to very low monomer conversions. In contrast, the reaction initiated with an azo-compound (i.e., AMBN) was moderately retarded and slightly inhibited only at high GTR percentages. The observed effects were mainly attributed to the chemical interactions induced by carbon black, additives and impurities present in the formulation of GTR. Finally, a simplified determination of the overall reaction activation energy showed that, in the case of BPO, the effective activation energy decreased compared to the one required for the polymerization of the neat monomer, while the effect was reversed in the case of AMBN. These effects were in agreement with the previous analysis.

A novel methodology to prepare GTR-reinforced polystyrene composites with improved mechanical properties.

Contents

3.1 Introduction	45
3.2 Mechanical properties of polymer composites	45
3.2.1 Tough and brittle behavior in polymers	45
3.2.2 Main parameters influencing toughness in thermoplastic composites based on GTR	46
3.2.2.1 GTR particle size and size distribution	46
3.2.2.2 GTR morphology and surface	48
3.2.2.3 Molecular weight of the polymer matrix	48
3.2.2.4 GTR content	48
3.2.2.5 Sequence of the processes	49
3.2.2.6 Effect of the type of mixing	50
3.2.2.7 State of dispersion	51
3.3 A novel methodology to prepare polystyrene composites with GTR	53
3.3.1 Product specifications	53
3.3.2 Proposed methodology for product preparation	54
3.4 Materials characterization	54
3.4.1 Ground tire rubber (GTR)	54
3.4.2 Polystyrene	55
3.4.3 Reagents	57
3.5 Process definition	57
3.5.1 Compatibility improvement	57
3.5.1.1 Polymerization reactor: building and operating an experimental setup	57
3.5.2 Reducing particle size	63
3.5.2.1 Intermeshing co-rotating twin-screw extruder	63
3.5.2.2 Influence of the compounding conditions on the diminution of the particle size	64
3.5.2.3 Setting up the compounding line	66
3.5.2.4 Characterization of the equipment	66

3.6 Process proposed	68
3.6.1 Experimental conditions to be tested	68
3.7 Operating methods	68
3.7.1 Free-radical grafting polymerization of styrene onto/into GTR particles	68
3.7.2 Free-radical solution polymerization of styrene	70
3.7.3 Compounding in a twin-screw extruder	71
3.8 Evaluation	72
3.8.1 Structural assessment	73
3.8.1.1 Monomer conversion	73
3.8.1.2 Polymer grafting efficiency	73
3.8.1.3 Polymer molar mass	74
3.8.1.4 Chemical structure of the composites	74
3.8.1.5 Chemical composition of the polymer	74
3.8.1.6 Number of double bonds in the molecular structure of GTR	75
3.8.1.7 Swelling capacity of GTR by styrene absorption.	75
3.8.2 Morphological characterization	76
3.8.2.1 Morphology of the composites and fracture surfaces	76
3.8.2.2 Particle size distribution	76
3.8.3 Thermal characterization	77
3.8.3.1 Glass transition temperature and thermal decomposition	77
3.8.4 Mechanical properties	78
3.8.4.1 Impact strength	78
3.8.4.2 Tensile strength	79
3.8.4.3 Fabrication of mechanical testing specimens	82
3.8.4.4 Fabrication of unfilled polystyrene testing specimens	83
3.9 Conclusions	83

3.1 Introduction

This chapter deals with a novel approach to toughen polystyrene by incorporation of significant quantities of rubber particles such as GTR. In the first part, a review of the main intrinsic and extrinsic parameters identified as influencing toughness of GTR-reinforced thermoplastics, is presented. Then, based on the bibliographic research, the targeted properties and desired specifications of the polystyrene compounds to be prepared are defined. Subsequently, a novel methodology is proposed to formulate and fabricate such materials.

3.2 Mechanical properties of polymer composites

As mentioned in Chapter 1, thermoplastic elastomers or TPE are made up of two distinct and usually incompatible phases having different properties. On the one hand, the elastomer phase is characterized by a high level of extensibility and a glass transition temperature (T_g) far below the room temperature (e.g. until $-70\text{ }^\circ\text{C}$). On the other hand, the thermoplastic phase is rigid (weakly extensible) and its T_g is higher (e.g. polystyrene up to $90\text{ }^\circ\text{C}$). As a result, the TPE combines the most interesting properties of elastomers with the processability of thermoplastics [81, 82].

The advantage of introducing an elastomer phase into a brittle polymer matrix lies in conferring it particular properties, widening the scope of application of a polymer [81, 82]. Since the objective here is to toughen or, in other words, increase the impact strength of polystyrene by the addition of GTR, it is imperative to focus on the key aspects in the improvement of this attribute. Nevertheless, the optimization of toughness results in inevitable changes of some other relevant mechanical properties, such as tensile properties (modulus, yield strength and capacity of deformation), which are also crucial in determining composite applications [10, 81, 82]. For this reason, in this work, both impact and tensile properties are considered to evaluate the performance of the prepared composites.

In this section, the definition of tough and brittle behavior in polymers is assessed. In addition, the main parameters influencing toughness in composites materials based on GTR and thermoplastics are reviewed.

3.2.1 Tough and brittle behavior in polymers

The integration of butadiene rubber in polystyrene to produce commercial reinforced materials, leads to variations in the overall mechanical behavior of key polymer properties such as the elastic or Young's modulus (E), yield strength (σ_y), ultimate strength (σ_r) and elongation at break (ϵ). Figure 3.1 shows an example of the variation of the stress-strain curve of polystyrene induced by the dispersion of butadiene rubber to obtain commercial HIPS (about 12% of rubber) and styrene-butadiene-styrene block copolymer rubber family (SBS) (>60% of rubber) [51].

The brittle behavior is represented by polystyrene (I) and designed when the polymer fractures at its maximum stress at quite low deformation (below 20%). A high-impact material as HIPS (II), is capable of sustaining larger plastic deformation to withstand the mechanical stresses before failing. This represents the tough behavior. Finally, the mechanical behavior of a toughened elastomer is observed at high contents of rubber (III). It has the ability to undergo deformations up to 100%, as for SBR and other elastomers such as the styrene-butadiene-styrene block copolymer rubber family (SBS) [83].

Brittle and tough behaviors can also be distinguished by means of the energy absorbed by the material before fracture. This latter can be determined via two different methods. First, the resistance to fracture or toughness may be related to the entire area beneath the stress-strain curve from the origin

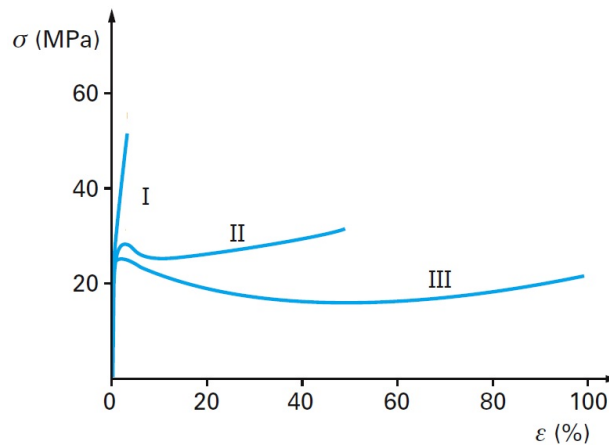


Figure 3.1 – Example of typical stress-strain curves for standard polystyrene (I), HIPS (II) and SBS block copolymers (III) at ambient temperature. Figure reproduced and modified from Heim (2002) [51].

to rupture. Thus, the energy absorbed per unit volume is designed as modulus of toughness (units of J/m^3).

Second, Charpy or Izod impact tests lead to a direct measurement of the energy required to promote material failure. Testing consists in striking at high speed a standard bar-shaped specimen with a heavy pendulum swing. The energy dissipated is transformed in terms of impact resistance or strength (units of J/m^2). Recently, instrumented pendulums lead to following the evolution of the load applied during the impact. Similarly to stress-strain curves, their shape is also representative of the material behavior.

3.2.2 Main parameters influencing toughness in thermoplastic composites based on GTR

In preparing thermoplastic composites with GTR, numerous factors play an important role in modifying all the linear (low strain) and nonlinear (high strain) mechanical properties [3, 81, 82]. These parameters can be grouped in two categories: intrinsic and extrinsic, as shown in Figure 3.2. On the one hand, intrinsic parameters are related to the physico-chemical characteristics of each of the individual phases. Extrinsic parameters, on the other hand, are related to the formulation and processing. In what follows, the way each of these parameters influences the properties is briefly highlighted. However, it is appropriate to clarify that such a list is not exhaustive of all the possible factors.

3.2.2.1 GTR particle size and size distribution

The average primary particle size and size distribution of the rubber particles are crucial parameters in controlling the reinforcing effect in polymer composites. For instance, the industry implements fillers with size ranges varying from the nano-size to the micron order, because these render better results in improving mechanical properties [3, 10].

It has been reported that, in order to increase impact resistance of rubber-toughened polymers, the size of the rubber particles should be limited to a narrow range [84, 85]. For example, Figure 3.3 illustrates the size range (delimited by points b and d) in which the maximum of toughness is achieved for a specific rubber-toughened nylon 6 (RTPA6) and where the optimum or critical size (c) is about $0.5 \mu\text{m}$ [84–86]. According to Bucknall and Paul 2009 [84], such a range for effective toughening exists for many rubber-toughened blends and the optimum seems to be about $0.3 \mu\text{m}$. In an extended work, Wu [87] demonstrated that in toughening nylon, the optimum size of the particles shifts to larger diameters

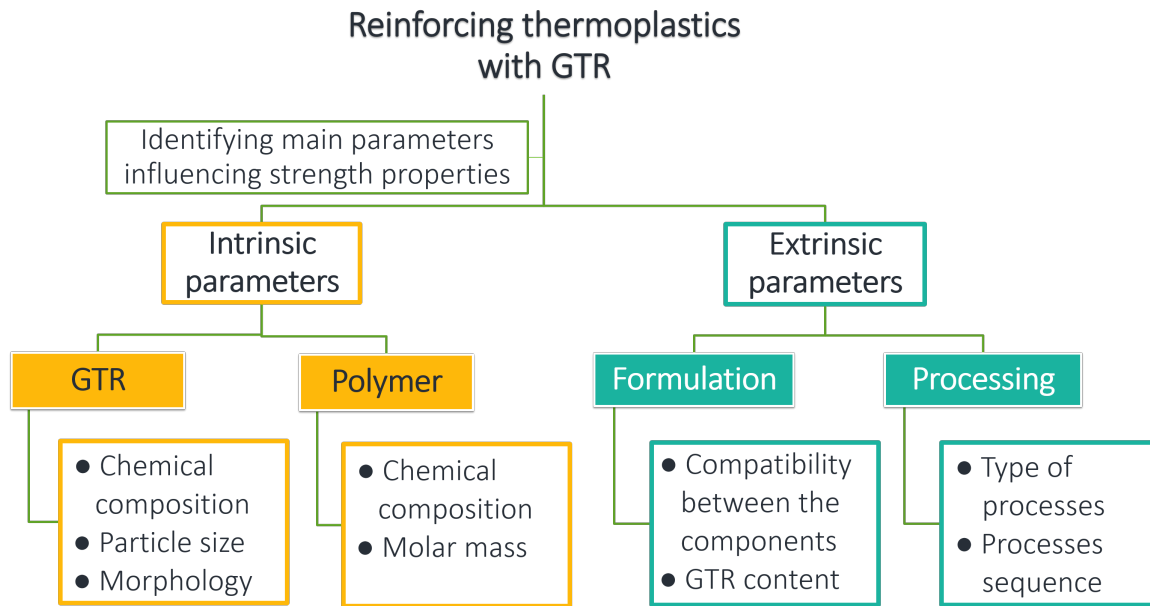


Figure 3.2 – Main parameters influencing toughness in thermoplastic composites reinforced with GTR.

when increasing the rubber content.

As regards toughened polystyrene, it has been reported that effective toughening can be reached by the addition of a monomodal distribution of rubber particles with mean size lying between $1\ \mu\text{m}$ and $3\ \mu\text{m}$ [54, 87, 88]. Moreover, Okamoto et al. (1991) [89], stated that impact toughness of polystyrene can be also increased when using a bimodal distribution of large and sub-micrometer particles, and the extent of the improvement depends on the size difference between the bimodal particles. For example, the notched Izod impact strength of HIPS (8,5 wt% of rubber), containing equivalent fractions of bimodal rubber particles of mean size of $1\ \mu\text{m}/4.9\ \mu\text{m}$, was increased in about 50% when using a bimodal system with a mean size of $0.2\ \mu\text{m}/4.9\ \mu\text{m}$ (at equivalent mass fraction).

In this context, GTR particles should be reduced to a few microns in size in order to obtain improved toughness levels in thermoplastics. Nevertheless, this is difficult to achieve by the conventional grinding techniques and therefore, most of the studies reported in the literature use crumbs with a minimum size of about $200\ \mu\text{m}$. For example, Ismail et al. [40], blended PP with waste tire granulates of different sizes ($250\text{-}500\ \mu\text{m}$, $500\text{-}700\ \mu\text{m}$, and $710\ \mu\text{m}\text{-}1\ \text{mm}$). From the set of blends, those with finer particles exhibited slightly improved tensile properties, in particular elongation at break. In a similar way, Colomb et al. [90] and Mujal-Rosas et al. [91], reported that when adding reused tire powders of size $<200\ \mu\text{m}$ to recycled high-impact polyethylene (HDPE) or ethylene vinyl acetate (EVA), respectively, the Young's modulus of the host polymers increased. Tantayon and Juikham observed that the impact strength of polypropylene increased until 20% when adding GTR particles of $420\ \mu\text{m}$ in size [92].

These results and additional literature on GTR toughened thermoplastics, suggest that the reinforcing effects of GTR can be observed when using particle sizes below $500\ \mu\text{m}$. Beyond that, the properties deteriorate drastically and continuously with increasing GTR size [37, 40, 90, 91].

Until recently, there have been no studies reporting the utilization of GTR particles having very narrow particle size distributions, around 3 to $5\ \mu\text{m}$, for polystyrene reinforcement. In fact, due to the elastic nature of GTR, the reduction of the particle size to a few micrometers became difficult and expensive.

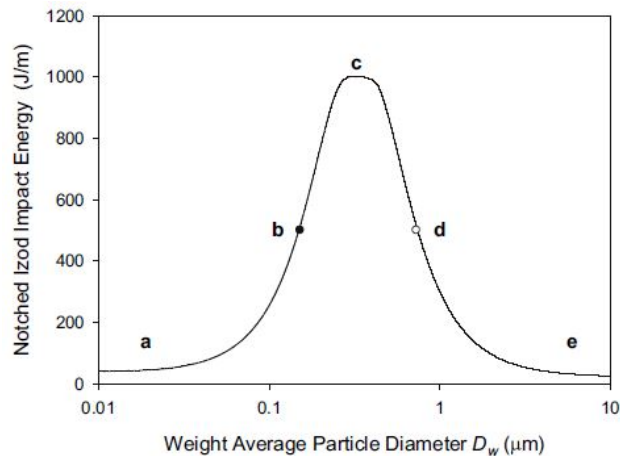


Figure 3.3 – Optimum particle size range for effective increase of Izod impact strength of a specific sample of nylon 6 with ethylene-containing rubber. Schematic representation and data from Bucknall and Paul 2009 [84, 86].

3.2.2.2 GTR morphology and surface

The morphology as well as the surface quality of reinforcing fillers influence the processing and targeted properties of thermoplastic composites [3, 93, 94]. With respect to the preferred morphology of the particles for enhancing the impact properties, asymmetric fillers having a medium to high aspect ratio (ratio of the longest dimension to the smallest one) such as fibers and flakes, are selected. In fact, high aspect ratio values (i.e. >20) and rough surfaces imply a larger contact area with the polymer, which allows better absorption and transfer through the material of the energy dissipated during the impact events [3].

According to Wiebking 1998 [94], variations in the aspect ratio have an influence on the tensile modulus rather than the impact strength, which is a function of the particle size instead. The morphology of the GTR crumbs varies considerably according to the source and the grinding processes. In general, GTR is obtained as irregular shaped particles with an average aspect ratio varying between 4 and 7 approximately [95]. However, the influence of the geometry of GTR particles in increasing the mechanical properties of thermoplastics has not been thoroughly addressed in the literature.

3.2.2.3 Molecular weight of the polymer matrix

The molecular weight (MW) is known to influence the impact resistance of pure polymers [83]. For instance, Cook et al. [96], reported data of notched Charpy impact strength of several commercial polystyrene samples having different MW , as shown in Figure 3.4 [96]. The reported values indicate that impact resistance in polystyrene increases exponentially with MW . Then, impact properties seem to drastically deteriorate at the weight average MW values below $2.1\text{E}+05$ g/mol. In a similar way, it is expected that MW will also affect the mechanical properties of polymer composites. However, in reinforcing thermoplastics with GTR, far too little attention has been paid to the influence of the polymer MW .

3.2.2.4 GTR content

As mentioned in Chapter 1, the integration of GTR in thermoplastics leads to a degradation of all their physical-chemical and mechanical properties [82]. The negative effects, which are magnified with increasing the amount of rubber, have been mainly attributed to the poor interfacial adhesion of their physical blend. For instance, some published studies reported the addition of amounts of GTR ranging

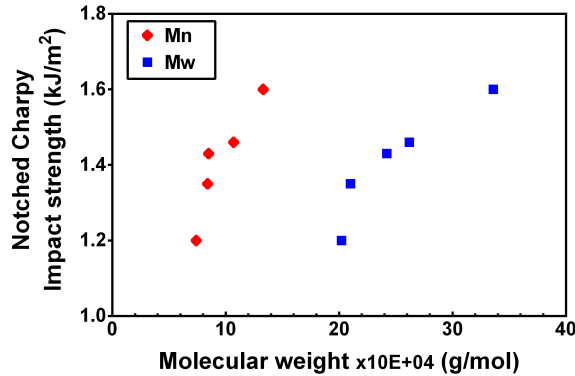


Figure 3.4 – Notched Charpy impact strength of different commercial polystyrenes measured by Cook and Rudin 1990 [96]. Testing speed 1.0 m/s, notch deep 0.5 mm and specimen size of 75x12x6.2 mm.

from 1 to 70 wt% to reinforce polymers such as recycled and fresh HDPE, LDPE, EVA [37, 90, 92]. In all cases, the tensile strength, elongation at break and toughness (calculated as the area beneath the stress-strain curves) were drastically decreased even at the lowest rubber contents. Besides, when using polyolefins such as PP, a similar effect as the one described for PE and EVA is observed, except for the strain at break which can be increased in about 20% [40].

Nonetheless, when GTR particles are bonded to the polymer matrix (e.g. by grafting), the reinforcing effects become obvious. Therefore, the following are examples of the influence of the GTR content on blends, prepared using some of the existing compatibilization techniques mentioned in section 1.4.3. Tantayanon and Juikham [92], toughened PP with different amounts of devulcanized GTR varying from 20 to 40 parts by weight (pbw). The blends were compatibilized by dynamic vulcanization by using sulfur and other cross-linking agents. Their results suggested that there is an optimum of rubber content equivalent to 30 pbw at which the notched Izod impact strength is maximized up to 20%. In comparison, only a marginal increase in the ultimate strength is reported for the non-compatibilized blends.

Zhang et al. [45] prepared a series of blends of GTR/PS with and without PS-g-SBR compatibilizer, at different amounts of GTR (5 to 30 wt%). The reported data showed that in both types of blends, the tensile strength diminished continuously with increasing rubber content. By contrast, impact strength increased and reached the highest value at 20 wt% of rubber for both blends, and then it decreased again. Colomb et al. [44] oxidized the surface of GTR with various chemical acids and used it as reinforcement material in recycled HDPE. Acid treatment led to an increase in the interactions between both components, and the Young's modulus of fresh HDPE was increased until 73%, when incorporating 40 wt% of recycled rubber particles.

3.2.2.5 Sequence of the processes

Fabrication of filled thermoplastics involves two steps: mixing and processing. In some cases, polymerization is also performed [70]. According to the moment at which the filler is integrated, two different cases are distinguished:

- 1st case: the reinforcing particles are added to the monomer solution and the polymerization is performed in-situ in a reactor. If the monomer conversion is incomplete, the residual monomer can be subsequently removed or post-polymerized in a second step.
- 2nd case: the polymer (synthesized previously) is heated until the molten state and the particulate-filler is added.

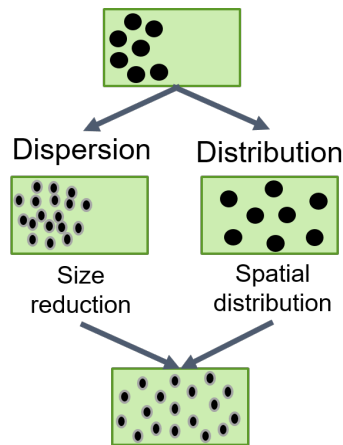


Figure 3.5 – Dispersion and distribution mixing types of particles in polymers. Figure reproduced from Manas-Zloczower, (2009) [3]

In both cases, the product is mixed to obtain a homogeneous and well integrated material, which is later transformed by a fabrication step or shaping via thermal processes, to give it its final shape.

3.2.2.6 Effect of the type of mixing

Reinforcing particles are introduced and dispersed into the polymeric medium by means of mixing processes involving different types of equipment and mixing configurations [3]. These control the microstructure, which is also crucial as it influences the mechanical behavior of the final material [3, 82]. The microstructure of the composite is defined by the degree of dispersion and distribution of the particles in the volume, which are achieved by different but complementary mixing mechanisms, dispersive and distributive respectively, as illustrated in Figure 3.5 [3].

According to the nature and characteristics of the components, one type of mixing configuration should be preferred [3, 97]. Thus, dispersive mixing consists in breaking up the agglomerates of particles that present strong cohesive forces (e.g. carbon black, talc). By contrast, distributive mixing is operative to distribute uniformly the free flowing particles (low cohesive character) or the agglomerates in the volume of the material. The appropriate combination of both types of mixing leads to achieve a uniform microstructure [3].

Whereas recycled rubber particles as GTR exhibit low interactions between particles at the micrometric size, the cohesive forces become more relevant when decreasing towards the sub-micrometer domains [84, 85]. In addition, the reduction of size increases the specific surface allowing the exposure of the carbon black nanoparticles contained in the GTR backbone, which tend to agglomerate under the effect of various cohesive forces (i.e. electrostatic, Van der Waals, capillary bridges, etc.) [71, 98]. When the dispersed phase forms clusters or agglomerates, these can be broken down and gradually dispersed by the application of high shear forces, stronger than the cohesive ones, to the flowing material during mixing [3]. Nevertheless, with respect to GTR, little is known about the parameters influencing GTR dispersion and distribution in polymeric melts to obtain a high dispersion quality.

Different types of mixing equipment have been used in published studies for the addition of GTR (dispersion and distribution) in thermoplastics. Some of the most common devices include two-roll mills, batch mixers and twin-screw extruders [11], from which the latter has the advantage of operating continuously and thus, at a lower cost. Twin-screw extruders are constituted of two counter- or co-rotating screws inside a temperature-regulated metal barrel, through which the filled polymer is transported, melted and mixed [3, 97]. A more detailed description about extruders use and configu-

ration is described later in this chapter.

3.2.2.7 State of dispersion

The state of dispersion of the particulate-fillers in polymeric materials is of paramount importance for ultimate tensile and strength properties. The presence of structural inclusions and inhomogeneities in the composite matrix, such as agglomerates and voids, act respectively as stress concentrators during mechanical tests. Large inclusions accumulate more stress, which detract the reinforcement effects. For example, the tensile and unnotched impact strength are strongly affected by the agglomerates since they initiate sample failure because of the high stresses developed around them during deformation [3, 99, 100].

By contrast, notched Izod impact strength seems to be less sensitive to the presence of agglomerates, at a reasonably good dispersion degree. In fact, the sharp notch in impact specimens concentrates larger stresses than inclusions and thus, the failure initiate right at the collision point of the weight [3, 83, 99]. Wang and Huang (1996) [100], demonstrated that notched impact strength was improved until 13% as the degree of dispersion of calcium carbonate agglomerates increased by 11% by using different configurations in a single-screw extruder.

This brief synopsis brings to light that interfacial adhesion is not the only parameter that dictates toughness in particulate-filled polymer composites. However, so far the interfacial adhesion issue has concentrated the attention of most of the cases. Table 3.1 consolidates all the parameters mentioned above, and indicates the manner in which they tend to improve and or decrease toughness of thermo-plastic composites reinforced with GTR.

Table 3.1 – Intrinsic and extrinsic parameters and their influence on toughness of composites based on GTR and thermoplastics.

Intrinsic parameters	How does this parameter improve toughness?	How does this parameter decrease toughness?	Ref.
GTR			
Particle size distribution	Mean size between 1 and 5 μm \rightarrow resist to multiple crazing	Mean size > 500 μm \rightarrow crazing predominates	[88][87][92] [37][90]
	Presence of monomodal micrometer particles	Presence of large particles	[54][84]
	Bimodal system of sub-micrometer and micrometer particles (e.g. 0,2 to 5 μm)		[85][89]
Particle morphology	Irregular shape: rough and irregular surfaces \rightarrow high specific area and volume	Regular shape: smooth and edgy surfaces \rightarrow low specific area	[10][93]
Treated surface	Devulcanized \rightarrow sol fraction increases miscibility		[92]
Porosity	High porosity \rightarrow high polymer interpenetration	Low porosity \rightarrow low polymer interpenetration	[3]
Polymer			
Chemical composition	High chemical reactivity \rightarrow favor interactions and grafting on the filler backbone		[50][10]
Molar mass	High molecular weight	Low molecular weight	[83][96]
Extrinsic parameters			
Formulation			
GTR load	Weight fractions of about 20 to 40%		[3][97]
Interfacial adhesion	Chemically bonded interfaces	No bonded interfaces	[92][55]
Processing			
Sequence of the processes	Compatibilization and mixing at the same time Compatibilization and subsequent mixing		[92],[55]
Type of mixing	Good degree of dispersion	Presence of large structural inclusions (agglomerates, voids, etc.)	[99][100]
	Homogeneous distribution	Inhomogeneous distribution	[3]

3.3 A novel methodology to prepare polystyrene composites based on GTR with improved mechanical properties

The conception of materials with targeted properties can be studied by using the approach of chemical products design [101]. Since the main goal is to reinforce polystyrene by introducing recycled rubber particles as GTR in order to obtain a high-resistance polystyrene, the question is therefore: how to recreate a material offering good impact resistance? In order to address this question, on the one hand, the specifications sought for the final product have been established. On the other hand, a novel methodology for the preparation of such toughened polystyrene is proposed and applied.

3.3.1 Product specifications

The desirable impact properties of the final composite should be comparable or superior to those of commercial HIPS. Table 3.2 presents some value ranges of the mechanical properties of interest for GPPS (unreinforced) and high impact polystyrene (butadiene-rubber reinforced). These data are used just to give orders of magnitude of the differences between both materials and cannot be interpreted as absolute values, since they vary with testing speed and formulation (e.g. polymer molecular weight, rubber loading, etc.). The addition of the butadiene-rubber phase to the polystyrene rigid matrix, improves the notched Charpy impact strength (IS) more than twice, and ϵ_r until 65 %. By contrast, E and σ_r are deteriorated.

Table 3.2 – Comparison of the mechanical properties of GPPS and HIPS. The values of the properties were extracted from the database published by Biron (2014) [53].

Property	GPPS	HIPS	Standard
Tensile strength at break (MPa)	40 - 60	20 - 50	ISO 527
Elongation at break (%)	1 - 4	20 - 65	ISO 527
Tensile Modulus (GPa)	3 - 3.4	2 - 2.5	ISO 527
Notched Charpy impact strength (kJ/m^2)	2	3 - 12	ISO 179

In addition to the mechanical properties sought for the product, this latter should aim to fulfill additional requirements or “needs”. These have been defined to confer supplementary characteristics to the product, in order to differentiate it from compounds reported in published literature. These needs are classed as essential and useful. In this work, the essential needs cover the critical aspects giving the added value to the product, and the useful ones are beneficial if achieved. The design of the composite material should meet three essential and two useful needs. The essential needs are:

- Polystyrene composites must contain high percentages of GTR (≥ 30 wt%) in the purpose of maximizing GTR recycling. This helps to reduce GTR wastes, thereby having a positive impact on the environment.
- GTR should be used as-received without further purification with organic solvents, first, to avoid the generation of chemical wastes and second, to reduce the production costs.
- GTR should be used as-received without additional grinding for size reduction, since this stage requires expensive processes (cryogenic grinding) and sophisticated equipment.

The two useful needs are:

- The final material can be easily processed by thermoforming.
- The finished product can be recycled and reprocessed several times without any substantial change of the initial properties.

Table 3.3 – Product specifications for the preparation of GTR-reinforced polystyrene composites

TECHNICAL PERFORMANCE	
Finished product	<p>Formulation: Materials with high GTR contents ≥ 30 wt% and ready to use.</p> <p>Preparation: Easy processing by thermoforming.</p>
Product performance in service	<p>Mechanical properties: Impact strength: 2 times higher than unreinforced PS. Comparable with commercial HIPS.</p> <p>Recycling: Easy to grind and reprocessed several times by extrusion and injection molding without decreasing the initial mechanical properties.</p>
SAFETY AND ENVIRONMENTAL REQUIREMENTS	
Protection of the user	<ul style="list-style-type: none"> ○ Low additive concentration, no aromatic solvents.
Protection of the environment	<ul style="list-style-type: none"> ○ Low wastes from fabrication process.

Table 3.3 consolidates the product specifications.

3.3.2 Proposed methodology for product preparation

In previous research work, Yu 2015 [55] proposed to combine two techniques widely used in polymer composite formulations to reinforce polystyrene by the addition of GTR particles. These techniques consist in grafting polystyrene directly to the GTR backbone and subsequent compounding in a twin-screw extruder. Experimental results demonstrated that the grafted polystyrene led to the formation of rigid PS domains inside the GTR elastic particles, which helped to break them down when compounding at high shear rate and low temperature conditions. This effective process allowed gradually decreasing the mean size of GTR from $350 \mu\text{m}$ to about $90 \mu\text{m}$ under specific operating conditions and composition. In addition, it was demonstrated that when reducing GTR particle size, polystyrene impact strength was effectively increased.

The present work, in addition to the contributions of the previous research [55], proposes a methodology to prepare particulate-filled polymer composites based on GTR and polystyrene. This methodology was developed from the qualitative and quantitative study of a set of experiments leading to a better understanding of the whole process: the chemical reaction and all the unit operations involved in the fabrication and transformation of the composite material. The process was redesigned in its entirety since a different set of equipment was implemented in order to produce larger quantities of product. Then, the equipment was characterized and as a consequence, most of the operating conditions were adapted and optimized.

The experimental procedure followed in this work accounts for three main parts, as indicated in Figure 3.6. Each part is developed in a detailed way in the following sections.

3.4 Materials characterization

3.4.1 Ground tire rubber (GTR)

GTR was obtained from two different suppliers, REGENE company from Brazil and DeltaGOM from France. To differentiate between both types of GTR, they will be referenced as **GTR1** and **GTR2** respectively. Both GTR are derived from the recycling of end-of-life tires of different categories (light, heavy goods and agricultural vehicles, motorcycles, etc.). The characteristics are listed in Table 3.4 and an

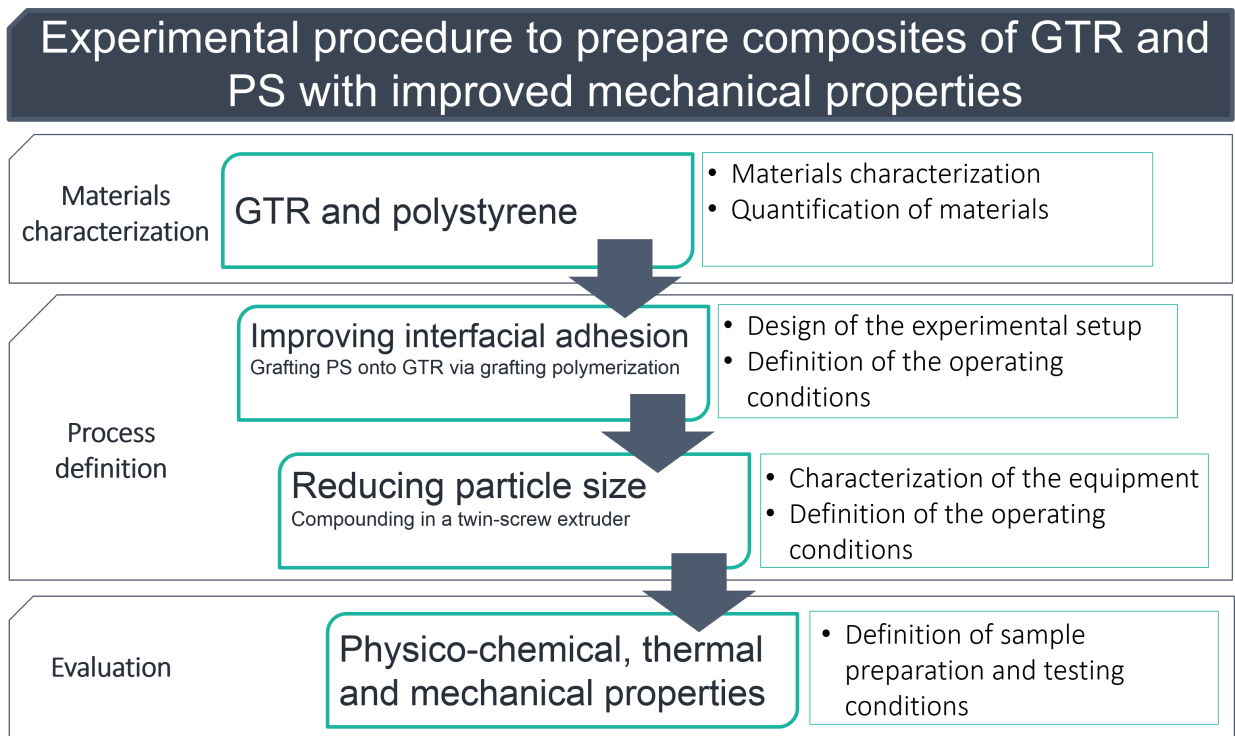


Figure 3.6 – Experimental procedure to prepare blends of GTR and PS with improved mechanical properties.

approximate composition of the constitutive elastomers is presented in Table 3.5.

One interesting characteristic of GTR is its high capacity of styrene absorption. This parameter is crucial defining the methods for samples preparation. The swelling capacity of both types of GTR as well as the absorption rate of styrene monomer are illustrated in Figure 3.7. The measurements were performed in this work (see Sect. 3.8.1.7). Both rubber particles are saturated after about 20 minutes. The absorption capacity of GTR1 and GTR2 is about 2,5 and 2,0 times their initial weight, respectively.

3.4.2 Polystyrene

Commercial general purpose polystyrene used is N1840 from EDISTIR, and the properties provided by the supplier are shown in Table 3.6.

Table 3.4 – Characteristics of the commercial GTR used for polystyrene reinforcement

Reference		GTR1	GTR2
Supplier		REGENE (Brazil)	DeltaGOM (France)
Grinding process*		Cryogenic	Mechanical
Particle diameter (μm)			
minimum	d(0.1)	335	295
mean	d(0.5)	540	580
maximum	d(0.9)	850	925
Real density (g/cc)		1.18 to 1.20	
Apparent density (g/cc)		0.375 to 0.420	

* Grinding process used by the supplier for GTR fabrication

Table 3.5 – Composition of GTR elastomers

Elastomers	Weight fraction approx. (%)
Natural rubber (NR)	30
Styrene-butadiene rubber (SBR)	40
Butadiene rubber (BR)	20
Butyl and nitrile butadiene rubber (IIR and NBR)	10

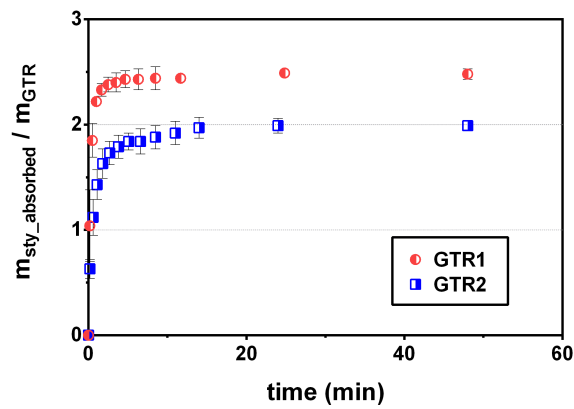


Figure 3.7 – Absorption rate of styrene by both types of GTR.

Table 3.6 – Physical and mechanical properties of GPPS E1840. Values were extracted from the supplier's data sheet.

Material	GPPS	Standard
Physical Properties		
Density	1.05 g/cc	ISO 1183
Melt mass-flow rate* (MFR)	10 g/10 min	ISO 1133
Mechanical Properties		
Tensile strength at break (5mm/min)	39.0 MPa	ISO 527
Elongation at break (5mm/min)	1.8 %	ISO 527
Tensile Modulus (1mm/min)	3.25 GPa	ISO 527
Izod Notched impact strength	1.7 kJ/m ²	ISO 180/1A
Processing properties		
Melt temperature	200 - 250 °C	
Mold temperature	30 - 50 °C	

3.4.3 Reagents

All the reagents used, namely, styrene monomer (with a purity 99.5% and stabilized with 0.005 % of 4-tert-butylcatechol), benzoyl peroxide - BPO (75% remainder water), dicumyl peroxide - DCP (with 98% of active mass), 2,5-dimethyl-2,5-di(tert.butylperoxy)hexane - DHBP (with 90% of active mass), hidroquinone - HQ (with a purity $\geq 99\%$), tetrahydrofurane - THF (anhydrous, $\geq 99\%$), chloroform (anhydrous, $\geq 99\%$) and chloroform-D (99.8b % atom) were purchased from Sigma-Aldrich and used without further purification, unless stated otherwise.

3.5 Process definition

3.5.1 Compatibility improvement by grafting PS onto GTR

The grafting polymerization of polystyrene in the presence of GTR was described in Chapter 1 (c.f. Sect. 1.6.1). Here, the objective is to define optimal conditions to perform the reaction by stimulating both the styrene conversion and formation of grafted polystyrene chains (grafted-PS) rather than free polymer chains (free-PS). This means therefore achieving a grafted-PS/free-PS ratio superior to 1.

With regards to the composition of the polymerization system, this was adopted from the extensive study of the kinetics of the bulk grafting reaction performed in the previous work [55]. Table 3.7 shows the composition and operating conditions proposed for the polymerization of two systems containing a mass ratio GTR/styrene equivalent to 1:1 and 1:1.5. The utilization of a binary initiating system, composed of BPO and DCP, fostered the total monomer conversion up to 80% with a reasonably high grafted-PS/free-PS ratio (St-g/St-f) close to 1, as illustrated in Figure 3.8.

Table 3.7 – Polymerization system composition proposed by Yu 2015 [55].

GTR/Styrene (w/w%)	Initiator (I)	I/styrene (by mole)	Temperature (°C)	Time (h)
1:1	BPO+DCP	BPO(2%)+ DCP(1%)	70	3
			80	3
90			2	
100			2	
1:1.5				

This radical grafting polymerization is usually performed in small glass tubes or reactors to produce only a few grams of product [28, 30, 47, 55]. Yu 2015 [55], implemented a one liter-capacity stainless-steel batch reactor to produce about 0.4 Kg of product per batch. However, the behavior of the system in laboratory scale reactors and process conditions, such as optimum mixing systems to promote homogeneity and heat transfer, was not addressed.

3.5.1.1 Polymerization reactor: building and operating an experimental setup

As part of this research work, an effort was undertaken to design a new experimental set-up to perform the polymerization of styrene in presence of GTR in a laboratory scale reactor. The set-up built consists of a 3L capacity batch reactor to produce quantities of composite ranging from 0.6 to 1.0 Kg/batch.

This section presents the specifications of the polymerization set-up system and the main difficulties encountered during its starting. Additionally, a qualitative and quantitative assessment details the aspects that interfere in the chemical reaction process in terms of unit operations such as mixing and heat transfer.

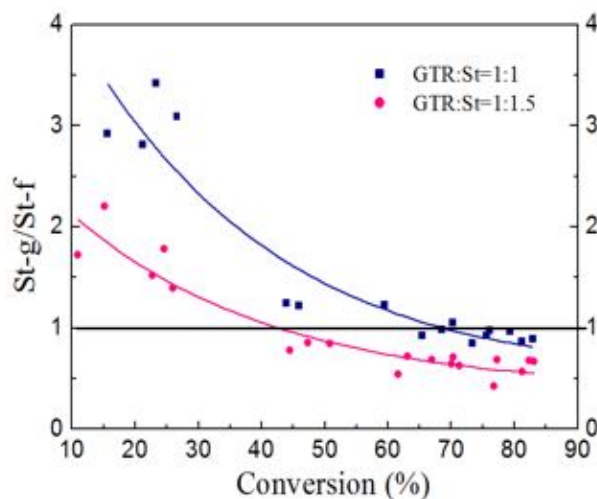


Figure 3.8 – Grafted-PS/free-PS ratio ($St-g/St-f$) as the function of styrene conversion. By using the binary initiator system BPO/DCP the final system conversion is up to 80% and the amounts of free-PS and grafted-PS formed are equivalent (ratio $St-g/St-f = 1$) [55].

Polymerization reactor set-up

Figure 3.9 presents the process diagram of the experimental set-up. It is mainly composed of a polymerization reactor (R-101), a cooling and heating system, and a spraying device (S-101). Detailed specifications of the equipment are presented in Table 3.8.

The benefits of implementing this new setup can be listed and detailed as follows:

- **Shorter time in reacting medium preparation.** As demonstrated before, GTR particles are able to absorb (almost instantaneously) in more than twice their weight in styrene. When preparing mediums containing more than 50% in mass of GTR (e.g. mass ratio GTR/Styrene up to 1), the liquid styrene cannot be directly poured onto the GTR particles since it is difficult to ensure its instantaneous contact with each of the particles. Consequently, styrene repartition inside all the particles is heterogeneous. To overcome this problem and promote homogeneous distribution of the monomer-initiator solution inside the GTR particles, a spraying system was installed. Then, the solution is atomized at low flow with high-pressure air to create a cloud of suspended microdroplets into the reactor, while GTR particles are agitated at high speed. It allows intimate contact particle surface-monomer droplets and therefore, an even repartition throughout the medium. This system is an efficient method to mix both phases.
- **Better monitoring of the reaction.** It involves:
 - Qualitative assessments: visual trailing through the translucent walls of the glass reactor to get information about mixing quality and evolution of the reacting medium appearance over all process stages.
 - Quantitative aspects: following-up of the internal temperature (into the medium and reactor atmosphere) and the mixing torque (τ).
- **Safer handling.** Isolation of the reactor to minimize the emissions of hazardous unreacted products. Protection of the operators from potential accidents, such as projections of chemical products or hot substances, cracking or breakage of glass materials, etc.

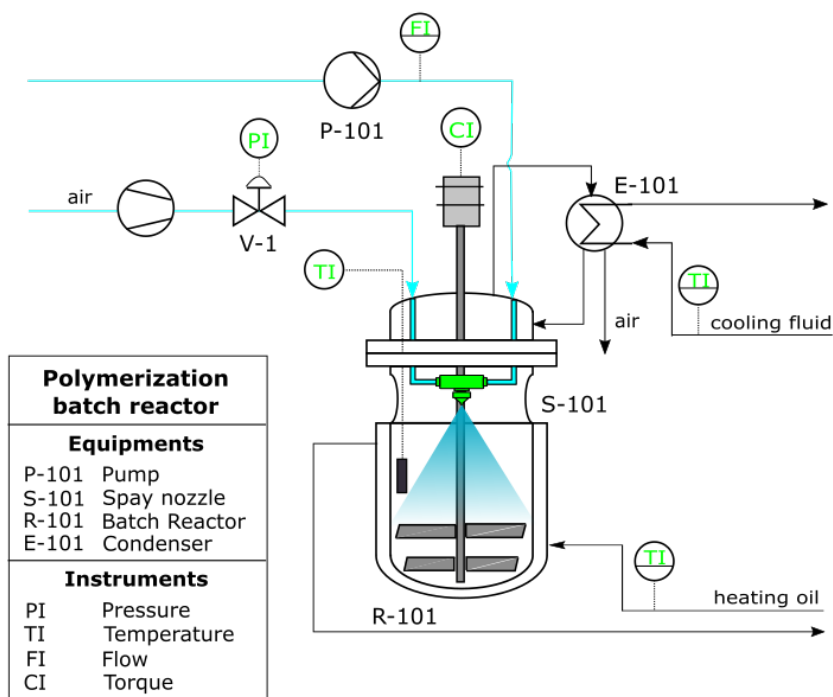


Figure 3.9 – Polymerization reactor set-up.

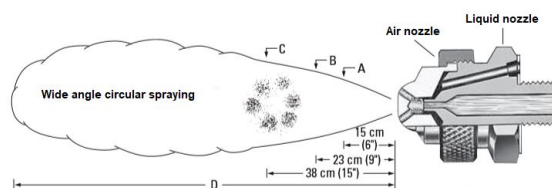


Figure 3.10 – Spraying nozzle for monomer solution atomizing. [102].

Characterization of the polymerization system

A series of runs was realized in order to get information about polymerization performance and define the mixing operating conditions. The polymerizations were performed by using the specifications in Table 3.7, for a system containing 30, 50 and 70 wt% of GTR. Here, the GTR percentage is defined as the weight of GTR present in the total mixture of GTR and styrene. The temperature of the reacting medium was monitored at three different points: next to the wall of the reactor, next to the agitator shaft (i.e. in the center of the reactor) and in the middle of these two points. In addition, variations in the viscosity of the medium were followed up by monitoring the mixing torque. Stirrer configurations used are helical (used in the previous work), helical with anchor, single blade and twin-blade paddles.

The progress of the grafting polymerization is strongly dependent on the composition of the system. A brief description of the medium is presented below. The appearance of the final product is displayed in Figure 3.11.

- The raw particles of GTR are shown in Figure 3.11a. In the system containing 30 wt% of GTR, the excess of monomer remains outside the rubber granulates, creating a continuous liquid phase with the embedded particles. The medium becomes high-viscous and sticky as reaction progress. The final product consists of rubber particles dispersed into a rigid polystyrene matrix (Fig. 3.11b).
- When increasing the GTR content to 50 wt%, most of the monomer polymerizes in the particles

Table 3.8 – Polymerization reactor set-up: equipment and devices specifications

Equipment/device	Specifications
Double jacketed glass reactor (R-101)	Capacity of 3 L and internal diameter of 15 cm. Reactor is fixed to a hand crank system to move it vertically to load and unload the product.
Overhead stirrer motor	Speed range 30-1200 rpm and torque operational range 0-110 Nm.
Cooling system (E-101)	Glass condenser is connected to a thermostatically-controlled bath (ethylene glycol). Temperature range -20 °C to 50 °C .
Heating oil bath circulator	Temperature operating range: 20 to 150 °C .
HPLC pump (P-101)	Pumping speed rate 1 to 1000 rpm.
Compressed air (valve V-1)	Pressure range 0.1 to 7 bars.
Air atomizing spray nozzle (S-101)	Wide angle circular pattern (See details in Figure 3.10). Jet diameters at points A, B, C and D vary according to air and liquid pressure. The configuration of the spraying nozzle implemented (from Spraying systems Co.)

core and a part of the monomer forms a thin layer around the particles, creating a semi-continuous phase. At the end, the rubber granulates are partially adhered by the polymer formed on their surface (Fig. 3.11c).

- At higher GTR content of about 70 wt%, the monomer remains exclusively inside the particles and therefore, the polymerization system is non-continuous. GTR granulates are kept separated until the end of the reaction (Fig. 3.11d).

From the descriptions and measurements raised, two relevant aspects were identified:

1. The viscosity of the medium can undergo drastic variations during the polymerization, principally for systems with high styrene concentration. Figure 3.12 illustrates the fluctuation in the mixing torque of a reaction system containing 50 wt% of GTR, when using the helical-anchor configuration. In this case, the torque increases more than two-fold during polymerization. For medium rich in styrene, mixing torque can attain values up to 120 Nm due to the highly viscous and sticky character of the mix. The permanent agitation of this medium has a negative effect and provokes product heterogeneity. In fact, granulates remains stuck to the reactor walls and accumulate gradually until these are compressed and squeezed, causing inhomogeneous styrene concentration.
2. The distribution of the temperature through the medium is not homogeneous. This leads to gradients of about 15 °C in the extreme cases, between the wall and center of the reactor as shown in Figure 3.13. The temperature differences are almost insignificant when the medium is continuous and by contrast, the non-continuous mediums display the highest temperature differences.

The difficulties encountered in inhomogeneous temperature distribution were attributed to the following factors:

- Low thermal conductivity of the components.

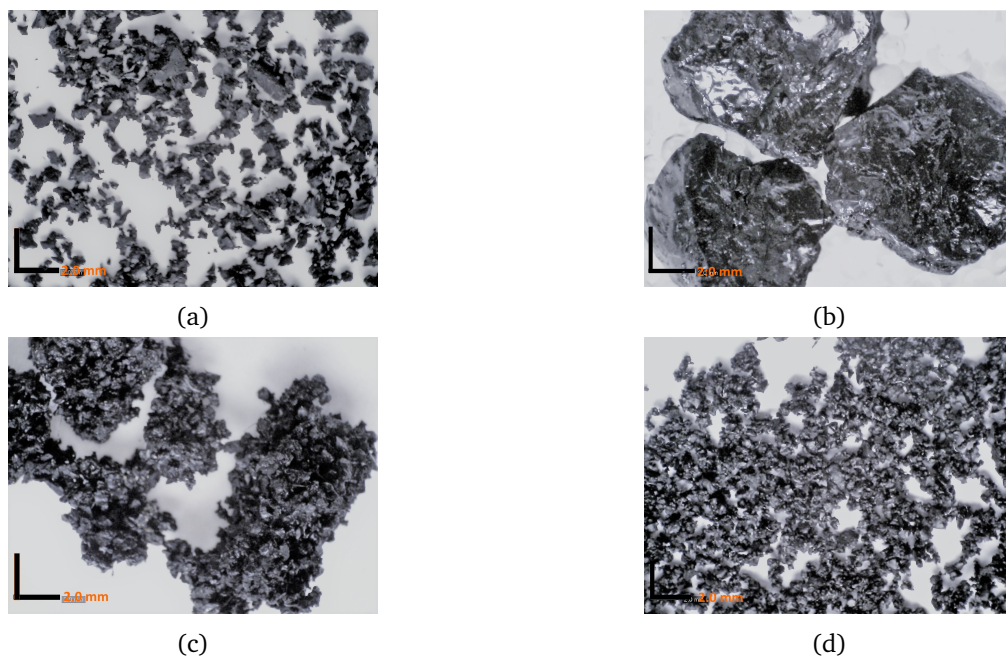


Figure 3.11 – Appearance of the raw GTR (a) and the product after grafting PS in the medium containing (b) 30, (c) 50 and (d) 70 wt% of GTR.

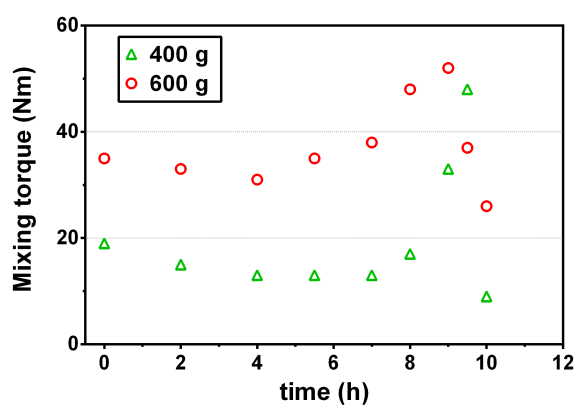


Figure 3.12 – Following the mixing torque during styrene polymerization in a batch reactor for system containing 50 wt% of GTR. Drastic torque increase is due to a high increase of the medium viscosity, when the rate of polystyrene formation accelerates. The mix styrene+polystyrene+GTR becomes highly sticky.

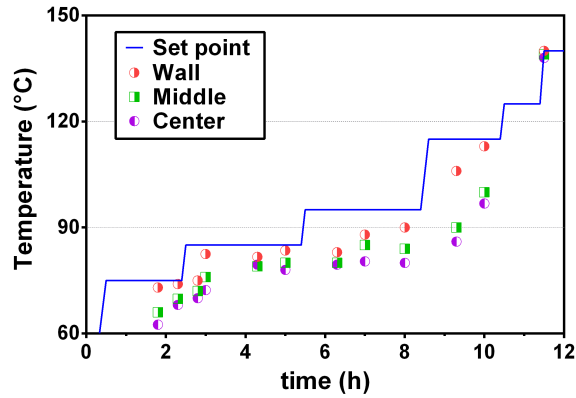


Figure 3.13 – Measurement of the temperature distribution through the batch reactor during styrene polymerization in a system containing 50 wt% of GTR.

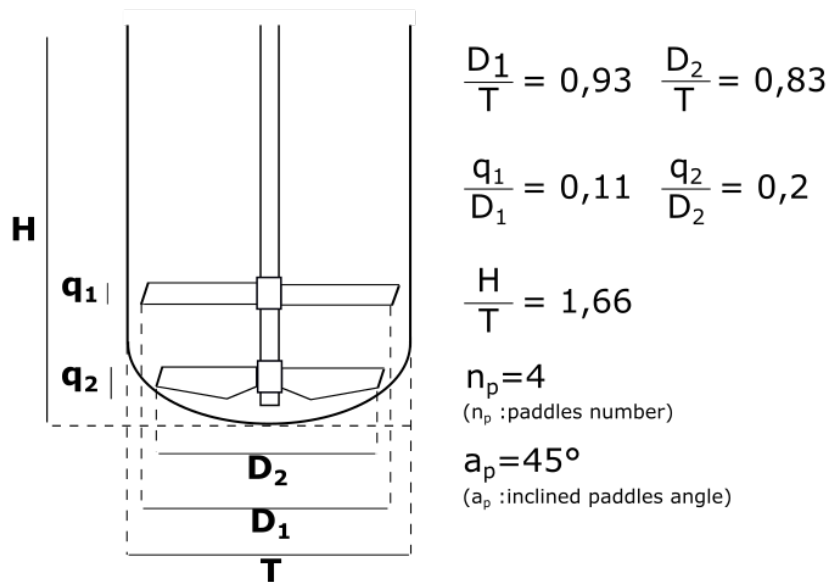


Figure 3.14 – Scheme of the system reactor-stirrer

- Presence of semi-continuous and non-continuous phases in the reacting medium.
- Inefficient mixing and limited heat transfer through the reacting medium.
- Insufficient reactor thermal insulation.

Temperature distribution and product homogeneity issues were overcome by adjusting the polymerization temperature profile and stirrer configuration, whose specifications are shown in Figure 3.14. The stirrer, an impeller with twin 45° pitched-blades was chosen to ensure the homogeneous mixing during polymerization. It creates a radial and axial movement of the medium. The optimum stirrer dimensions are closer to those of the reactor diameter, to scrape off the walls and permanently renew the layer formed on it. This configuration promotes a better heat transfer from the heating fluid through the reactor walls. Some additional advantages of the stirrer are:

- Limitation in the formation of dead zones at the bottom and next to the walls,
- prevention of the adhesion and accumulation of particles on the reactor walls, and
- homogeneous mixing of the reacting medium on the range of compositions studied.

3.5.2 Reducing particle size by compounding in a twin-screw extruder

The next stage, after the compatibilization of GTR with polystyrene via grafting polymerization in the batch reactor, consists in compounding the product taken from the stirred reactor in a twin-screw extruder. In addition to the improved interfacial adhesion by the polystyrene grafts, the polystyrene formed inside the elastic rubber particles confers a brittle character that helps them break down through mechanical treatments, which are otherwise inefficient for breaking raw GTR.

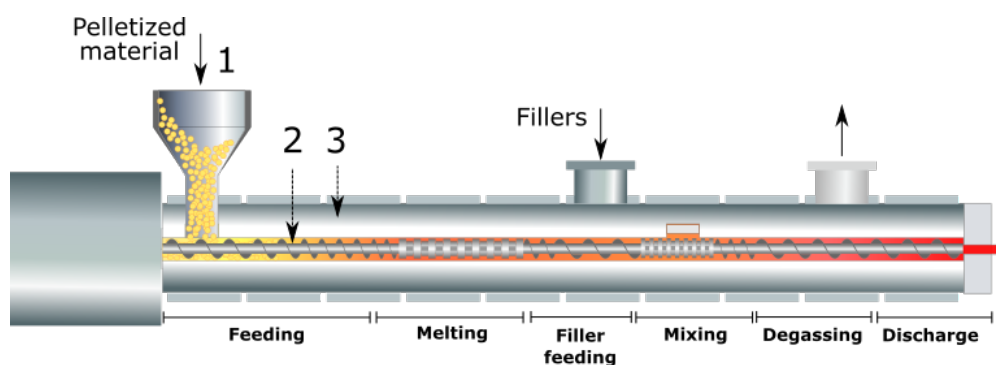


Figure 3.15 – Processing zones in a twin-screw extruder

Compounding is commonly used to combine polymer resins with different classes of additives, to improve the aesthetic and technical properties at reasonable prices [3]. For example, an application of compounding in extruders consists in dispersing high aspect ratio fibers (glass, carbon, lignin, etc.) in thermoplastic matrices to increase their impact resistance [3, 103]. In this particular case, special attention is paid to the compounding conditions due to the possibility of fiber attrition and thus, deterioration of their reinforcing capacity.

Paradoxically, the undesirable effect of fibers breakage will be used in this work as the strategy to reduce the size of GTR particles to a few tens of microns, preferably to a few microns, e.g. 3 to 5 μm , according to values reported in Table 3.1. This application results unusual for compounding in extruders and little is known about the operating conditions that maximizes attrition of particles of rubbery nature.

3.5.2.1 Intermeshing co-rotating twin-screw extruder

The modular intermeshing co-rotating twin-screw extruder is the most important machine used for continuous processing in thermoplastic industry [104]. This equipment consists in two screws rotating in the same direction. Each screw possesses a geometry or profile that can be modified according to the envisaged application thanks to the different modular elements. Finally, both screws are intermeshed and the elements wipe each other to clean [3, 104].

Figure 3.15 is a side view of the internal configuration of a twin-screw extruder. The polymer pellets are introduced in the hopper (1). By the action of a motor driver, the screws (2) rotate in a temperature-controlled barrel (3) with several heaters. Compounding in extruders consists of a series of zones that accomplish specific unit operations, including feeding, melting, mixing (dispersive and distributive), possible reaction, devolatilization and discharge [3, 103]. At the end of the extruder, the material is pushed through a die (4) of defined cross-section geometry and dimensions. In the following, the zones are briefly described.

- **Feeding zone.** The solid granulates of polymer are introduced in the feed hopper and transported forward by conveying elements (Fig. 3.16a). The barrel is cooled to avoid product adhesion and

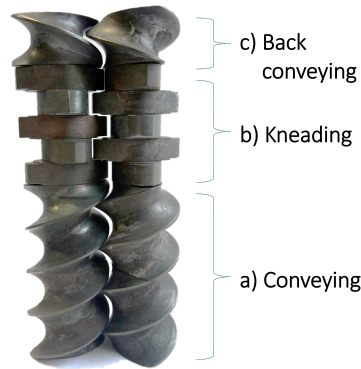


Figure 3.16 – Intermeshed screw elements: (a) conveying, (b) kneading elements staggered at 90° and (c) back conveying or forward pumping elements.

thus, reduce the flow resistance against the fed material. Feeding conditions are fixed in such a way as to promote high filling rates and material compression in the transition towards the melting zone [3, 103, 104].

- **Melting zone.** The solid polymer undergoes a phase change to the molten state. Melting process starts by the formation of a polymer melt film on the barrel wall. This film is essential since it helps to create the shear gradient between the wall and the screw shafts [3]. As polymer moves forward, the melt film thickens. At the end of the zone, complete melting can be achieved or not. Zone configuration typically includes conveying elements and narrow kneading elements to accelerate melting (Fig. 3.16b)
- **Mixing.** Consists in the homogenization of the melt. When combining polymers such a polystyrene with fillers such as GTR, blocks of kneading elements are integrated to impart both distributive and dispersive mixing. Fibers or particulate fillers are added to the molten polymer before the mixing zones. The intensity of the mixing can be managed by varying the elements geometry, dimensions and stagger angle between them (30, 45, 60 or 90°) [105]. Restrictive conveying elements with reverse helix (Fig. 3.16c) are placed to at the end of the zone to restrict material flow and thus, increase the filling degree and residence time.

Depending on the characteristics of the material to be compounded, a series of mixing tasks are required. Each task combines several elements that define the screw configuration. In addition to the screw profile, the series of setting and process parameters listed in Table 3.9 need to be considered when setting up the compounding line [3, 103–105].

Table 3.9 – Setting and process parameters identified in the compounding process.

Setting parameters	Process parameters
• Feeding rate	• Torque
• Screw speed	• Temperature profile
• Die geometry	• Pressure/filling degree profile
• Barrel heating	• Dispersion/mixing quality
	• Residence time distribution

3.5.2.2 Influence of the compounding conditions on the diminution of the particle size

The screw profile implemented in the previous research, for compounding the product obtained from the grafting polymerization, i.e., GTR-grafted-PS+free-PS, is displayed in Figure 3.17 [55]. The configuration has four blocks of kneading discs with a stagger angle of 90 between successive elements,

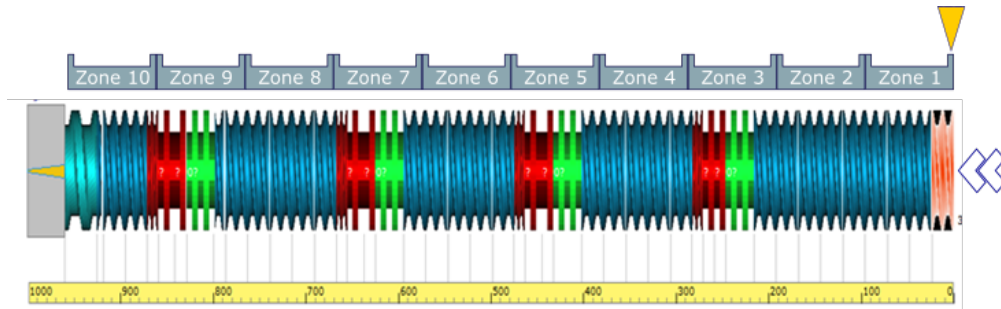


Figure 3.17 – Screw profile used for compounding in the previous research [55]

Table 3.10 – Compounding conditions implemented by Yu 2015. Constant screw speed at 200 rpm. [55]

Extrusion	Barrel zone number and temperature (°C)										Torque (Nm)
	1	2	3	4	5	6	7	8	9	10	
1	20	20	125	125	125	140	140	155	160	165	130
2	20	20	110	110	115	125	130	140	160	165	140
3	20	20	100	100	105	105	130	130	160	165	155

whose role is to impart both dispersive and distributive mixing.

In order to maximize the breakage of the GTR-grafted-PS particles by the action of high-shear forces, the extruder was operated at its maximum torque capacity (140 Nm). It was assumed that to fulfill this condition, the extruded should be performed at low temperatures, close to the polymer T_g (e.g., 90 to 100 °C) and high screw speed. The material was extruded three times at the operating conditions specified in Table 3.10.

The mean size of the GTR-grafted-PS particles was measured after each extrusion. The results reported suggested that compounding in the twin-screw extruder was successful to break the particles down, and the size reduction progressed with the number of extrusions. For example, Figure 3.18 shows that the mean size of the GTR-grafted-PS particles can be gradually reduced during 1, 2 and 3 extrusions by applying the operating conditions above. The grafting polymerization product (GTR-g-PS) was ground by cryogenic grinding before extrusion.

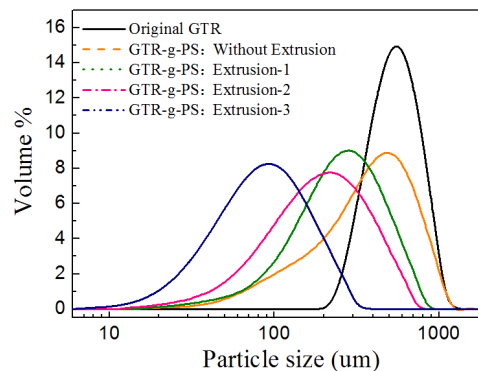


Figure 3.18 – Gradual diminution of the size of GTR-g-PS particles after several extrusions. The particle size of the GTR-g-PS particles taken from the batch reactor was reduced by cryogenic grinding before the first extrusion (c.f. GTR-g-PS: Without extrusion). Results from the previous research [55].

Table 3.11 – *Technical specifications of the twin-screw extruder implemented in this work.*

Parameter	Value
Screw diameter D (mm)	24
Screw length	40xD
Maximum torque (Nm)	140
Maximum operating temperature (°C)	400
Maximum operating pressure (bar)	100
Feeding (kg/h)	0.5 to 5

3.5.2.3 Setting up the compounding line

To continue the research of the previous work, the purpose of equipment characterization was to optimize the compounding stages to achieve smaller size domains (i.e. 3 to 5 μm). The choice of the screw configuration and extrusion conditions were based by considering the following assumptions:

- **Screw configuration:** Breakage effect can be boosted if instead of having several short mixing zones on the screw, these are arranged successively in order to create a unique large block accomplishing the whole mixing tasks. The concentration of the shear rates imparted by all the elements could create a synergy and intensify the shear stresses and particle-particle friction.
- **Barrel temperature:** Lower working temperatures, ranging between 90 and 100 °C , were applied for all the extrusion stages. Under these conditions, polystyrene is in the transition zone between the solid and high viscous state. Then, the shear forces generated by the kneading elements can break down the GTR particles easily. In addition, higher particle-particle interactions are expected since both components are at the solid phase, mainly at the feeding barrel where temperatures are more than 10 °C below.
- **Feeding rate:** The bulk density of the material varies with the GTR content. For a constant feed rate, the filling degree of the extruder increases along with the GTR loading. Therefore, at high filling rate the material is more compressed in the mixing zones, which in turns leads to higher thermal dissipation and mixing torque.
- **Number of extrusion stages:** A first extrusion passage at high temperatures, about 200 °C , was implemented to complete the polymerization of the remaining styrene present in the product from the grafting stage. Subsequently, this material is extruded several times at lower temperatures at the conditions of the items mentioned here above.

3.5.2.4 Characterization of the equipment

Technical specifications

- **Extruder.** Compounding is performed in a pilot scale modular intermeshing co-rotating twin-screw Thermo Scientific HAAKE Rheomex PTW24. The barrel has 10 independent temperature controlled sections. The technical specifications of the equipment are listed in the Table 3.11. The extrusion die at the discharge zone has a circular section of diameter ($d=8$ mm).
- **Feeders.** Material feeding is performed by using a twin-screw volumetric feeder K-TRON. The rotating screws gently transport the material at a constant speed towards the hopper of the extruder. Maximum feeding rate is 5 kg/h. For lateral GTR feeding, a second twin-screw feeder of 1 kg/h feeding rate is connected directly to the extruder barrel.
- **Grinder.** The extruded material is ground in a cutting mill machine SM 300 Restch with grinding speed range of 700 to 3000 rpm, and size mesh of 0.8 x 0.8 mm.

Definition of the compounding conditions

Due to their enhanced mixing effects and shear rates, the selected configuration of the kneading blocks consist of narrow discs (see Fig. 3.16b) with staggered angle at 90. By increasing the number of elements in the kneading zone, it is possible to achieve higher extrusion torque. Preliminary compounding tests to prepare blends of raw GTR and commercial polystyrene (50/50 wt%) were carried out by using the screw profile shown in Figure 3.19. This configuration has two mixing zones: one short (7 elements) to accelerate polymer melting, and one long (19 elements) for GTR dispersion. The barrel temperature set is detailed in Table 3.12.

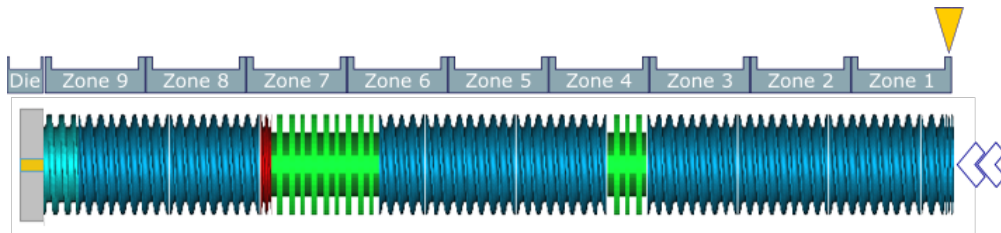


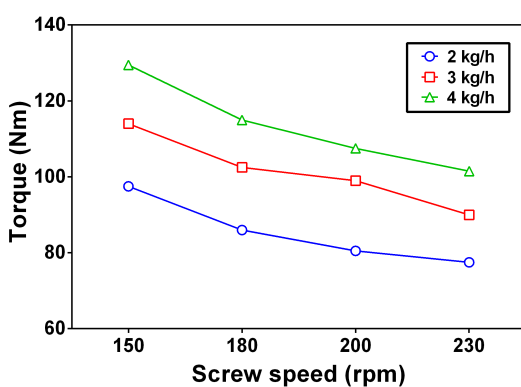
Figure 3.19 – Screw configuration used for preliminary tests.

Table 3.12 – Compounding conditions of the preliminary tests. [55]

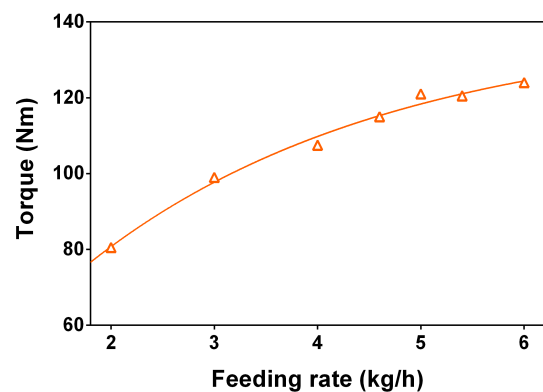
Barrel zone number and temperature (°C)									
1	2	3	4	5	6	7	8	9	Die
70	70	110	130	120	100	100	100	120	140

Figure 3.20a shows the variation of the compounding torque with the screw speed and feeding rate. Higher feeding rates at lower screw speed ensure a high filling degree of the extruder. Nevertheless, shear strain also decreases along with screw speed. The right balance between torque and shear stress is found experimentally by keeping a relative high screw speed and increasing throughput, as shown in Figure 3.20b. The extrusion torque is automatically calculated by using a correlation involving the force applied by the screws and the maximum screw speed during extrusion.

Figure 3.20 – Variation of the extrusion torque in function of the screw velocity for different feeding rates of raw GTR and a screw speed of 200 rpm. The maximum extrusion torque of the extruder machine is about 140 Nm.



(a)



(b)

3.6 Process proposed

The design of the experimental setup and the characterization of the equipment performed above, led to develop a complete fabrication process in agreement with the initial goals pursued. All the stages of the process, proposed to transform recycled rubber particles and polystyrene into a polymer composite with improved mechanical properties, are shown in Figure 3.21. This is divided in four principal stages, namely A, B, D and F, which were completely explored and optimized in this work. Uncolored stages were not optimized.

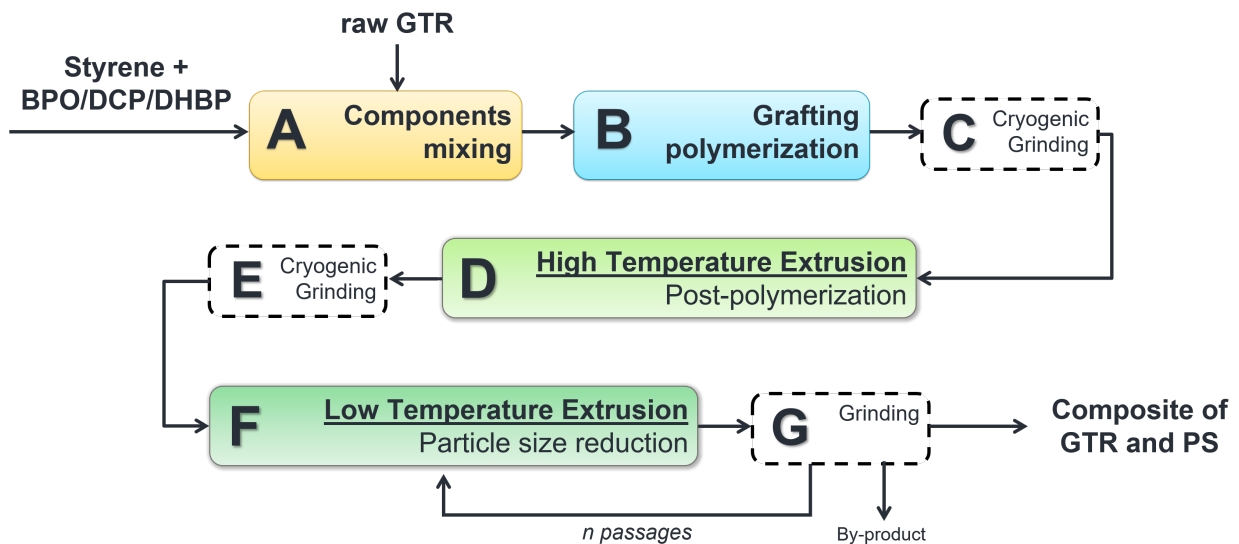


Figure 3.21 – Schema of the implemented process steps

There are no waste products generated in this process and only a derived by-product is obtained from the whole transformation, at the last stage of the process. This is generated during the first and last minutes of the extrusion stages, when the material is not compounded under steady-state processing conditions (i.e. maximum torque). Nevertheless, this could be recycled to the process if desired.

3.6.1 Experimental conditions to be tested

This process will be applied through the experimental conditions presented in Figure 3.22. These involve the fabrication of composites by varying three parameters through three different pathways. Thus, condition 1 and 2 pretend to prepare compatibilized blends of GTR and PS by the method of grafting polymerization and subsequent compounding, by using two different screw profiles. Condition 3 is a control experiment that consists in compounding raw GTR with commercial polystyrene without pre-treatments or compatibilization, but with the same formulations and equipment.

In what follows, the detailed conditions and operating methods established for each of the stages are presented.

3.7 Operating methods

3.7.1 Free-radical grafting polymerization of styrene onto/into GTR particles

Grafting polymerization involves two main stages: the mixing of the components and the reaction. The operating conditions of each stage are shown in Tables 3.13 and 3.14, respectively. The volume occu-

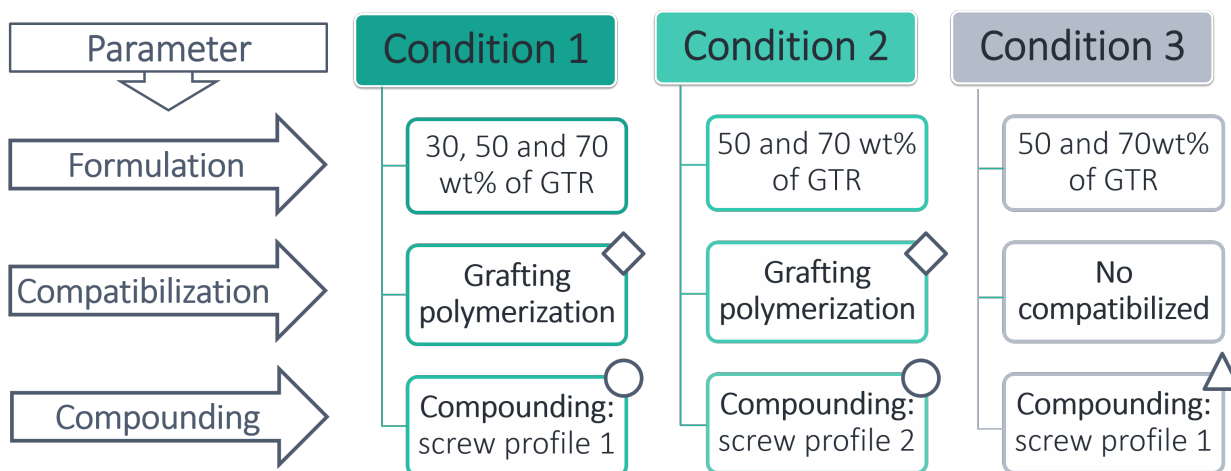


Figure 3.22 – Experimental conditions tested.

pied by the swollen GTR particles restrains the amount of product that can be produced by batch. In this respect, the maximum effective capacity of the reactor corresponds to about 800 gr of GTR/styrene mixture.

Table 3.13 – Conditions for components mixing.

Parameter	Value
Monomer solution pumping rate (ml/min)	5 to 8
Compressed air pressure (bar)	1.1 to 1.2
Stirring speed (rpm)	100
Condenser temperature (°C)	-7

The consecutive stages of the grafting polymerization are:

a) Preparation of the monomer solution

The initiators are dissolved in the monomer with magnetic stirring for 15 min at room temperature. The solution must contain 12% of additional mass, with respect to the nominal mass, to compensate mass loss during the next spraying step. Then, the monomer solution is stored overnight at 4 °C .

b) Mixing of the components

The GTR is introduced in the reactor before closing it hermetically. The rubber powder is stirred permanently while the monomer solution is pumped and sprayed with compressed air at room temperature. After complete dispersion of the monomer solution, the air is stopped and stirring is kept for one hour at 50 rpm. A batch of maximum 0.4 Kg is mixed at each time qt room temperature. The polymerization medium is removed from the reactor with a spatula and weighted to quantify the mass loss of monomer solution during spraying. This is equivalent to about 12 wt% for the set-up implemented. Then, the medium is stored overnight at 4 °C . The spraying system is removed.

c) Polymerization

The polymerization medium is introduced into the reactor. Stirring is turned on and the reactor is heated to the initial polymerization temperature (e.g. 75 °C). The reaction is carried out without inert

Table 3.14 – *Operating conditions for grafting polymerization.*

Parameter	Value	
	Temperature (°C)	time (h)
Temperature profile	75	2
	85	3
	95	3
	115	1.5
	125	1
	140	1
Total reaction time (h)	12	
Stirring speed (rpm)	30	
Condenser temperature (°C)	15	
Heating rate (°C /min)	2	
Cooling rate (°C /min)	2	

atmosphere (air) and in two stages of 6 hours per day since one single day is not enough to perform the whole reaction. At the end of the first day, the reactor is cooled at room temperature at a rate of 2 °C /min. The day after, the reactor is started again at the same operating conditions.

d) Stopping the polymerization

At the end of the total polymerization time, the medium is kept under stirring and cooled to 100 °C . The product is removed from the reactor with a spatula and stored in a hermetic flask at 4 °C . The monomer remaining in the polymerized product is not removed.

3.7.2 Free-radical solution polymerization of styrene

Isothermal polymerization of styrene in toluene was performed to prepare unfilled polystyrene with controlled molar mass. The polystyrene obtained was used as reference material to compare the mechanical properties with those of the composites. The composition of the polymerization system is presented in Table 3.15.

Table 3.15 – *Composition and operating conditions*

Parameter	Value
Composition	
Ratio solvent/monomer	1:1
Ratio BPO/monomer (w/w %)	0.8, 1.18, 1.22
Operating conditions	
Reaction temperature (°C)	80 or 90
Reaction time (h)	4
Stirring (rpm)	300

i) Preparation of the reagents

The initiator is dissolved in the solvent with magnetic stirring for 15 min. In parallel, the stabilizers present in the monomer (4-tert-butylcatechol) are removed by filtration in a column containing aluminum oxide (Al_2O_3).

ii) Polymerization

The solution is introduced into the reactor and stirring is turned on. Subsequently, the phase is purged with nitrogen for 30 minutes. Then, the uninhibited monomer is added to the solution and the reactor is heated to the polymerization temperature.

iii) Stopping the polymerization

When the polymerization reaction ends, the medium is kept under stirring and cooled to room temperature. Then, the polymer is precipitated from the solution with methanol and subsequently dried up in a vacuum oven during 7 hours.

3.7.3 Compounding in a twin-screw extruder

This operating method is implemented for compounding two kinds of products (c.f. Sect. 3.6.1). On the one hand, the product obtained from the grafting polymerization. On the other hand, the control experiment which consists in compounding raw GTR with commercial polystyrene, without pre-treatments or compatibilization. The minimum quantity of material required to perform the three extrusion passages is about 1.2 kg.

The compounding stages are:

First extrusion:

A) Feeding

The product obtained from grafting polymerization is cryogenically ground if necessary, to get granulates of size of about 1 to 2 mm. The granulates are introduced in a twin-screw feeder and the feeding rate is fixed to 1 kg/h.

For control experiments, the pellets of commercial polystyrene are fed in the feeding zone (Zone 1). The raw GTR is introduced through a feeder device located downstream from the polymer melting section (Zone 5). The feeding rate of each component is set up according to the desirable composition.

B) Compounding

Due to the high extrusion temperature at this stage, some gases of the curative additives contained in the GTR formulation are produced, mainly at the feeding and discharge zones. Smoke aspiration systems are disposed over these zones.

C) Extrudate recovery

With heat-resistance gloves, the extruded wire is recovered by hand and carefully arranged to prevent the product from sticking together. Material is cooled at room temperature and subsequently broken down into sticks of a few centimeters.

D) Granulation

The sticks are cooled with liquid nitrogen and ground into particles with a diameter of less than 1 mm.

Subsequent extrusions:

I) Feeding

The granulates of the material, extruded in the previous stage, are introduced in the feeder. The initial feeding rate is fixed to 3 kg/h until a stable extrusion torque is reached. Then, the feeding rate is gradually increased until reaching the maximum torque value. The significant process parameter here is the torque, regardless of the feeding rate.

II) Compounding

The aspiration systems operate while remaining gases are still produced. The torque of the extruder is supervised continuously and only the product extruded at constant high torques is selected.

III) Extrudate recovery and granulation

The steps of recovery of the extrudate and granulation are similar to stages C and D of the first extrusion.

3.8 Evaluation

The characteristics of the composites fabricated were assessed by the set of analytical techniques listed in Table 3.16. More precisely, the analysis is carried out at four main levels: structural assessment, morphological characterization, thermal properties and mechanical properties. The general purpose of applying each of the techniques is presented in the right column. In what follows, the experimental conditions and procedures are detailed.

Representative elementary volume (REV)

The representative elementary volume (REV) is a crucial parameter in determining the effective mechanical and physical properties of composite materials [106]. In fact, despite the efforts for good mixing and homogenization of the constitutive phases, composites may include a large number of micro and macro heterogeneities such as agglomerates, voids, etc. As a consequence, the volume of the sample to be analyzed has to be statistically representative of the heterogeneities present in the composite. The REV is defined as the volume of material required to measure the desired property in a way that will be representative of the composite [106, 107].

The REV size depends on the property and the composite formulation [107]. For this reason, in this work, the adequate size of the sample for some of the analytical methods implemented (i.e. gravimetry, soxhlet extraction, granulometry) was determined experimentally. Then, for the measurement of all properties, a sufficient number of measurements and repetitions were considered in order to calculate the standard deviation (Stand. Dev.) and report the precision of the estimations. The studies performed for REV are not presented here, but the optimal simple sizes are already included in the experimental protocols.

Table 3.16 – Analytical techniques implemented for evaluating the properties of the composites.

Analytical technique	Purpose of the measurements
Structural assessment	
<ul style="list-style-type: none"> Gravimetry Soxhlet extraction Gel permeation chromatography (GPC) Fourier transform infrared (FTIR) Nuclear magnetic resonance (NMR) Wijs method 	<ul style="list-style-type: none"> Monomer conversion PS grafting efficiency PS molar mass Chemical structure of the composites Chemical composition of PS Number of double bonds in the GTR structure
<ul style="list-style-type: none"> Swelling 	<ul style="list-style-type: none"> Absorption capacity of styrene by GTR
Morphological characterization	
<ul style="list-style-type: none"> Scanning electron microscopy (SEM) 	<ul style="list-style-type: none"> Morphology of the composite and fracture surfaces.
<ul style="list-style-type: none"> Granulometry 	<ul style="list-style-type: none"> Particle size distribution of GTR
Thermal properties	
<ul style="list-style-type: none"> Differential scanning calorimetry (DSC) 	<ul style="list-style-type: none"> Glass transition temperature of PS and composites
<ul style="list-style-type: none"> Thermogravimetric analysis (TGA) 	<ul style="list-style-type: none"> Degradation temperature of PS and composites
Mechanical properties	
<ul style="list-style-type: none"> Impact strength 	<ul style="list-style-type: none"> Impact resistance of PS and composites
<ul style="list-style-type: none"> Tensile strength 	<ul style="list-style-type: none"> Tensile properties of composites

3.8.1 Structural assessment

3.8.1.1 Monomer conversion

The purpose of this characterization is to determine the total monomer conversion achieved during the free-radical polymerization of styrene in presence of GTR. The measurement is performed in a heating halogen balance. A sample of about 2.5 g is weighted in the aluminum pan of the balance and moisten with a known quantity (at least twice the sample mass) of hydroquinone (HQ) solution 0.5 g/ml (water/ethanol 4:1 v/v%) to inhibit further styrene polymerization during measurement. The mix is heated at 170 °C during 30 min or until constant weight. The monomer vaporizes, and the monomer conversion (x) is calculated from the mass difference as follows:

$$x = \frac{m_{PS}}{m_{i_{sty}}} = \frac{m_{f_{sample}} - m_{i_{GTR}} - m_{i_{HQ}}}{m_{i_{sty}}} \quad (3.1)$$

where:

- m_{PS} : mass of polystyrene in the sample (g).
- $m_{i_{sty}}$: initial mass of styrene in the sample before measurement (g).
- $m_{f_{sample}}$: final mass of the sample after measurement (g).
- $m_{i_{GTR}}$: initial mass of GTR in the sample before measurement (g). About 2.6% of the initial mass of GTR, from volatile curatives and additives, is removed during measurement.
- $m_{i_{HQ}}$: mass of HQ added to the initial sample before measurement (g).

3.8.1.2 Polymer grafting efficiency



The total percentage of styrene grafted into/onto the GTR particles after the free radical polymerization is measured by Soxhlet extraction. Chloroform was used as extracting agent to remove the remaining monomer and the non grafted polystyrene from the sample. About 70 mL of the solvent are poured into the bottom flask (1). Then, a sample of 1 g is placed into a porous thimble (cellulose) in the extraction chamber (2). If necessary, the sample is ground previously to granulates of less 2 mm of diameter. The solvent is heated to the boiling temperature (65 °C approx.). The evaporated solvent moves up until the condenser (4), where it is condensed and trickles into the extraction chamber. After 6 hours under reflux, the solvent is recovered in the funnel (3) and the removed components remain into the flask. Finally, the insoluble material in the thimble is dried under vacuum. Grafting efficiency can be calculated as:

$$GE(\%) = \frac{m_{PS_{grafted}}}{m_{PS_{total}}} = 1 - \frac{m_{PS_{free}}}{m_{i_{sample}} \cdot W_{0_{sty}} \cdot x} \quad (3.2)$$

Figure 3.23
– Soxhlet

where:

- $m_{PS_{grafted}}$: mass of polystyrene grafted onto GTR present in the sample (g).
- $m_{PS_{free}}$: mass of free polystyrene present in the sample (g).
- $m_{PS_{total}}$: total mass of polystyrene (grafted + free) in the sample (g).
- $m_{i_{sample}}$: initial mass of the sample before soxhlet extraction (g).
- $w_{0_{sty}}$: theoretical mass fraction of styrene in the formulation before polymerization in the batch reactor (g).
- x : monomer conversion after polymerization in the batch reactor.

3.8.1.3 Polymer molar mass

The molecular weight distribution (*MWD*) and the number average (M_n) and weight average (M_w) molecular weight of the polystyrene were determined by size exclusion chromatography (SEC) in an instrument SEC-MALS. The device is equipped with two detectors: a refractive index Obtilab REX (RI) for concentration detection and a multi-angle light scattering MALS WYATT mini dawn TREOS for absolute molecular weight measuring. Separation is performed through three columns PLgel with pore size of 100 Å (*MW* range up to 500), 10E+03 Å (*MW* range 500 to 60000) and 10E+05 Å (*MW* range 60000 to 1700000). Samples were prepared by dissolving the polymer in THF at a concentration of about 6 to 8 mg/mL. Measurements are carried out at a flow rate of 1 mL/min in THF at 40 °C.

3.8.1.4 Chemical structure of the composites

The chemical structure of GTR-grafted-PS composites was confirmed by fourier-transform infrared (FTIR) measurements on a Bruker Alpha instrument, equipped with the software Opus 6.5 to process the infrared spectrum of absorption. The device crystal The analysis consists in radiating a sample under powder form with a beam of multiple frequencies of light and measuring its capacity for light absorption. The spectra were recorded between a wavelength range from 600 to 4000 cm^{-1} , with a spectral resolution of 4 cm^{-1} ; a total of 64 spectra were averaged for each measurement to reduce the noise.

3.8.1.5 Chemical composition of the polymer

Analysis on the free polystyrene formed during grafting polymerization), to identify traces of remaining styrene monomer, was performed by nuclear magnetic resonance (NMR). The measurements were performed in liquid phase in an apparatus Bruker with a resonance frequency of 300 MHz. Polymer samples were dissolved in deuterated chloroform at a concentration of about 10 mg/mL.

3.8.1.6 Number of double bonds in the molecular structure of GTR

The concentration of double bonds of the elastomer chains of GTR was determined according to the “Standard test method for iodine value of drying oils and fatty acids” (ASTM D-1959) [47, 108]. In this method, unsaturated bonds are quantified by indirect titration with iodine.

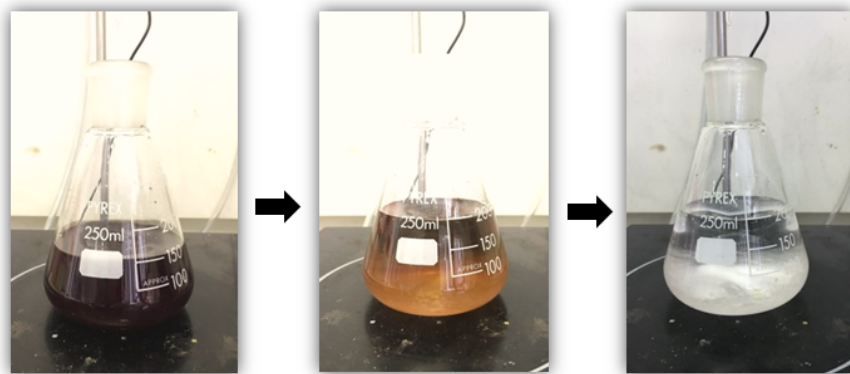


Figure 3.24 – GTR titration for double-bonds quantification.

GTR was used as-received or previously purified with chloroform. Firstly, the Wijs agent, which is a solution of iodine monochloride (ICl) in acetic acid (17 g/L), was prepared and stored in a dark place.

In an Erlenmeyer flask, the Wijs solution was added in excess (25 mL) to a sample of GTR (0.5 g) with $CHCl_3$ (30 mL). The medium was agitated vigorously and stored in a dark place (during 40 min). In this step, the iodine gets mainly fixed to the double bonds. Subsequently, distilled water (100 mL) and a solution of potassium iodide (KI) (0.2 g/mL) were added to the medium. The latter form a complex with the ICl remaining in the mixture to get diiodide. Then, the solution was titrated with a standard solution of sodium thiosulfate ($Na_2S_2O_3$) (14 g/mL) in presence of a starch indicator, which turns off the solution color from clear yellow to intense blue-black. Finally, the solution became translucent at the equivalent volume as shown in Figure 3.24. The same procedure was followed in an additional flask without GTR to prepare the blank.

The content of double-bonds (mole/gr of GTR) is calculated as follows:

$$I = (V_0 - V)C/M \quad (3.3)$$

where V_0 and V correspond to the $Na_2S_2O_3$ solution volume (L) required for titration of the GTR and the blank, respectively, C is the concentration (mol/L) of the $Na_2S_2O_3$ and M is the sample mass of GTR (g).

3.8.1.7 Swelling capacity of GTR by styrene absorption.

This test was conducted to determine the styrene absorption rate and maximum absorption capacity by GTR. The measurement methodology was adapted from the ASTM standard D471 [40, 109]. Slabs of GTR with dimensions of 2.9 x 1.3 x 2 mm were fabricated by compression molding at 150 °C during 20 min. Final weight of the specimens was about 0.5 to 0.6 g. Slabs were weighted (W_0) and then completely immersed in an excess of monomer (100 mL) at room temperature. Slabs were removed and weighted periodically to calculate the weight change, (W). At each time, the excess of monomer was wiped dry. Then, the percent weight change or swelling percentage (S) was determined from the following expression:

$$S = [(W - W_0)/W_0] * 100\% \quad (3.4)$$

3.8.2 Morphological characterization

3.8.2.1 Morphology of the composites and fracture surfaces

Microscopic images of the composite particles and fracture surfaces were realized by scanning electron microscopy (SEM) in a device Jeol 6490-IV. The particulate samples were deposited on the surface of the metallic plots, which were previously covered with double-side adhesive. It was possible to have good contrast between rubber and polymer phases without metallizing the sample surface. Observations were performed under high vacuum at a voltage of 10 kV. For fracture surface observations, only unfilled polystyrene specimens were sputter-coated to better contrast.

3.8.2.2 Particle size distribution

Particle size distribution (PSD) of the GTR in the prepared composites (compatibilized or not) was measured before and after the compounding stages, by laser diffraction in a Mastersizer 2000 device (Malvern Instruments). The particles are dispersed in liquid media and the laser consists of two light sources, He and Ne, which are diffracted by the particles. Whilst the blue light detects the small particles, the red light is used for measuring the larger ones. The diffraction pattern is determined by the particles size and is measured by detectors, where the signal is transformed to particle size distribution data.

(A) Sample preparation

GTR particles can be found as raw GTR particles or dispersed GTR-grafted-PS particles in polystyrene composites. In the latter case, particles are agglomerated during the grafting polymerization and/or thermomechanical treatment due to the presence of polystyrene on their surface. The procedure for particles separation is illustrated in Figure 3.25 and detailed step by step as follows:

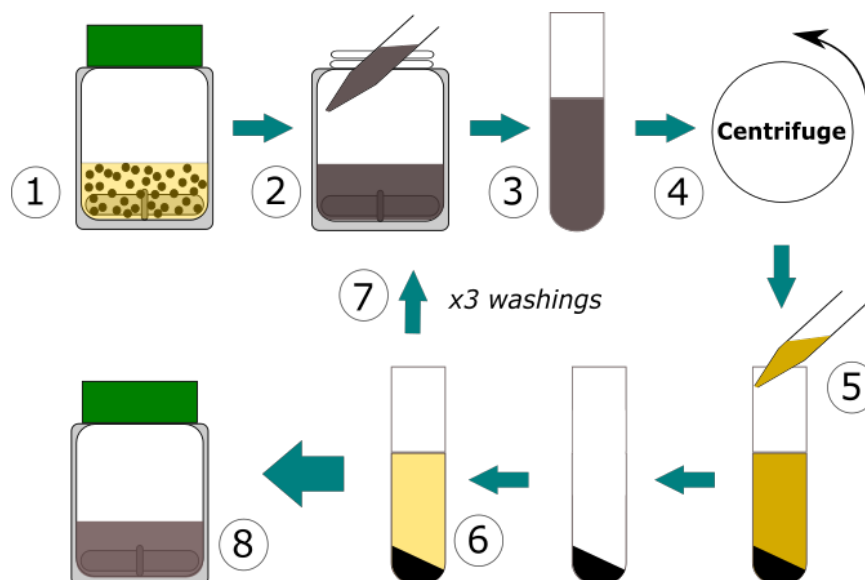


Figure 3.25 – Procedure for GTR and GTR-grafted-PS particles' separation.

1. A sample of the composite product is reduced by cryogenic grinding into granulates with diameter of less than 2 mm. Then, 0.5 g of the material is added to 20 mL of THF, and the media is stirred at 130 rpm during seven days. To achieve good separation, the length of the magnetic stirrer shall be close to the containing flask diameter. In addition, a small volume of solvent is used to create enough turbulence in the media.

2. Particles are washed once daily for three consecutive days by partially replacing the polluted solvent with fresh solvent. To do this, the agitation is stopped to allow precipitation of the big granulates during 15 min.
3. By using a pipette, 15 mL of the supernatant is removed from the flask and poured in 2 or 3 centrifugation flasks of 15 mL. Then, the flasks are filled up with fresh acetone and gently closed without this being hermetic (hermetically-closed flasks can implode or explode during centrifugation).
4. Samples are centrifuged at 8500 rpm during 15 min.
5. The supernatant is carefully removed with a pipette to avoid particles re-suspension.
6. Fresh THF solvent is added to the pellet until completing the initial volume of the sample (15 mL). Then, the flasks are mixed vigorously.
7. All the flasks are poured again into the initial agitation flask and the sample is placed under permanent agitation. This procedure is repeated three times.
8. After seven days, the same procedure is repeated but THF is replaced by fresh acetone. The suspension is hermetically stored and measured the same day.

(B) Measuring

Ethanol (98% purity) is used as dispersion media for the measurement. The acetone suspension is stirred and sampled with a pipette (having a large diameter tip up to 2 mm), and poured in the sampler (stirring at 2000 rpm). The concentration of particles is limited by the obscurity index of the device on the range of 12 to 15%. The result of each measurement is the average of three consecutive measurements and each sample is measured twice.

3.8.3 Thermal characterization

3.8.3.1 Glass transition temperature and thermal decomposition

Thermal analysis of the raw materials and composites was conducted by differential scanning calorimetry (DSC) and thermogravimetric analysis (TGA) in a device Mettler Toledo TGA/DSC 1, equipped with the software Star to process and calculate the data from the thermograms from both analyses.

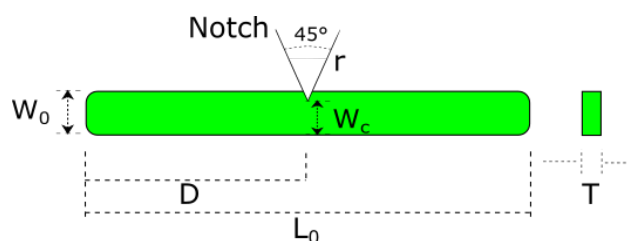
(i) DSC measurements

For glass transition temperature (T_g) measurements, a sample of mass between 7 to 10 mg is introduced in hermetic aluminum pans of 40 to 100 μ L. Particulate samples were slightly compressed with a small stick to ensures a good contact with the bottom of the pan. Samples were scanned twice in the DSC module using nitrogen at a volume flow rate of 50 ml/min. All runs were performed at heating rates varying between 3 and 5 $^{\circ}$ C /min. The first run was performed in the temperature range from 30 to 150 $^{\circ}$ C to eliminate the thermal history of the material. Subsequently, the T_g was measured at the mid-point through the tangent method and from the second run performed at different temperature ranges according to the materials as follows:

- Raw GTR: -80 to 20 $^{\circ}$ C
- Composites GTR/PS: -80 to 200 $^{\circ}$ C
- Polystyrene: 30 to 150 $^{\circ}$ C

(ii) TGA measurements

Table 3.17 – *Standard dimensions of impact specimens.*



Dimension	Value (mm)
W_o	10
W_c	8
L_o	100
D	50
T	4
r	0.25 radius

Table 3.18 – *Instrumented hammer specifications.*

Parameter	Value
Energy (J)	7.5
Falling angle (degrees)	150
Impact velocity (m/s)	3.8

Thermogravimetry analysis consists in following the mass changes of a sample while the temperature is increased over time. In this work, TGA is used to track the decomposition of the constitutive components of the raw GTR and the GTR/PS composites. For thermogravimetric analysis, samples of about 15 mg were placed in open alumina pans of 100 μ L and measurements were carried out under inert nitrogen atmosphere, under a heating rate of 10 $^{\circ}$ C /min. GTR containing samples were scanned between 40 to 600 $^{\circ}$ C and polystyrene samples in the range of 40 to 300 $^{\circ}$ C .

3.8.4 Mechanical properties

3.8.4.1 Impact strength

Impact resistance of the polymer composites was measured by notched Charpy impact strength, according to the standard ASTM D6110-10 or the equivalent ISO 179 for plastics. The mechanical test was performed with a standard specimen in a machine INSTRON CEAST 9020 pendulum with an instrumented Charpy impact hammer DAS 64k to acquire the force signal and equipped with VisualIMPACT software. In contrast to the uninstrumented hammer, the instrumented one includes a force sensor on the tip that offers a reliable control of the impact test.

(a) Impact standard specimens

The standard dimensions of the impact specimens are detailed in Table 3.17. The fabrication procedure is described in detail below (c.f. Sect. 3.8.4.3). The notch was milled at least 24 h after the specimen fabrication with a manual notching machine CEAST AN20 Notchvis. The minimal waiting period before impact testing was three days.

(b) Impact testing conditions and procedure

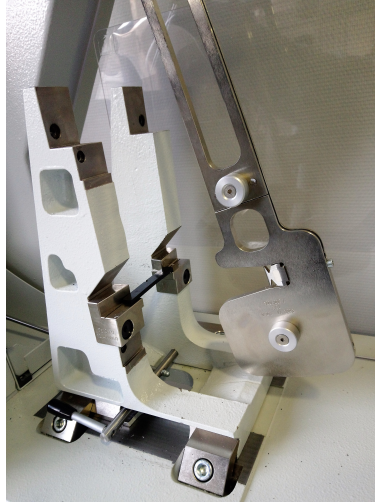


Figure 3.26 – Charpy impact testing.

At least five specimens were tested to determine the impact resistance. The specifications of the instrumented hammer used are listed in Table 3.18. The pendulum was calibrated before measuring. The width (W) and thickness (T) under the notch were measured with a caliper. In Charpy impact testing, the specimen is clamped horizontally in the center of the support with the unnotched face facing the direction of the impact. Then, the pendulum is released to strike the specimen, as shown in Fig 3.26. The software records the evolution of the force (N) applied to the specimen during the collision event, and the neat breaking energy E_b (J).

The only parameter controlled by the device is the impact velocity v_{impact} , which is initially 3.8 m/s. Then, the impact energy at break point E_{break} is calculated according to the Equation 3.5, where m_{hammer} is the hammer mass.

$$E_{break} = \frac{1}{2} m_{hammer} v_{impact}^2 \quad (3.5)$$

The impact strength of each specimen IS (kJ/m^2) is obtained by the Equation 3.6. The final impact resistance is calculated from the average of the values of the set of specimens. The samples that do not break or are partially damaged were discarded.

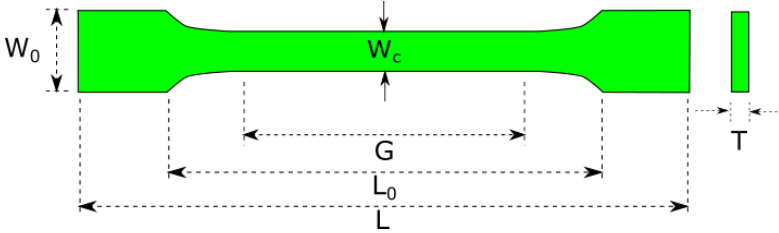
$$IS = \frac{E_b}{W \cdot T} \quad (3.6)$$

The instrumented pendulum used in this work measures both the uninstrumented and instrumented breaking energy. Whilst the former is read directly from the pendulum, the latter is calculated via the construction of the load-displacement curve with the data provided by the force sensor on the hammer. The area beneath this curve corresponds to the impact energy absorbed by the specimen. In theory, both measurements lead to similar results, but in some cases, large discrepancies can be observed (for example, due to hammer rebounding).

3.8.4.2 Tensile strength

Tensile properties, namely the Young's modulus (E), yield strength (σ_y), ultimate strength (σ_r) and elongation at break (ϵ), were measured in agreement with the standard ASTM D638-10 (ISO 597) for plastics. Testing was performed in a machine INSTRON 5569 equipped with Bluehill software.

Table 3.19 – Standard dimensions of tensile specimens.



Dimension	Value (mm)
W_0	20
W_c	10
L_0	100
L	150
G	50
T	4



Figure 3.27 – Tensile strength testing

(I) Tensile standard specimens

Table 3.19 shows the dimensions of the standard specimens fabricated (c.f. Sect. 3.8.4.3). In order to concentrate the stresses during the application of the tension, two small lateral notches (about 1 mm depth) were machined by hand in middle zone of the specimen. In addition, the edges were carefully polished with sandpaper to eliminate defects that may initiate failure.

(II) Tensile testing conditions and procedure

It is recommended to wait a time interval of 40 hours between specimens' fabrication and testing. A set of at least three specimens was required for accurate properties estimation. The width (W_0) and thickness T at the notched zone were measured with a caliper. The testing conditions are indicated in Table 3.20. For test execution, the specimen is aligned the long axis with the grips and held in such a way to prevent slippage, as illustrated in Fig 3.27. Specimen misalignment can lead to apparently lower resistance. Then, the specimen is subjected to tension at a high-strain deformation at constant cross-head speed, causing permanent deformation until it breaks.

In contrast to typical testing, the utilization of an extension indicator (extensometer) for accurate

Table 3.20 – Tensile testing conditions

Parameter	Value
Load cell capacity (N)	10
Initial deformation (%)	0.5
Cross-head speed (mm/min)	10
Initial length* (mm)	50

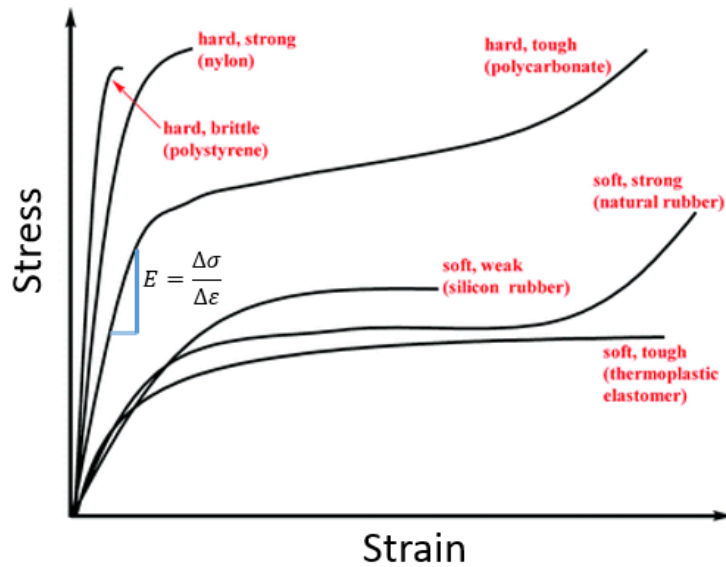


Figure 3.28 – Stress-strain curve and tensile properties.

modulus calculation is not recommended for samples containing GTR. In fact, this device is gripped firmly on the specimen to record the distance as a function of the load at strains below 10%. Nevertheless, the edge of the extensometer in contact with the specimen consists of a fine blade that pierces the surface (due to the presence of the soft elastic phase). Consequently, this distorts the measurement and causes the premature fracture of the sample.

The device records the tensile force (F) applied as a function of the displacement of the grids (ΔL). These values are then normalized with respect to the initial cross sectional area (A_o) and length (L) of the specimen, in order to calculate the nominal stress (s) and strain (ε) by the Equations 3.7 and 3.8, respectively:

$$s = \frac{F}{A_o} \quad (3.7)$$

$$\varepsilon = \frac{\Delta L}{L_o} \quad (3.8)$$

Figure 3.28 is an example of a typical stress-strain curves for different polymers. Tensile properties are obtained from such curves as follows:

- Young's modulus (E) is measured at low stress and strain. Under these conditions, most of materials suffer an elastic or reversible deformation. Then, the material behaves as a linear elastic solid and therefore, the stress-strain curve is linear at strain values less than 0.25%. The elastic

modulus or Young's modulus corresponds to the slope of this linear portion:

$$E = \frac{\Delta\sigma}{\Delta\varepsilon} \quad (3.9)$$

- Tensile strength at yield (σ_y) is the initial maximum stress at which the stress-strain behavior starts to be non-linear. Then, this point denotes the end of the elastic behavior and the onset of the plastic behavior or permanent deformation.
- Fracture tensile strength or strength at break (σ_r) is the corresponding value of the stress at the specimen break point, regardless of whether the specimen necks (reduction of the specimen cross-section) or fractures before necking.
- Elongation or strain at break (ε) is the strain at the rupture point.

3.8.4.3 Fabrication of mechanical testing specimens

Specimens for impact and tensile testing were fabricated by means of injection molding in an inter-meshing co-rotating twin-screw micro-compounder DSM Xplore. The machine is equipped with a temperature controlled mixing chamber and an injection device able to work at high injection pressures. Both types of specimens were prepared at the operating conditions listed in Table 3.21.

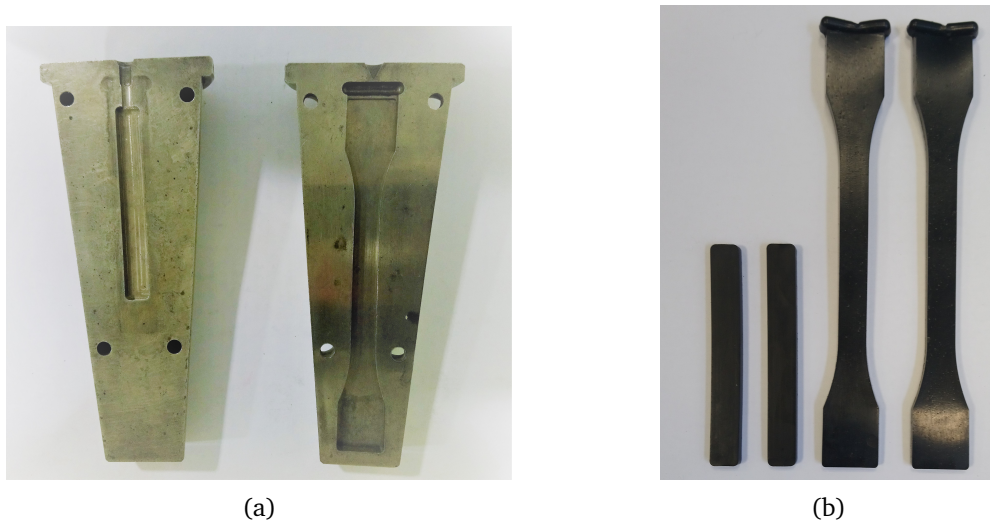
Table 3.21 – *Injection-molding conditions*

Parameter	Value
Mixing	
Screw speed (rpm)	100
Barrel temperature (°C)	140 to 180
Time of mixing (min)	5
Screw force (N)	>2300
Molding	
Cylinder temperature (°C)	140 to 180
Injection pressure (bar)	6 to 10
Time of injection (s)	30
Mold temperature (°C)	50

The consecutive stages for specimens' preparation are the following:

- The material in the form of particles of less than 2 mm of diameter was feed into the mixing chamber. To ensure high shear mixing rates and thus, good homogenization, the chamber was filled up until reaching the minimal screw force.
- The barrel temperature was fixed according to the nature and formulation of the sample. Samples containing commercial PS required higher mixing temperatures than compatibilized ones. In addition, barrel temperature was increased with the content of GTR, and in some cases, with the number of extrusions.
- At the end of the mixing time, the material was injected to the preheated mold (Figure 3.29a). Finally, specimens were carefully removed and cooled at room temperature. These were free from scratches, pits, sinks, marks and other surface defects (Figure 3.29b).

Figure 3.29 – Injection molds (a) and specimens (b) for impact and tensile testing.



3.8.4.4 Fabrication of unfilled polystyrene testing specimens

Specimens of unfilled polystyrene of different molecular weight, such as commercial PS and PS synthesized by free-radical solution polymerization (c.f. Sect. 3.7.2), were fabricated by molding compression in a mechanical press. Both types of PS are so brittle that specimens break down when unmolded from the molds used in the injection-molding microcompounder. Therefore, a stainless-steel two-part mold with the standard dimensions was fabricated (Figure 3.30).



Figure 3.30 – Compression molding of polystyrene impact specimens.

For specimens' fabrication, the internal walls of the mold were covered with both a protective anti-adhesion spray and heat-resistant film, to avoid polymer adhesion to the metallic walls. Polystyrene powder (finely ground at cryogenic temperature) was poured in the mold layer by layer, with intermediate heating stages at 120 °C during 5 min. Finally, the specimen was compressed at 120 °C by gradually increasing the pressure as follows: 1 bar for 4 min, 4 bar for 6 min and 10 bar for 10 min.

3.9 Conclusions

GTR may accomplish the function of impact modifier to fabricate high-resistance polystyrene composites, similar to HIPS. The main intrinsic and extrinsic parameters influencing toughness in thermoplastic compounds reinforced with GTR have been identified. Although the interfacial adhesion is one of the most important parameters, it is not the single most relevant. Despite this, most studies consider only

a portion of these parameters instead of considering them as a whole. In this respect, it became crucial to identify clearly such microstructure, i.e. degree of particle dispersion (particle size) and distribution, which dictates the final mechanical behavior of GTR-reinforced thermoplastics and most notably, the one that leads to polystyrene toughening.

This chapter proposed a novelty methodology for the fabrication of reinforced polystyrene compounds with GTR, having defined specifications and targeted mechanical properties. All the aspects related to the experimental procedure that involves definition of the materials, processing, equipment and characterization techniques implemented, are detailed. The preliminary studies of the radical polymerization reaction revealed that depending on the relative amounts of GTR and styrene in the system, the polymerization medium is continuous or non-continuous. Therefore, it was possible to identify the difficulties related to mixing and the limitations of heat and mass transfer when performing the reaction in a batch reactor. These findings enhanced the understanding of this polymerization system in a larger scale laboratory set-up.

A comprehensive kinetic model of radical styrene polymerization and grafting polymerization onto ground tire rubber

Contents

4.1	Introduction	87
4.1.1	Styrene polymerization	87
4.1.2	Grafting polymerization of styrene onto rubber	88
4.2	Experimental	89
4.2.1	Materials and reagents	89
4.2.2	Methods	90
4.2.2.1	Solution styrene polymerization	90
4.2.2.2	Free-radical bulk polymerization in a batch reactor	90
4.2.2.3	Monomer conversion	91
4.2.2.4	Grafting efficiency	91
4.2.2.5	Molecular weight	91
4.2.2.6	Number of saturations in GTR	91
4.3	Styrene homopolymerization model	92
4.3.1	Model developments	92
4.3.1.1	The kinetic mechanism	92
4.3.1.2	Polymerization rate functions	93
4.3.1.3	Moment rate functions	94
4.3.1.4	Reactor design equations	95
4.3.1.5	Polymer properties	96
4.3.1.6	Diffusion controlled reactions	96
4.3.1.7	Kinetic rate constants	97
4.3.2	Results and discussion	98
4.3.2.1	Free-radical bulk polymerization	98
4.3.2.2	Free-radical solution polymerization	101
4.3.3	Conclusions	102
4.4	Styrene grafting polymerization onto GTR model	103
4.4.1	Introduction	103
4.4.1.1	Synthesis experiments in a batch reactor	103

4.4.1.2	DSC measurements	104
4.4.1.3	Oxidation-redox reactions between CB and peroxide initiators BPO/DCP	105
4.4.2	Model developments	105
4.4.2.1	The kinetic mechanism	106
4.4.2.2	Polymerization rate functions	108
4.4.2.3	Moments rate functions	109
4.4.2.4	Reactor design equations	110
4.4.2.5	Polymer properties	111
4.4.2.6	Kinetic rate constants and parameters estimation	112
4.4.2.7	Adopted model assumptions and possible extensions	114
4.4.3	Conclusions	116

4.1 Introduction

Standard polystyrene (PS) is one of the most commercialized thermoplastic polymer resins in spite of its brittle character. In fact, due to the high compatibility with numerous monomers and polymers, polystyrene is usually modified by co-polymerization in order to confer it interesting properties such as opacity, impact resistance, elasticity, thermal resistance, etc., and thus broaden its scope [51]. Polystyrene is commercially produced by free-radical bulk, suspension or solution polymerization. Although the production costs and wastes generation are reduced for the bulk process, this is difficult to control, implying safety risks [51, 115].

4.1.1 Styrene polymerization

Free-radical polymerization of styrene involves both the chemical initiation with distinct nature agents (e.g. peroxides, azo-compounds, etc.) at relatively low reaction temperatures ($< 120\text{ }^{\circ}\text{C}$), and the sporadic thermal initiation ($> 100\text{ }^{\circ}\text{C}$), which arises particularly above $150\text{ }^{\circ}\text{C}$ [116, 117]. A great number of experimental studies has been performed and reported in the literature. Moreover, in an attempt to describe this polymerization system, researchers have proposed and developed different mathematical models. From a series of experiments, Mayo (1968) [117, 118] explained the phenomena of the self-initiated thermal polymerization as a three-step process. According to this, two styrene molecules first interact by Diels-Alder mechanism to form an intermediate species named “adduct” (1-phenyl-1,2,3,9-tetrahydronaphthalene). In a second step, the adduct reacts with a third styrene unit, leading to two radical species that subsequently initiate the polymerization. This mechanism was later confirmed by the simulations performed by Pryor and Coco (1970) [119]. In 1972, Hui and Hamielec (1972) [116], developed a kinetic model to study the influence of the monomer concentration and diffusion-controlled termination on thermal polymerization rate in the temperature range of 100 to $200\text{ }^{\circ}\text{C}$, at which the industrial thermal processes operate. To this purpose, two limiting forms of initiation were evaluated: a second- and third-order one, in terms of styrene concentration. Authors recommended the use of the third-order model to get more accurate predictions on rate and average molecular weight distributions. Later, Husain and Hamielec (1978) [120] extended this kinetic study to higher polymerization temperatures (200 to $240\text{ }^{\circ}\text{C}$). They found that the model of Hui and Hamielec may be applied to describe system behavior at temperatures up to $230\text{ }^{\circ}\text{C}$.

Mathematical modeling of the combined chemical and thermal free-radical polymerization of styrene has seen several developments by the contributions of numerous studies since the early 1970s. Relevant authors such as Marten and Hamielec (1982) [62], Achilias and Kiparissides (1992) [121], Tefera et al., (1997) [122], O’Neil et al. (1998) [123], proposed kinetic models considering the physical phenomenon of autoacceleration at intermediate conversion of the polymerization rate, known as gel effect or Tromsdorff-Norrish effect [75]. The later models also included the diffusion-controlled dependence of the elementary reactions, as well as the initiator efficiency f (fraction of radicals leading to initiate new polymer chains). Moreover, the effects of the transfer of small molecules through chain transfer reactions to monomer and adduct, were considered as being of major importance in controlling the average molecular weight of the polymer [116, 119]. To validate their simulations, authors compared with experimental data from diverse sources and mainly using azobis(isobutyronitrile) (AIBN) as initiator over a wide range of temperature (30 to $80\text{ }^{\circ}\text{C}$).

The most relevant kinetic models recently published were reported by Kotoulas et al. (2003) and Woloszyn et al. (2013). These account for the combined chemically and thermally initiated polymerization, and thus, can be applied over a wide range of temperature conditions of interest for industrial polymerization processes (50 to $200\text{ }^{\circ}\text{C}$). The model developed by Kotoulas et al. [124] predicts with accuracy the experimental data obtained for the styrene polymerization using dicumyl peroxide (DCP) as chemical initiator (120 to $150\text{ }^{\circ}\text{C}$), in addition to the thermal polymerization at higher temperatures (150 to $180\text{ }^{\circ}\text{C}$). Since no information about the method for parameters estimation was reported,

Woloszyn et al. [125, 126] implemented a ranking algorithm to identify the parameters according to their influence on model predictions. The top ranked list parameters were estimated and the rest were kept at their literature values. Nevertheless, simulation results of the polymerization initiated with benzoyl peroxide (BPO) and DCP, showed a poor predictability of the polymer molecular weight data trends obtained from industrial batch reactions.

Estimation and adjustment of the different types of model parameters concerned in the reactions and mechanisms of the free-radical polymerization system, i.e. initiation, propagation, termination, chain transfer and diffusion-control, is still a challenge [63, 125]. For example, techniques such as pulsed laser polymerization (PLP) in combination with molecular weight MW measurements by size exclusion chromatography (SEC) have lead to acquire with accuracy the values of the propagation and termination rate coefficients, k_p and k_t , respectively [127, 128].

Nevertheless, experimental literature values of rate constants often exhibit large divergences, which may be mainly associated to widely different experimental reaction conditions (e.g., solvent viscosity, discrepancies in conversion), experimental error or methods of calculation (e.g., differences in the initial values of rate coefficients used for the estimation of the reaction rates) [63, 128]. Horie and co-workers (1969) [129, 130], and Ebdon and Hunt (1973) [131], demonstrated the use of differential scanning calorimetry (DSC) to obtain directly, continuously and over the whole range of conversion, reliable quantitative information about the bulk polymerization of styrene. The DSC device records the heat flow released during the exothermic polymerization reaction, which is assumed as proportional to the reaction rate. From the experimental data it is then possible to calculate the instantaneous rate, monomer conversion and heat of reaction [58, 129]. Bera et al., (2011) [61], implemented the DSC to confirm the existence of changes on the rate of polymerization close to the maximum rate. Results demonstrated that, from the DSC thermograms it is possible to identify, over a range of temperatures from 70 to 90 °C, the onset and the maximum of the gel effect and the maximum of the polymerization rate that is followed by a deceleration stage with a minimum and a maximum of conversion (i.e. ultimate monomer conversion) at the end of polymerization. These data were implemented to develop a simple model, describing the autoacceleration mechanism and its temperature-dependence.

4.1.2 Grafting polymerization of styrene onto rubber

As mentioned above, impact resistance of standard polystyrene is usually improved by copolymerization with an elastomer phase such as polybutadiene rubber (PB) [51]. Recently, a new approach has been considered to replace the fresh elastomer by rubber particles derived from recycled tires [10, 11, 17, 28, 30]. These are fine powders commercially called ground tire rubber or GTR, which are obtained through mechanical grinding of the rubber phase of end-of-life tires. GTR consists of a sulfur-crosslinked reinforced elastomer phase which displays interesting mechanical properties such as high extensibility and elasticity. Nevertheless, GTR and PS are incompatible phases and thereby, it is difficult to produce a homogeneous material simply by blending them. To overcome this problem and render both phases compatible, the polystyrene phase can be directly grafted onto the surface of the GTR particles via free-radical polymerization [23, 28, 56].

GTR is constituted of a mix of natural and synthetic elastomers such as styrene-butadiene rubber (SBR), butadiene rubber (BR) and butyl and halogenated butyl rubber (IIR), reinforcing agents (carbon black, clays and amorphous silicas), curatives (e.g. sulfur and peroxides) and additives (antioxidants, stabilizers, etc.) [9, 11, 15]. Peroxide initiators such as BPO and DCP have the ability to attack the double bonds or abstract allylic hydrogen atoms from the elastomer chains, creating new radicals on the surface of the rubber particles to which the growing polymer chains can attach [56, 132]. During polymerization, two main parallel and competitive reactions take place: homopolymerization forming free polystyrene chains (free-PS), and grafting polymerization, which produces PS chains grafted (grafted-PS) to GTR backbone. Coiai et al. (2006) [28], grafted PS onto GTR by using BPO in bulk poly-

merization. Authors noticed that by adding 10 wt% of rubber particles (ratio mol BPO to mol styrene of 0.4%, at 80 °C and during 24 h) the monomer conversion decreased to 55% and continued decreasing with the increment of GTR content, whereas the same system in absence of rubber reached a final conversion of 99.6%. Moreover, the portion of PS grafted, quantified as grafting efficiency "GE" (i.e., the ratio of the mass of grafted polystyrene over the total mass of formed polystyrene) increases along with the amount of rubber and, by contrast, seems to be independent of the initiator concentration. The effects of GTR on the radical polymerization of styrene were partially elucidated in a previous work (Chapter 2), and these are briefly discussed further in this chapter. However, no published studies have been found that surveyed the theoretical study and modeling of the bulk polymerization of styrene onto GTR.

Theoretical and modeling studies reported in the literature related to the grafting of styrene, have been mainly focused on the preparation of high-impact polystyrene in bulk or solution polymerization. Manaresi et al., (1975) [132], studied experimentally and theoretically the initial stages of the graft bulk polymerization of styrene with *cis*-1,4-polybutadiene (*cis*-PB) by using DCP. Experimental results showed that the polymerization rate was lowered in the presence of *cis*-PB (1 to 9 wt% of the total mass, 60 °C) and exhibited a minimum value at a relatively high rubber concentration (about 8 wt%). Authors proposed a model predicting the initial stages, i.e. at low extents of reaction, with low rubber contents (below 9 wt%). The reaction mechanism included, in addition to the significant reactions of chemical and thermal initiation, the grafting initiation by radicals attacks to the rubber chains and, propagation, chain transfer and termination reactions for both polymer species formed, free and grafted chains. In another study, Huang and co-workers (1995) [133], considered a similar mechanism to describe the grafting of styrene onto *cis*-PB with BPO. Thermal initiation was not considered since experiments for model validation were conducted at low temperatures (60 °C). To simulate their experimental measurements on monomer conversion, polymerization rate, GE and average molecular weight, they assumed that the reactivity of both polymer macroradicals, free and grafted, was equivalent, as well as their growing rates.

In Chapter 2 of this dissertation, the course of the isothermal free-radical bulk polymerization of styrene, in presence and absence of GTR, was monitored by using DSC. On the basis of the generated data, this chapter attempts to propose a mechanistic model, capable of accurately simulating the system in the absence and presence of GTR. In the following section, the kinetic model for the free-radical bulk polymerization of styrene is developed. This involves a comprehensive kinetic scheme including chemical and thermal initiation, propagation, termination and chain-transfer reactions. Chemical initiation is primarily achieved by using a single or a mixture of initiator agents (e.g. BPO, DCP, AIBN, AMBN etc.) while thermal initiation is promoted by the reversible Diels-Alder dimerization of styrene. The diffusion-controlled model proposed by Martin and Hamielec [62] related to the gel, glass and cage effect phenomena is also included. The developed kinetic model allows for the calculation of the evolution of the monomer conversion and the average properties of the chain-length distributions of the different polymer species (e.g. the number- and weight-average molecular weights) formed during the reaction, via the application of the well-established method of moments.

4.2 Experimental

4.2.1 Materials and reagents

GTR was obtained from two different suppliers, REGENE Company from Brazil and DeltaGOM from France. Both GTR are derived from the recycling of end-of-life tires of different categories (light, heavy goods and agricultural vehicles, motorcycles, etc.). Both types of GTR have the capacity to absorb about twice their initial weight in styrene. All the reagents used, namely, styrene monomer (with a purity 99.5% and stabilized with 0.005 % of 4-tert-butylcatechol), benzoyl peroxide (BPO, 75% remainder

water), dicumyl peroxide (DCP, with 98% of active mass), hydroquinone (HQ, with a purity $\geq 99\%$), tetrahydrofuran (THF anhydrous, $\geq 99\%$), chloroform ($CHCl_3$ anhydrous, $\geq 99\%$) and chloroform-D (99.8b % atom) were purchased from Sigma-Aldrich and used without further purification, except if indicated otherwise.

4.2.2 Methods

4.2.2.1 Solution styrene polymerization

Isothermal free-radical solution polymerization of styrene in toluene was carried out in a batch reactor of 1 liter capacity. The styrene monomer was purified by filtration in a column containing aluminum oxide (Al_2O_3) to remove the stabilizers before use. The ratio toluene to styrene was fixed to 1:1 (by weight). Polymerizations were performed by setting the weight ratio BPO to monomer to three different values, namely, 0.8, 1.18 or 1.22%. All polymerizations were carried out at constant temperature, set either to 80 °C (for all the studied BPO/styrene ratios) or 90 °C (for BPO/styrene = 0.8 w/w%). BPO was previously dissolved in the solvent and the mixture was introduced in the reactor and purged with nitrogen atmosphere during 20 minutes under permanent agitation. Subsequently, the monomer was added and the medium was heated to the reaction temperature at a heating rate of 2 °C /min. The reaction was performed during 4 to 5 h at a permanent stirring rate of 300 rpm. The degree of conversion was measured by gravimetry and the number- and weight-average molecular weights were determined by SEC.

4.2.2.2 Free-radical bulk polymerization in a batch reactor

For model developments and validation, two different data sets were obtained from the experiments performed in two different batch reactors. A first series of 20 experiments was carried out in a stainless-steel reactor of 1 L, under the conditions presented in Table 4.1. Two parameters were varied each time, the ratio GTR to monomer and the initiator concentration. GTR was purified with $CHCl_3$ to remove all the additives and plasticizing oils contained in the GTR formulation. The monomer solution containing the initiators was added drop-by-drop to the GTR in order to ensure a homogeneous distribution of the monomer in the granulates. Then, the medium was charged to the reactor and purged with nitrogen during the whole reaction.

Table 4.1 – Bulk polymerization conditions tested in the batch reactor of 1 L capacity

Parameter	Values
GTR/(styrene + GTR) (w/w %)	15; 17.5; 20
(BPO + DCP)/styrene (mol/mol)	0.2; 0.6; 0.76; 1
BPO/DCP (mol/mol)	0.25; 1; 1.27; 4
Temperature profile	90 °C (2.5 h), 120 °C (2.5 h)

Secondly, additional experiments were performed in a glass batch reactor of 3 L capacity. The only variable parameter was the amount of GTR in the polymerization system, as indicated in Table 4.2. For the preparation of the reacting medium, the raw GTR (without previous purification) was introduced into the reactor and mixed at high speed, while the monomer solution was atomized throughout a spraying nozzle by mixing it with compressed air. This created a cloud of micro-droplets that allowed an intimate contact with the rubber granulates, ensuring an even concentration through the medium. The reaction was performed in air atmosphere and the temperature was frequently monitored next to the reactor walls and in the center of the vessel. Monomer conversion was determined by gravimetry.

Table 4.2 – Bulk polymerization conditions tested in the batch reactor of 3 L capacity

Parameter	Values
GTR/(styrene + GTR) (w/w %)	30; 50; 70
(BPO + DCP)/styrene (mol/mol)	0.3
BPO/DCP (mol/mol)	2
Temperature profile (°C - h)	75 °C (2 h), 85 °C (3 h), 95 °C (3 h), 115 °C (1.5 h), 125 °C (1 h), 140 °C (1 h)

The average molecular weight was measured by SEC after extracting the free polystyrene with THF and precipitating it with an excess of methanol.

4.2.2.3 Monomer conversion

Monomer conversion was measured in a heating halogen balance. A sample of about 2.5 g was weighted in the aluminum pan of the balance and moisten with a known quantity (at least twice the sample mass) of HQ solution 0.5 g/ml (water/ethanol 4:1 v/v%) to inhibit further styrene polymerization during measurement. The mix was heated at 170 °C during 30 min or until constant weight.

4.2.2.4 Grafting efficiency

The amount of polystyrene grafted onto the GTR particles after the free radical polymerization was measured by Soxhlet extraction. Chloroform was used as extracting agent to remove the remaining monomer and the non grafted polystyrene from the sample. A sample of 1 g was placed into a porous thimble (cellulose) in the extraction chamber of a Soxhlet apparatus. The solvent was heated to the boiling temperature for 6 hours under reflux. The insoluble material remaining in the thimble, namely, GTR-grafted-PS, was dried under vacuum until constant weight.

4.2.2.5 Molecular weight

The number- (M_n) and weigh- average (M_w) molecular weight of free polystyrene were determined by SEC in an instrument SEC-MALS. The device is equipped with two detectors: a refractive index Obitlab REX (RI) for concentration detection and a multi-angle light scattering MALS WYATT mini dawn TREOS for absolute molecular weight measuring. Separation is performed through three columns PLgel with different pore size. Measurements were carried out at a flow rate of 1 mL/min in THF at 40 °C. Samples were extracted by Soxhlet to remove the free-PS, which was subsequently precipitated with an excess of methanol. Then, the polymer was dissolved in THF at a concentration ranging from 6 to 8 mg/mL.

4.2.2.6 Number of saturations in GTR

The concentration of double bonds of the elastomer chains of GTR was quantified according to the "Standard test method for iodine value of drying oils and fatty acids" (ASTM D-1959) [47, 108]. In this method, unsaturations are quantified by indirect titration with iodine. The measurement procedure was detailed in Chapter 3, Sect. 3.8.1.6.

4.3 Styrene homopolymerization model

4.3.1 Model developments

4.3.1.1 The kinetic mechanism

The kinetic mechanism considered in this work for the free-radical styrene polymerization is presented from Equations 4.1 to 4.14. This involves four significant reactions: initiation, propagation, termination and transfer. The initiation reaction (Eq. 4.1) considers the chemical initiation by the thermal decomposition of the initiator (I) to form free primary radicals (PR), which subsequently initiate the polymer radicals via reaction with a monomer unit (Eq. 4.2). Depending on the nature of initiator agent, this chemical initiation process can take place at significant rates even at temperatures significantly lower than 100 °C. This initiation mechanism is completed by the thermal initiation of styrene that becomes important mainly at temperatures above 100 °C [118, 120]. This mechanism includes the reversible Diels-Alder dimerization of the styrene molecule (Eqs. 4.3) that forms the adduct (AH), an intermediate species. This can subsequently react with M to form other intermediate products as styryl (MR) and 1-phenyltetralyl (AR) radicals (Eqs. 4.4) that at the same time, can further react with M (Eqs. 4.5 and 4.6) and initiate new radical chains, denoted R_2 and R_3 , respectively. The reaction of AH with M (Eq. 4.7) gives a short "dead" molecule or trimer (D_3).

In the propagation stage, the reaction proceeds by the successive addition of M to the radicals, generated according to the previously described mechanism. The active growing polymer species are denoted as "live" chains (R_n), whose propagation takes place very rapidly (Eq. 4.8). The active radical centers can be transferred to another molecule such as M a/o AH (Eqs. 4.9 and 4.10, respectively), producing new chain initiating radicals and polymer chains that stop growing, denoted as "dead" polymer chains (D_n). At the same time, these polymer chains can be also attacked by primary radicals, resulting in their scission to two shorted polymer chain segments (Eq. 4.11), a "live" one and a "dead" one. In the termination reactions, the propagating radicals in styrene polymerization are almost exclusively terminated by the combination of two polymer radicals (Eq. 4.12) and by reaction with primary radicals (Eq. 4.14). Less commonly for this system, growth chains can also terminate by disproportionation through the transfer of a hydrogen radical (Eq. 4.13) [63]. In this kinetic scheme, only the reaction of chain-transfer to polymer molecules was considered negligible since indication of their occurrence (i.e., related to the formation of branched polymer molecules) has been reported for this radical polymerization system.

Chemical initiation:



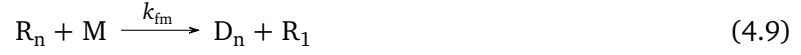
Thermal initiation:



Propagation:



Chain transfer to monomer:



Chain transfer to AH (adduct):



Scission:



Termination by combination:



Termination by disproportionation:



Termination by primary radicals:



4.3.1.2 Polymerization rate functions

The polymerization rate functions of the formation and consumption of the reactants can be obtained from their mass balances, on the basis of the chemical scheme above. The properties of each type of polymer populations such as the molecular weight, can be obtained by writing the mass balance equations for all possible chain lengths. This could lead, for example, to predict the full molecular weight distribution. Nevertheless, this requires a set of infinite number of differential equations that is numerically difficult to solve.

Equations 4.15 and 4.16 present the rate functions of the macromolecular species in the system, which correspond to the "live" and "dead" polymers of chain length "n", represented as R_n and D_n , respectively. All rate functions are expressed in molar concentration over time units (e.g. $mol \cdot l \cdot s^{-1}$), and the species molar concentrations are denoted in brackets [.]. The *quasi-steady state approximation* (Q.S.S.A.) has been adopted for rate functions of both types of primary radicals, PR and AH .

Rate of "live" polymer chains:

$$\begin{aligned} rR_n = & \left[k_I[PR][M] + k_{fm}[M] \sum_{k=1}^{\infty} [R_k] \right] \cdot \delta(n-1) \\ & + k_A[AR][M] \cdot \delta(n-3) + k_B[MR][M] \cdot \delta(n-2) + k_p[M]([R_{n-1}] - [R_n]) \\ & - (k_{fm}[M] + k_{fAH}[AH])[R_n] + k_S[PR] \sum_{k=n+1}^{\infty} [D_k] \\ & - (k_{tc} + k_{td})[R_n] \sum_{k=1}^{\infty} [R_k] - k_{tPR}[PR][R_n] \end{aligned} \quad (4.15)$$

Rate of "dead" polymer chains:

$$\begin{aligned}
rD_n = & k_c[AH][M] \cdot \delta(n-3) + (k_{fm}[M] + k_{fAH}[AH])[R_n] - k_S[PR](n-1)[D_n] \\
& + k_S[PR] \sum_{k=n+1}^{\infty} [D_k] + \frac{1}{2}k_{tc} \sum_{k=1}^{n-1} [R_k][R_{n-k}] + k_{tPR}[PR][R_n] \\
& + k_{td}[R_n] \sum_{k=1}^{\infty} [R_k]
\end{aligned} \tag{4.16}$$

where $\delta(n)$ denotes the Kronecker's δ function as follows:

$$\delta(n-i) = 1 \text{ for } n = i \text{ or } 0 \text{ for } n \neq i \tag{4.17}$$

4.3.1.3 Moment rate functions

In order to reduce the infinite-order system of the rate functions to a simpler subset of equations, the method of moments is implemented. This strategy allows to calculate and compare the average properties of each polymer type, instead of predicting the properties of the individual chains [134]. The moments of the chain-length distributions of the "live" system and "dead" polymer chain populations, denoted by λ_k and μ_k respectively, are defined as follows:

$$\lambda_k = \sum_{n=1}^{\infty} n^k [R_n] \tag{4.18}$$

$$\mu_k = \sum_{n=1}^{\infty} n^k [D_n] \tag{4.19}$$

The moment rate functions are obtained by multiplying the respective rate functions (c.f. Eqs. 4.15 and 4.16) by n^k and summing over all values of n . Equations 4.20 and 4.21 present the developed moment balances for the "live" and "dead" polymer chains, respectively.

Moments of the "live" polymer chains

$$\begin{aligned}
r\lambda_k = & k_I[PR][M] + 3^k k_A[AR][M] + 2^k k_B[MR][M] + k_{fm}[M]\lambda_0 \\
& + k_p[M] \left(\sum_{r=0}^k \binom{k}{r} \lambda_r - \lambda_k \right) - (k_{fm}[M] + k_{fAH}[AH])\lambda_k \\
& + k_S[PR]T_1 - (k_{tc} + k_{td})\lambda_0\lambda_k - k_{tPR}[PR]\lambda_k
\end{aligned} \tag{4.20}$$

Moments of the "dead" polymer chains

$$\begin{aligned}
r\mu_k = & 3^k k_c[AH][M] + (k_{fm}[M] + k_{fAH}[AH])\lambda_k - k_S[PR](\mu_{k+1} - \mu_k) \\
& + k_S[PR]T_1 + \frac{1}{2}k_{tc} \sum_{r=0}^k \binom{k}{r} \lambda_r \cdot \lambda_{k-r} + (k_{td}\lambda_0 + k_{tPR}[PR])\lambda_k
\end{aligned} \tag{4.21}$$

where the term T_1 corresponds to the following expression, in which B_m is the Bernoulli number series [$B_0 = 1; B_1 = -1/2; B_2 = 1/6, \dots$]:

$$T_1 = \sum_{m=0}^k \frac{B_m}{k-m+1} (\mu_{k-m+1} - \mu_0) \tag{4.22}$$

Finally, the Zabinsky's closure technique [135], is applied to solve the closure problem of the "dead" polymer moment balances derived from the scission reaction (Eq. 4.11).

$$\mu_3 = \mu_0 \left(\frac{\mu_2}{\mu_1} \right)^3 \quad (4.23)$$

4.3.1.4 Reactor design equations

Once the moments of the principal polymer populations are known, the design equations of the batch reactor are written to complete the mathematical model. From the kinetic scheme, the mole balances for the generation and consumption of the species, at any time instant, t , are given by Equations 4.24 to 4.31. These involve the chemical initiators, monomer, primary radicals and the other intermediate radicals, AH , AR and MR . The system volume V (Eq. 4.32) varies during the reaction with the production of the polymer chains, affecting the rate of formation of all species.

Initiator:

$$\frac{1}{V} \frac{d(V \cdot I)}{dt} = -k_d \cdot [I] \quad (4.24)$$

Monomer:

$$\begin{aligned} \frac{1}{V} \frac{d(V \cdot M)}{dt} = & 2k_{-1}[AH] - 2k_1[M]^2 - (k_I[PR] + k_2[AH] + k_A[AR] \\ & + k_B[MR] + k_c[AH] + k_p\lambda_0 + k_{f_m}\lambda_0)[M] \end{aligned} \quad (4.25)$$

Primary radical, PR:

$$\frac{1}{V} \frac{d(V \cdot PR)}{dt} = 2fk_d[I] - (k_I[M] + k_S\mu_0 + k_{tPR}\lambda_0)[PR] \quad (4.26)$$

Diels-Alder adduct, AH:

$$\frac{1}{V} \frac{d(V \cdot AH)}{dt} = k_1[M]^2 - k_{-1}[AH] - ((k_2 + k_c)[M] + k_{f_a}\lambda_0)[AH] \quad (4.27)$$

Styryl radical, MR:

$$\frac{1}{V} \frac{d(V \cdot MR)}{dt} = k_2[AH][M] - k_B[MR][M] \quad (4.28)$$

1-Phenil tetraryl radical, AR:

$$\frac{1}{V} \frac{d(V \cdot AR)}{dt} = k_2[AH][M] - k_A[AR][M] + k_{f_a}\lambda_0[AH] \quad (4.29)$$

'Live' and 'dead' polymer chain moments:

$$\frac{1}{V} \frac{d(V \cdot \lambda_k)}{dt} = r \cdot [\lambda_k] \quad (4.30)$$

$$\frac{1}{V} \frac{d(V \cdot \mu_k)}{dt} = r \cdot [\mu_k] \quad (4.31)$$

Reactor volume, V :

$$\frac{1}{V} \frac{dV}{dt} = r_M \left(\frac{1}{d_m} - \frac{1}{d_p} \right) MW_m \quad (4.32)$$

where d_m and d_p are the monomer and polymer density, respectively, r_M is the monomer reaction rate (cf. 4.25) and MW_m is the molar mass of the monomer.

4.3.1.5 Polymer properties

The conversion yield of monomer into polymer is calculated from the expression in Equation 4.33. Moreover, based on the zeroth (μ_0, λ_0), first (μ_1, λ_1) and second (μ_2, λ_2) moments, M_n and M_w are given by the Equations 4.34 and 4.35. The zeroth and first moments are theoretically related the concentration and the mass of the polymer chains, respectively [134]. The course of the reaction is described by calculating these properties at each instantaneous time t .

Monomer conversion, x :

$$x = \frac{V_0[M_0] - V[M]}{V_0[M_0]} \quad (4.33)$$

Number- and weight-average molecular weights of free polymer:

$$M_n = \frac{\mu_1 + \lambda_1}{\mu_0 + \lambda_0} MW_m \approx \frac{\mu_1}{\mu_0} MW_m \quad (4.34)$$

$$M_w = \frac{\mu_2 + \lambda_2}{\mu_1 + \lambda_1} MW_m \approx \frac{\mu_2}{\mu_1} MW_m \quad (4.35)$$

4.3.1.6 Diffusion controlled reactions

As polystyrene production progresses, the viscosity of the reacting medium increases and the mobility of the polymer species is reduced. In radical polymerization of some monomers such as styrene, the evolution in time of the rate of polymerization, under isothermal reaction conditions, is characterized by diffusion-controlled phenomena [136–138]. These are designed as the gel, glass and cage phenomena, which are related to termination of "live" radicals, propagation of these "live" growing polymer chains and initiation reactions, respectively [138].

The diffusion phenomena, affecting the above-mentioned kinetic rate constants, can be explained on the basis of the free volume theory and involves four stages, quantified with the Equations 4.36 to 4.50. At low monomer conversions (1st stage), the free volume of the reaction system is high and the radical chains move by *translational diffusion*. Nevertheless, the encounter of two radical ends and the chemical reaction between them, which is performed by *segmental diffusion*, is diffusion-controlled. Afterwards, the viscosity of the reacting medium increases due to the augmentation of the concentration of long polymer chain radicals, until the free volume reaches a critical value (i.e. when $K = K_{cr}$). During the gel effect (2nd stage), the diffusion of these chains is reduced and their termination rate becomes slower. Since the motion of the smaller monomer units is less hindered, these are rapidly consumed at accelerated polymerization rate. When the system reaches a very high conversion yield the total free volume of the system decreases to a critical free volume, $V_{f,crm}$. The glass effect appears (3rd stage) if the polymerization temperature is inferior than the T_g of the polymer formed. Under this condition, k_p is affected and begins to decrease. The cage effect (4th stage) takes place at the highest viscosity levels, when the initiator is surrounded and caged by the macromolecular polymer chains and cannot diffuse, leading to an increase of the rate of bi-radical deactivation reactions, expressed in the model by a decrease in the value of the efficiency factor, f .

First stage of diffusion control

$$k_{t,seg} = k_{t0}(1 + \delta_c C_p MW_m) \quad (4.36)$$

Second stage of diffusion control - gel effect

$$K = M_w^{0.5} \cdot \exp\left(\frac{A}{V_f}\right) \quad (4.37)$$

$$K_{cr} = A_{cr} \cdot \exp\left(\frac{E_{cr}}{RT}\right) \quad (4.38)$$

$$V_f = [0.025 + \alpha_p(T - T_{gp})] \frac{V_p}{V_t} + [0.025 + \alpha_m(T - T_{gm})] \frac{V_m}{V_t} \quad (4.39)$$

$$k_T = k_{t0} \left(\frac{M_{wrc}}{M_w}\right)^n \cdot e^{\left(\frac{A}{1/V_f,cr-1/V_f}\right)} \quad (4.40)$$

$$k_{t,rd} = k_{t,rd,min}X + k_{t,rd,min}(1 - X) \quad (4.41)$$

$$k_{t,rd,min} = 10^3 \cdot A_{min}k_{p,eff}[M]N_{av} \quad (4.42)$$

$$k_{t,rd,max} = 10 \cdot A_{min}k_{p,eff}[M]N_{av} \quad (4.43)$$

$$A_{min} = \frac{4}{3} \pi \sigma \delta^2 \quad (4.44)$$

$$A_{max} = \frac{8}{3} \pi \delta^3 j c^{0.5} \quad (4.45)$$

$$k_{t,eff} = \left(\frac{1}{k_{t,seg} + \frac{1}{k_T}}\right)^{-1} + k_{t,rd} \quad (4.46)$$

Third stage of diffusion control - glass effect

$$V_{f,crm} = A_{crm} \cdot \exp\left(\frac{E_{crm}}{RT}\right) \quad (4.47)$$

$$k_{p,eff} = k_{p0} \cdot \exp\left[-B\left(\frac{1}{V_f} - \frac{1}{V_{f,crm}}\right)\right] \quad (4.48)$$

Fourth stage of diffusion control - cage effect

$$C_{rRatio} = \frac{V_{f,creff}}{V_{f,crm}} \quad (4.49)$$

$$f_{i,eff} = f_{io} \cdot \exp\left[-C\left(\frac{1}{V_f} - \frac{1}{V_{f,creff}}\right)\right] \quad (4.50)$$

In the expressions above, δ_c is the segmental diffusion parameter for styrene, C_p is the concentration of polymer in the system, m and P denote the monomer and polymer, respectively; T is the polymerization temperature (K); V is the reactor volume and V_t is the total volume ($V_m + V_p$) of the system (L).

4.3.1.7 Kinetic rate constants

The model parameters include the kinetic rate constants of the set of chemical reactions and the diffusion-controlled mechanism. In order to consider the influence of the temperature variations on the reaction rates, the rate constants are expressed as Arrhenius-type functions, in terms of the activation energy E_a and the pre-exponential factor k_0 , as follows:

$$k = k_0 \cdot \exp\left(\frac{-E_a}{RT}\right) \quad (4.51)$$

Parameter estimation requires first to identify and rank those inducing major changes on model predictions. According to Woloszyn et al. [125, 126], the evolution of both the monomer conversion and

Table 4.3 – Final estimated pre-exponential and activation energies used in styrene polymerization model.

Parameter	Pre-exponential factor (s^{-1})*	Activation energy ($kCal \cdot mol^{-1}$)	Reference
$k_{d,BPO}$	2.2896E+14	27.233	this work
$k_{d,DCP}$	5.50E+17	36.65	this work
k_1	4.38E+08	26.440	[124]
k_{-1}	6.84E+03	13.533	[124]
k_2	9.8E+07	23.883	[124]
k_A	1.149E+09	7.5126	this work
k_B	1.149E+09	7.5126	this work
k_C	2.36E+06	21.346	[124]
k_p	1.149E+09	7.5126	this work
k_{fm}	1.0324E+07	10.545	this work
k_{fAH}	7.36E+07	30.800	this work
k_{tc}	7.404E+10	1.6632	[124]
k_{td}	7.53E+10	1.677	[124]

molecular weight in function of the reaction time, is mainly influenced by the variation of the parameters related to the chemical initiation, transfer to adduct and the onset of the gel effect [125, 126].

A preliminary sensitivity analysis of the most influencing parameters of the model, carried out in this work, concluded to similar results with the ones indicated by Woloszyn et al., (2013) [126]. Then, the values of the top list parameters were adjusted through hand tuning, by comparing the simulation predictions of conversion and molecular weight with experimental data obtained from numerous experimental data produced in this work (c.f. Section 4.2.2). Relevant literature reported values of rate constants were used as starting points for parameter estimation [62, 124–126]. Conversion measurements were primarily used to tune the initiation- and propagation-related constants, while the *MW* measurements were mainly used to tune the constants of the transfer and termination reactions.

Parameter estimation concluded to the single set of values of E and k_0 listed in Table 4.3, which was used for all the simulations in this work. The column at right indicates if the value was held as reported in the literature, and in this case the reference is indicated, or otherwise, if the value was adjusted in this work.

The literature values of the physical and transport parameters, associated to the diffusion-controlled mechanism, are reported in Tables 4.4 and 4.5 [124, 139].

4.3.2 Results and discussion

4.3.2.1 Free-radical bulk polymerization

In Figure 4.1, the course of the isothermal free-radical bulk polymerization of styrene is plotted at 85 °C, 90 °C and 120 °C at a constant ratio BPO to styrene of 4.6 wt%. Model predictions (solid continuous lines) are compared with the experimental measurements (discrete points) obtained through monitoring the reaction by DSC (Chapter 2). Results of the simulations show that the developed model and the set of estimated parameters proposed above, lead to describe with accuracy the evolution of the overall polymerization system over the range of temperatures tested. At 80 and 90 °C, the gel effect is evidenced at conversions around 55%. The model trends for the number- and weight-average molecular

Table 4.4 – Diffusion control parameters in styrene polymerization model.

Parameter	Value	Units	Reference
α_m	1.40E-03	K^{-1}	this work
α_p	4.8E-04	K^{-1}	[126][62]
A	0.4315	unitless	this work
n	2.5	$cal \cdot mol^{-1}$	[126][62]
E_{crm}	1670	$cal \cdot mol^{-1}$	this work
A_{crm}	0.231	unitless	this work
B	0.7	unitless	this work
C_{rRatio}	0.8	unitless	[126]
C	$0.9 \cdot B$	unitless	this work
jc	175	num	[126][124]
δ	3.8E-09	$m \cdot num^{-0.5}$	this work
σ	3.7E-09	m	this work
δ_c	5.0E-04	$L \cdot g^{-1}$	[126]
A_{cr}	9.0	$(g \cdot mol^{-1})^{0.5}$	this work
E_{cr}	$1960 \cdot R$	K^{-1}	this work
f	0.65	unitless	this work

Table 4.5 – Physical properties of styrene and polystyrene

Parameters	Units
$d_m = 0.9236 - 0.887 * 10^{-3}(T - 273.15)$	$g \cdot cm^{-3}$
$d_p = 1.085 - 6.05 * 10^{-4}(T - 273.15)$	$g \cdot cm^{-3}$
$d_{IBPO} = 1.16; d_{IDCP} = 1.56$	$g \cdot cm^{-3}$
$k_B = 1.3806488 * 10^{-23}$	$m^2 \cdot kg \cdot s^{-2} \cdot K^{-1}$
$T_{gm} = 185; T_{gp} = 378$	$^{\circ}C$

weights are shown in Figure 4.2 (not experimental data available). Both M_n and M_w present a marked increase starting at the onset of the autoacceleration.

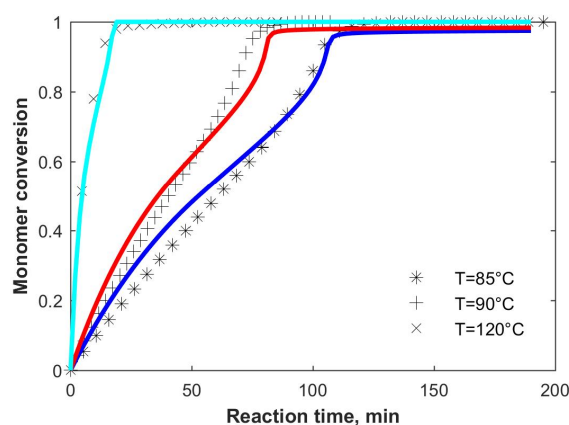


Figure 4.1 – Predicted (—) and DSC monitored monomer conversion (symbols) in function of time during the isothermal free-radical bulk polymerization of styrene by using a ratio BPO to styrene of 4.6 wt%.

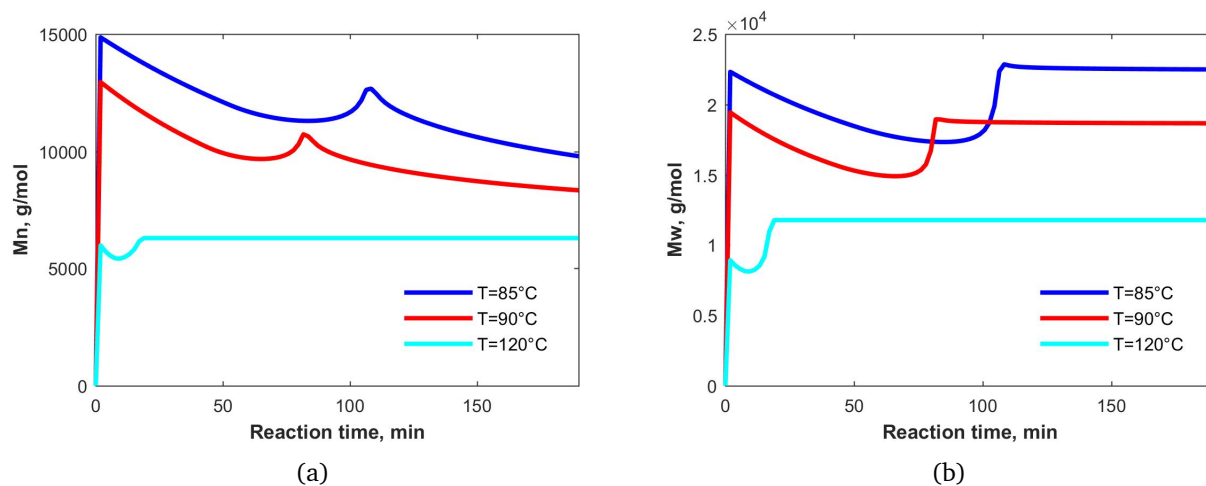


Figure 4.2 – Predicted evolution of M_n and M_w of polystyrene during the isothermal free-radical bulk polymerization of styrene by using a ratio BPO to styrene of 4.6 wt%.

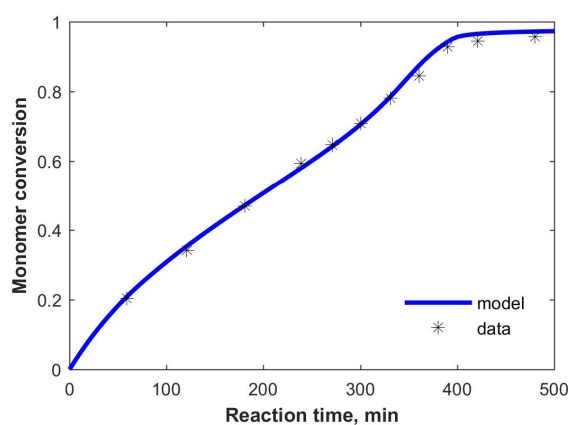


Figure 4.3 – Comparison of predictions (—) and experimental measurements (*) of the conversion history of the bulk polymerization of styrene at 90 °C initiated with 0,29 wt% of BPO. Experimental data from Villalobos et al. (1993) [140]

The capability of the model to describe the experimental results reported in two relevant literature studies is also proved. Data from Villalobos et al. (1993), on the styrene bulk polymerization, initiated at 90 °C, with BPO (0,29% by weight) are used for this purpose [140]. As evidenced in Figure 4.3 and 4.4, the agreement between experimental and reported data at 90 °C is quite satisfactory with respect to both the conversion and the evolution of the average molecular weights in function of monomer conversion.

In other publication, Kotoulas et al. (2003) [124], reported the experimental data on monomer conversion and average molecular weight of the isothermal free-radical bulk polymerization of styrene at different temperatures (i.e. 120, 130, 140 and 150 °C) by using DCP as initiator agent (0,4 wt%). Figure 4.5 compares reported monomer conversion in function of time with the respective predictions of the model developed in this work, at two temperatures, namely, 120 and 150 °C. The agreement between model predictions and data set at 150 °C is good for the evolution of both conversion and molecular weight. Nevertheless, in contrast to model predictions presented by the authors, the deviations between predicted and reported monomer conversion at 120 °C and high yield percentages are more important and matching between curves comparing the molecular weight is rather poor. This may be due to the experimental errors associated to the measurement of M_n and M_w by SEC, as mentioned by the authors.

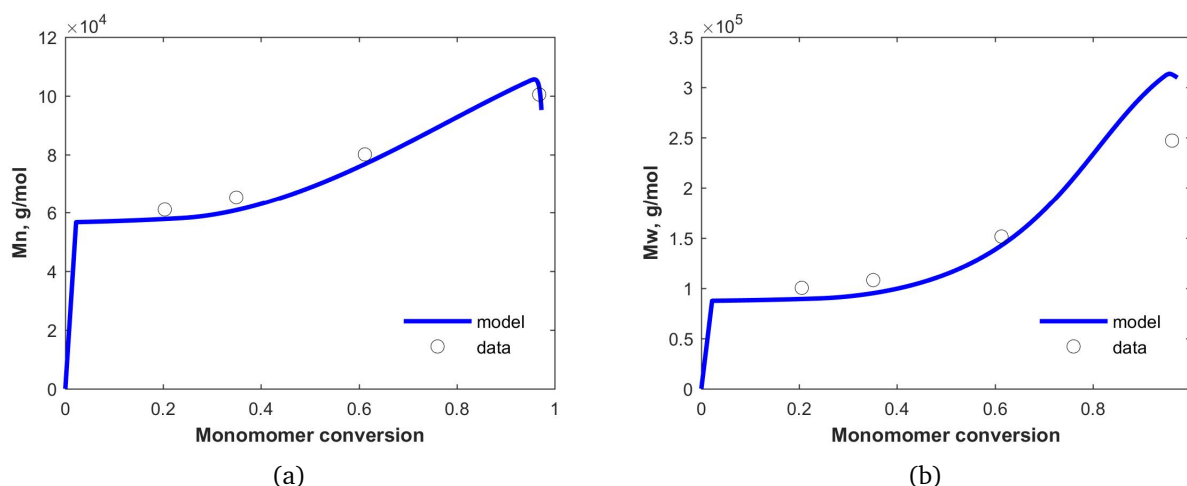


Figure 4.4 – Model predictions (—) and experimental measurements (○) of the evolution of M_n and M_w of during the BPO initiated bulk polymerization of styrene at 90 °C . Experimental data from Villalobos et al. (1993), [140]

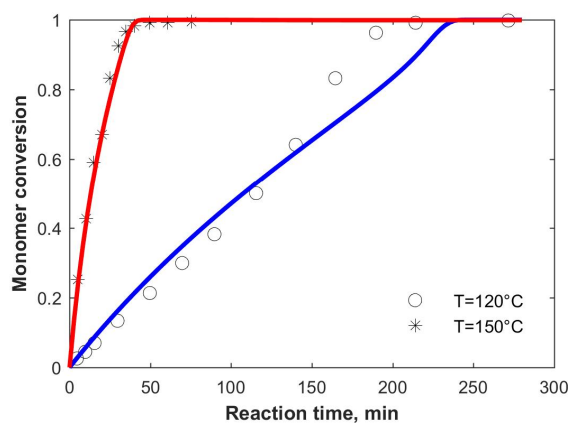


Figure 4.5 – Predicted (—) and experimental data of conversion evolution in time of the bulk polymerization of styrene at 120 °C (○) and 150 °C (*) initiated with 0,29 wt% of BPO. Experimental data from Kotoulas et al. (2003) [124]

4.3.2.2 Free-radical solution polymerization

Experimental data produced by isothermal styrene polymerization, produced in toluene, was also used for model validation. The polymerization was performed in a batch reactor and by varying the BPO concentration, as detailed in section 4.2.2.1. The experimental results of the ultimate monomer conversion and the average molecular weights, for the reaction at 80 °C with 1,22 and 1,8 wt% of BPO, are compared with model predictions in Figures 4.7 and 4.8, respectively. Since the solvent acts as diluent, the viscosity of the reacting medium remains much lower than in the bulk system and thus, the translational diffusion of the growing polymer is less disturbed. As a consequence, the overall polymerization rate slightly falls close to the end of the reaction time (240 min) along with the decrease of monomer and initiator concentrations, as described by model results. The overall rate of reaction increases with initiator concentration, as expected. The ultimate conversion “reached at the end of the measuring time” matches well with the experimental data at both initiator contents. Moreover, it is noticed from the evolution of the polymer molecular weight that the gel-effect did not occur during the reaction time.

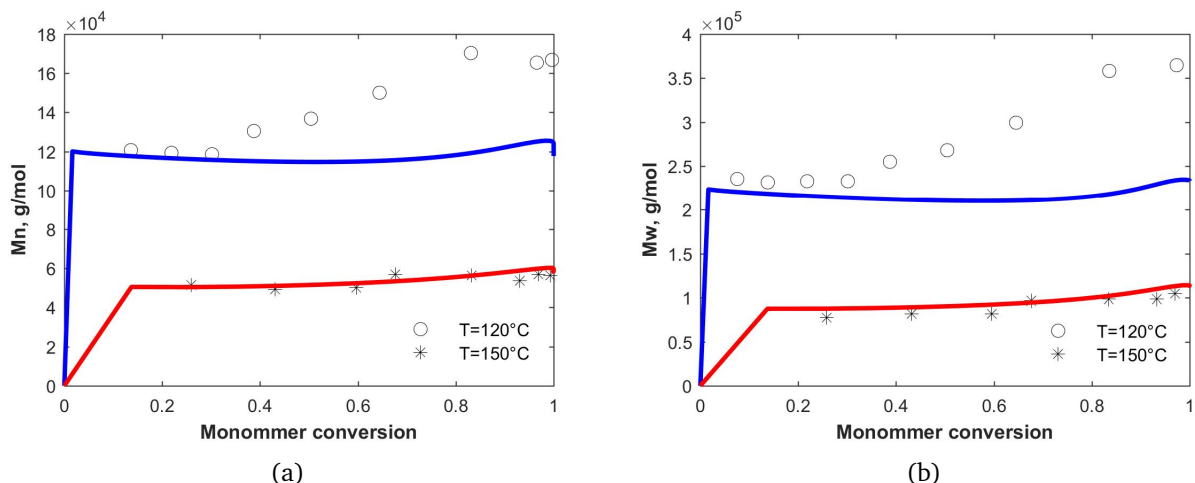


Figure 4.6 – Predicted (—) and experimental M_n and M_w of the bulk polymerization of styrene at 120 °C (○) and 150 °C (*) initiated with 0,29 wt% of BPO. Experimental data from Kotoulas et al. (2003) [124]

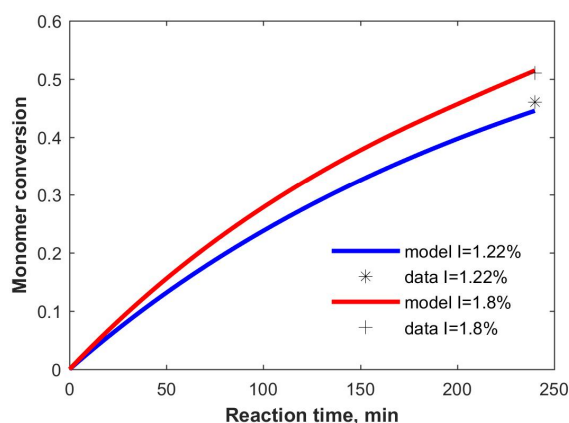


Figure 4.7 – Predicted evolution (—) and experimental ultimate conversion of the free-radical solution polymerization of styrene in toluene (weight ratio styrene to solvent 1:1) at 80 °C with two different contents of BPO (*) 1,22 wt% and (+) 1,8 wt%.

At the lowest BPO content (i.e. 1,22 wt%), the predicted trends of M_n and M_w are in good agreement with the experimental values, in contrast to the small deviations noticed when increasing the amount of BPO.

4.3.3 Conclusions

The purpose of this section was to present the mechanistic kinetic model proposed to describe the free-radical polymerization of styrene. This model combines both the chemical and thermal initiation, and accounts for diffusion-controlled initiation, propagation, termination and chain transfer reactions. By implementing reliable data of the overall course of the bulk polymerization of styrene obtained through DSC monitoring, it was possible to adjust the model parameters ensuring a satisfactory matching of the changes in the polymerization rates at all stages of the reaction. The model developed and the updated set of model parameters proposed in this work, is capable of predict solution and bulk polymerization systems over different conditions of temperature and initiator concentration, and show accurate agreement with the experimental data reported in relevant literature.

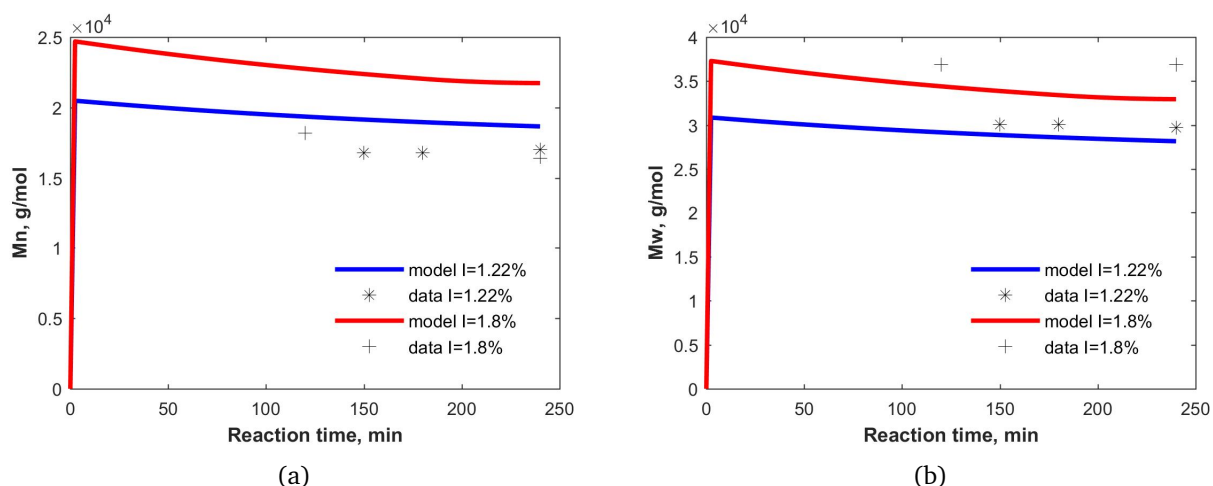


Figure 4.8 – Predicted trends (—) and experimental measurements of M_n and M_w of the polystyrene formed during the BPO initiated radical solution polymerization of styrene at 80 °C with different amount of BPO (\ast) 1,22 wt% and (+) 1,8 wt%. The ratio toluene to styrene was fixed to 1:1 (by weight).

4.4 Styrene grafting polymerization onto GTR model

4.4.1 Introduction

The mechanical properties of polystyrene may be enhanced by the integration of dispersed rubber particles such as GTR. For this purpose, strong interfacial interactions between both GTR and PS have to be created since these are incompatible phases. In this respect, the surface of GTR is usually modified to promote the interfacial adhesion with the polymer matrix. Grafting the polymer directly onto the surface of the recycled rubber particles, is one of the most widely and low cost strategies implemented for effective interfaces compatibilization [10, 11, 17]. This is achieved by performing the free-radical polymerization of styrene *in-situ* with peroxide initiator agents.

4.4.1.1 Synthesis experiments in a batch reactor

Free-radical bulk polymerization of styrene in presence of GTR is chemically initiated by the action of a peroxide agent such as BPO or DCP, or a mix of them, as mentioned above. The reaction occurs on the bulk monomer and on the surface of the GTR particles, and two main parallel and competitive reactions take place, producing grafted PS chains onto/into GTR and non-grafted PS chains or free-PS. Both polymer populations have distinct characteristics and properties. Polystyrene grafting is achieved in two consecutive steps. First, active radicals are created on the GTR backbone. Second, the polymerization is mainly promoted (besides some transfer phenomena) by the propagation of these grafted radicals (via monomer addition) [28, 56, 132]. Therefore, by stimulating polymer grafting, quantified in terms of GE , it is possible to strengthen the particle-polymer interfaces.

In contact with styrene, GTR is able to absorb a certain amount of monomer. The critical absorption threshold varies according to the GTR composition and it is about 2. When the styrene/GTR ratio is less than this value, the monomer migrates completely inside the particles swelling them. By contrast, when the styrene/GTR ratio exceeds the critical threshold, the particles get saturated and the excess of monomer remains outside. Therefore, depending on the styrene/GTR ratio in the system, the polymerization proceeds exclusively inside or in both inside/outside the rubber particles.

Numerous experiments have been performed to study this polymerization system in a batch reactor

and over a wide range of composition and temperature conditions, as described in Section 4.2.2.2. A total of 50 runs were carried out under isothermal (between 70 and 110 °C) and non-isothermal conditions (ranging from 70 to 140 °C). The polymerization systems, loaded with 15 to 70 wt% of GTR, were chemically initiated by using two peroxide initiator agents, namely BPO or DCP, either individually or combined at different concentrations (i.e., 0.2 to 3.0 mol/mol % of styrene). From the results of monomer conversion and molecular weight obtained from the series of reactions, the following worth noting conclusions were drawn:

- Styrene polymerization in presence of GTR is never complete. The evolution of the monomer conversion in function of time decreases along with increasing the GTR content.
- The ultimate monomer conversion increases under non-isothermal conditions and by using the mix of peroxide initiator agents.
- The number- and weight-average molecular weights of free PS decrease when increasing the amount of GTR.
- When the styrene/GTR ratio is superior to the critical threshold, the excess of monomer solution remaining outside the particles forms a continuous phase, in which the rubber particles are dispersed. Therefore, the reacting medium may be considered as homogeneous.
- When the styrene/GTR ratio is below the critical threshold, the polymerization takes place almost exclusively inside the particles and no continuous phase is formed. As a consequence, the reacting medium is rather heterogeneous and temperature distribution through the reactor is not uniform.

4.4.1.2 DSC measurements

In an effort to better understand the phenomena observed from batch reactor experiments, the radical styrene polymerization system in presence of GTR was monitored by DSC (Chapter 2). This study produced results which corroborate the earlier experimental findings above. It was demonstrated that GTR has a negative effect on the overall course of the free-radical styrene polymerization when using a peroxide initiator such as BPO. Moreover, it may have a positive or negative influence on the rate of polymerization and the effects are more pronounced with increasing the GTR content.

These findings have been mainly attributed to the chemical interactions taking place between the peroxide radicals and the additives contained in the formulation of GTR, in particular with the reinforcing carbon black "CB" agent. The series of factors that have been identified to explain such phenomena are summarized in the following items:

- Existence of competitive reactions between the dissociated BPO radicals with the additives present in the formulation of GTR. The surface of CB is mainly covered with oxygen-containing groups and some of the carbon atoms have unsatisfied valences, leading to high electron transfer. In addition, other additives such as stabilizers and antioxidants, have the function of radical scavengers. Therefore, the interactions with the peroxide radicals give rise to new high or low active radical sites on the CB surface to which the primary radicals and growing radical polymers compete to react.
- Oxidation-reduction of the peroxide initiators when they get in contact with the functionalized surface of CB. The redox decomposition produces new active radicals on the CB surface that may react with the intermediate radical species participating in the reaction. The catalytic dissociation of the peroxides through redox reactions is favored at lower activation energies (i.e., 40-60 kJ/mol) than thermal decomposition (i.e., 120-150 kJ/mol).

- Inhibition and retardation of the styrene polymerization system when this is chemically initiated with peroxide agents such as BPO. Since the dissociated peroxide radicals display a higher affinity towards GTR rather than the monomer, the overall polymerization rate and ultimate monomer conversion are negatively affected.
- Mobility limitation of the macromolecular radical species participating in the polymerization. Similarly to the gel effect, the three-dimensional cross-linked network of GTR may affect the translational diffusion of the long radical species. Consequently, this induces earlier diffusion-controlled termination reactions and therefore, leads to a precipitated acceleration of the polymerization rate.

The results of the study demonstrated that the formulation and crosslinked structure of GTR can produce various and sometimes even antagonistic effects, annulling one another, within the polymerization system. As a consequence, it is very difficult to identify the extent, or even the existence, of each effect individually.

4.4.1.3 Oxidation-redox reactions between CB and peroxide initiators BPO/DCP

In systems involving redox initiation, typically, only one radical per oxidant-reductant pair is produced [63]. With regard to BPO, it has been suggested that fast redox dissociation is mainly due to the direct transfer of an unpaired electron from the CB surface, which causes the scission of the $-O-O-$ bond. This produces one anion radical trapped on the CB surface and one free radical. It is uncertain the portion of free radicals that initiate polymerization, since they may be also captured instantaneously after the redox dissociation and before reaching the bulk monomer [60, 63].

By contrast to BPO, it has been reported that oxidation-reduction reaction of DCP is much slower when in presence of CB [60]. This has been attributed to differences in their chemical structure. In fact, BPO possesses two electron-withdrawing groups $[-CO-]$ that draw electrons (e^-) away from the reaction center (left Fig. 4.9). As a consequence, this decreases the e^- density of the molecule, favoring e^- transfer towards the $-O-O-$ bond. By contrast, DCP substituents $[-C(CH_3)_2]$ are e^- donating groups that release e^- to the reacting center. This increases e^- density and creates steric effects (Fig. 4.9 right), slowing down oxidation-reduction reactions.

Although the redox decomposition of DCP is almost negligible compared with BPO, the polymerization may be strongly inhibited in comparison to the case where a non-peroxide agent, as AMBN, is used (c.f. Chapter 2). In the absence of radicals production by redox, the active sites on the CB surface are not occupied by peroxide anion radicals, as for example, during BPO dissociation. As a result, these are vacant to capture the cumyloxy radicals produced by the thermal dissociation of DCP and the growing polymer chains.

4.4.2 Model developments

From the extended experimental studies performed in the batch reactors and the kinetic study using DSC, it is clear that the free-radical polymerization of styrene in the presence of GTR is a system that presents a complex kinetic mechanism that has not been completely elucidated. Therefore, modeling of this system is such an ambitious and complex task in terms of the kinetic scheme definition and model parameters estimation.

On the basis of the model developed above for the bulk free-radical styrene polymerization, a comprehensive kinetic model of the free-radical grafting polymerization of styrene onto GTR has been developed. This model takes into account the aforementioned phenomena related to the reactions of grafting, redox initiation and inhibition, via transfer to the CB surface. It consists of an initial approach to describe, for the first time, the kinetic developments of this complex polymerization system in a complete

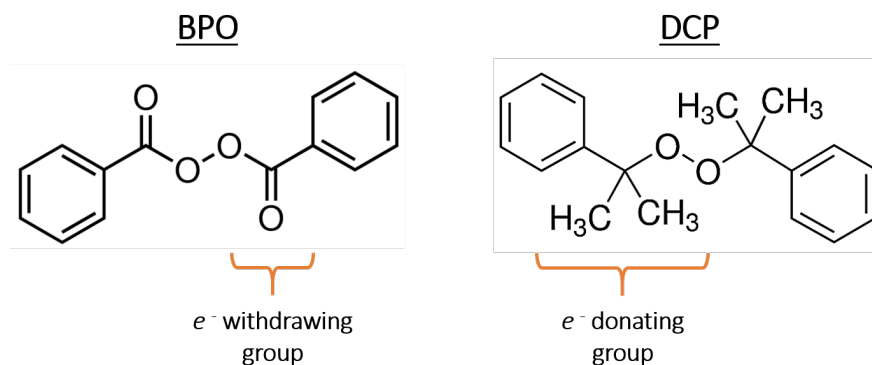


Figure 4.9 – Electron withdrawing groups in BPO (left) and electron release substituents in DCP (right)

mechanistic model, on the basis of the experimental observations and relevant literature indications. At the same time, specific assumptions have been adopted with respect to the system homogeneity. Finally, by no means does this approach constitute a detailed kinetic analysis of all possible chemical reactions of the system, but rather an attempt to model the polymerization system on the basis of lumped reaction developments. All these adopted assumptions are further elaborated in section 4.4.2.7.

4.4.2.1 The kinetic mechanism

The postulated free-radical polymerization kinetic scheme for the grafting polymerization of styrene onto/into GTR accounts for the following reactions:

- The chemical reactions of the styrene homopolymerization model, as described previously in Eqs. 4.1 to 4.14 and which are written in black.
- Reactions taking place on the surface and inside GTR (denoted here as G) and marked in green. G is considered into the model as a quantity proportional to the molar concentration of GTR double bonds, which are prompt to create grafted-radicals according to the mechanism described previously.
- A set of reactions that can occur on the functionalized surface of carbon black "CB" and written in red. In this case, "CB" represents the active sites (unpaired e^- and oxygen-containing groups) capable of interacting with initiators and radical species participating in the polymerization.

Chemical initiation:



Thermal initiation:



Propagation of homo-polymerization:



Propagation of graft-polymerization:



Chain transfer to monomer:



Chain transfer to GTR:



Chain transfer to CB:



Chain transfer to AH (Diels-Alder adduct):



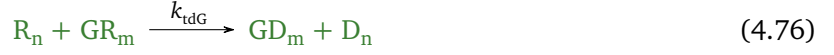
Scission:



Termination by combination:



Termination by disproportionation:



Termination by primary radicals:



4.4.2.2 Polymerization rate functions

According to the kinetic scheme above, the net production and consumption rate functions of the participating molecular species can be established. The rate functions of both the "live" and "dead" of free and grafted polymer are defined as follows:

Rate of "live" polymer chains (radicals):

$$\begin{aligned} rR_n = & \left[k_I[PR][M] + k_{fm}[M] \sum_{k=1}^{\infty} [R_k] \right] \cdot \delta(n-1) \\ & + k_A[AR][M] \cdot \delta(n-3) + k_B[MR][M] \cdot \delta(n-2) + k_p[M]([R_{n-1}] - [R_n]) \\ & - (k_{fm}[M] + k_{fAH}[AH])[R_n] + k_S[PR] \sum_{k=n+1}^{\infty} [D_k] \\ & - (k_{tc} + k_{td})[R_n] \sum_{k=1}^{\infty} [R_k] - k_{tPR}[PR][R_n] + \left[k_{fmG}[M] \sum_{k=1}^{\infty} [GR_k] \right] \cdot \delta(n-1) \\ & - k_{fG}[G][R_n] + k_{sG}[PR] \sum_{k=n+1}^{\infty} [GD_k] - (k_{tcG} + k_{tdG})[R_n] \sum_{k=1}^{\infty} [GR_k] \\ & - k_{fCB}[CB][R_n] \end{aligned} \quad (4.79)$$

Rate of "dead" polymer chains:

$$\begin{aligned} rD_n = & k_c[AH][M] \cdot \delta(n-3) + (k_{fm}[M] + k_{fAH}[AH])[R_n] - k_S[PR](n-1)[D_n] \\ & + k_S[PR] \sum_{k=n+1}^{\infty} [D_k] + \frac{1}{2} k_{tc} \sum_{k=1}^{n-1} [R_k][R_{n-k}] + k_{tPR}[PR][R_n] \\ & + k_{td}[R_n] \sum_{k=1}^{\infty} [R_k] + k_{fG}[G][R_n] \\ & + k_{tdG}[R_n] \sum_{k=1}^{\infty} [GR_k] + k_{fCB}[CB][R_n] \end{aligned} \quad (4.80)$$

Rate of "live" grafted polymer chains (G-radicals):

$$\begin{aligned}
rGR_n = & (k_{pG}[GPR][M]) \cdot \delta(n-1) + k_p[M]([GR_{n-1}] - [GR_n]) \\
& - (k_{fmG}[M] + k_{fAHG}[AH])[GR_n] \\
& - (k_{tcG} + k_{tdG})[GR_n] \sum_{k=1}^{\infty} [R_k] - k_{tPRG}[PR][GR_n] \\
& - k_{fCBG}[CB][GR_n]
\end{aligned} \tag{4.81}$$

Rate of "dead" polymer chains:

$$\begin{aligned}
rGD_n = & (k_{fmG}[M] + k_{fAHG}[AH])[GR_n] \\
& + \frac{1}{2}k_{tcG} \sum_{k=1}^{n-1} [R_k][GR_{n-k}] + k_{tdG}[GR_n] \sum_{k=1}^{\infty} [R_k]
\end{aligned} \tag{4.82}$$

$$\begin{aligned}
& + k_{tPRG}[PR][GR_n] + k_{fCBG}[CB][GR_n]
\end{aligned} \tag{4.83}$$

4.4.2.3 Moments rate functions

To reduce the infinite order of the resulting system of ODEs, the method of moments is implemented to the macromolecular "live" and "dead" of free and grafted polymer chains, through the following equations:

$$\lambda_k = \sum_{m=1}^{\infty} n^k R_n \tag{4.84}$$

$$\mu_k = \sum_{m=1}^{\infty} n^k D_n \tag{4.85}$$

$$\nu_k = \sum_{m=1}^{\infty} n^k GR_n \tag{4.86}$$

$$\xi_k = \sum_{m=1}^{\infty} n^k GD_n \tag{4.87}$$

Thus, the moment rate functions can be expressed on the basis of the above kinetic scheme. The balances of the free and grafted "live" and "dead" polymer chains are presented here:

Moments of the "live" polymer chains (Radicals) :

$$\begin{aligned}
r_{\lambda_k} = & k_I[PR][M] + k_{fm}[M]\lambda_0 + 3^k k_A[AR][M] + 2^k k_B[MR][M] \\
& + k_p[M] \left(\sum_{r=0}^k \binom{k}{r} \lambda_r - \lambda_k \right) - (k_{fm}[M] + k_{fAH}[AH])\lambda_k \\
& + k_S[PR]T_1 - (k_{tc} + k_{td})\lambda_0\lambda_k - k_{tPR}[PR]\lambda_k \\
& + k_{fmG}[M]\nu_0 - k_{fG}[G]\lambda_k + k_{sG}[PR]T_{1G} - (k_{tcG} + k_{tdG})\lambda_k\nu_0 \\
& - k_{fCB}[CB]\lambda_k
\end{aligned} \tag{4.88}$$

Moments of the "dead" polymer chains:

$$\begin{aligned}
r_{\mu_k} = & 3^k k_c [AH][M] + (k_{fm}[M] + k_{fAH}[AH])\lambda_k \\
& + k_s [PR](T_1 - (\mu_{k+1} - \mu_k)) + k_{tPR}[PR]\lambda_k \\
& + \frac{1}{2} k_{tc} \sum_{r=0}^k \binom{k}{r} \lambda_r \lambda_{k-r} + k_{td} \lambda_k \lambda_0 \\
& + k_{fG}[G]\lambda_k + k_{tdG} \lambda_k \nu_0 + k_{fCB}[CB]\lambda_k
\end{aligned} \tag{4.89}$$

Moments of the "live" grafted polymer chains (G-radicals):

$$\begin{aligned}
r_{\nu_k} = & k_{pG}[GPR][M] + k_p[M] \left(\sum_{r=0}^k \binom{k}{r} \nu_r - \nu_k \right) \\
& - (k_{fmG}[M] + k_{fAHG}[AH])\nu_k \\
& - (k_{tcG} + k_{tdG})\nu_0 \nu_k - k_{tPRG}[PR]\nu_k \\
& - k_{fCBG}[CB]\nu_k
\end{aligned} \tag{4.90}$$

Moments of the "dead" grafted polymer chains:

$$\begin{aligned}
r_{\xi_k} = & (k_{fmG}[M] + k_{fAHG}[AH])\nu_k + k_{tdG} \nu_k \lambda_0 \\
& + \frac{1}{2} k_{tcG} \sum_{r=0}^k \binom{k}{r} \lambda_r \nu_{k-r} + k_{tPRG}[PR]\nu_k \\
& + k_{fCBG}[CB]\nu_k
\end{aligned} \tag{4.91}$$

$$\tag{4.92}$$

4.4.2.4 Reactor design equations

To complete the mathematical model, the rate functions for each of the species present in the mixture are developed from Equations 4.93 to 4.102.

Initiator:

$$\frac{1}{V} \frac{d(V \cdot I)}{dt} = -(k_d + k_{dCB}[CB])[I] \tag{4.93}$$

Monomer:

$$\begin{aligned}
\frac{1}{V} \frac{d(V \cdot M)}{dt} = & -(k_I[PR] + (k_p \lambda_0 + k_{fm} \lambda_0))[M] \\
& - ((k_2 + k_C)[AH] + k_A[AR] + k_B[MR])[M] \\
& - (k_{pG}([GPR] + \nu_0) + k_{fmG} \nu_0)[M] \\
& - 2k_1[M]^2 + 2k_{-1}[AH]
\end{aligned} \tag{4.94}$$

Ground tire rubber (acting as comonomer), G:

$$\frac{1}{V} \frac{d(V \cdot G)}{dt} = -(k_{IG}[PR] + k_{fG} \lambda_0)[G] \tag{4.95}$$

Carbon black, CB:

$$\frac{1}{V} \frac{d(V \cdot CB)}{dt} = -(k_{dCB}[I] + k_{fCB}\lambda_0 + k_{fCBG}\nu_0)[CB] \quad (4.96)$$

Adduct, AH:

$$\begin{aligned} \frac{1}{V} \frac{d(V \cdot AH)}{dt} = & k_1[M]^2 - (k_{-1} + (k_2 + k_c)[M])[AH] \\ & - (k_{fAH}\lambda_0 + k_{fAHG}\nu_0)[AH] \end{aligned} \quad (4.97)$$

...after the application of the Q.S.S.A.:

$$[AH] = \frac{k_1[M]^2}{k_{-1} + (k_2 + k_c)[M] + k_{fAH}\lambda_0 + k_{fAHG}\nu_0} \quad (4.98)$$

Styryl radicals, MR:

$$\frac{1}{V} \frac{d(V \cdot MR)}{dt} = k_2[AH][M] - k_B[M][MR] \quad (4.99)$$

1-Phenil tetraryl radicals, AR:

$$\frac{1}{V} \frac{d(V \cdot AR)}{dt} = k_2[AH][M] - k_A[M][AR] \quad (4.100)$$

Primary radicals, PR:

$$\begin{aligned} \frac{1}{V} \frac{d(V \cdot PR)}{dt} = & 2(f_1 \cdot k_d + f_2 \cdot k_{dCB}[CB])[I] - k_I[M][PR] \\ & k_{IG}[G][PR] - (k_S\mu_0 + k_{sG}\xi_0)[PR] \\ & (k_{tPR}\lambda_0 + k_{tPRG}\nu_0)[PR] \end{aligned} \quad (4.101)$$

Rubber primary radicals, GPR:

$$\frac{1}{V} \frac{d(V \cdot GPR)}{dt} = k_{IG}[G][PR] - k_{pG}[M][GPR] + k_{fG}[G]\lambda_0 \quad (4.102)$$

4.4.2.5 Polymer properties

After determining the moment balances, the following expressions can be defined to describe the evolution in function of time of the monomer conversion, grafting efficiency and the average molecular weights of both grafted-PS and free-PS chain populations.

Monomer conversion, x :

$$x = \frac{V_0M_0 - VM}{V_0M_0} \quad (4.103)$$

Grafting efficiency, GE:

$$GE = \frac{\xi_1}{\xi_1 + \mu_1} \quad (4.104)$$

Number- and weight-average molecular weights of the free polymer:

$$M_n = \frac{\mu_1 + \lambda_1}{\mu_0 + \lambda_0} MW_m \approx \frac{\mu_1}{\mu_0} MW_m \quad (4.105)$$

$$M_w = \frac{\mu_2 + \lambda_2}{\mu_1 + \lambda_1} MW_m \approx \frac{\mu_2}{\mu_1} MW_m \quad (4.106)$$

Number- and weight-average molecular weights of the grafted polymer:

$$M_n = \frac{\xi_1 + \nu_1}{\xi_0 + \nu_0} MW_m MW_m \approx \frac{\xi_1}{\xi_0} \quad (4.107)$$

$$M_w = \frac{\xi_2 + \nu_2}{\xi_1 + \nu_1} MW_m MW_m \approx \frac{\xi_2}{\xi_1} \quad (4.108)$$

4.4.2.6 Kinetic rate constants and parameters estimation

Estimation of model parameters can be performed on the basis of the parameters for the styrene homopolymerization (c.f. Table 4.3). Table 4.6 lists all the rate constants involved in the kinetic scheme above. The grafting reactions related to propagation k_{pG} and termination k_{tcG} are expected to occur at lower rates than homopolymerization due to decreased mobility in the crosslinked network of GTR. Under these assumptions, instead of estimating each of the new individual parameters, these can be expressed as ratios between parameters such as k_{pG}/k_p and k_{tcG}/k_{tc} .

Table 4.6 – Kinetic constant parameters involved in the grafting polymerization mechanism of styrene in presence of GTR.

Styrene	GTR	CB
$k_{d,BPO}$	k_{IG}	$k_{d,CB}$
$k_{d,DCP}$	k_{pG}	$k_{f,CB}$
k_1	k_{fmG}	$k_{f,CBG}$
k_{-1}	k_{fAHG}	
k_2	k_{fG}	
k_A	k_{sG}	
k_B	k_{tcG}	
k_C	k_{tdG}	
k_p	k_{tPRG}	
k_{fm}		
k_{fAH}		
k_{tc}		
k_{td}		

At the same time, literature reported values can also be found and used as starting points for some of the above constants, as is the case for the rate constant of redox decomposition of BPO. For example, Odian (2004) [63] reported that in presence of N-diethylaniline, the redox dissociation rate of BPO is about $2.29 \cdot 10^{-3} L \cdot mol^{-1} \cdot s^{-1}$ at 30 °C and $1.25 \cdot 10^{-2} L \cdot mol^{-1} \cdot s^{-1}$ at 60 °C, which are one or two order of magnitude greater than the simple thermal homolysis.

As mentioned above, the initial concentration of GTR, $[G]$, corresponds to the number of double bonds susceptible of being attacked by the peroxide radicals during the free-radical polymerization. This varies according to the composition of the used tires recycled to produce GTR. In the model developed, $[G]$ was quantified theoretically by considering the type, average molar mass and weight fraction

of the main elastomers present in GTR (Table 4.7), according to suppliers data sheets and literature values. The estimated mean number of double bonds, expressed in mol, is shown in the last column of Table 4.7. It is considered that only a fraction of the total calculated amount of double bonds is exposed to initiator attacks, represented by a parameter in the model. For example, if this fraction is set to 35%, then the calculated initial value of $[G]$ is equal to approximately $3.44 \cdot 10^{-2}$ mol/g of GTR.

In addition, $[G]$ was also quantified experimentally by using the procedure detailed in section 4.2.2.6. Table 4.8 presents the results obtained. These indicate that double bonds concentration is almost the same for both types of GTR used and that it slightly decreases when GTR is purified with chloroform. These values are also comparable to the calculated theoretical value.

Table 4.7 – Mole mean number of double bonds contained in the different types of elastomers present in GTR

Elastomer	Weight fraction (w/w%)	Average molar quantity of double bonds (mol)
Styrene-butadiene rubber	0.4	0.498
Polyisoprene	0.3	0.087
Polybutadiene	0.2	0.074
Butadiene-acrylonitrile	0.05	0.032
Isobutylene-isoprene rubber	0.05	0.001

In other, $[CB]$ represents the concentration of active sites that induce peroxide redox dissociation and in parallel, interact with the reactive species. According to Xiong (2005) [60], oxidation-reduction of BPO is mainly induced by the transfer of unpaired electrons from the CB surface. Ohkita et al., (1975) [66], reported that the number of unpaired electrons present in commercial carbon black is usually lower than those of the quinone groups. For example, the furnace carbon black used by the authors (from Phillips Chemical Co.) contained about $9.2E+19/g$ of unpaired electrons and $3.2E+20/g$ of quinone groups [65, 74]. Since the exact quantification of the groups that are prone to react in this system is rather difficult and exceeds the purpose of this study, an initial approach would be to consider this quantity as directly proportional to the concentration of GTR in the reacting system.

The increased number of parameters in the model, with respect to the homopolymerization model, certainly complicates the parameter estimation process. This is even more true taking into account the aforementioned antagonistic actions of certain reactions (e.g., redox decomposition and radical deactivation on the surface of CB). Nonetheless, the initially adopted simplifying assumptions, described in the previous paragraphs of this section, as well as the large number of available experimental data under different conditions and from different sources (i.e., DSC and reactor runs), should act beneficially, especially if combined with the implementation of advanced statistical techniques for the ranking and estimation of the parameters. For example, Eghtesadi and McAuley (2014) [141], have proposed a relevant methodology for highly-parametric systems, making use of previously existing models and available data sets. Unfortunately, by the time of the reduction of the present manuscript, this process has not yet been sufficiently advanced as to be reported here, but it is underway and should be concluded within the near future.

Table 4.8 – Concentration of double-bonds present in GTR (mole/g GTR)

GTR supplier	Raw GTR		Chloroform-treated GTR	
	REGENE	DeltaGOM	REGENE	DeltaGOM
Double-bond content (mole/g GTR)	3.43E-03	3.68E-03	3.15E-03	3.49E-03

4.4.2.7 Adopted model assumptions and possible extensions

As described above, this grafting polymerization system may behave as a pseudo-homogeneous fluid system or as a completely segregated particulate-solid system, depending on the relative amounts of GTR and styrene. This has direct implications to the heat and mass transfer phenomena and, consequently, to the rate of the different chemical reactions across the reacting medium. In the case where the ratio of St/GTR is above the threshold of 2 (i.e., as identified in the present work - c.f. Ch. 3, Sect. 3.8.1), the hypothesis of homogeneous reacting mixture can be adopted, as the GTR particles are suspended within a continuous styrene liquid phase. In this case, the experimental measurements in the reactor have also demonstrated that the temperature distribution is quasi-uniform, thus supporting such hypothesis. On the other hand, when the ratio St/GTR is lower than the threshold, the above assumption does not hold true and a different approach must be employed, taking into account the heterogeneity of the system and the associated transfer limitations. These two cases are detailed below. In the present work, the first approach has been considered for the moment (parameter estimation work in progress), while the second approach remains subject for future developments.

- **First case: polymerization in a pseudo-homogeneous fluid system.** In presence of an excess of monomer solution (styrene/GTR ratio ≥ 2), GTR particles are embedded in the bulk monomer. Therefore, the overall polymerization rate, the rate of conversion and product formation (grafted and free PS chains) may be significantly influenced by the mass diffusion from the bulk phase to the GTR particles and viceversa. To simplify the development of this model, it is assumed that the reactants get into the pores of the rubber particle by convective flow instead of diffusion. Under these conditions, diffusion limitations across the particle boundary layer and within the particles may be neglected and do not affect the polymerization rates [142]. Moreover, it is also supposed that the heat transfer is mainly conductive from the reactor walls and through the monomer/polymer continuous phase, ensuring heat transfer and homogeneous temperature outside and inside the particles.

Similarly to the diffusion-controlled mechanism detailed above for the styrene homopolymerization (c.f. Sect. 4.3.1.6), the four stages of diffusion control as well as the equations describing each of them are also valid for the present system. These stages are considered as being less important in the presence of low amounts of rubber particles (i.e. below 33 wt% of the total mass of the mix GTR+styrene), except for the premature accelerating effects promoted by the polymerization inside the crosslinked network, which cannot be neglected. Nevertheless, the acceleration in the crosslinked network would be taken into account via the consideration of the different kinetic rate constants of the reactions of propagation and termination.

- **Second case: polymerization in a segregated particulate-solid system.** When the monomer solution migrates completely inside the GTR particles (styrene/GTR ratio < 2), the reacting medium is not continuous and the polymerization takes place almost exclusively in the core of their crosslinked network. In this heterogeneous system, by contrast to the above homogeneous one, the phenomena of mass and heat transfer inside the GTR particles play a crucial role and further dictate the overall polymerization rate and final properties of the polymer product. Therefore, these phenomena need to be considered in the development of the mathematical model to

accurately describe the behavior of the polymerization system. For this purpose, the heterogeneous grafting polymerization of styrene inside GTR may be compared, to some extent, to the polymerization systems involving supported catalysts.

In the industry, homopolymers and copolymers of some olefins, such as propylene and ethylene, may be produced at high rates (50 to 100 Kg per gram of catalyst) and short times (1 to 2 hours) by using heterogeneous catalysts [142, 143]. These latter are solid porous carriers with high specific surface areas covered with catalyst molecules or active sites available for polymerization. In contact with the catalyst, the monomer diffuses first through the boundary layer around the support and then into the pores. When the reactants reach the active sites, the polymerization takes place at high rates [143]. The polymer produced is continuously deposited on the catalyst surfaces, covering the active sites. At this state, the monomer must diffuse through the formed polymer layers to get in contact with the catalyst molecules. As reaction goes forward, the polymer gradually fills up the pores of the catalyst support until complete encapsulation of the support. Then, the polymer particles continue expanding with monomer conversion, generating radial mass and heat gradients with the surroundings [142–144].

This kind of polymer systems is studied through the *single particle modelling* or "*granule*" reactor approach [143, 145]. This associates physical and chemical phenomena to two characteristic length scales. First, the molecular scale or microscale concerns the kinetic mechanism and nature of the catalytic sites. Second, the particle scale or meso-scale involves the interphase and intraphase heat and mass transfer phenomena, and the particle-wall interactions that influence single particle growing [143, 144]. A series of mathematical models have been developed to describe the polymerization kinetics and diffusion phenomena involved in these heterogeneous systems. Although these are not the subject of this study, the following example gives a general idea of some of the aspects considered in numerical models based on single particle approach.

Debling and Ray (1995) [146] developed a kinetic/diffusion model for the production of impact polypropylene (PP), containing semi-crystalline PP and ethylene-propylene rubber (EPR), in two steps. First, microparticles of PP homopolymer are produced and subsequently, the rubbery phase is copolymerized *in-situ* in presence of the PP micrograins. Since PP and EPR are different in nature and immiscible, the particles obtained are designed as "heterophasic" and their morphologies vary according to the content of each polymeric phase. For example, at high contents of EPR, this progressively fills up the pores of the PP microparticles (0.1 to .3 μm) and then covers them until forming copolymer macroparticles (1000 to 5000 μm) having a continuous rubber phase. The model proposed accounts for material balances at the micro- and meso-scale. The particle equations consider the reactants diffusion and fluxes through the polymer layers and pores existing in the micro- and macroparticles. The energy balances take into consideration the temperature gradients at the boundary layers and within the particles. Finally, the kinetic model implemented leads to predict the average polymer properties of both polymer species formed. The set of differential equations obtained are solved in space and time. Simulations showed that the occlusion of the pores by the formation of EPR reduces monomer diffusivity. Since ethylene is more reactive than polypropylene, the former is more diffusion limited, creating granulates having a center rich in PP copolymer. Another important conclusion is that by increasing the pore volume in the homopolymer PP microparticles, higher contents of rubber can be incorporated to the impact polypropylene product. In further studies, Hamba et al., (1997) expanded this model to describe the changes in particle morphology and intraparticle reactants diffusivity as polymerization progress at different temperature conditions [147].

In the heterogeneous system regarding the grafting polymerization of styrene inside GTR, the con-

struction of a kinetic/diffusion model increases the complexity of this system. According to the published literature, and in spite of considering the diffusion-controlled reaction mechanism, additional diffusion limitations of the reactants are expected. For example, mass transfer resistance due to the production of homopolymer in the pores crosslinked network. Similarly to catalyst supports, the active sites on the surface of the carbon particles uniformly dispersed through GTR, trap the initiator molecules and growing polymer chains. These latter are progressively deposited on the CB surfaces, thereby reducing the diffusion of the radicals produced by redox catalyst towards the bulk monomer, or inversely, preventing the capture of the initiator molecules from the bulk. Moreover, by contrast to most catalytic systems for which the supports are rigid, the elastic GTR particles may significantly expand while being progressively filled by the amorphous polymer. This means that important amounts of polymer can be incorporated to the particles, which implies higher heat and mass transfer resistances and radial gradients through the particles.

4.4.3 Conclusions

On the basis of both the developments of the kinetic model for the free-radical polymerization of styrene and relevant experimental evidence obtained in a previous work, a model is proposed to describe the graft polymerization of styrene onto/into rubber particles from recycled tires. This is a general framework that accounts for a triple initiation mechanism (chemical, thermal and redox), the formation of both grafted and homopolymer chains and the inhibition of the polymerization reaction. Since the phenomena displayed by the presence of GTR are not - to this date - completely elucidated, it is difficult to develop detailed models on the elementary mechanisms. Although the proposed approach reposes on specific simplifying assumptions, it can be easily modified to account for varying concentration and/or temperature conditions. Even under this simplifying prism and to the best of the authors' knowledge, this is the first time that such a complete model is postulated for this complex system, laying the basis for future, more detailed developments.

Experimental results and discussion

Contents

5.1	Introduction	119
5.2	Free-radical bulk polymerization of styrene in presence of GTR in a batch reactor	119
5.2.1	Influence of the GTR content on polystyrene qualities: x and GE	119
5.2.2	Morphology of the GTR-grafted-PS particles	121
5.2.3	Verifying polystyrene grafting onto GTR	123
5.2.3.1	Chemical characterization by FTIR analysis	123
5.2.3.2	Glass transition temperature (T_g)	123
5.2.4	Effect of GTR content on the molecular weight of free-PS	125
5.2.5	Discussion and interpretation	125
5.3	Compounding of the polystyrene grafted GTR composites in a twin-screw extruder	128
5.3.1	Effect of a single extrusion by using screw Profile-1 on the microstructure and mechanical properties of polystyrene composites containing 30 wt% and 50 wt% of equiv-GTR	131
5.3.1.1	Effect of high temperature compounding on polystyrene qualities: x , GE and molecular weight	131
5.3.1.2	Influence of the GTR content on Charpy impact strength (IS)	131
5.3.1.3	Fracture surfaces of impact specimens	133
5.3.1.4	Intermediate discussion and interpretation	135
5.3.1.5	Effect of the grafting compatibilization on tensile mechanical properties	136
5.3.1.6	Fracture surfaces of tensile specimens	137
5.3.1.7	Effect of a single extrusion on the morphology and PSD of GTR-g-PS particles	137
5.3.1.8	Influence of the grafting compatibilization on PSD of GTR-g-PS particles	140
5.3.1.9	Influence of the amount of GTR on PSD of GTR-g-PS particles	140
5.3.1.10	Discussion and interpretation	142
5.3.2	Effect of 1, 2 and 3 extrusions by using screw Profile-1 on the microstructure and mechanical properties of polystyrene composites containing 30 wt% and 50 wt% of equiv-GTR	144
5.3.2.1	Influence of the number of extrusions on IS	144
5.3.2.2	Effect of the number of extrusions on tensile strength properties	146
5.3.2.3	Changes in the morphology of GTR-g-PS particles after 1, 2 and 3 extrusions.	147
5.3.2.4	Changes in PSD of GTR-g-PS particles after 1, 2 and 3 extrusions	147

5.3.2.5	Evolution of the <i>IS</i> of the composites after multiple extrusions	150
5.3.2.6	Notch sensitivity of polystyrene composites	150
5.3.2.7	Discussion and interpretation	151
5.3.3	Influence of the extruder screw configuration after 1, 2 and 3 extrusions on the microstructure and mechanical properties of polystyrene composites containing 50 wt% of equiv-GTR.	153
5.3.3.1	Qualities of polystyrene: α , <i>GE</i> and molecular weight	153
5.3.3.2	Variations in the <i>IS</i> when using screw Profile-2	154
5.3.3.3	Influence of the screw configuration on the tensile properties	155
5.3.3.4	Changes in the morphology and PSD of the GTR-g-PS particles with screw Profile-2.	157
5.3.3.5	Discussion and interpretation	158
5.3.4	Influence of increasing the GTR content on the microstructure and tensile properties of polystyrene composites extruded 1 and 2 times.	160
5.3.4.1	Influence of the GTR content on the qualities of polystyrene: α and molecular weight	160
5.3.4.2	Tensile properties of composites extruded with screw Profile-1	161
5.3.4.3	Tensile properties of composites extruded with screw Profile-2	162
5.3.4.4	Changes in the morphology and PSD of GTR-grafted-PS particles extruded with screw Profile-1 or Profile-2	163
5.3.4.5	Discussion and interpretation	164
5.4	Conclusions	166

5.1 Introduction

In Chapter 3, a novel methodology was proposed to prepare polystyrene-reinforced composites filled with recycled rubber particles as GTR and exhibiting improved mechanical properties. This proposes a systematic method for appropriate product fabrication through in-situ free-radical grafting polymerization of styrene and multiple compounding in a twin-screw extruder. Hence, the particular contribution of this chapter is to focus on the role of each of the proposed strategies in toughening polystyrene and trying to answer the question: can there be any synergistic effects by combining both techniques?

To find the answer, the methodology proposed was applied to prepare three different polystyrene composites filled with different amounts of GTR. First, the GTR was grafted with PS by free-radical grafting polymerization in a batch reactor and by using a mix of peroxide initiators. The influence of the GTR content on the quality indexes of polystyrene, namely monomer conversion, efficiency in polymer grafting and molecular weight is discussed. Then, the products of the grafting polymerization were transformed by compounding through several extrusion passages (i.e., 1-3 passages). The changes in the microstructure and mechanical strength properties of the different composites obtained were studied.

5.2 Free-radical bulk polymerization of styrene in presence of GTR in a batch reactor

The compositions tested for the free-radical bulk polymerization systems of styrene in presence of GTR are shown in Table 5.1. In total, a series of 14 polymerizations were conducted at three different GTR contents: 30, 50 and 70 wt%. Here, the GTR content is defined as the percentage by weight (wt%) present in the total mixture of styrene and GTR ($GTR/[Sty+GTR]$). The initiator system selected (I) was a mixture of BPO, DCP and DHBP. All compositions were prepared by keeping a constant molar ratio of initiator to styrene equal to 3.2 mol/mol%, with 1% of BPO, 2% of DCP and 0.2% of DHBP (percentages expressed as mol of I/mol of sty). The polymerization temperature profile was 75 °C for 2h, 85 °C for 3h, 95 °C for 3h, 115 °C for 1h, 125 °C for 1h and 140 °C for 1h.

Table 5.1 – Composition of the grafting polymerization systems tested.

GTR content ^a (wt%)	Initiators ^b (I) (wt%)	I/GTR (wt%)	Number of experiments (numbering sequence)
30	6.2	22.1	5 (1 to 5)
50	4.5	9.5	7 (6 to 12)
70	2.8	4.1	2 (13 to 14)

^a Weight/weight*100% (w/w or wt%)

^b I: mix of BPO, DCP and DHBP

5.2.1 Influence of the GTR content on polystyrene qualities: x and GE

The effects of the amount of GTR on the ultimate monomer conversion (x) are displayed in Figure 5.1. It is observed that x is never complete and decreases with increasing the amount of GTR in the polymerization systems. Note that x is reduced by about 9.5% when passing from 30 wt% to 50 wt% of GTR, and subsequently it drops markedly (45.5% approx.) when increasing to 70 wt% of GTR.

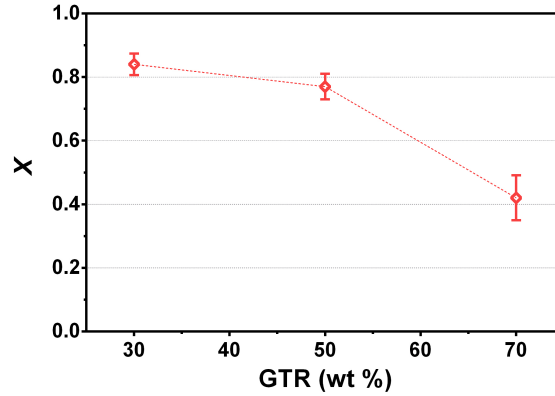


Figure 5.1 – Effect of GTR content on monomer conversion.

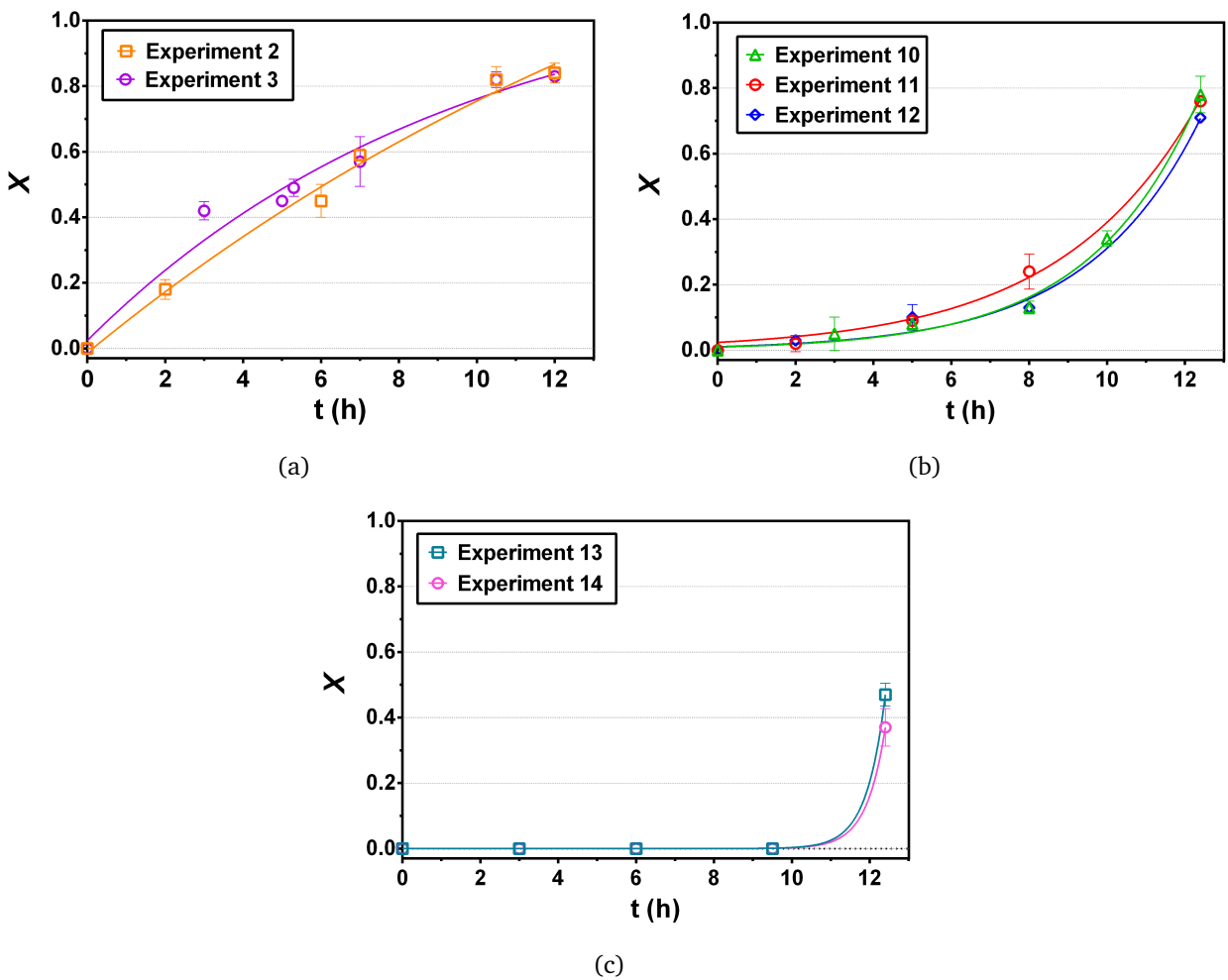


Figure 5.2 – Effect of GTR content on x in function of t for polymerization systems containing (a) 30 wt%, (b) 50 wt% and (c) 70 wt% of GTR. The full line is just a guide to illustrate the trend.

These effects can better be addressed by following the evolution of x as a function of time (t), of some representative experiments, as shown in Figure 5.2. It is interesting to note that the presence of GTR not only affects x , but also deviated the course of all reactions from the typical evolution of the polymerization of neat styrene (i.e., without GTR), as recorded via DSC in Chapter 2 (cf., Figure 2.1).

Compared with this latter, the polymerization systems with 30 wt% of GTR (Fig. 5.2a) exhibit the lowest deviations. By contrast, the systems containing 50 wt% and 70 wt% of GTR (Figures 5.2b and 5.2c, respectively) are strongly affected. In this latter, styrene conversion is detected after 9 hours of reaction, at the highest temperature steps above 125 °C .

On the other hand, the results of grafting efficiency (*GE*) of the polymerization systems containing 50 wt% of GTR are shown in Table 5.2. This indicates that from the total amount of styrene transformed into polystyrene (i.e., grafted-PS + free-PS), the formation of grafted-PS is favored over free-PS. The measurements displays a higher degree of disparity and are located around a mean value of approx. 72%. Unfortunately, it was not possible to get accurate measurements of *GE* for the composites with 30 wt% and 70 wt% of GTR. In the former case, the samples permeated the filters used for free-PS extraction. By contrast, in the latter case, the mass balances applied for *GE* calculation were not coherent. This is explained in more detail below.

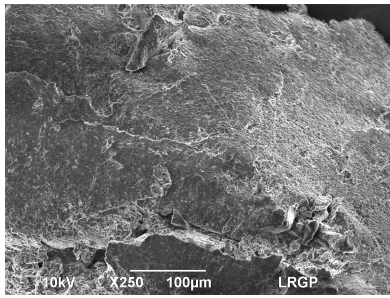
Table 5.2 – Effect of GTR on *GE* of polymerization systems containing 50 wt% of GTR.

Experiment No.	$\frac{\text{grafted-PS}}{\text{free-PS}}$ (w/w%)	<i>GE</i> (%)
6	1,7	61,4
7	1,9	65,0
8	3,8	79,2
9	2,6	72,0
10	3,3	80,0
11	3,4	78,0
12	2,3	69,7
Mean	2,7	72,1
Stand. Dev.	0,8	7,3

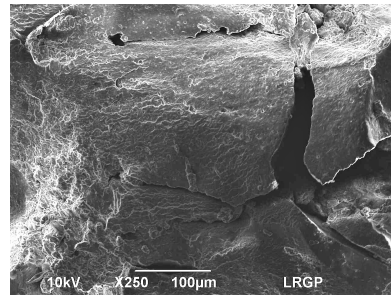
5.2.2 Morphology of the GTR-grafted-PS particles

SEM micrographs of the GTR particles before grafting (i.e., as received), reveals that their surfaces are rough and contain sharp edges (Fig. 5.3). Figure 5.4 shows the micrographs of the surfaces of the GTR particles after modification via grafting polymerization. The amount of GTR in the composites increases from top to bottom: (a-b) 30 wt%, (c-d) 50 wt% and (e-f) 70 wt%. Left images display the GTR particles obtained after polystyrene grafting, which product is designed as GTR-grafted-PS+free-PS. In composites with 30 wt% of GTR (a), the particles are completely coated with a glossy layer of polystyrene (grafted-PS + free-PS) which makes the surface smoother. When increasing the GTR content to 50 wt% (c), the particles are partially coated and, when passing to 70 wt% of GTR (e), it is difficult to find any evidence of polystyrene onto the surface of GTR.

Right images show the particles after extraction of free-PS with chloroform and thus, only the GTR-grafted-PS particles are observed. Note that for composites containing 30 wt% (b) and 50 wt% of GTR (d), the polystyrene layer initially evidenced onto the particles (i.e., before free-PS removing), is less visible and particle surfaces become rougher. For the composite containing 70 wt% of GTR (f), no visible changes are detected by the micrographs.

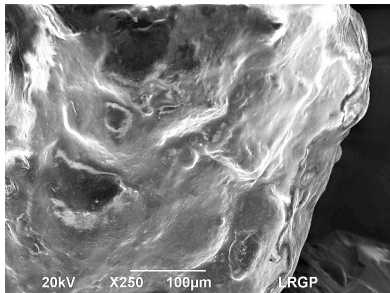


(a)

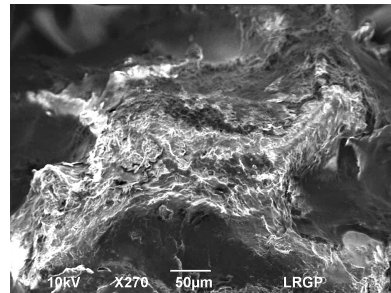


(b)

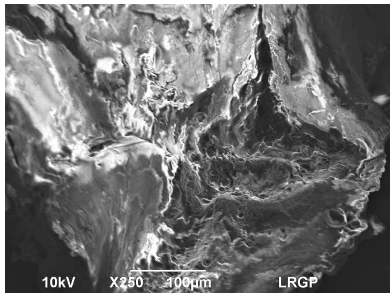
Figure 5.3 – Morphology of GTR particles before grafting: (a) from Regene Co. Brazil and (b) from DeltaGom France.



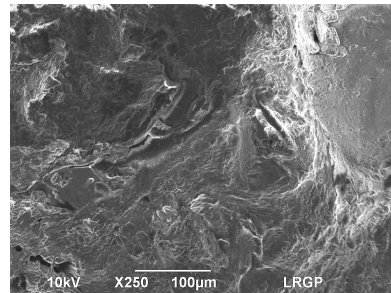
(a)



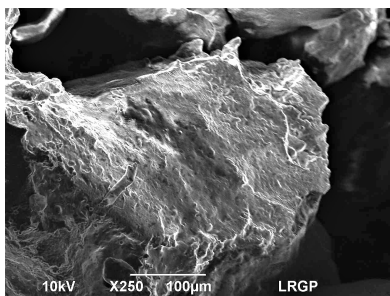
(b)



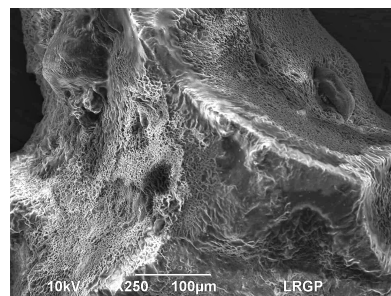
(c)



(d)



(e)



(f)

Figure 5.4 – Morphologies of the GTR particles after modification via polystyrene grafting. The content of GTR in the composites increases from top to bottom: (a-b) 30 wt%, (c-d) 50 wt% and (e-f) 70 wt%. From left to right the figures display the particles before (GTR-grafted-PS+free-PS) and after (GTR-grafted-PS) extraction of free-PS.

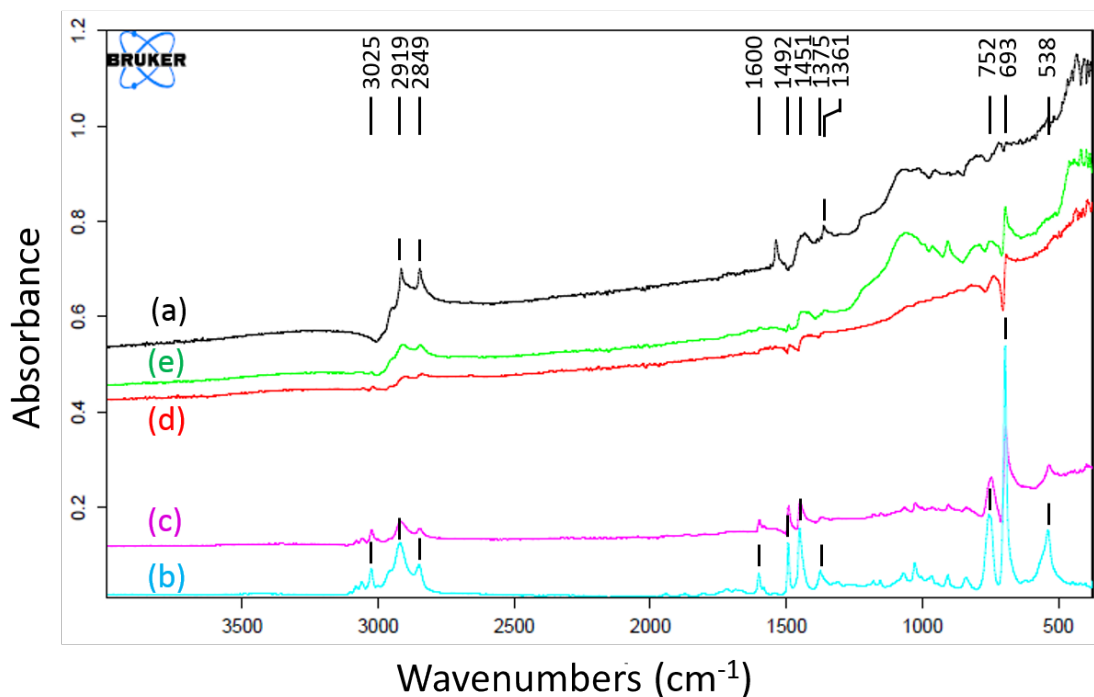


Figure 5.5 – FTIR spectrum of: (a) GTR particles before grafting, (b) free-PS and GTR-grafted-PS particles from composites containing (c) 30 wt%, (d) 50 wt% and (e) 70 wt% of GTR.

5.2.3 Verifying polystyrene grafting onto GTR

5.2.3.1 Chemical characterization by FTIR analysis

Grafting of polystyrene chains onto GTR was verified by examination of chemical bonds formation by FTIR. For this purpose, the composites were analyzed after free-PS extraction with chloroform. Figure 5.5 compares the FTIR absorption spectra of GTR particles before grafting (a), free-PS (b) and the GTR-grafted-PS particles from composites containing 30 wt% (c), 50 wt% (d) and 70 wt% of GTR (e). The sample of free-PS was obtained by chloroform extraction and subsequent precipitation in methanol. The spectrum of this latter is representative of the samples analyzed and exhibits some characteristic vibrational bands (Table 5.3), which correspond to the C-H stretch of the benzene ring (3025 cm^{-1}), C=C bending vibration of benzene (between 1600 and 1450 cm^{-1}) and C-H vibration of monosubstituted benzene (at 754 to 696 cm^{-1}). Like free-PS, the spectrum of GTR particles before grafting (a) displays two peaks assigned to the vibrations of C-H alkane bonds (near 2919 and 2846 cm^{-1}).

By comparing with the spectra of GTR before grafting, the characteristic vibrational bands of free-PS, such as the vibrating bonds of the benzene rings described in Table 5.3, are clearly identified in the spectrum of the GTR-grafted-PS particles. Moreover, the higher the content of GTR, the more similar the absorption vibrational bands of the grafted particles to those of GTR, and otherwise more similar to free-PS. This indicates that there exist polystyrene chains chemically linked to the surface of GTR. Negative bands observed may be attributed to the presence of residual solvents traces or bad realigning and calibration of the FTIR device.

5.2.3.2 Glass transition temperature (T_g)

In a similar way, GTR-grafted-PS particles were analyzed by DSC to corroborate effective grafting of polystyrene through changes in the T_g of the individual phases (i.e., GTR and polystyrene). Figure 5.6

Table 5.3 – Characteristic vibrational bands of neat free-PS and raw GTR measured by FTIR.

Polystyrene		GTR	
Wavenumber (cm^{-1})	Chemical group	Wavenumber (cm^{-1})	Chemical group
3000 to 3015	C-H stretch of benzene on the PS side chain	2919 to 2846	C-H alkane bonds
2919	CH_2 stretch on the main PS chain	1361 to 1550	Additives
2849	C-H stretch on the main PS chain	1100	Silice
1600 to 1450	C=C stretch of benzene		

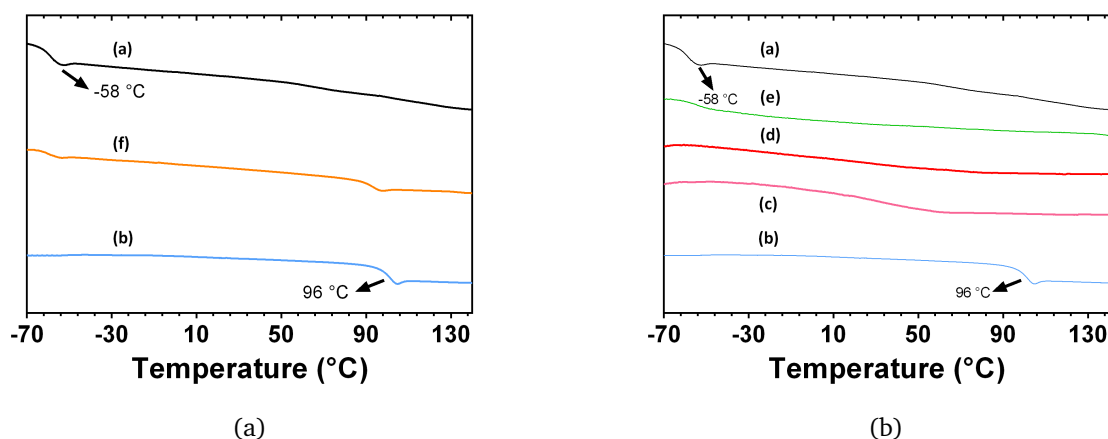


Figure 5.6 – Effect of grafted-PS onto/into GTR on the thermal properties of the composites obtained. Comparison of: (a) GTR before grafting, (b) free-PS, GTR-grafted-PS particles from composites with (c) 30 wt%, (d) 50 wt% and (e) 70 wt% of GTR, and (f) simple blend of GTR and commercial polystyrene.

compares the thermograms of GTR before grafting (curve a) and free-PS (curve b). GTR displayed a low T_g of about $-58\text{ }^{\circ}\text{C}$ (very close to that of natural rubber $-58.8\text{ }^{\circ}\text{C}$ approx.), whereas that of free-PS (curve b) was around $96\text{ }^{\circ}\text{C}$. This latter value was used as a guide, since it may vary approx. from $80\text{ }^{\circ}\text{C}$ to $100\text{ }^{\circ}\text{C}$, according to the molecular weight (e.g. $10\ 000$ to $180\ 000\text{ g/mol}$, [51]). Curve f is an example of a thermogram for a sample prepared by simple blending of polystyrene (e.g., commercial polystyrene) with GTR as received (without previous grafting). In this case, the T_g of both individual phases were easily identified.

In contrast, the thermogram of the GTR-grafted-PS particles from the composites with 70 wt% of GTR (Fig. 5.6b, curve e), displayed a marked but less pronounced transition close to the T_g of GTR before grafting (curve a). Otherwise, at 30 wt% of GTR (curve c), the thermogram shows a large transition occurring over a wide temperature range starting at $30\text{ }^{\circ}\text{C}$. Finally, when the composite contained 50 wt% of GTR (curve d), the changes in the T_g were too small to be detected by the DSC device at the measurement conditions fixed.

Table 5.4 – Influence of the GTR content on the molecular weight and T_g of free-PS.

GTR content (wt%)	M_n (g/mol)	M_w (g/mol)	M_w/M_n	T_g (°C)
30	6,75E+04 ($\pm 1,7E+04$)	1,38E+05 ($\pm 3,9E+04$)	2,04 ($\pm 0,07$)	95 ($\pm 1,5$)
50	2,26E+04 ($\pm 0,3E+04$)	3,88E+04 ($\pm 1,4E+04$)	1,69 ($\pm 0,04$)	80 ($\pm 2,1$)
70	2,90E+04 ($\pm 0,2E+04$)	3,62E+04 ($\pm 0,3E+03$)	1,25 ($\pm 0,01$)	84 ($\pm 1,6$)

5.2.4 Effect of GTR content on the molecular weight of free-PS

As mentioned above, the grafting polymerization lead to the formation of grafted and free polystyrene chains. Only these latter can be removed from the composites by the method implemented in this work, namely the soxhlet extraction with chloroform. Then, the free-PS was precipitated and its average molecular weight was measured by GPC. Therefore, the effect of GTR content on the number- (M_n) and weight-average molecular weight (M_w) is illustrated in Figure 5.7. The results correspond to the mean of the measurements of the set of experiments performed. It is seen that both M_n and M_w decreases drastically when increasing the amount of GTR, and more precisely, there is a nearly 3-fold decrease when passing from 30 wt% to either 50 wt% or 70 wt% of GTR, as shown in Table 5.4. In addition, according to the results of polydispersity (M_w/M_n), the molecular weight distributions are also affected and seem become narrower at higher GTR contents.

On the other hand, the T_g of the free-PS is marked by the changes of molecular weight and exhibits the same trend when increasing the GTR content in the polymerization systems.

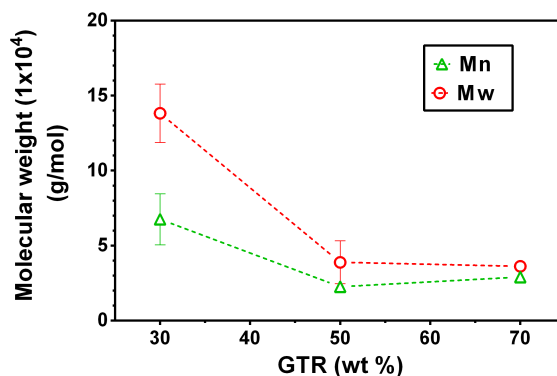


Figure 5.7 – Effect of the GTR content on the average molecular weight of free-PS.

5.2.5 Discussion and interpretation

The strategy adopted in this study to modify the surface of GTR, namely the bulk free-radical grafting polymerization of styrene with a mix of peroxide initiators, has demonstrated effectiveness in creating polystyrene grafts onto/into GTR. These latter are expected to reduce the interfacial tension between the incompatible GTR and polymer phases, thereby promoting a good interfacial adhesion and miscibility. However, the properties of the produced polymer are strongly affected by the presence of GTR.

Microscopic examinations suggest that styrene polymerizes almost exclusively in the bulk particles of the composites containing 50 and 70 wt% of GTR. This may be associated to the GTR absorption capacity of styrene, which, as mentioned in the previous chapter, ranges between 2 to 2.4 times its weight.

Then, it is assumed that most of the monomer remains within the GTR particles during polymerization, and both grafted-PS and free-PS form rigid PS domains through the cross-linked structure of GTR. These domains are expected to further help the break and fine dispersion of GTR through the polymer matrix, as will be studied in the following sections of this chapter.

The ultimate x decreases with increasing the content of GTR in the polymerization system. These results are also consistent with the findings of the study of the polymerization system conducted by DSC in Chapter 2 of this work. Returning briefly to the results of such study, it was found that the carbon black (CB) and additives, contained in the formulation of GTR, have a strong inhibitory effect on the BPO-initiated radical polymerization of styrene. Therefore, the increase of the amount of GTR in the polymerization system decreases x . Moreover, when increasing the polymerization temperature the negative effects on x are more pronounced. Since the initiator system used to perform the reaction in the batch reactor is a cocktail of peroxides (BPO, DCP and DHBP), it is expected that DCP and DHBP also undergo similar chemical interactions with the additives contained in GTR, in the same way as BPO. Nevertheless, from the experiments performed here it is not possible to identify the extent of the individual effects of GTR when using exclusively DCP or DHBP in the polymerization system.

The course of the polymerization system with 30 wt% of GTR seems to be less sensitive towards the presence of GTR, by contrast to the systems containing 50 wt% and 70 wt% of GTR. From the beginning of the reaction and as it progresses, the peroxide radicals are captured by the CB and additives before they initiate a polymer chain. The ratio of initiator to styrene being kept constant (3.2 mol/mol%), the radicals are scavenged by the CB and their concentration drastically decreases with the increase of GTR content. Consequently, the polymerization proceeds at lower rates or is completely inhibited, resulting in a significant diminution of the ultimate monomer conversion.

It is not possible to determine if there is a correlation between x and GE , since it was not possible to get accurate values of GE for all the polymerization systems. Despite this, the results of ultimate x (78%) and the average percentages of GE (65%) obtained for the polymerization system with 50 wt% are encouraging. In fact, these results imply that it is possible to stimulate the formation of grafted chains ($GE > 50\%$, ratio grafted-PS/free-PS > 1) by reaching a high monomer conversion around 80%, as initially desired for the polymerization systems. The disparity of the GE measurements seems to be due to an underestimation of the size of the samples used for measurement. Nevertheless, it was not possible to use higher sample masses due to the limited capacity of the soxhlet apparatus used.

The polystyrene grafts onto/into GTR, created during the grafting polymerization of styrene in-situ, can be chemically bonded to both, the elastomer chains and the CB surface. Indeed, the peroxide radicals may attack the unsaturated double bonds of the elastomer chains that form the cross-linked structure of GTR. This creates new active radicals to which the growing polystyrene chains can be grafted. However, peroxide radicals can also interact with the chemical functions present on the surface of CB. This may promote the formation of active sites that capture the radical polymer chains.

With regard to the qualities of the grafted and free-PS, it is assumed that both have similar molecular weight. The largest M_n and M_w of free-PS are obtained for the formulation containing 30 wt% of GTR. Afterwards, both decrease when increasing the GTR content. Due to the excess of CB and additives in the polymerization systems, the radicals concentration diminishes and thus, the polymerization rate declines as the reaction progresses. The radical polymer chains are probably captured on the CB surface and thus, their growing is inhibited, leading to the formation of polymer chains with rather intermediate molecular-weight (e.g., M_n and M_w of the order of $3E+04$ and $1E+05$). This result is in agreement with Kiatkamjornwong (2003) [67] findings on the synthesis of styrenic-based polymerized CB particles, using BPO as initiator (ratio BPO to styrene of 1/80 parts, at 70 °C during 8 h). It was reported that the M_w of the resulting product decreased markedly from about $10E+04$ to $4E+04$ g/mol

when increasing the CB feed level from 1 to 3 wt%, whereas M_n was relatively constant at very low values around $5E+03$ g/mol.

The low value of polydispersity, i.e., approx. 1.25, obtained for the free-PS extracted from the composite containing 70 wt% of GTR, is theoretically impossible in free-radical polymerization systems. This result may be associated with limitations in extracting the free-PS chains from the core of the particles. Since the polymerization takes place almost exclusively within the GTR particles, it is possible that the larger entangled polymer chains have more trouble diffusing through the cross-linked structure. As a result, mainly the smaller chains are removed by soxhlet extraction with chloroform, suggesting a narrow molecular weight distribution. These limitations in free-PS extraction may also explain the incoherences founded during the calculation of GE for these systems.

One interesting observation is that, when the styrene/GTR ratio is lower than 2.0 (e.g., for systems loaded with 50 and 70 wt% of GTR), the polymerization takes place mainly inside GTR. Under these conditions, the polymerization system behaves as a completely segregated particulate-solid system (not continuous) and the temperature distribution through the reactor is affected. In fact, due to the low thermal conductivity of GTR (e.g. used as thermal isolator), the heat transfer from the reactor walls to the center is poor, creating temperature gradients. It is possible, therefore, that temperature within the particles is lower than the desired set point and consequently the polymerization rate is decelerated. Moreover, poor heat transfer may result in local hot spots inside the particles due to poor evacuation of the heat of polymerization.

Although the heat transfer problems were partially overcome by optimizing both the mixing system of the batch reactor and temperature profile, as reported in Chapter 3, it seems that the reactor configuration implemented in this work is not the optimal one to perform the reaction in this type of segregated particulate-solid systems. Further studies in scaling up this polymerization process aiming to use a large-capacity reactor, need to integrate techniques leading to promote a good heat exchange between the heating jacket of the reactor and the polymerization system within each of the GTR particles.

5.3 Compounding of the polystyrene grafted GTR composites in a twin-screw extruder.

The experimental study of compounding was performed in an intermeshing co-rotating twin-screw extruder. The above composites, obtained via free-radical grafting polymerization of styrene onto/into GTR, were extruded in three consecutive extrusion passages under identical screw configuration. The first extrusion was mainly performed to complete the polymerization of the remaining styrene monomer. The second and third extrusions were carried out to promote the reduction in size of the GTR-grafted-PS particles. For this last purpose, the extrusion torque was fixed the nearest possible to the upper limit of the extruder machine (approx. 140 Nm). Overall, two different screw configurations were used. These are illustrated in Figure 5.8 and the compounding conditions are detailed in Table 5.5. The feeding rate in the first extrusion was fixed to 1 kg/h. For subsequent extrusions, this was adjusted until reaching the maximum torque value, regardless of the feeding rate.

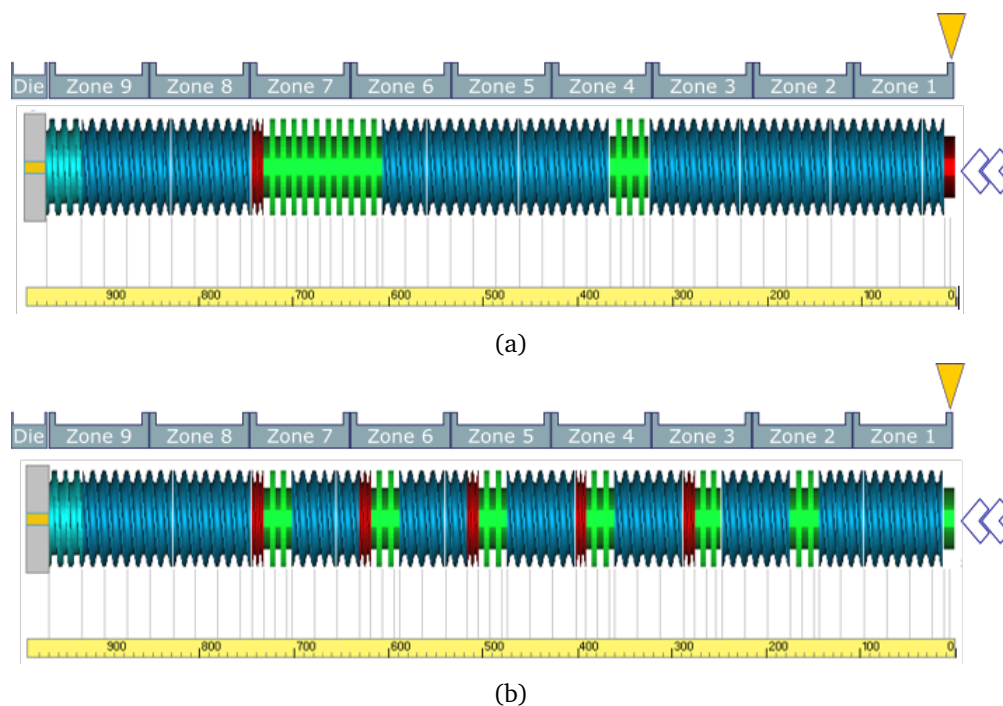


Figure 5.8 – Screw configurations tested. (a) Profile-1 and (b) Profile-2

Table 5.5 – Compounding conditions.

Number of extrusion	Barrel zone number and temperature (°C)										Screw speed (rpm)
	1	2	3	4	5	6	7	8	9	Die	
1	80	110	160	← 180 to 200 →				170	160		200
2	80	110	110	← 90 to 100 →				120	140		200
3	80	110	110	← 90 to 100 →				120	140		200

- **Profile-1** (Fig. 5.8a). This was composed of three conveying zones (blue color) and two kneading blocks (green color). A first short block (7 discs) was placed at the end of the feeding barrel (Zone 4) to accelerate polystyrene melting. In the second block, 23 kneading elements were arranged

to create a long mixing zone. Staggered angle between the successive kneading discs was 90°. This zone ended with a back conveying element (red color).

- **Profile-2** (Fig. 5.8b). To create the second profile, the total of kneading discs integrated in Profile-1 were redistributed in six zones along the screw. The first mixing block (Zone 2) had the function of accelerating melting. Then, a back conveying element was added at the end of each of the mixing zones.

Two sets of composites were extruded and their characteristics are summarized in Tables 5.6 and 5.7:

- a first set of 5 composites was prepared via free-radical grafting polymerization of styrene onto/into GTR. These correspond to the composites prepared and analyzed in the previous section (cf. Sect. 5.2). These composites consist exclusively of GTR-grafted-PS+free-PS which will be designed as yGTR-g-PS/f-PS_z, where:
 - y refers to the percent of GTR (by weight) in the composite, namely 30 wt%, 50 wt% or 70 wt%.
 - f-PS_z or free-PS_z, corresponds to the polystyrene chains that are not grafted to the GTR particle. z is a value between 1 and 5, which lead to differentiate the free-PS, since its molecular weight is different for each of the composites.
- a second set of 2 composites, corresponding to the control experiments, was prepared in the extruder by simple blending of commercial PS with raw GTR (as received), without neither previous purification nor polystyrene grafting. The composites prepared for control experiments contain 50 wt% or 70 wt% of GTR, and are designated as 50GTR/PS6 or 70GTR/PS6, respectively. The commercial PS is named as PS6 to distinguish it from the free-PS generated in-situ via grafting polymerization (f-PS1 to f-PS5).
- To distinguish between the raw GTR and the GTR in the GTR-g-PS/f-PS, the GTR (grafted) in the GTR-g-PS/f-PS is designated as equivalent GTR or equiv-GTR.

Table 5.6 – Set of composites extruded.

GTR content (wt%)	Polystyrene matrix origin	Product code for extrusion	Extruder screw profile
equiv-GTR			
30	Styrene grafting	30GTR-g-PS/f-PS1	Profile-1
50	Styrene grafting	50GTR-g-PS/f-PS2	Profile-1
		50GTR-g-PS/f-PS3	Profile-2
70	Styrene grafting	70GTR-g-PS/f-PS4	Profile-1
		70GTR-g-PS/f-PS5	Profile-2
raw GTR			
50	Commercial	50GTR/PS6	Profile-1
70	polystyrene	70GTR/PS6	

The study of compounding took place in four phases as follows:

- firstly, the grafted composites 30GTR-g-PS/f-PS1 and 50GTR-g-PS/f-PS2, and the non-grafted 50GTR/PS6 were extruded once by using screw Profile-1;

Table 5.7 – Average molecular weight of the polystyrene matrices.

Product code for extrusion	Average molecular weight of the polystyrene matrix		
	Polystyrene matrix code	M_n (g/mol)	M_w (g/mol)
30GTR-g-PS/f-PS1	free-PS1	7,95E+04 ($\pm 0,09E04$)	1,66E+05 ($\pm 0,03E04$)
50GTR-g-PS/f-PS2	free-PS2	1,98E+04 ($\pm 0,04E04$)	3,04E+04 ($\pm 0,03E04$)
50GTR-g-PS/f-PS3	free-PS3	2,31E+04 ($\pm 0,04E04$)	3,60E+04 ($\pm 0,05E04$)
70GTR-g-PS/f-PS4	free-PS4	3,02E+04 ($\pm 0,04E04$)	3,80E+04 ($\pm 0,05E04$)
70GTR-g-PS/f-PS5	free-PS5	2,78E+04 ($\pm 0,02E04$)	3,44E+04 ($\pm 0,08E04$)
50GTR/PS6 70GTR/PS6	PS6	1,12E+05 ($\pm 0,26E04$)	2,38E+05 ($\pm 0,18E04$)

- secondly, the composites obtained in the previous step were extruded a second and third time by using screw Profile-1;
- then, the effects of changing the screw profile were studied by extruding 3 times the 50GTR-g-PS/f-PS3 composite with screw Profile-2;
- and finally, the influence of increasing the GTR content to 70 wt% was analyzed by extruding 2 times the 70GTR-g-PS/f-PS4 composite with screw Profile-1 and the 70GTR-g-PS/f-PS5 composite with screw Profile-2. The non-grafted 70GTR/PS6 composite was extruded with Profile-1.

Ultimate x , GE and molecular weight of the grafted composites were measured after the first extrusion passage. The mechanical properties of all composites were characterized after each extrusion passage by both Charpy impact and tensile testing. Their microstructure was analyzed by granulometry and SEM images.

5.3.1 Effect of a single extrusion by using screw Profile-1 on the microstructure and mechanical properties of polystyrene composites containing 30 wt% and 50 wt% of equiv-GTR

5.3.1.1 Effect of high temperature compounding on polystyrene qualities: x , GE and molecular weight

During the first single extrusion, the unreacted styrene remaining in both the 30GTR-g-PS/f-PS1 and 50GTR-g-PS/f-PS2 composites polymerizes almost completely. Table 5.8 shows, for example, the results of x , amount of grafted-PS and GE of the composite containing 50 wt% of equiv-GTR. The formation of grafted-PS chains remains favored over free-PS, and GE varies slightly. By contrast, it was not possible to calculate GE of the composite containing 30 wt% equiv-GTR as mentioned above.

Table 5.8 – Ultimate x and GE of polystyrene after a single extrusion at high temperature

Composite	Number of extrusion	x	$\frac{\text{grafted-PS}}{\text{free-PS}}$ (w/wt%)	GE (%)
50GTR-g-PS/f-PS2	0	0,80 ($\pm 0,02$)	1,8 ($\pm 0,4$)	63,1 ($\pm 3,8$)
	1	0,96 ($\pm 0,02$)	1,6 ($\pm 0,4$)	61,4 ($\pm 0,01$)

Table 5.9 shows the measurements of molecular weight, M_n and M_w , of free-PS1 and free-PS2 before and after a single extrusion of the composites at 200 °C . It can be seen that the molecular weight of free-PS2 increases slightly, contrary to free-PS1, which is reduced by almost half. Despite this, the molecular weight remains higher in the composite containing more polystyrene (i.e., 30GTR-g-PS/f-PS1). Note that these values are very low compared to the molecular weight of PS6 (cf. Table 5.7), and thus, the low-molecular-weight polymer chains on both free-PS are always dominant.

Table 5.9 – Molecular weight of free-PS in grafted composites after a single extrusion.

Polystyrene matrix	Number of extrusion	M_n (g/mol)	M_w (g/mol)	M_w/M_n
free-PS1	0	7,95E+04 ($\pm 0,09E04$)	1,66E+05 ($\pm 0,03E04$)	2,10 ($\pm 0,07$)
	1	4,22E+04 ($\pm 0,11E04$)	8,22E+04 ($\pm 0,15E04$)	2,30 ($\pm 0,07$)
free-PS2	0	1,98E+04 ($\pm 0,04E04$)	3,04E+04 ($\pm 0,03E04$)	1,53 ($\pm 0,02$)
	1	2,11E+04 ($\pm 0,02E04$)	3,27E+04 ($\pm 0,03E04$)	1,55 ($\pm 0,02$)

5.3.1.2 Influence of the GTR content on Charpy impact strength (IS)

Three sets of notched specimens of 30GTR-g-PS/f-PS1, 50GTR-g-PS/f-PS2 and 50GTR/PS6, were analyzed by high-speed Charpy impact testing and the evolution of the events was recorded. Figure 5.9 displays the evolution of the impact load (N) as a function of the displacement (mm). Here, the load is the force required to provoke plastic deformation (peak force) and complete rupture (total force) of the specimen. The displacement is an indication of specimen deformation before it fails. These curves are the average of three of the most representative results of the observed behavior for each composite.

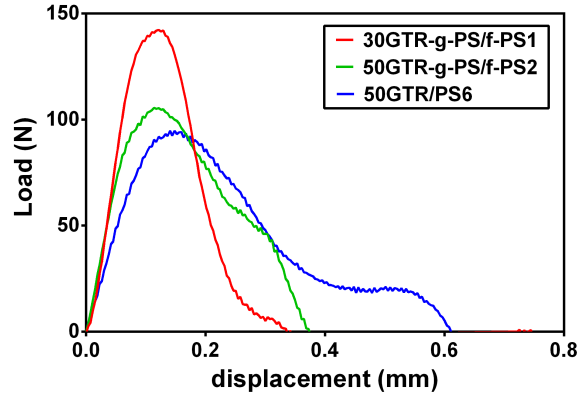


Figure 5.9 – Load cell responses during the impact events.

It is seen that the peak force is the highest for the 30GTR-g-PS/f-PS1 composite, however, it breaks at lower deformations. In contrast, the deformation of both 50GTR-g-PS/f-PS2 and 50GTR/PS6 composite is more important, especially for the latter. On the one hand, these profiles represent the mechanical behavior attributable to ductile materials as in the case of the composites containing 50 wt% of equiv-GTR or raw GTR. On the other hand, when decreasing the content of equiv-GTR to 30 wt%, the composites present a combined ductile/brittle behavior.

The integration of the area beneath the load-displacement curve corresponds to the total energy exchanged during the impact event until the specimen rupture. Then, this impact energy is normalized to the cross-section of the notched specimen to determine the notched Charpy impact strength (IS). However, these values need be interpreted with caution and cannot be directly compared. Indeed, the impact resistance of the polymer matrices, namely free-PS1, free-PS2 and PS6, is not identical, since these have different molecular weight. Therefore, to establish if these polystyrene matrices are effectively toughened by the presence of 30GTR-g-PS, 50GTR-g-PS or raw GTR particles, respectively, the notched Charpy IS of each of the composites must be exclusively compared with that of its respective polystyrene matrix (i.e., neat polystyrene without GTR-g-PS or raw GTR).

Table 5.10 presents both the notched and unnotched Charpy IS of the three polystyrene matrices. The values for PS6 were directly measured from notched and unnotched specimens. It is noticed that the impact resistance of PS6 decreases in about 61% when the specimens are notched. By contrast, the notched Charpy IS of each of the free-PS was predicted by means of a correlation function between the IS of polystyrene and its M_w , presented in Equation 5.1. This function was determined from values reported in the literature and experimental measurements carried out in this work. These latter were performed on a series of impact specimens made of polystyrene of different M_w , but similar to those of free-PS1 and free-PS2 after extrusion. A detailed explanation of the experiments and calculation of the correlation is presented in Appendix 2.

$$IS_{PS} \quad (kJ/m^2) = (8 \cdot 10^{-11} \cdot M_w^2 + 1 \cdot 10^{-5} \cdot M_w) \cdot 0.39 \quad (5.1)$$

Note that the M_w of PS6 is approximately 60% to 86% higher than those measured for all the free-PS. As a consequence, both the notched and unnotched Charpy IS of PS6 are significantly higher compared to that of the free-PS.

Figure 5.10 compares the notched Charpy IS of each composite with the notched and unnotched values of their respective polystyrene matrices. The Y scales are different to better observe the variations. For example, the notched Charpy IS of the 50GTR-g-PS/f-PS2 composite is about 0.78 kJ/m^2 , which

Table 5.10 – Notched and unnotched Charpy IS of the polystyrene matrices

Polystyrene matrix	M_w (g/mol)	Charpy IS (kJ/m ²)	
		Unnotched	Notched
free-PS1	9,72E+04 (±0,15E04)	1,30 (±0,09)	0,51 (±0,04)
free-PS2	3,04E+04 (±0,03E04)	0,65 (±0,01)	0,25 (±0,03)
PS6	2,38E+05 (±0,18E04)	5,16 (±0,06)	2,02 (±0,06)

Table 5.11 – Improvement or deterioration percentages of the notched Charpy IS of polystyrene matrices. Compounds after a single extrusion.

Composite	IS_{var} (%)
30GTR-g-PS/f-PS1	+40 (± 1,4)
50GTR-g-PS/f-PS2	+207 (± 3,2)
50GTR/PS6	-54 (± 1,6)

outperforms in approx. 0.5 kJ/m² and 0.12 kJ/m² the notched and unnotched IS of its polystyrene matrix, free-PS2, respectively. By contrast, the Charpy IS of PS6 is drastically degraded by the addition of raw GTR.

What stands out in this figure is that the notched Charpy IS of both GTR-g-PS/f-PS composites, outperforms that of their respective polystyrene matrices. This suggests that the presence of GTR-g-PS particles effectively enhances the impact resistance of free-PS, and it seems to increase with the content of equiv-GTR. To a better comprehension of these results, the improvement or deterioration effects by the presence of GTR-g-PS or raw GTR particles, on the notched Charpy IS of the polystyrene matrices may be quantified as follows:

$$IS_{var}(\%) = \frac{IS_{composite} - IS_{polystyrene}}{IS_{polystyrene}} * 100 \quad (5.2)$$

where $IS_{composite}$ is the notched Charpy IS of the composite and $IS_{polystyrene}$ is the notched Charpy IS of the respective polystyrene matrix. Thus, the variation (by percent) of the impact strength (IS_{var}), may be reported as positive or negative to indicate the improvement or deterioration, respectively. These percentages are valid to compare the notched Charpy IS of the distinct composites regardless of the molecular weight differences of their polystyrene matrices.

Table 5.11 shows the calculated percentages of IS_{var} . Thus, in presence of 50 wt% of raw GTR, and under the same compounding conditions, there are two possibilities: improve polystyrene Charpy IS substantially in more than 200% by partially grafting the polymer matrix onto/into the raw GTR particles, or largely deteriorate it in more than 50% by simply mixing them.

5.3.1.3 Fracture surfaces of impact specimens

Figure 5.11 displays the SEM micrographs of the fracture surfaces of the impact specimens. Some rubber particles on the fracture surface of the 50GTR/PS6 specimens (Fig. 5.11a) are exposed and others have been pulled out forming cavities. The porous appearance of the regions around crumbs and cavities is evidence of the plastic deformation of the polymer matrix. As a result, the matrix defects and weakly

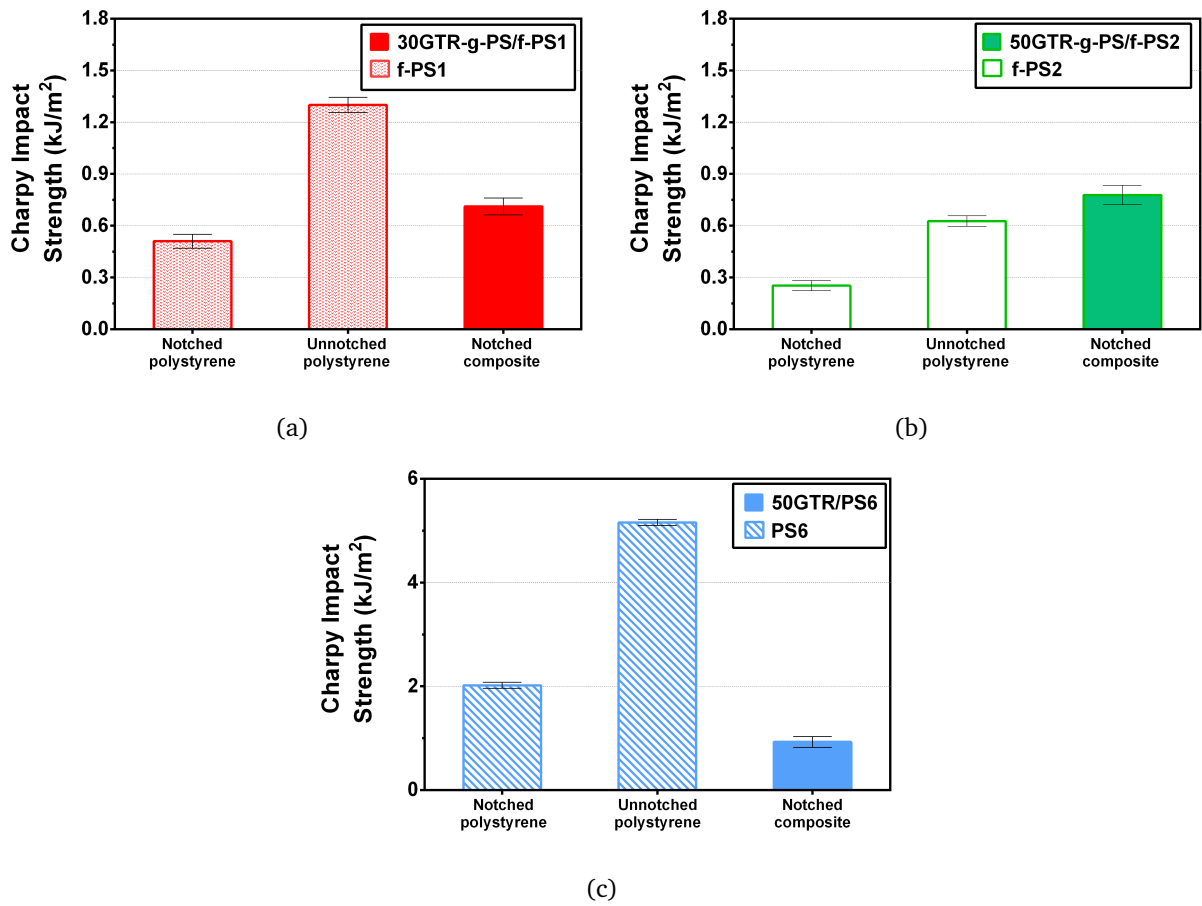


Figure 5.10 – Comparison of the Charpy IS of polystyrene and polystyrene composites after a single extrusion: (a) 30GTR-g-PS/f-PS1, (b) 50GTR-g-PS/f-PS2 and (c) 50GTR/PS6.

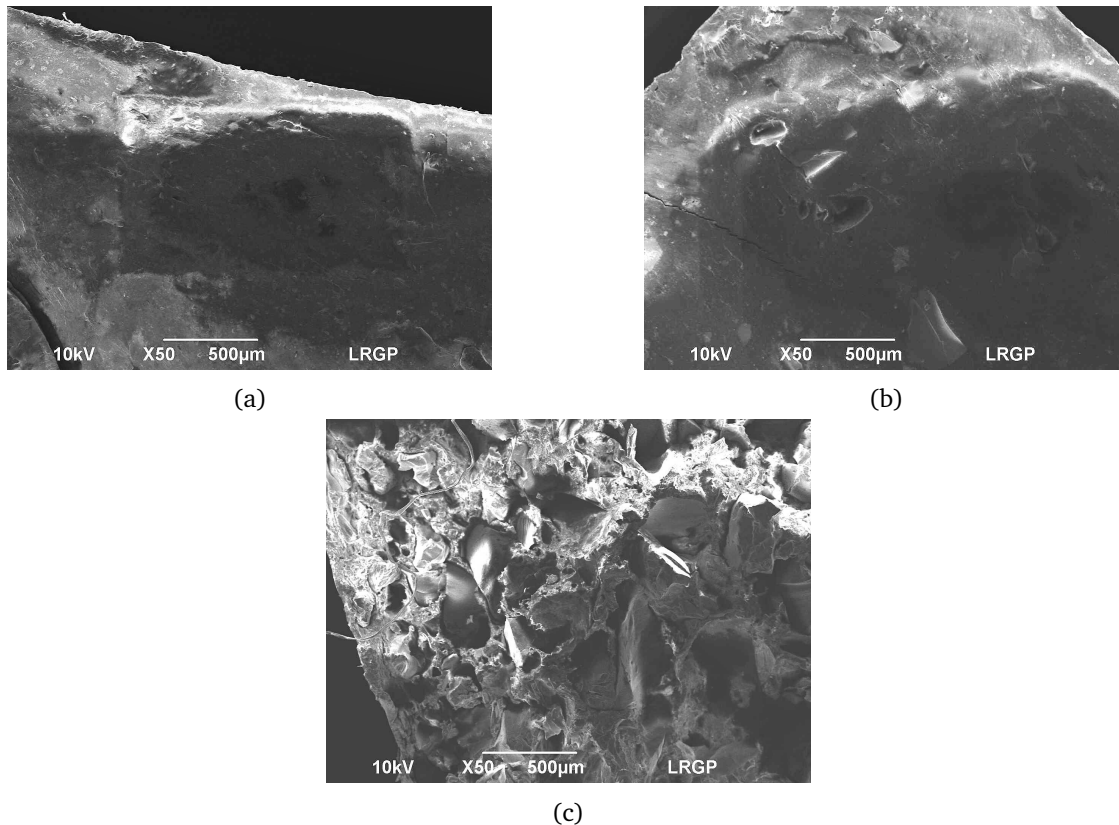


Figure 5.11 – Fracture surfaces of impact specimens of the composites after a single extrusion: (a) 30GTR-g-PS/f-PS1, (b) 50GTR-g-PS/f-PS2 and (c) 50GTR/PS6.

adhered particles seem to be the precursors of the interfacial fracture.

On the other hand, the surfaces of both polystyrene grafted GTR specimens (GTR-g-PS/f-PS) are smoother and the rubber granulates are much less visible. A well interpenetration of both GTR-g-PS particles with free-PS is reached and therefore, the individual phases cannot be distinguished. Stronger bonding produces a moderately ductile (i.e., ductile/brittle) fracture. The cavities observed on the fracture surface of the 30GTR-g-PS/f-PS1 specimen (Fig. 5.11b) are probably formed during specimens' fabrication.

5.3.1.4 Intermediate discussion and interpretation

Through the measurement of the Charpy *IS*, it has been demonstrated that under specific conditions, polystyrene can be effectively toughened by the addition of recycled rubber particles as GTR. In fact, the simple dispersion of raw GTR into PS6 by mixing in the extruder, decreases drastically the Charpy *IS* of PS6. By contrast, under the same compounding conditions, the reinforcing effects are only evidenced when the polystyrene phase is partially grafted beforehand into/onto the raw GTR.

When comparing the notched Charpy *IS* of the three composites obtained, it is noticed that the increased interfacial adhesion, achieved via polystyrene grafting, is an important parameter but not the only one influencing the ultimate impact strength. This suggests that it is necessary to consider other possible influencing parameters, such as the particle size distribution and morphology. Indeed, the micrographs of the fracture surfaces reveal that the microstructure of the composite suffered substantial changes during mixing in the twin-screw extruder. For example, the individual phases, i.e., the GTR-g-

PS particles and free-PS matrix, cannot be distinguished and coarse particles are absent, by contrast to the 50GTR/PS6 composite. Therefore, it is possible that such differences are responsible for effective polystyrene toughening.

These results are consistent with those of the previous research [55] and suggest that the grafting polymerization strengthens the interfacial adhesion between GTR-g-PS and free-PS. This is favored by the reactive extrusion that takes place when compounding at high temperature conditions (180 to 200 °C), during which the polymerization of the remaining styrene is completed. Under these conditions, the radical peroxide initiators (BPO, DCP and DHBO) are consumed very rapidly and thus, the polymerization is rather thermally initiated.

Moreover, devulcanization and reclaiming of the cross-linked structure of GTR is also expected to occur at some extent. Then, the cleavage of mono and polysulfide bonds -C-S- and -S-S-, and elastomer -C-C- bonds may lead to form new radicals that can initiate polymerization or serve as grafting sites for the growing radical chains. This could explain that the formation of grafted-PS continues to be favored and *GE* remains almost unchanged. It is possible therefore, that the more amount of polystyrene grafts, the higher interfacial adhesion between GTR-g-PS and free-PS, which may be associated to the increased capability of these composites to absorb higher impact energies and withstand larger plastic deformation before failure.

The notched Charpy *IS* of standard polystyrene, represented here by the free-PS, can be increased by about 50% and continues rising up to 200% when passing from 30 wt% to 50 wt% of equiv-GTR. This result differs from some published studies that reported the existence of an optimum of GTR content (modified or blended with compatibilizer agents) ranging from 20 to 30 wt% at which the *IS* of PS and PP can be maximized. [45, 92]. Moreover, as mentioned in the literature review (c.f. Sect. 3.2.2.3), a prior study has noted that the notched Charpy *IS* of standard polystyrene is drastically deteriorated at M_w values below 210 000 g/mol [96]. In contrast to this approach, the findings above indicate that the 50GTR-g-PS/f-PS2 composite is the material that better withstands the impact events in spite of having the lowest M_w . This result suggests that the interfacial adhesion between the GTR-g-PS particles and free-PS is a parameter of higher influence, over the free-PS molecular weight, on the measured Charpy *IS*. Nevertheless, additional characterizations were performed to better identify the effects of mixing in the twin-screw extruder.

5.3.1.5 Effect of the grafting compatibilization on tensile mechanical properties

The above effects of reinforcing polystyrene with GTR-g-PS particles were observed through the measurement of the impact properties. Additional tests were carried out to determine whether those effects still exist when studying the mechanical behavior of the composites by tensile testing. Figure 5.12 shows the nominal stress-strain curves of tensile specimens of both 50GTR-g-PS/f-PS2 and 50GTR/PS6 composites. It can be seen that the stress at yield σ_y , stress at break σ_r and Young' modulus E of the 50GTR/PS6, are rather representative of the rigid behavior of the PS6 matrix, which seems to predominate over the elasticity of the raw GTR. By contrast, despite the lower values of σ_r and E , the elongation at break point ε_r of the 50GTR-g-PS/f-PS2 composite is significantly increased by more than 55%, as shown in the summary in Table 5.12. In this case, it is possible to notice the high extensibility capability of the dispersed GTR-g-PS phase. Note that, the value of E is calculated from the slope of the linear stress-strain curve at strain values below 0.25% for all the composites.

As reported above (cf., Table 5.7), the molecular weight of PS6 is almost 5 times higher than that of free-PS2. Despite this large difference, the presence of polystyrene grafts into/onto the raw GTR surfaces seems to strengthen the interfacial bonding of GTR-g-PS with free-PS. Therefore, the resulting composite is a more ductile material, which is able to endure higher strains before rupture. This also

accords with the observations on impact strength properties.

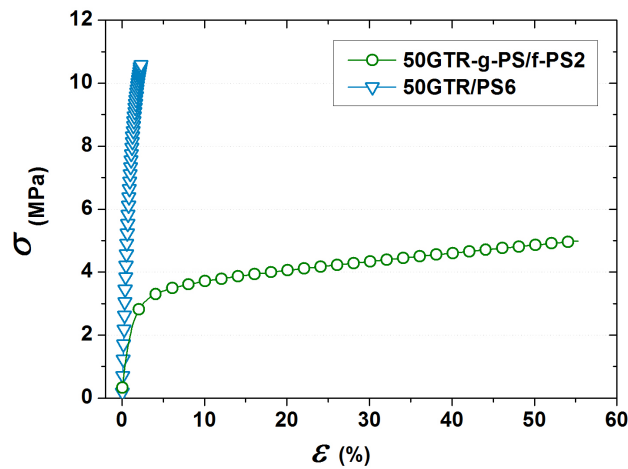


Figure 5.12 – Stress-strain curves of tensile specimens of composites with 50 wt% of equiv-GTR or raw GTR after a single extrusion.

Table 5.12 – Tensile properties of the composites after a single extrusion.

Composite	$E, 0.25\%$ (MPa)	σ_y (MPa)	σ_r (MPa)	ε_r (%)
50GTR-g-PS/f-PS2	230 ($\pm 4,6$)	3,6 ($\pm 0,18$)	5 ($\pm 0,23$)	55,5 ($\pm 4,96$)
50GTR/PS6	921 ($\pm 18,4$)	8,3 ($\pm 0,42$)	10,5 ($\pm 1,22$)	2,3 ($\pm 0,05$)

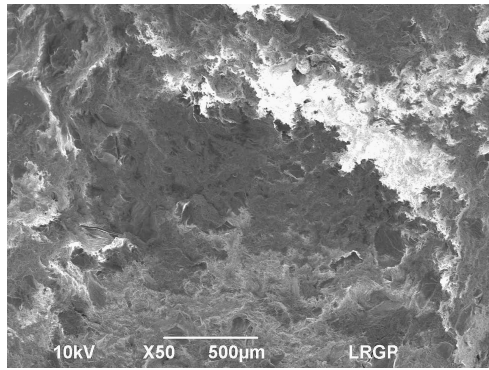
5.3.1.6 Fracture surfaces of tensile specimens

SEM micrographs of the fracture surfaces of the tensile specimens are displayed in Figure 5.13. The 50GTR/PS6 specimen exhibits a fracture surface that is similar to that of the impact specimens. Due to the weak particle-matrix interactions, there are voids around the raw GTR particles and some are pulled-out forming large cavities. In a similar way, the particles seem to be primarily responsible for the initiation of interfacial rupture.

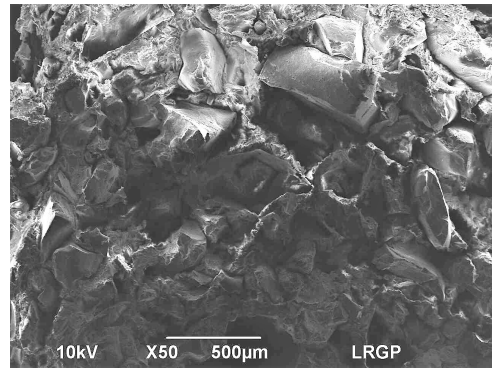
In contrast, the appearance of the 50GTR-g-PS/f-PS2 specimen reveals that both the GTR-g-PS and free-PS2 phases are well integrated, since the individual particles cannot be distinguished. The roughness of the fracture surface indicates that the interpenetrated phases follow an important plastic deformation and a more ductile fracture than the one obtained during impact testing.

5.3.1.7 Effect of a single extrusion on the morphology and PSD of GTR-g-PS particles

Figure 5.14 shows the SEM micrographs of the particles contained in both 30GTR-g-PS/f-PS1 and 50GTR-g-PS/f-PS2 composites, namely the 30GTR-g-PS (a-b) and 50GTR-g-PS (c-d), respectively. The particles were observed after removal of free-PS. In addition, the PS6 in the 50GTR/PS6 composite was also removed to observe the 50GTR ones (e-f). The particles before extrusion are shown on the left and after the extrusion on the right. Images reveal that there has been a drastic size reduction of both

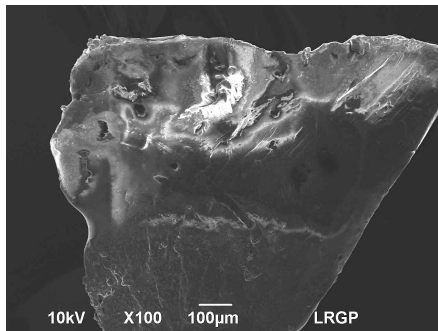


(a)

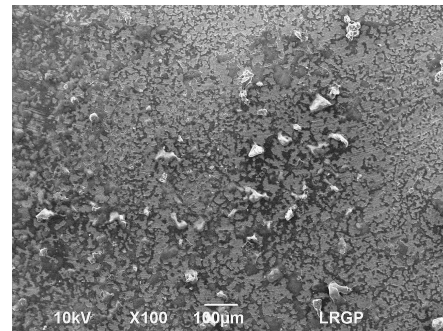


(b)

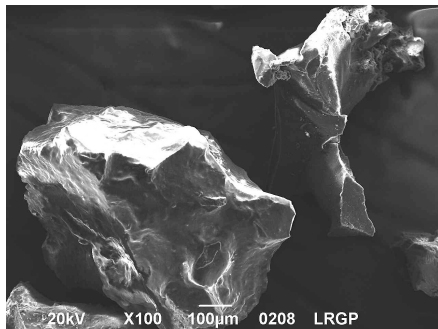
Figure 5.13 – Fracture surfaces of tensile specimens of: (a) 50GTR-g-PS/f-PS2 and (b) 50GTR/PS6.



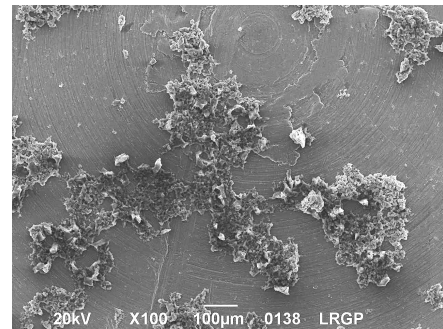
(a)



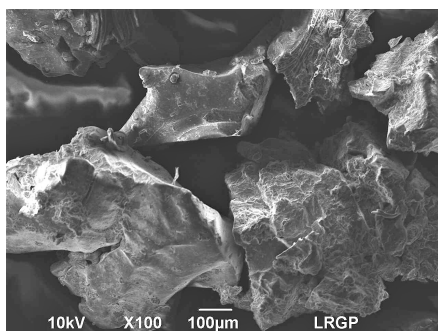
(b)



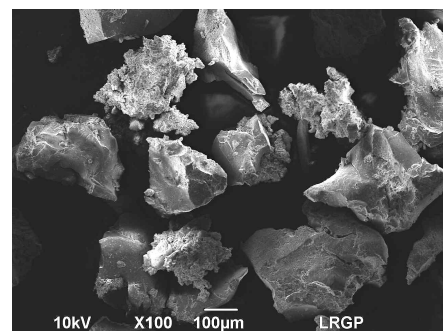
(c)



(d)



(e)



(f)

Figure 5.14 – Morphology of the particles contained in the composites before (at left) and after (at right) a single extrusion: (a-b) 30GTR-g-PS (c-d) 50GTR-g-PS and (e-f) 50GTR.

GTR-g-PS particles as a consequence of the compounding step at 200 °C .

By zooming on 50GTR-g-PS particles before and after extrusion (Fig. 5.15), it is observed that their surfaces are very rough and the shape changes from irregular granulates to completely irregular clusters or agglomerates, for which individual particles are difficult to identify.

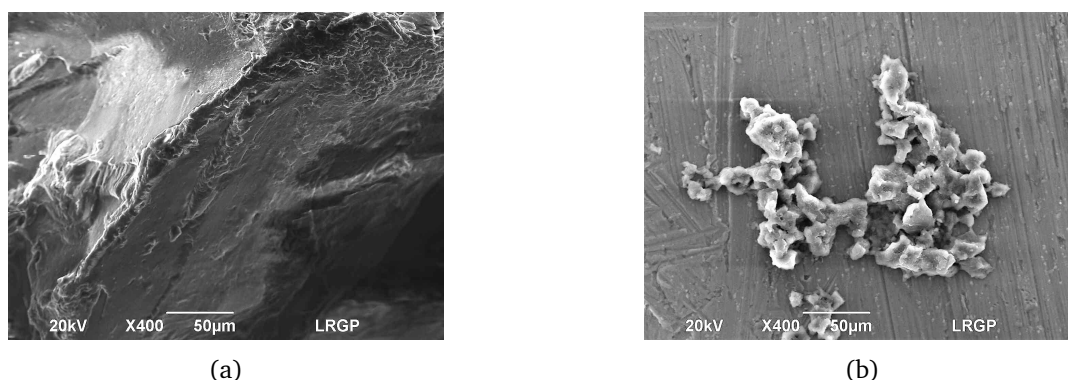


Figure 5.15 – Zoom of the morphology of 50GTR-g-PS particles before and after a single extrusion.

The differences in particle size were quantified by granulometry. For example, Figure 5.16 compares the particle size distribution (PSD) of raw GTR (as-received GTR, dotted line) with those of 50GTR-g-PS ones (solid green line) after a single extrusion of the 50GTR-g-PS/f-PS2 composite. Results are expressed as the volume fraction distribution of particles in the range of size categories present in the sample. For instance, the volume occupied by raw GTR particles having a size ranging from 500 to 600 µm, represents about 10,1 % (area beneath the curve between the size range) of the total volume occupied by all the particles in the sample.

It is observed that, after a single extrusion of the 50GTR-g-PS/f-PS2 composite, the size of the 50GTR-g-PS particles decreases and their distribution is not unimodal. In a similar way, and as will be seen along this chapter, the distribution curves obtained for most of the samples exhibit bimodal or multimodal distributions. Therefore, these curves are deconvoluted to simplify the analysis. Figure 5.17, shows an example of the deconvolution of the PSD curve of 50GTR-g-PS particles (solid green line). The graph reveals how this specific PSD distribution can be considered as a mixture of three normal distributions or populations, having different individual volume fractions (Φ) and mean characteristic diameters or mean sizes (\varnothing). Note that Φ is defined as the volume fraction occupied by a single population over the total volume occupied by all populations.

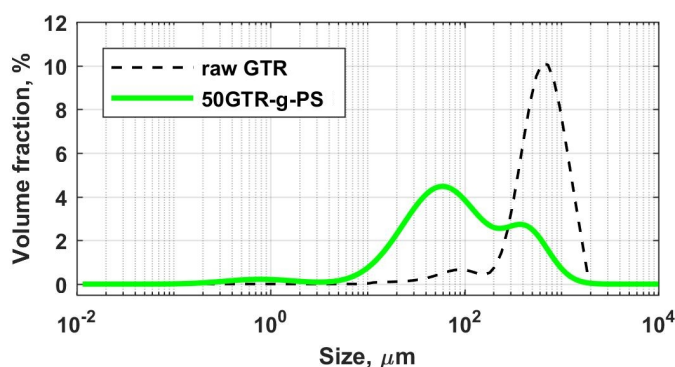


Figure 5.16 – Comparison of the PSD between raw GTR and 50GTR-g-PS particles after a single extrusion.

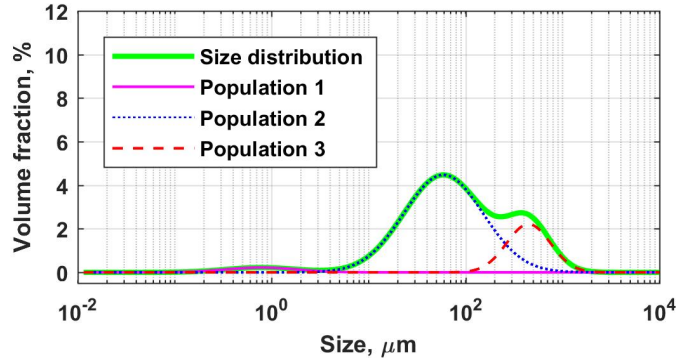


Figure 5.17 – Example of deconvolution of the PSD curve of 50GTR-g-PS particles after a single extrusion.

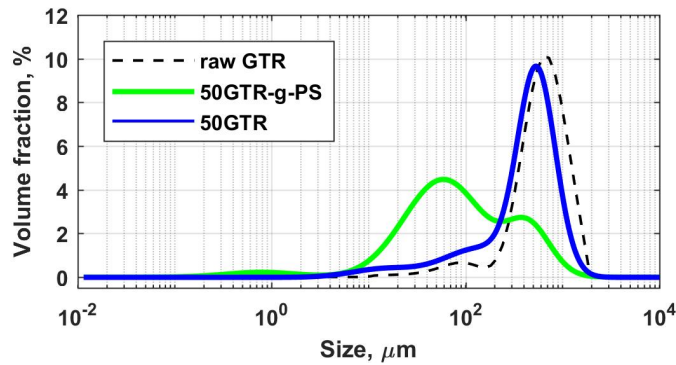


Figure 5.18 – Comparison of the PSD of particles of raw GTR and particles of 50GTR and 50GTR-g-PS after a single extrusion

5.3.1.8 Influence of the grafting compatibilization on PSD of GTR-g-PS particles

Figure 5.18 compares the PSD of raw GTR with both the 50GTR-g-PS and 50GTR particles. The distribution curves reveal that the grafted particles are reduced in size gradually by forming two main mixed populations having very distinct mean sizes. By contrast, size reduction is more uniform, i.e., the unimodal distribution is almost preserved, for the non-grafted ones and both the distribution profile and mean size remain similar to that of the raw GTR.

Table 5.13 summarizes the values of mean size for the populations having the two largest Φ (cumulative volume fraction up to 80 %), in each of the curves. What stands out in this table is the drastic decrease of almost 90% in the mean size of most of the 50GTR-g-PS particles ($\Phi = 76\%$ in volume) after a single extrusion.

5.3.1.9 Influence of the amount of GTR on PSD of GTR-g-PS particles

Size distribution curves of both 30GTR-g-PS and 50GTR-g-PS particles are compared in Figure 5.19. It is observed that the distribution of the former is multimodal and covers a large size range from 1 to 1000 μm . The characteristic diameters of both populations are shown in Table 5.14. The bigger population of 30GTR-g-PS is similar in Φ and mean size to the one in 50GTR-g-PS. Nevertheless, the second most important population of 30GTR-g-PS has a mean size of only a few microns.

By comparing the mixing torques τ (Tables 5.13 and 5.14), it is seen that for a constant feeding rate of 1 kg/h, it increases with the GTR content. In particular for 50GTR-g-PS/f-PS2, the torque was

Table 5.13 – Characteristic diameters of particles of raw GTR and particles of 50GTR and 50GTR-g-PS after a single extrusion.

Particles	Mean diameter ^a \varnothing (μm)	Volume fraction ^b Φ	Extrusion torque τ (Nm)
raw GTR	585	0,97	
50GTR	139	0,20	45
	541	0,75	
50GTR-g-PS	59	0,76	76
	446	0,21	

Stand. Dev. range from: ^a. 1,0 to 1,21 and ^b. 0,003 to 0,03

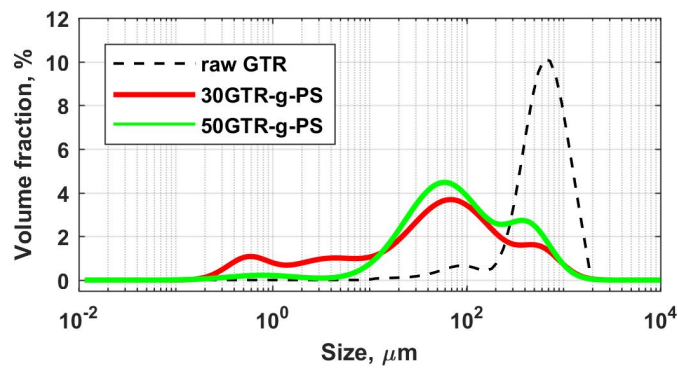


Figure 5.19 – Comparison of the PSD of raw GTR particles and grafted ones of 30GTR-g-PS and 50GTR-g-PS.

Table 5.14 – Characteristic diameters of raw GTR particles and grafted ones of 30GTR-g-PS and 50GTR-g-PS after a single extrusion.

Particles	\varnothing^a (μm)	Φ^b	τ (Nm)
raw GTR	585	0,97	
30GTR-g-PS	4	0,15	22
	69	0,66	
50GTR-g-PS	59	0,76	76
	446	0,21	

Stand. Dev. range from: ^a. 1,0 to 1,21 and ^b. 0,001 to 0,04

about 76 Nm, in comparison to 22 Nm for the 30GTR-g-PS/f-PS1 composite. Despite the significant differences on M_w between free-PS2 and PS6, τ is superior in about 68%.

5.3.1.10 Discussion and interpretation

The results above indicate that the mechanical behavior of the composites obtained is dictated by the co-action of the two fabrication processes implemented. On the one hand, the grafting polymerization by using a mix of peroxide initiators to promote good interfacial adhesion between GTR-g-PS particles and free-PS, and on the other hand, the modification of the composite microstructure via twin-screw extrusion, i.e., PSD and morphology of the rubber particles, as well as degree of dispersion and distribution through the polymer matrix.

In the first part of this section, it was demonstrated that polystyrene can be effectively toughened when this is partially grafted to raw GTR. The notched Charpy IS is increased when containing 30 wt% and 50 wt% of equiv-GTR. These results are corroborated by the stress-strain curves. In the 50GTR/PS6 composite, the linear shape of the stress-strain curve is representative of the brittle behavior of standard polystyrene, represented by the PS6 matrix, shown in Figure 3.1. This behavior seems to be transformed, in presence of the GTR-g-PS particles, to that of a toughened polystyrene, which elastic and plastic deformation capability are significantly enhanced in detriment of E , σ_y and σ_r properties.

In addition to the effective modification of the GTR surface, the ultimate microstructure leading to increase the impact strength involves irregular GTR-g-PS particles having a multimodal size distribution. The mean sizes after one extrusion mainly lie between 60 and 70 μm . These findings differ from those of the relevant literature [54, 84, 85], according to which the optimal mean particle size ranges from 3 to 5 μm , with a PSD combining sub-micrometer and larger particles (c.f. Table 3.1). It has been possible, therefore, to demonstrate that significant improvements in IS are not only observable in the sub-micrometer size domain.

One interesting finding is the drastic reduction of the size of GTR-grafted-PS particles and morphological changes during high temperature extrusion. This result may be explained by a number of different factors. As mentioned in Chapter 3, the grafted polystyrene leads to particle dispersion during extrusion, or in other words, the reduction in size of the GTR-g-PS particles. Nevertheless, the ultimate particle size is rather determined by the mixing shear, which depends, at the same time, on the viscosity of both polymer phases.

When compounding the grafted composites, the dispersion of GTR-g-PS particles begins from the first mixing section of the screw, where polymer melting takes place. Then, polystyrene is at the molten state (low viscous) and the cross-linked GTR contained in the GTR-g-PS particles remain almost unchanged at the rubbery state. It is possible that, under these conditions, the viscosity of the material flowing through the extruder is rather high. This could favor the development of high mixing shear, noticeably through the kneading blocks of the screw profile. When the shear stresses are high, the particles are subjected to numerous and large deformations, and thereby, strain is cumulated until the particles break down under the effect of the mechanical fatigue. [3, 24].

At the same time, and as mentioned above, some GTR devulcanization and reclaiming are also expected to take place during extrusion. Then, a gel rubber fraction and a soluble rubber fraction are formed. Both mechanisms, dispersion and devulcanization generate higher surface areas that increase the intimate contact with free-PS. This promotes a fine dispersion, homogeneous distribution and therefore, well integrated particle-polymer phases, as evidenced on SEM images of the fracture surfaces.

The effects above demonstrate that the extrusion conditions and screw configuration defined lead to obtain a size distribution of GTR particles, which is specific for each of the composites. In addition,

the toughening effects are evidenced, regardless of the content of GTR added to the formulation.

It was also found that for a fixed content of 50 wt% of equiv-GTR or raw GTR and feeding rate of 1 kg/h, the highest mixing torques were reached when extruding the polystyrene grafted GTR composites. This may be associated to the presence of free and grafted polystyrene into/onto GTR. Since the simple mixing of raw GTR with PS6 leads to weak particle-polymer interfaces and inefficient size reduction, the polymer can hardly penetrate the rubber phase and remains around the raw GTR particles. Thus, when the polymer forms a superficial molten film, the transfer of shear mixing is poor, by contrast to the grafted composites. It is therefore possible that this facilitates particles flowing, reducing the filling degree of the kneading zones and the mixing torque.

Another important result is that the fracture surfaces reveal that the 50GTR-g-PS/f-PS2 composite is highly sensitive to the speed of the mechanical testing. Then, high-speed forces applied during impact events change the fracture mode of this composite. In spite of the increased impact strength, the fracture surface presents a flatter surface representative of the brittle behavior. By contrast, the tensile specimens deformed at lower cross-head speeds, exhibit a ductile performance.

5.3.2 Effect of 1, 2 and 3 extrusions by using screw Profile-1 on the microstructure and mechanical properties of polystyrene composites containing 30 wt% and 50 wt% of equiv-GTR

In the previous section it was observed that during a single extrusion step, the mean size of the GTR-g-PS particles was reduced to a few tens of μm . Would the particle size be further reduced to the sub-micrometer domain by additional extrusion steps? Based on the experimental evidence of Yu (2015) [55] (c.f. Sect. 3.5.2.2), the composites obtained were extruded a second and third time at low temperature and by using screw Profile-1.

The extrusion conditions are shown at the beginning of this section 5.3. For the second and third extrusions, the barrel temperature ranges between 90 and 110 °C at the kneading blocks and screw speed is always 200 rpm. The feeding rate is adjusted for each composite and extrusion passage in order to work at the highest possible torque, which is the paramount parameter in this stage.

5.3.2.1 Influence of the number of extrusions on IS

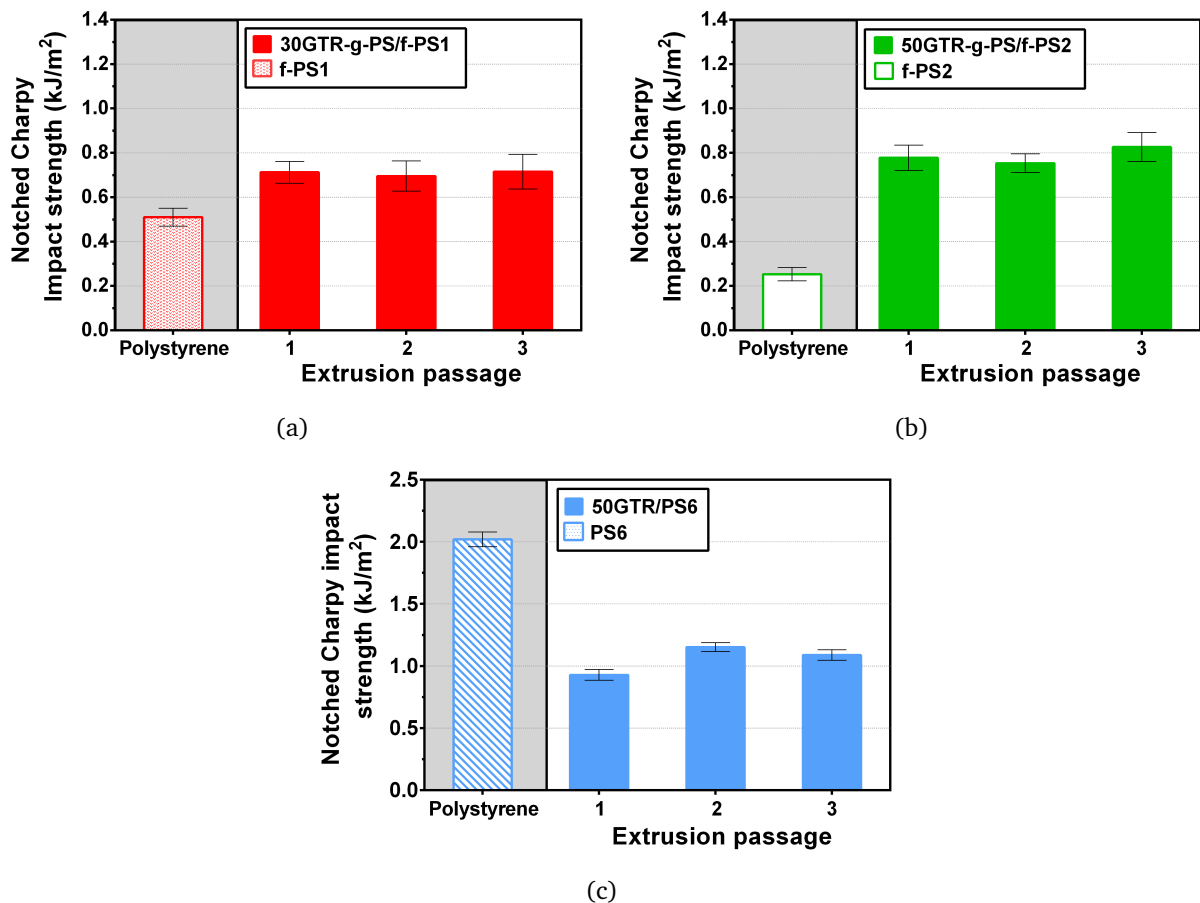


Figure 5.20 – Comparison of the Charpy IS between the polystyrene matrices and composites after 1, 2 and 3 extrusions: (a) 30GTR-g-PS/f-PS1, (b) 50GTR-g-PS/f-PS2 and (c) 50GTR/PS6.

Figure 5.20 compares the notched Charpy IS measurements of the three composites after 1, 2 and 3 extrusions, with those of their respective polystyrene matrix. Y-axis scales are different to better appreciate the variations. The 50GTR/PS6 composite exhibits a gradual increment after the second extrusion (Fig. 5.20c). By contrast, it seems that Charpy IS of the GTR-g-PS/f-PS composites remains almost

unchanging after the second extrusion (Figures 5.20b and 5.20a). After the third extrusion, though, there is a slightly increase in particular for 50GTR-g-PS/f-PS2.

Values of IS_{var} after each extrusion are shown in Table 5.15. The notched Charpy IS values of the composites are compared with those calculated for the polystyrene matrices after the first extrusion. These values corroborate that the Charpy IS of the 30GTR-g-PS/f-PS1 remains almost unchanged after the first extrusion, whereas the one of 50GTR-g-PS/f-PS2 displays a supplementary increase of about 10% after the third extrusion.

Table 5.15 – Improvement or deterioration percentages of the notched Charpy IS of of the polystyrene matrices. Compounds after a 1, 2 and 3 extrusions.

Composite	IS_{var} (%)		
	1st extrusion	2nd extrusion	3rd extrusion
30GTR-g-PS/f-PS1	+40 ($\pm 2,4$)	+37 ($\pm 2,2$)	+41 ($\pm 1,2$)
50GTR-g-PS/f-PS2	+207 ($\pm 6,2$)	+198 ($\pm 5,3$)	+226 ($\pm 5,5$)
50GTR/PS6	-54 ($\pm 2,6$)	-43 ($\pm 2,1$)	-46 ($\pm 2,3$)

The fracture surfaces of the impact specimens of the 50GTR-g-PS/f-PS2 composite are shown in Figure 5.21. It is observed that the failure mode after each extrusion seems to be representative of the brittle/ductile behavior, with smoother and partially flattened surfaces. The individual phases cannot be identified, except for some visible but very small granulates dispersed through the fracture surface.

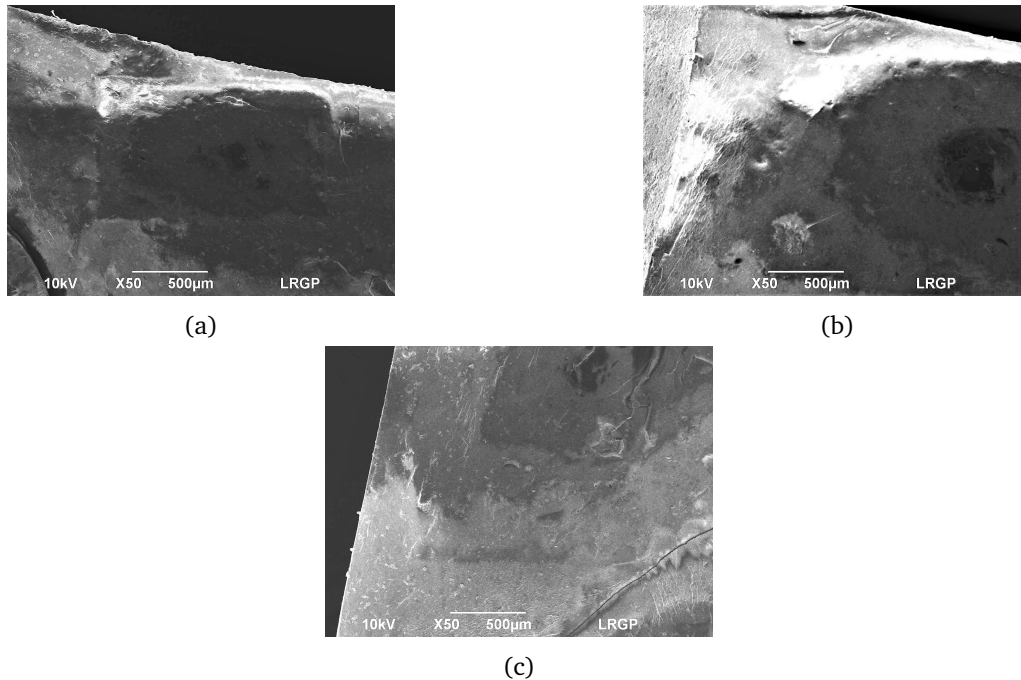


Figure 5.21 – Fractured surfaces of impact specimens of the 50GTR-g-PS/f-PS2 composite after (a) 1, (b) 2 and (c) 3 extrusions.

5.3.2.2 Effect of the number of extrusions on tensile strength properties

The behavior under mechanical stress of the tensile specimens of the 50GTR-g-PS/f-PS2 and 50GTR/PS6 composites after 1, 2 and 3 extrusions, is plotted in Figure 5.22. Y-axis scales are different to better appreciate the variations. Note that σ_r and ε_r of the 50GTR/PS6 composite (Fig. 5.22b) exhibit a slight increase, of about 4,5% and 11,5% after the second extrusion, respectively. These improvements are in agreement with impact testing results.

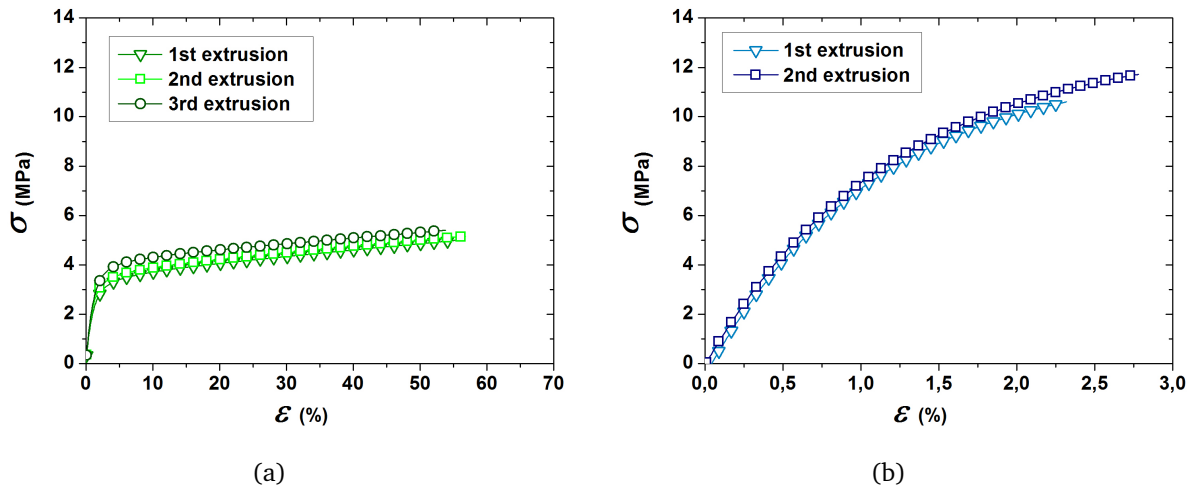


Figure 5.22 – Stress-strain curves of tensile specimens of: (a) 50GTR-g-PS/f-PS2 and (a) 50GTR/PS6 composites after 1, 2 and 3 extrusions.

It is interesting to note that for the 50GTR-g-PS/f-PS2 composite (Fig. 5.22a), both σ_y and σ_r show a gradual increase with the number of extrusions. Note that E also increases progressively, passing from 230 MPa to 277 MPa between the first and the last extrusion, respectively. By contrast, ε_r remains almost unchanged around 55%. The progressive variations in these properties, i.e., σ_y , σ_r and E , seem to be more relevant, mainly after the second extrusion, than those observed for the impact properties. Hence, this may suggest that tensile properties are more sensitive to the possible changes, in the PSD and morphology of the particles, induced during the second and third extrusions. The values obtained for the tensile properties are shown in Table 5.16.

Table 5.16 – Tensile properties of the 50GTR-g-PS/f-PS2 and 50GTR/PS6 composites after 1, 2 and 3 extrusions.

Composite	Number of extrusion	$E, 0.25\%$ (MPa)	σ_y (MPa)	σ_r (MPa)	ε_r (%)
50GTR/PS6	1	921 ($\pm 18,4$)	8,3 ($\pm 0,42$)	10,5 ($\pm 1,22$)	2,3 ($\pm 0,05$)
	2	887 ($\pm 14,4$)	9,2 ($\pm 0,46$)	11 ($\pm 0,7$)	2,6 ($\pm 0,48$)
50GTR-g-PS/f-PS2	1	230 ($\pm 4,6$)	3,6 ($\pm 0,18$)	5 ($\pm 0,23$)	55,5 ($\pm 4,96$)
	2	264 ($\pm 5,2$)	3,8 ($\pm 0,19$)	5,2 ($\pm 0,65$)	57 ($\pm 3,98$)
	3	277 ($\pm 5,4$)	4,3 ($\pm 0,21$)	5,4 ($\pm 0,95$)	54 ($\pm 6,13$)

The fracture surfaces of tensile specimens of 50GTR-g-PS/f-PS2 are shown in Figure 5.23. The surfaces are very rough in contrast to those of the impact specimens. This may be associated to the large

plastic deformation suffered by phases and thus, the fracture mode in the three cases may be associated with a ductile/brittle behavior.

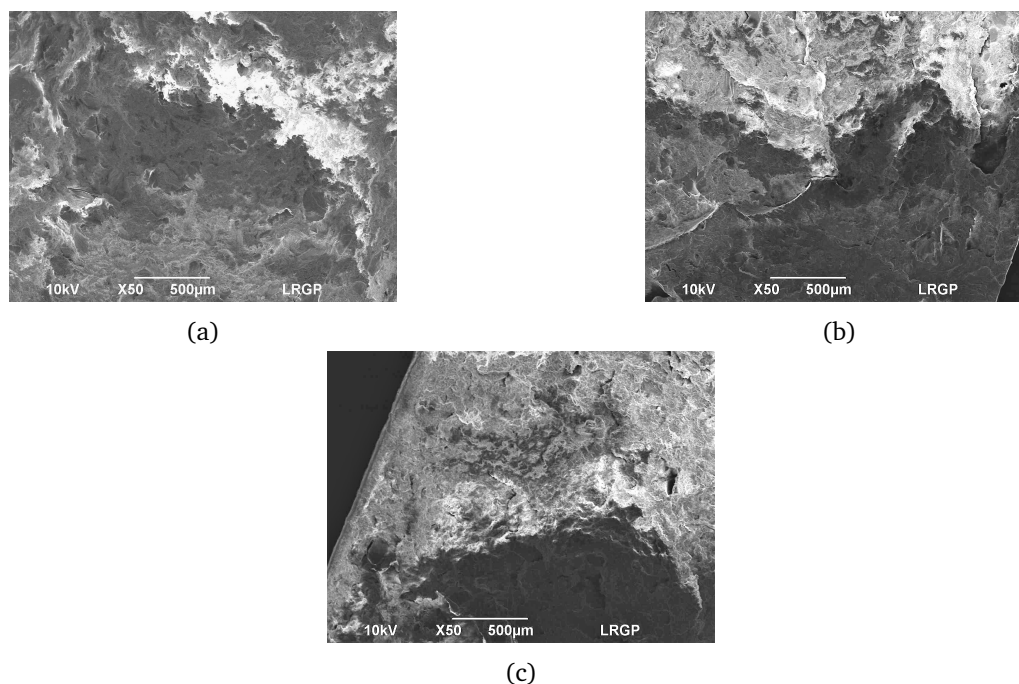


Figure 5.23 – Fracture surfaces of tensile specimens of the 50GTR-g-PS/f-PS2 composite after (a) 1, (b) 2 and (c) 3 extrusions.

5.3.2.3 Changes in the morphology of GTR-g-PS particles after 1, 2 and 3 extrusions.

Changes in the microstructure of the 50GTR-g-PS/f-PS2 composite after 1, 2 and 3 extrusions are appreciated in SEM micrographs in Figure 5.24. The 50GTR-g-PS may be appreciated after removing free-PS2. It seems that the number and size of the irregular agglomerates formed during the first extrusion, decrease gradually after the subsequent extrusion and at the last stage.

5.3.2.4 Changes in PSD of GTR-g-PS particles after 1, 2 and 3 extrusions

The changes in the composite's microstructure were also determined through granulometry measurements. PSD curves are shown in Figure 5.25.

What stands out in these figures is that for GTR-g-PS particles, the number of populations and distribution size ranges decrease gradually during the second and third extrusions, as evidenced in the SEM images. This effect is more pronounced for the 50GTR-g-PS particles, for which the ultimate distribution becomes unimodal during the last extrusion. Contrarily, the tendency is reversed for the 50GTR particles. This means that the presence of large particles predominates and their distribution gradually evolves to broaden size ranges with increasing the number of extrusions. This suggests that gradually dispersion of the raw GTR particles through PS6 matrix also takes place, but a slower size reduction rate compared to the grafted ones. Values of mean particle size and volume fraction for the two main populations of each distribution are shown in Table 5.17.

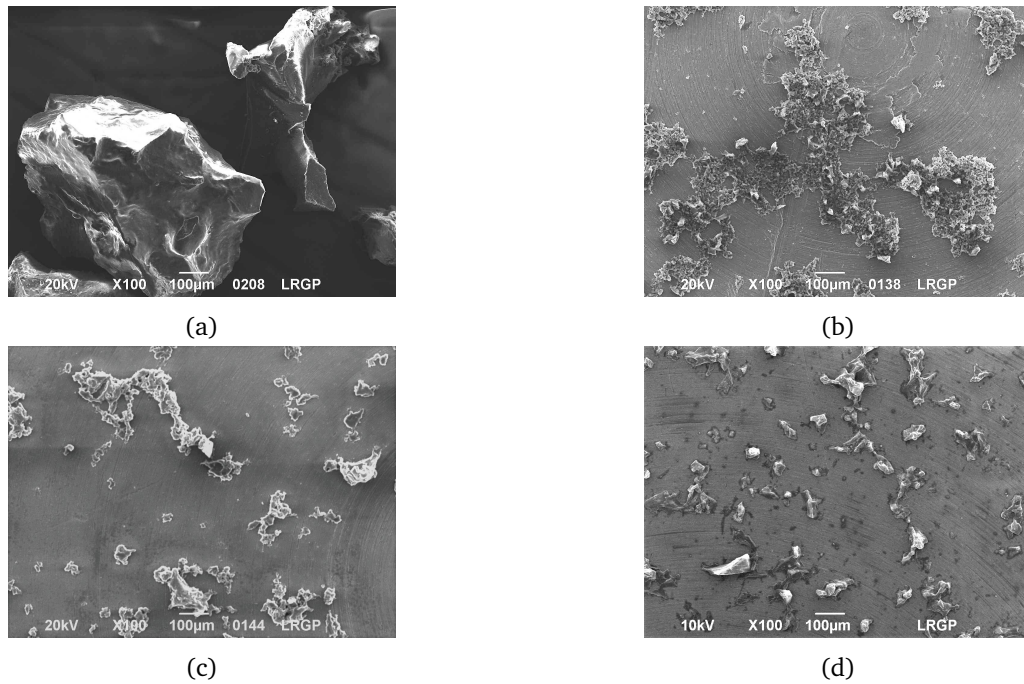
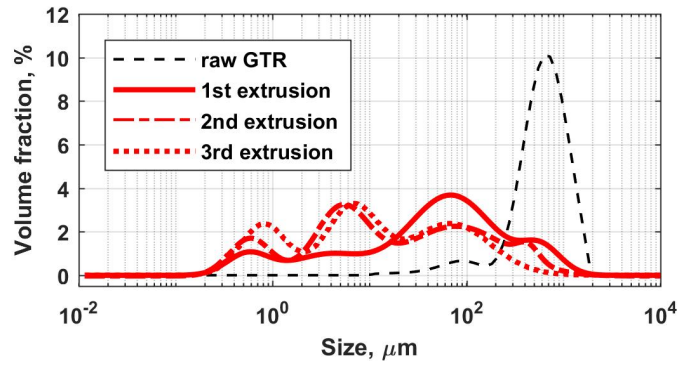


Figure 5.24 – Morphology of the 50GTR-g-PS particles (a) before and after (b) 1, (c) 2 and (d) 3 extrusions.

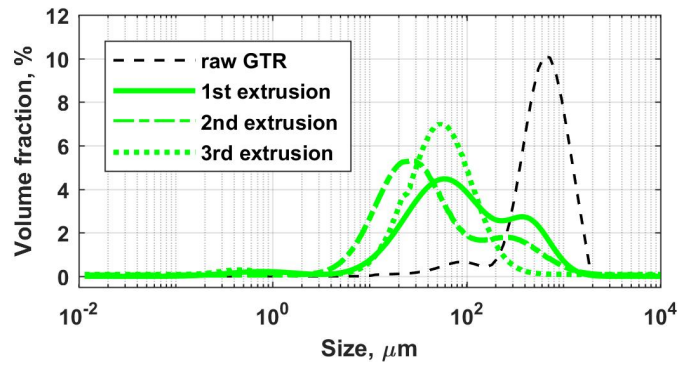
For results understanding and interpretation, the evolution of the mean particle size needs to be analyzed by considering both the PSD curves and the two largest populations in Φ . In Figure 5.25b, for example, the PSD after the first extrusion of the 50GTR-g-PS particles exhibits two main populations, where the largest one ($\Phi = 0,76$) has a mean size about $59 \mu\text{m}$. During the second extrusion, the mean sizes of both populations are slightly reduced. Finally, the second largest population is drastically decreased in size after the third extrusion, forming thus an unimodal distribution ($\Phi = 0,98$), which mean size is approx. of $74 \mu\text{m}$. The increase of the mean particles size suggests that the second largest population was reduced to a size close but superior to the one of the largest population. For this reason, the ultimate mean size shifts to the right.

It is observed that the mean size is reduced with the increment of the number of extrusions. Nonetheless, the progressive transition of the multimodal PSD of the 50GTR-g-PS particles towards an unimodal distribution (c.f. Fig. 5.20c), may be responsible for the gradual increase of the tensile properties of 50GTR-g-PS/f-PS2 such as σ_y and σ_r with the number of extrusions, as well as the improvement on the notched Charpy *IS* after the last extrusion. These results are also in agreement with the observations of the SEM images (c.f. Figure 5.24). In fact, it is possible that the largest irregular agglomerates produced during the first extrusion are gradually broken and finely dispersed during the successive extrusions.

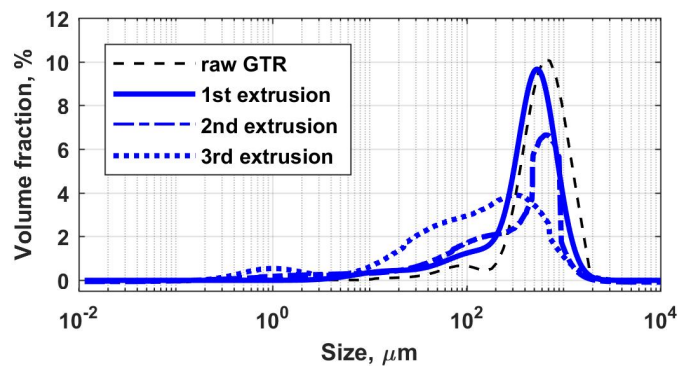
Table 5.17 also shows that the desired working torque, i.e., about 140 Nm, was effectively reached when compounding the composites containing the GTR-g-PS particles. In fact, it was observed that the feeding rate required to attain such τ increased along with the number of extrusions. Nevertheless, it is necessary to clarify that, in some cases it was not possible to get the desired τ due to two main factors: first, the insufficient filling degree of the extruder due to the limited capacity of the feeding system (5 kg/h) and second, the difficulties in quickly adjusting the adequate filling rate without extruder overloading.



(a)



(b)



(c)

Figure 5.25 – Comparison of the PSD of raw GTR with (a) 30GTR-g-PS, (b) 50GTR-g-PS and (c) 50GTR particles.

Table 5.17 – Characteristic diameters of particles of 50GTR, 30GTR-g-PS and 50GTR-g-PS after 1, 2 and 3 extrusions.

Particles	1st extrusion			2nd extrusion			3rd extrusion		
	\varnothing^a (μm)	Φ^b	τ (Nm)	\varnothing^a (μm)	Φ^b	τ (Nm)	\varnothing^a (μm)	Φ^b	τ (Nm)
30GTR-g-PS	4 69	0,15 0,66	22	5 78	0,34 0,47	103	5 48	0,35 0,41	138
50GTR-g-PS	59 446	0,76 0,21	76	43 433	0,76 0,24	141	0,7 74	0,02 0,98	140
50GTR	139 540	0,20 0,75	45	98 426	0,38 0,47	121	61 340	0,58 0,34	114

raw GTR: $\varnothing = 585 \mu\text{m}$ and $\Phi = 0,97$

Stand. Dev. range from: ^a. 1,01 to 1,23 and ^b. 0,002 to 0,035

5.3.2.5 Evolution of the IS of the composites after multiple extrusions

The 50GTR-g-PS/f-PS2 composite was successively extruded five times more, at the same compounding conditions fixed above for the second and third extrusions. The notched Charpy IS was measured for impact specimens of the composite obtained after each extrusion. The mean values are compared in Figure 5.26. It is seen that the notched Charpy IS varies on the range from 0,63 and 0,82 kJ/m^2 . As can be seen, the reinforcing capability of the GTR-g-PS particles is still evidenced even after several extrusions. By comparing these values with the one of free-PS2 (0.3 kJ/m^2), the increment of the impact resistance the polystyrene matrix may vary between 150% and 250%.

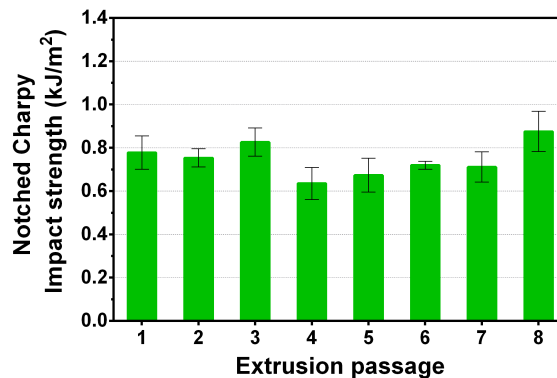


Figure 5.26 – Evolution of the notched Charpy IS after multiple extrusions of the 50GTR-g-PS/f-PS2 composite.

5.3.2.6 Notch sensitivity of polystyrene composites

The unnotched Charpy IS of the 50GTR-g-PS/f-PS2 composite was measured after multiple extrusions (e.g., 6, 7 and 8 extrusions). Figure 5.27 compares both the average notched and unnotched Charpy IS values, in order to get an estimation of the reduction of the impact resistance due to specimen notching (notch sensitivity). It is observed that the variations in the measurements of Charpy IS are significantly lower compared to the reduction of about 61% determined for the PS6 matrix.

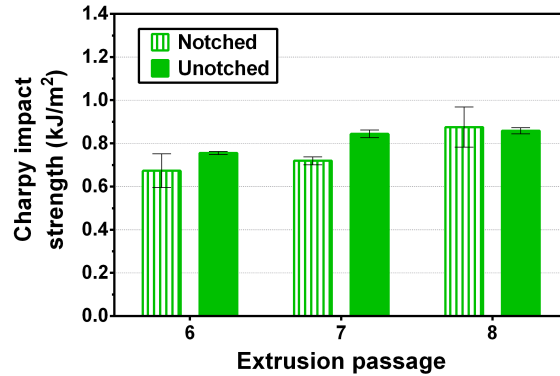


Figure 5.27 – Comparison between notched and unnotched Charpy *IS* of impact specimens of the 50GTR-g-PS/f-PS2 composite.

5.3.2.7 Discussion and interpretation

The effectiveness of high-temperature compounding on decreasing the size of dispersed raw GTR particles - chemically bounded or not - into the polystyrene matrix, was evidenced. Despite the elastic character of the cross-linked structure of GTR, the current study found that the GTR-g-PS particles can undergo a drastic size reduction when extruding in the polymer molten state, e.g., at temperatures about 180 to 200 °C .

The notched Charpy *IS* of the composites displays slight variations after the second and third extrusion. After the successive extrusions, the size of the raw GTR particles dispersed through PS6 are partially reduced forming a broader distribution, in which the coarse particles predominate. However, the presence of smaller particles does not reduce the adverse effects that the raw GTR has on the Charpy *IS* of PS6. By contrast, the toughening effects of the free-PS matrices by the presence of the GTR-g-PS particles are always evidenced after each extrusion. Moreover, the IS_{var} percentages suggest that the notched Charpy *IS* follows slightly variations after the first extrusion.

With regard to the tensile properties of the 50GTR-g-PS/f-PS2 composite, the gradual increase of σ_y , σ_r and E , implies that the elastic deformation capability of the composite material is enhanced. Therefore, it is able to withstand higher stresses without altering its initial behavior and properties, this means, without undergoing permanent damages.

Another important observation is the marked relationship between the PSD and the mechanical behavior. In fact, the tensile properties of the 50GTR-g-PS/f-PS2 composite seem to be more sensitive to variations in the state of dispersion of the GTR-g-PS particles. Therefore, the gradually increase of σ_y , σ_r and E , may be associated to the evolution from a multimodal to an unimodal distribution via the successive extrusions. Such dependence seems to be also relevant when considering the observed increase of the notched Charpy *IS* of the composite (about 10% higher) after the last extrusion. This result suggests that the impact resistance remains almost unchanging while PSD is multimodal, but it continues to increase when such distribution become unimodal and narrower.

The variations evidenced on the mechanical behavior may be attributed to the changes produced in the microstructure of composites. As evidenced by the SEM micrographs and granulometry measurements, the modification of the mean particle size and morphology after the second and third extrusions are less marked than after the first extrusion. These results may be due to the low size of the GTR-g-PS particles after the first extrusion. In fact, as the particle size is reduced, their aspect ratio decreases and their shape become more spherical. During low temperature extrusion, the viscosity of the flowing

material is expected to increase as well as the mixing torque. Nevertheless, the smaller particles may be less deformed during and therefore, and thereby, the shear effects are less efficient. Despite this, it was evidenced that the larger particles remaining from the first extrusion are gradually dispersed, leading to narrower PSD at the end of the three extrusions. These results are in good agreement with the study of Di-Giuseppe et al. (2002), about lignocellulosic fiber breakage in a molten polymer by compounding in a twin-screw extruder. The authors demonstrated that the reduction of the fibers size through the extruder mainly depends on the initial dimensions of the fibers. Thus, the longer the initial fibers are, the more they will break [110].

From the composites prepared, the 50GTR-g-PS/f-PS2 one is compounded at the highest mixing torques. Due to the bulk density of the rubber particles, the volumetric feeding capacity of the extruder increases with the amount of equiv-GTR in the formulation. Then, when reaching high filling degrees at the kneading blocks, this helps to increment the flow compression and mixing torque. Moreover, the mixing torque may be also incremented by working at low temperatures close to the free-PS T_g . It may be the case therefore that these variations help to achieve a better dispersion and distribution of the GTR-g-PS particles during the second and third extrusion.

The differences in the notch sensitivity of the compounds also corroborates the modification of the brittle behavior of free-PS by the presence of GTR-g-PS particles. The Charpy *IS* of PS6 decreased in about 61%, whereas the 50GTR-g-PS/f-PS2 composite displays an average diminution from 0% to 15%. These results are in good agreement with the statements of Takano et al., (1976) [111], who demonstrated that both polymers and composites with brittle behavior are more sensitive to notch than ductile materials.

The toughening effects of free-PS in the 50GTR-g-PS/f-PS2 composite are still evidenced after compounding several times. An implication of this is that the composite may be recycled without apparently losing its mechanical properties. However, this observation must be interpreted with caution, since this is founded on data obtained from measurements which do not consider the variation of the properties during the service life of the composites. Thus, further research should be done to investigate such effects.

5.3.3 Influence of the extruder screw configuration after 1, 2 and 3 extrusions on the microstructure and mechanical properties of polystyrene composites containing 50 wt% of equiv-GTR.

Up to this point, it has been evidenced that the microstructure of GTR-g-PS/f-PS composites can undergo substantial changes when compounded at specific operating conditions and by using screw Profile-1. On this latter, the kneading elements constitute a main large block that has been assumed to magnify the effects of the mixing shear forces during extrusion. Screw Profile-1 has demonstrated to be effective to change the microstructure of such composites and therefore, have positive impact on their mechanical properties. Although this, it has been proposed to investigate the influence of uniformly distributing the kneading elements to create five short kneading zones along the extruder (screw Profile-2).

In what follows, the mechanical properties and microstructure of the 50GTR-g-PS/f-PS3 composite extruded 1, 2 and 3 times by using screw Profile-2 at the same compounding conditions used above, are analyzed. Note that the free-PS of this composite corresponds to the free-PS3, which has a different molecular weight of free-PS2.

5.3.3.1 Qualities of polystyrene: x , GE and molecular weight

The values of x and GE after the first extrusion are presented in Table 5.18. The polymerization of the remaining monomer is completed. The slight decrease of GE indicates that the styrene polymerized has instead formed free-PS chains during this stage. Although, the amount of grafted-PS predominates over free-PS.

Table 5.18 – Ultimate x and GE of free-PS after a single extrusion at high temperature with screw Profile-2.

Composite	Number of extrusion	x	$\frac{\text{grafted-PS}}{\text{free-PS}}$ (w/w%)	GE (%)
50GTR-g-PS/f-PS3	0	0,81 ($\pm 0,04$)	3,2 ($\pm 0,3$)	75,6 ($\pm 2,8$)
	1	0,96 ($\pm 0,02$)	2,7 ($\pm 0,1$)	67,5 ($\pm 2,9$)

The molecular weight of free-PS3 before and after the first extrusion of the composite is shown in Table 5.19. After the complete polymerization of the residual monomer, the molecular weight is slightly increased. As can be seen, the variations of x , GE and molecular weight after the first extrusion with screw Profile-2, are similar to those evidenced when using screw Profile-1. The variations of the polydispersity (M_w/M_n) indicate that the formation of large free-PS chains was rather favored.

Table 5.19 – Molecular weight of free-PS3 after a single extrusion of the 50GTR-g-PS/f-PS3 composite with screw Profile-2.

Polystyrene matrix	Number of extrusion	M_n (g/mol)	M_w (g/mol)	M_w/M_n
free-PS3	0	2,31E+04 ($\pm 0,04E04$)	3,60E+04 ($\pm 0,05E04$)	1,55 ($\pm 0,03$)
	1	2,76E+04 ($\pm 0,07E04$)	5,15E+04 ($\pm 0,07E04$)	1,86 ($\pm 0,06$)

5.3.3.2 Variations in the IS when using screw Profile-2

Notched Charpy IS of the sets of impact specimens fabricated with the 50GTR-g-PS/f-PS3 composite are shown in Figure 5.28. Figure 5.28a compares both the notched Charpy IS after a single extrusion of the composite with the notched and unnotched Charpy IS of its polymer matrix, i.e., free-PS3. These latter values were estimated from the correlation indicated in Eq. 5.1. As can be seen, the notched Charpy IS of free-PS3, which is about $0,3 \text{ kJ/m}^2$, exhibits a three-fold increase (i.e., $0,93 \text{ kJ/m}^2$) in the presence of the GTR-g-PS particles.

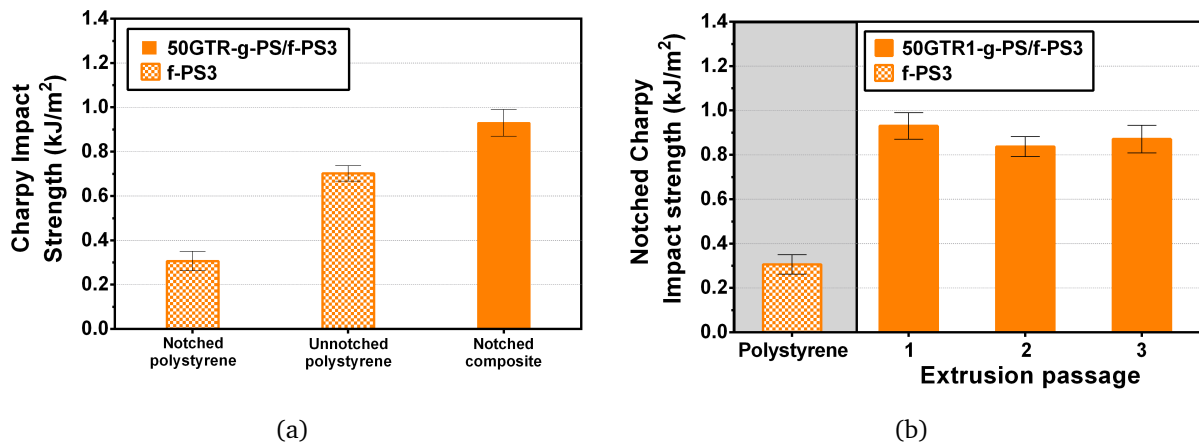


Figure 5.28 – Comparison of the Charpy IS of free-PS3 vs the 50GTR-g-PS/f-PS3 composite after 1, 2 and 3 extrusions with screw Profile-2. (a) Comparison after a single extrusion. (b) Comparing the evolution after 1, 2 and 3 extrusions.

It is observed that the notched Charpy IS varies slightly with increasing the number of extrusions by using screw Profile-2 (Fig. 5.28b). The quantification of the respective increments of the impact resistance of free-PS3 are shown in Table 5.19. These values are compared with those obtained for the 50GTR-g-PS/f-PS2 composite extruded with the screw Profile-1. The increment of the notched Charpy IS after the first extrusion is almost equivalent for both composites. By contrast, after the second and third extrusions, the impact resistance of the 50GTR-g-PS/f-PS3 composite displays an average diminution of 13%.

Table 5.20 – Comparison of the improvement of notched Charpy IS of polystyrene when changing the screw profile.

Composite	Screw profile	IS_{var} (%)		
		1st extrusion	2nd extrusion	3rd extrusion
50GTR-g-PS/f-PS2	Profile-1	+207 ($\pm 6,2$)	+198 ($\pm 5,3$)	+226 ($\pm 5,5$)
50GTR-g-PS/f-PS3	Profile-2	+204 ($\pm 1,9$)	+174 ($\pm 5,3$)	+185 ($\pm 5,7$)

On the fracture surface of the impact specimens of the 50GTR-g-PS/f-PS3 composite fabricated with screw Profile-2 (Fig. 5.29), there is evidence of the plastic deformation suffered by the material before it breaks down. In fact, the surfaces are roughly and more irregular, contrary to the smooth ones observed for the specimens with free-PS2. This suggests that the composite has a larger capability to better withstand the impact events and therefore, it fails in a more ductile manner. To complement these results, the tensile properties and characteristics of the composite microstructure, created by extruding with the

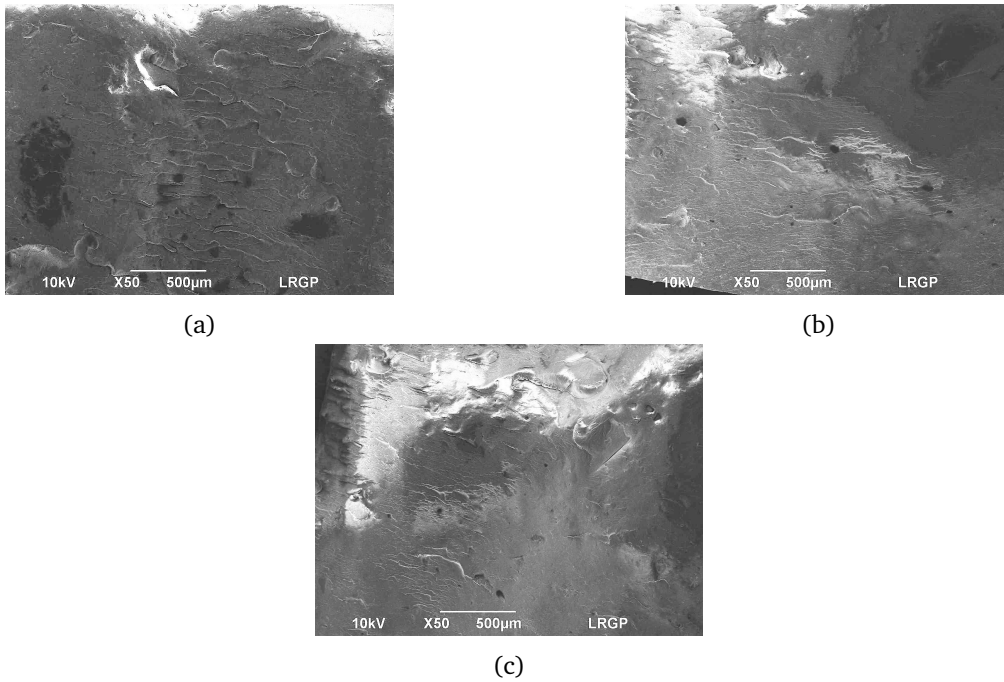


Figure 5.29 – Fracture surfaces of impact specimens of the 50GTR-g-PS/f-PS3 composite after (a) 1, (b) 2 and (c) 3 extrusions with screw Profile-2.

screw Profile-2, were also characterized.

5.3.3.3 Influence of the screw configuration on the tensile properties

The stress-strain curves of the 50GTR-g-PS/f-PS3 composite are illustrated in Figure 5.30. The graph reveals that the tensile properties are gradually incremented with the number of extrusion. There is not evidence of reduction of the cross-section of the specimen during testing.

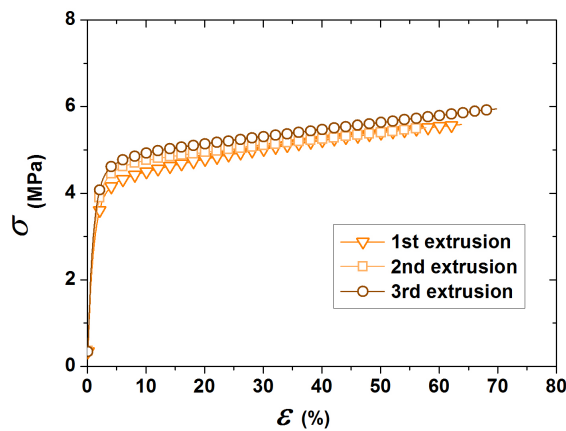


Figure 5.30 – Stress-strain curves of tensile specimens of the 50GTR-g-PS/f-PS3 composite extruded 1, 2 and 3 times with screw Profile-2

Table 5.21 shows the mean values of the tensile properties. It can be seen that all of them are

Table 5.21 – Effect of the screw profile on the tensile properties of the composite containing 50 wt% of equiv-GTR and extruded with screw Profile-2

Composite	Screw profile	Number of extrusion	$E, 0.25\%$ (MPa)	σ_y (MPa)	σ_r (MPa)	ϵ (%)
50GTR-g-PS/f-PS3	Profile-2	1	323 ($\pm 6,46$)	4,4 ($\pm 0,18$)	5,6 ($\pm 0,23$)	63 ($\pm 4,96$)
		2	344 ($\pm 6,88$)	4,7 ($\pm 0,19$)	5,6 ($\pm 0,35$)	58 ($\pm 3,98$)
		3	367 ($\pm 7,34$)	4,8 ($\pm 0,21$)	5,9 ($\pm 0,55$)	70 ($\pm 6,13$)

be gradually improved with the number of extrusion. For example, note that E is increased in about 13% between the first and the third extrusion. Moreover, the capability of the material to be deformed reaches high strain percentages up to 70%, at the rupture point. This suggests that the GTR-g-PS particles are well dispersed through the free-PS3 matrix.

On the fracture surfaces of the tensile specimens (Fig. 5.31) there are not visible particles and the individual phase domains cannot be distinguished. The surfaces are highly rough and there are some dimples or microvoids dispersed through the fractured area. Hence, it is possible that the material failure is initiated by the presence some of such inclusions. Despite this, the high plastic deformation evidenced may be associated to a ductile deformation behavior. These results corroborate the SEM observations of the fracture surfaces of the impact specimens.

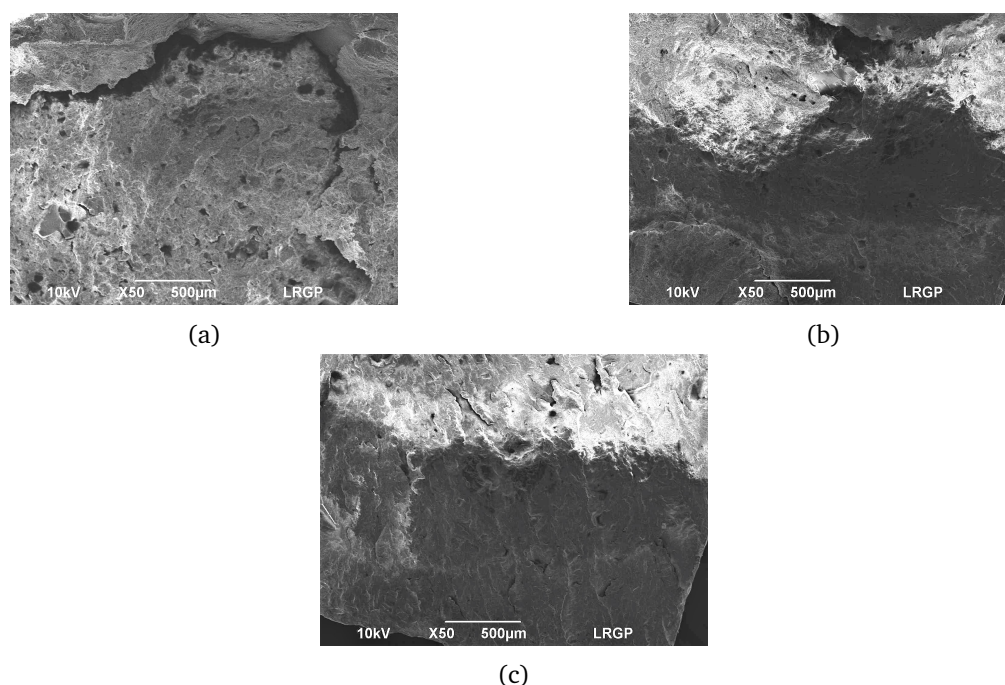


Figure 5.31 – Fractured surfaces of tensile specimens of the 50GTR-g-PS/f-PS3 compound after (a) 1, (b) 2 and (c) 3 extrusions with screw Profile-2.

5.3.3.4 Changes in the morphology and PSD of the GTR-g-PS particles with screw Profile-2.

Changes in particles morphology may be observed through the set of images in Figure 5.32, which are representative of the whole samples analyzed. These micrographs show that during the multiple extrusions of the 50GTR-g-PS/f-PS3 composite, the drastic diminution of the size and the morphological changes suffered by the 50GTR-g-PS particles, are pretty similar to those observed for the composite extruded with screw Profile-1. Nevertheless, the number of the large irregular agglomerates seems to be less important when using the screw Profile-2 (Fig. 5.32b). After the last extrusion, mainly small individual particles are perceived. Moreover, the diminution of the size is determined from the PSD curves illustrated in Figure 5.33.

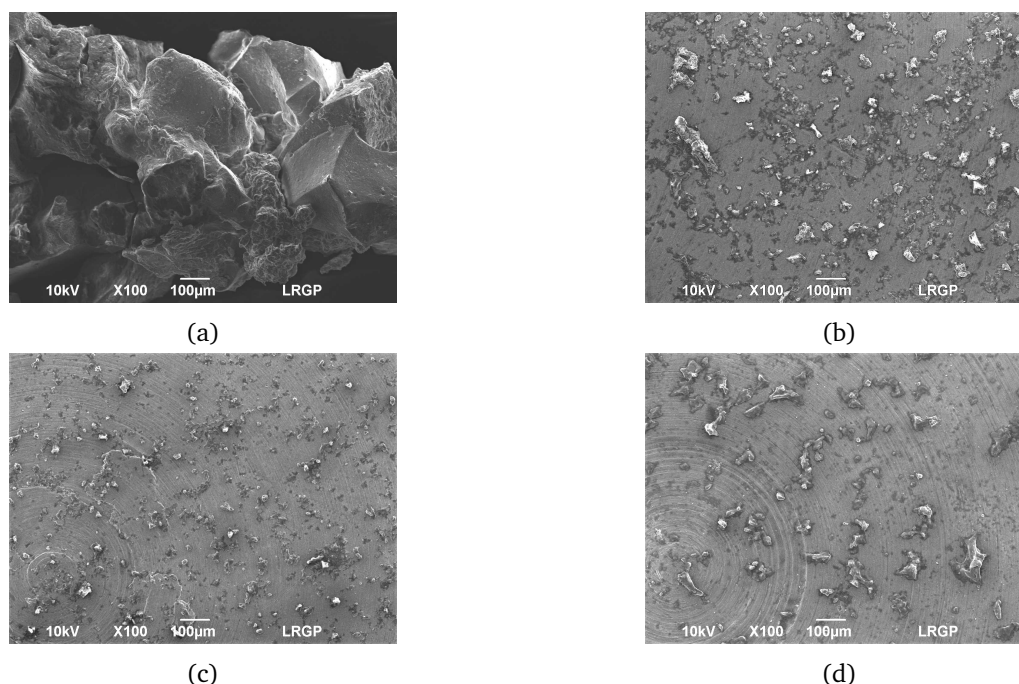


Figure 5.32 – Changes in the morphology of the GTR-g-PS particles (a) before and after (b) 1, (c) 2 and (d) 3 extrusions with screw Profile-2.

It is interesting to note that the distribution curves in this figure, by contrast to the above results produced with Profile-1, almost preserves the unimodal distributions after each extrusion. Although the size distribution range is larger than the one measured for raw GTR, this lies from a few sub-microns to about 310 μm . The characteristic diameters of the largest populations in volume and the maximal mixing τ are detailed in Table 5.22.

An important finding is that the mean size of the GTR-grafted-PS particles in the composite (approx. 82% volume fraction) is reduced in about 92% after a single extrusion. At the end of the sequence of extrusions, the total decrease has been estimated in 93% ($\Phi = 86\%$). Then, by comparing with the measurements acquired when implementing screw Profile-1 (Table 5.17), it is seen that the effect of screw Profile-2 on changing the microstructure of the composites seems to be more relevant, since higher volume fraction of particles can be reduced to lower mean sizes from the first extrusion.

On the question of τ during compounding with screw Profile-2, it is possible to reach higher values even during the high-temperature extrusion (first extrusion at 200 $^{\circ}\text{C}$) and for a fixed feeding rate of 1 kg/h. In addition, the desired mixing τ of 140 Nm was easily reached and even exceeded.

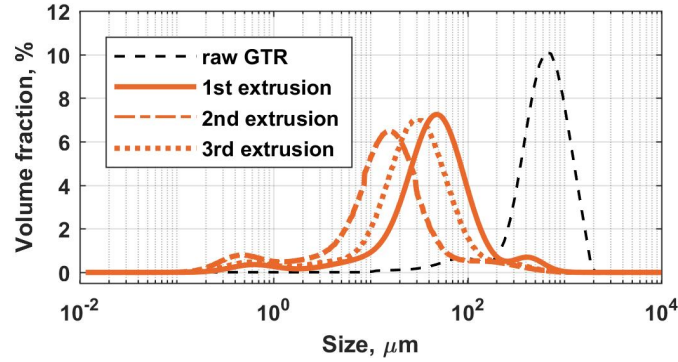


Figure 5.33 – Comparison of the PSD of raw GTR with 50GTR-g-PS particles after 1, 2 and 3 extrusions with screw Profile-2.

Table 5.22 – Characteristic diameters of raw GTR and particles of GTR-g-PS after 1, 2 and 3 extrusions with screw Profile-2.

Particles	1st extrusion			2nd extrusion			3rd extrusion		
	\varnothing^a (μm)	Φ^b	τ (Nm)	\varnothing^a (μm)	Φ^b	τ (Nm)	\varnothing^a (μm)	Φ^b	τ (Nm)
50GTR-g-PS (Screw Profile-2)	11 49	0,11 0,82	86	5 24	0,14 0,75	142	4 36	0,04 0,87	138

raw GTR: $\varnothing = 585 \mu\text{m}$ and $\Phi = 0,97$

Stand. Dev. range from: ^a. 1,0 to 1,01 and ^b. 0,005 to 0,023

5.3.3.5 Discussion and interpretation

Screw Profile-2 appears most advantageous than screw Profile-1, since it leads to reach higher mixing torques and thus, to provoke greater modifications in the microstructure of the composites containing GTR-g-PS particles. The degrees of dispersion and distribution of these particles seem to be improved. The findings above demonstrate that a severe reduction of the initial size of these particles can be performed in one step.

The notched Charpy *IS* of free-PS3 after the first extrusion of the 50GTR-g-PS/f-PS3 composite is increased by about 207%. This result may be attributed to the drastic reduction, in about one order of magnitude, of the mean size of the GTR-g-PS particles. When compounding with screw Profile-2, particle size reduction is performed so that the PSD remains almost unimodal with low volume fractions of coarse particles, by contrast to results obtained when using screw Profile-1. This suggests that the shear mixing, mainly developed at the multiple kneading blocks of screw Profile-2, is more effective in performing fine dispersion of the GTR-g-PS particles through the free-PS3 matrix. The high degree of dispersion and integration of both phases is also evidenced on the appearance of the fracture surfaces. In addition, the evidence of plastic deformation on the fracture surfaces of the specimens also corroborates such enhanced dispersion.

After the second and third extrusion, the reinforcement percentage of free-PS3 by the presence of the 50GTR-g-PS particles, declines slightly (about 13%). It is difficult to explain this result, but it might be related to the limited reinforcing capacity of the GTR-g-PS particles on the range of sizes reached. In other words, it is possible that while the mean particle size varies between 20 and 80 μm , in the presence or absence of low volume fractions of coarse ones, the reinforcement capability of the GTR-g-PS is almost the same. Therefore, it seems that the impact resistance of the free-PS may be further

increased, provided that the mean particle size shifts to the sub-micrometer domains, as reported by Bucknall et al., (2009, 2013) [84, 85]. In addition, it is also possible that such reinforcement capability also decreases with increasing the molecular weight of the polymer matrix. This implies that to achieve similar reinforcing effects (as those observed in this work, approx. 200%) in polymers having higher molecular weights than free-PS, it may be necessary to use smaller diameter particles (e.g., $< 10 \mu\text{m}$).

The tensile properties of the composite extruded with screw Profile-2, cannot be directly compared with those of the one extruded with the screw Profile-1. Even though the content of equiv-GTR in both composites is the same, i.e., 50 wt%, the molecular weight of free-PS2 and free-PS3 is distinct. For this reason, it is difficult to accurately attribute such properties to the differences observed in mean particle size and distribution, since the extent to which the molecular weight of free-PS influences these characteristics is unknown. According to the literature, the tensile behavior of neat polymers and thermoplastic composites is sensitive to the polymer molecular weight, as well as the impact properties [83, 112, 113]. Nevertheless, this study is not able to identify the extent of the positive or negative contributions of the molecular weight on each of the tensile properties.

The differences in the ultimate PSD due to the utilization of screw Profile-2, may be associated to the marked increase of the mixing torque. This can be explained by the flow of the product developed through the kneading blocks. In fact, the successive elements in the kneading sections have an offset angle of 90. Although this configuration is considered as highly efficient in imparting dispersive and distributive mixing, it also allows leak flow to occur [103]. Then, the product leaks from one element to the next through the staggered openings and creates preferential passages of lower flow resistance. Thus, the longer the kneading zones, the longer the preferential passages. This leads, on the one hand, to a lower filling degree of the extruded product, which reduces the shear stresses imparted by the kneading blocks. On the other hand, the mixing shear applied on the different fluid elements varies with the flow pathlines. Thus, the rupture of the different GTR particles (grafted or not) passing through the preferential passage is less important compared to those passing through the higher shear pathlines. Consequently, the size variation of the dispersed phase is not homogeneous and coarse particles are preserved.

Moreover, during dispersive mixing, the ultimate particle size is reached by repeated ruptures. This requires repeated passages through the high-shear zones of the screw. When using a screw configuration with multiple and short kneading zones as screw Profile-2, the residence time of a fluid element is shorter compared to the longer mixing zone in screw Profile-1. This may reduce the formation of preferential passages and the small mixing zones remain fuller. Therefore, high shear may be developed through the screw Profile-2 thus to cause a finer and more uniform dispersion, i.e., creating an unimodal PSD of the GTR-g-PS particles.

According to the experimental evidence on the impact properties of both 50GTR-g-PS/f-PS2 and 50GTR-g-PS/f-PS3 composites, it seems that the improvements achieved on the notched Charpy IS and ϵ_r of their respective free-PS, are independent of the screw configuration implemented. In other words, standard polystyrene can be toughened by using any of both screw Profile-1 or Profile-2.

5.3.4 Influence of increasing the GTR content on the microstructure and tensile properties of polystyrene composites extruded 1 and 2 times.

So far the sections above are focused on composites containing 30 wt% and 50 wt% of equiv-GTR. The following section will discuss the mechanical behavior of composites with 70 wt% of equiv-GTR. In fact, at this higher content, the composites have the capability to undergo large elastic deformations, thus exhibiting a mechanical behavior different from the above impact resistant thermoplastics.

Hence, the presentation of the results began by displaying the tensile properties and fracture surfaces of two composites, namely 70GTR-g-PS/f-PS4 and 70GTR/PS6. Both composites are extruded three times at the same operating conditions above and by using screw Profile-1. In parallel, a third composite, namely 70GTR-g-PS/f-PS5, is extruded with screw Profile 2. Subsequently, the microstructure of the composites is described and quantified, as well.

5.3.4.1 Influence of the GTR content on the qualities of polystyrene: x and molecular weight

After the high-temperature extrusion of both 70GTR-g-PS/f-PS4 and 70GTR-g-PS/f-PS5 composites, the values of ultimate x are shown in Table 5.23. Despite of the low conversion reached during the grafting polymerization, this is almost completed. As reported above, it was not possible to get accurate measurements of GE for this polymerization system.

Table 5.23 – Ultimate x of polystyrene after a single extrusion of composites containing 70 wt% of equiv-GTR.

Composite	Number of extrusion	x
70GTR-g-PS/f-PS4	0	0,47 ($\pm 0,04$)
(Screw profile-1)	1	0,93 ($\pm 0,05$)
70GTR-g-PS/f-PS5	0	0,37 ($\pm 0,06$)
(Screw profile-2)	1	0,90 ($\pm 0,02$)

The variations in the molecular weight of free-PS4 and free-PS5 are reported in Table 5.24. The high temperature of the first extrusion leads to an increase of both M_n and M_w , as well as the polydispersity values, which indicates the formation of both larger free-PS chains and a broader distribution.

Table 5.24 – Molecular weight of free-PS4 and free-PS5 after a single extrusion.

Polystyrene matrix	Number of extrusion	M_n (g/mol^{-1})	M_w (g/mol^{-1})	M_w/M_n
free-PS4	0	3,02E+04 ($\pm 0,04E04$)	3,80E+04 ($\pm 0,05E04$)	1,26 ($\pm 0,03$)
(Screw profile-1)	1	3,70E+04 ($\pm 0,06E04$)	5,71E+04 ($\pm 0,08E04$)	1,54 ($\pm 0,03$)
free-PS5	0	2,78E+04 ($\pm 0,02E04$)	3,44E+04 ($\pm 0,08E04$)	1,24 ($\pm 0,02$)
(Screw profile-2)	1	3,43E+04 ($\pm 0,04E04$)	5,07E+04 ($\pm 0,05E04$)	1,48 ($\pm 0,03$)

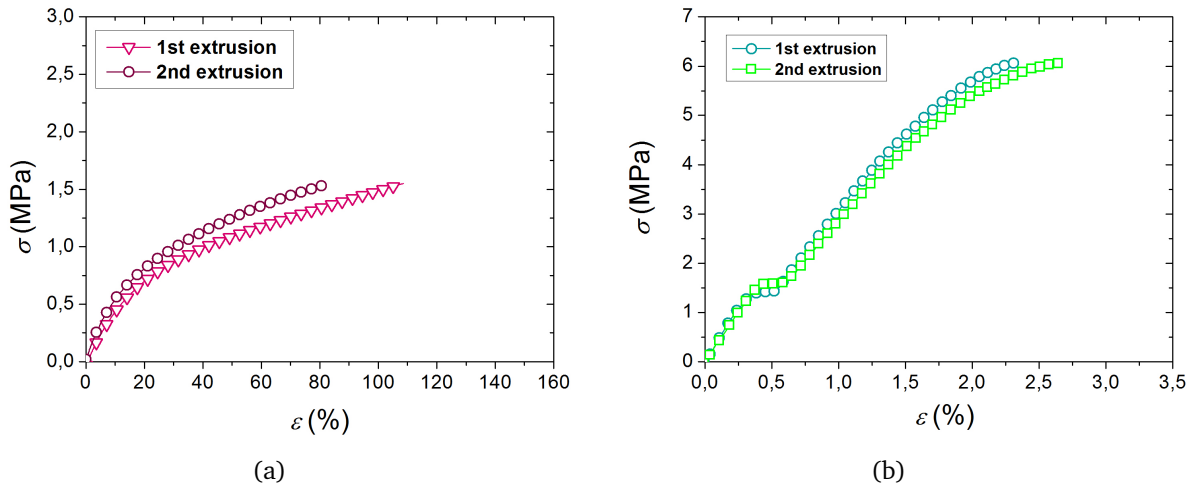


Figure 5.34 – Stress-strain curves of tensile specimens of (a) 70GTR-g-PS/f-PS4 and (b) 70GTR/PS6 compounds after 1 and 2 extrusions with screw Profile-1.

5.3.4.2 Tensile properties of composites extruded with screw Profile-1

In Figure 5.34, stress-strain curves of 70GTR/PS6 (Fig. 5.34b) and 70GTR-g-PS/f-PS4 (Fig. 5.34a) composites, are displayed. The X and Y scales are different to better observe the variations. The discrepancies in the mechanical behavior are clearly visible, such as the low ϵ_r (<3.0%) of the 70GTR/PS6 composite compared with the much higher (>80%) ϵ_r of the composite containing the GTR-g-PS particles. In contrast, note that ϵ_r of this latter is lower. In both cases, σ_r shows a slight increase after the second extrusion in detriment of ϵ_r .

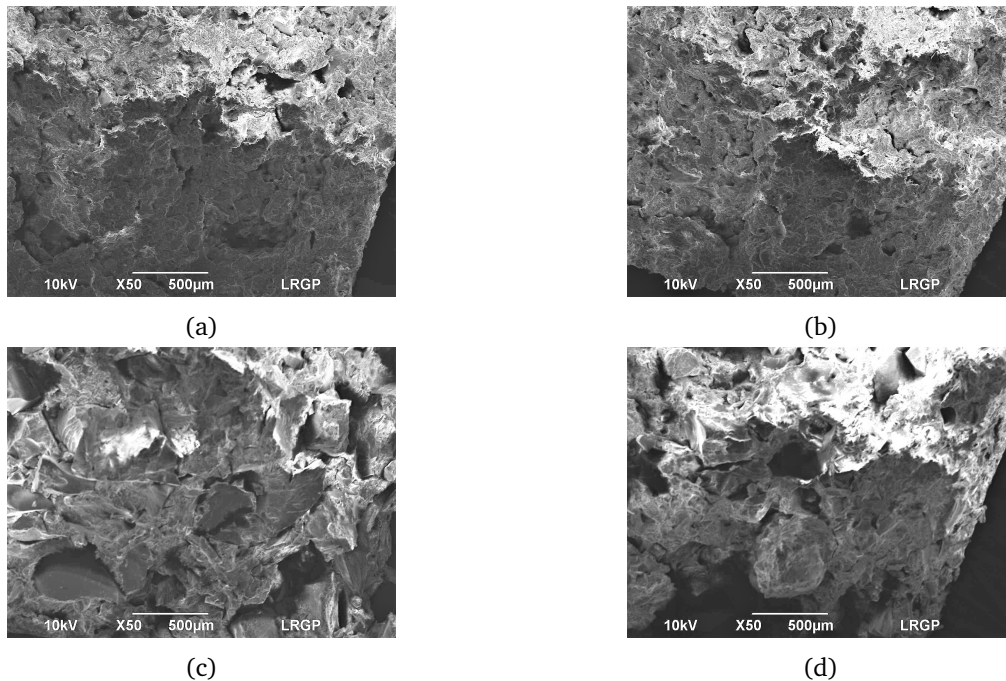


Figure 5.35 – Fractured surfaces of tensile specimens of: (a-b) 70GTR-g-PS/f-PS4 and (c-d) 70GTR/PS6 composites after 1 (left) and 2 (right) extrusions with screw Profile-1

For all specimens of the 70GTR/PS6 composite, the curves show a short step of deformation (from about 0.3 to 0.6%) at constant σ . This suggests that the rupture takes places in two times, which may be associated to failure initiation or partial rupture of the matrix and subsequent propagation until the total rupture.

SEM images of the fracture surfaces of the corresponding tensile specimens are shown in Figure 5.35. Left and right figures correspond to the composites after the first and second extrusion, respectively. On the surface of the 70GTR/PS6 specimens (bottom figures), large granulates and microvoids, due to weak interfaces and poor particle-matrix adhesion, are distinguished. These seem to be less numerous after the second extrusion (Fig.5.35c). Therefore, it is possible that the rupture is initially promoted by the interfacial failure of the matrix caused by the presence of the large inclusions and discontinuities.

By contrast, upper figures (i.e., Figs. 5.35a and 5.35b) reveal that the specimens made of the 70GTR-g-PS/f-PS4 composite have highly rough surfaces, no individual particles are evidenced and both phases seem to be well integrated. Moreover, the fracture profile exhibits a rugged surface, which is characteristic of the ductile failure.

5.3.4.3 Tensile properties of composites extruded with screw Profile-2

When using a different screw configuration, such as Profile-2, the mean stress-strain curves in Figure 5.36 reveal that ε_r can reach 120%. In addition, a significant increment of σ_y and σ_r is produced after the second extrusion. The shape of the stress-strain curves of both composites, i.e., 70GTR-g-PS/f-PS4 and 70GTR-g-PS/f-PS5, shows an uniform extension without reduction of the cross-section of the specimen.

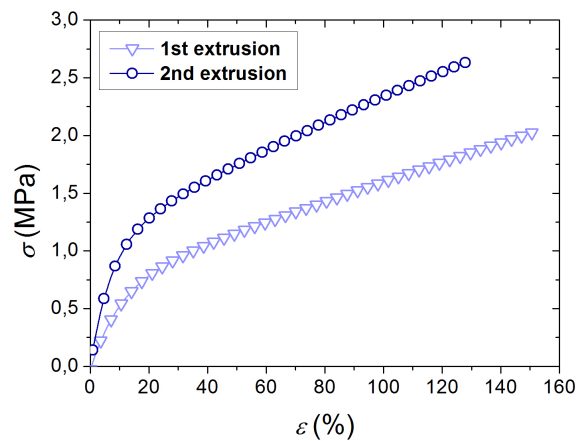


Figure 5.36 – Stress-strain curves of tensile specimens of the 70GTR-g-PS/f-PS5 composite after 1 and 2 extrusions with screw Profile-2.

The tensile properties of the three composites are summarized in Table 5.25. The fifth column reveals the “modulus” of the compound at 100% (E-100%), which is an additional measurement implemented for materials characterization in the elastomer industry. It differs from the engineering elastic Young’s modulus E , since this solely represents the stress required to deform the material at 100% [114]. Moreover, the value of E at a strain of 0,25% was not considered as a representative measurement of the mechanical behavior of these materials, which have a high deformation capability up to 80%. The total length of all specimens, before and after testing, was measured in order to determine the length recovery. Interestingly, all specimens showed a total recovery ranging from about 90 to 95%.

Table 5.25 – Tensile properties of 70GTR/PS6, 70GTR-g-PS/f-PS4 and 70GTR-g-PS/f-PS5 composites after 1 and 2 extrusions.

Composite	Number of extrusion	$E, 0.25\%$ (MPa)	σ_r (MPa)	ε_r (%)	$E, 100\%$ (MPa)
70GTR/PS6	1	450 ($\pm 9,0$)	6,0 ($\pm 0,41$)	2,3 ($\pm 0,22$)	–
(Screw profile-1)	2	406 ($\pm 8,1$)	6,1 ($\pm 0,16$)	2,6 ($\pm 0,09$)	–
70GTR-g-PS/f-PS4	1	–	1,5 ($\pm 0,23$)	108,5 ($\pm 2,69$)	–
(Screw profile-1)	2	–	1,5 ($\pm 0,25$)	80,9 ($\pm 7,49$)	1,3 ($\pm 0,06$)
70GTR-g-PS/f-PS5	1	–	2,0 ($\pm 0,11$)	151,2 ($\pm 10,9$)	1,6 ($\pm 0,07$)
(Screw profile-2)	2	–	2,6 ($\pm 0,37$)	127,9 ($\pm 4,6$)	1,6 ($\pm 0,08$)

5.3.4.4 Changes in the morphology and PSD of GTR-grafted-PS particles extruded with screw Profile-1 or Profile-2

The SEM micrographs of the GTR-g-PS particles contained in the 70GTR-g-PS/f-PS4 composite extruded with screw Profile-1, are shown in Figure 5.37. Immediately obvious from these images is that, in spite of the high content of equiv-GTR, the size of the particles is decreased drastically. During the second extrusion, the large irregular agglomerates seem to be reduced in number to smaller and individual particles. These images are representative of the morphology and size of those obtained for the compound extruded with screw Profile-2, which are not presented here.

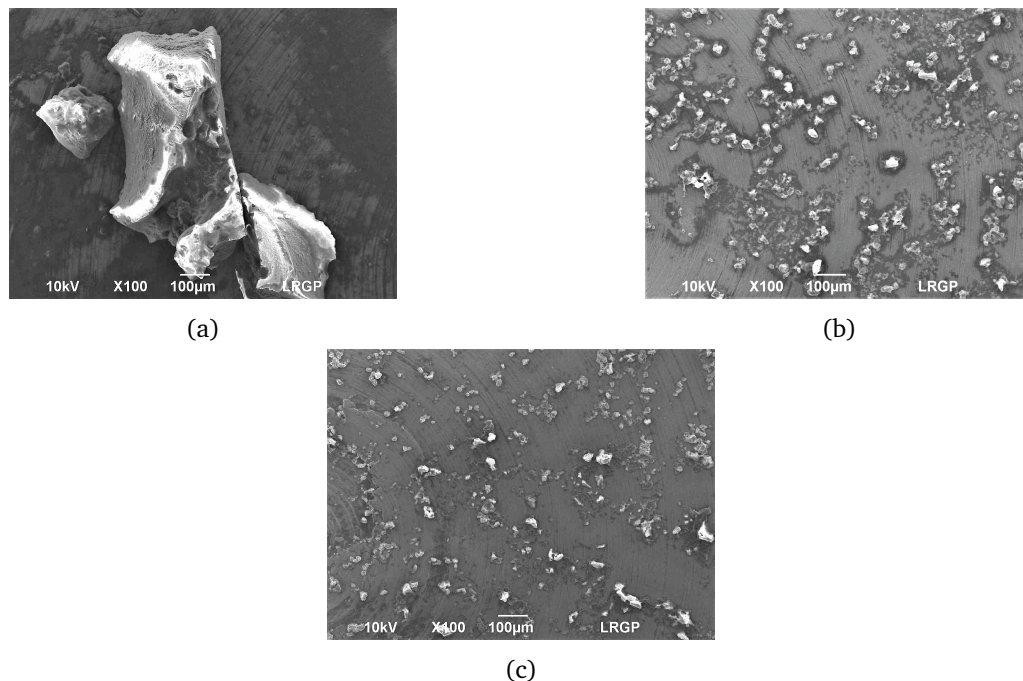


Figure 5.37 – Changes in the morphology of the 70GTR-g-PS dispersed particles in free-PS4 (a) before and after 1 (b) and 2 (c) extrusions with screw Profile-1.

Granulometry measurements (Figure 5.38) revealed that during the first and second extrusions with

Table 5.26 – Characteristic diameters of raw GTR and particles contained in the composites after 1 and 2 extrusions: (a) 70GTR in PS6 with, (b) 70GTR-g-PS in free-PS4 and (c) 70GTR-g-PS in free-PS5.

Particles	1st extrusion			2nd extrusion		
	\varnothing^a (μm)	Φ^b	τ (Nm)	\varnothing^a (μm)	Φ^b	τ (Nm)
70GTR in PS6 (Screw profile-1)	139 540	0,20 0,75	40	98 426	0,38 0,47	140
70GTR-g-PS in free-PS4 (Screw profile-1)	49 425	0,64 0,31	120	54 508	0,7 0,30	140
70GTR-g-PS in free-PS5 (Screw profile-2)	31 200	0,65 0,30	145	1 35	0,04 0,96	165

raw GTR: $\varnothing = 578 \mu\text{m}$ and $\Phi = 0,97$

Stand. Dev. range from: a . 1,01 to 1,23 and b . 0,001 to 0,05

screw Profile-1, the particles dispersed in PS6 (Fig. 5.38a) and free-PS4 (Fig. 5.38b) display PSD having multiple populations. By contrast, the particles dispersed in free-PS5 exhibit an unimodal distribution after the second extrusion.

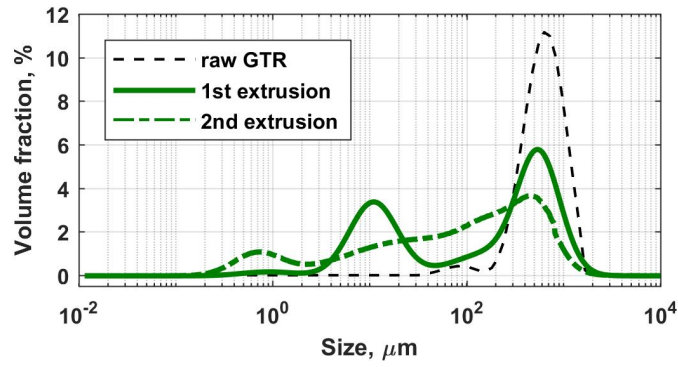
Interestingly, the mean size of about 65% (volume fraction) of the GTR-g-PS particles (Fig. 5.26), displays a diminution ranging from 90 to 95% of their initial size. These percentages are as high as the reduction observed for the composites containing 50 wt% of equiv-GTR. In addition, the mixing torques reached by compounding with screw Profile-2 largely exceeded the sought threshold of 140 Nm.

5.3.4.5 Discussion and interpretation

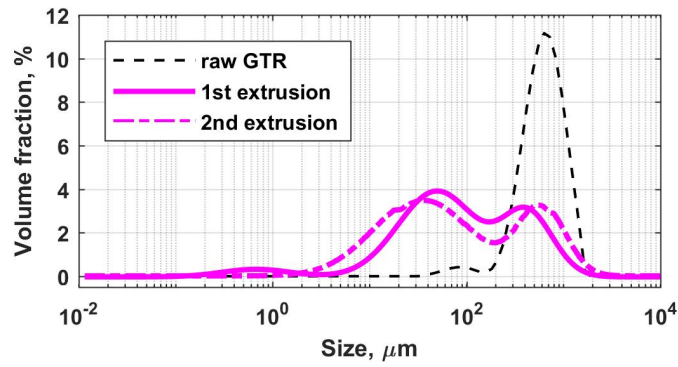
Once again, by coupling the processes of grafting polymerization and compounding, it was possible to fabricate polystyrene compounds rich in GTR-g-PS particles and displaying interesting tensile properties. Most noticeably, the compounds containing 70 wt% of equiv-GTR can reach a ϵ_r up to 120% and be reversibly elongated. According to the ASTM D-412 standard (“Standard test methods for vulcanized rubber thermoplastics elastomers - Tension”), such materials display a performance similar to that of a thermoplastic elastomer vulcanizate.

Thermoplastic vulcanizates (TPVs) are a class of thermoplastic elastomers fabricated by the dynamic vulcanization process, which involves the crosslinking of the rubber phase while it is being mixed with a thermoplastic at elevated temperature. The products consist of crosslinked rubber particles dispersed in a continuous thermoplastic matrix, exhibiting both high elasticity and good melt processability. Some most commercially important TPVs include blends of polypropylene (PP)/ethylene propylene diene rubber (EPDM) widely used in biomedical, automotive and wire/cables applications [babu2011].

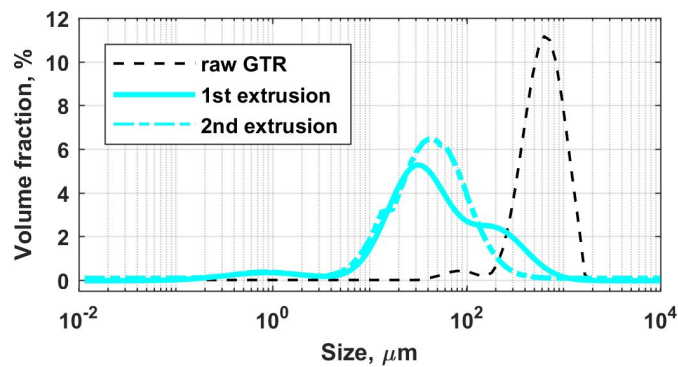
The first extrusion leads to complete the polymerization of the remaining styrene in the grafted composites. The increase of the molecular weight of free-PS may be attributed to the polymerization of larger free-PS chains. Nevertheless, the presence of polymer chains having intermediate-molecular-weight, compared to PS6, predominates. The polydispersity of the polymer chains remains relatively low, about 1.5, compared to the typical values expected for a free radical polymerization system (i.e., > 1.5). As mentioned in the first part of this chapter, this may be attributed to the limitations in extracting the largest free-PS chains polymerized within the particles. Then, only the smaller chains can diffuse



(a)



(b)



(c)

Figure 5.38 – Comparison of the PSD of raw GTR with particles contained in the composites after 1 and 2 extrusions: (a) 70GTR in PS6, (b) 70GTR-g-PS in free-PS4 and (c) 70GTR-g-PS in free-PS5.

through the cross-linked structure of the GTR particles. Nevertheless, it seems that this problem can be partially solved when reducing the particle diameter size during the extrusion. Thus, the largest polymer chains are exposed and can be easily removed by the solvent.

The stress-strain curves reveal that a second extrusion passage at low temperature may be necessary to increase the tensile properties such as $E_{100\%}$ and σ_r . This demonstrates that when increasing the GTR content, the tensile properties exhibit a more important dependence upon the dispersion degree of the particles. For this reason, the microstructure developed in the composite processed with screw Profile-2 leads to greater tensile properties. Thus, the enhanced ε_r and the fracture surfaces are evidence of important plastic deformations due to strongly adhered interfaces and a good state of dispersion and distribution.

Moreover, as pointed out earlier, both free-PS and grafted-PS are expected to be present almost exclusively within the particles. Since both free-PS and grafted-PS are the matrix and the compatibilizer agent, respectively, it is surprising that the composites containing 70 wt% of equiv-GTR may reach such a degree of deformation in the presence of so little polystyrene (i.e., 30 wt%).

One of the most interesting finding is that the reduction of the size of the GTR-g-PS particles is even higher with increasing the amount of equiv-GTR. It is evidenced that such modifications are responsible for the enhanced tensile properties observed. The microstructure is developed in a similar way as described in the previous discussions (c.f. Sect. 5.3.1.10 and 5.3.2.7).

As mixing progress during the first extrusion a high temperature, the GTR-g-PS particles suffer repeated ruptures when passing through the zones of higher mixing shear levels, at the same time that the remaining styrene polymerizes. Nonetheless, the filling degree of the kneading zones is higher due to the greater volume occupied by the particles. Therefore, the mixing torque increases and high shear stresses are imparted to the flowing material. Consequently, fine dispersion of the particles is more efficient, in particular when working with screw Profile-2. At the same time, the cross-linked structure of GTR may be devulcanized an/or reclaimed, which is also likely to enhance the integration of both the GTR-g-PS and free-PS phases.

By decreasing the extrusion temperature, it is possible to increase the mixing torque beyond 140 Nm, when compounding with screw Profile-2. This is due to the increase of the flow viscosity when working close to the polymer T_g . This step leads to increase the dispersion of most of the coarse particles, as displayed by the PSD curves. These findings corroborate the results obtained above, when extruding the 50GTR-g-PS/f-PS3, and demonstrate that the configuration of the screw Profile-2 provides enhanced dispersive mixing effects.

The simply mixing raw GTR particles with PS6 leads to weak particle-matrix interfaces and therefore, poor tensile properties. Despite this, it is possible to progressively reduce the size of the raw GTR. This result indicates that there is an important contribution of the volumetric feeding degree of the extruder to increasing the overall mixing shear. This also supports the fact that for the same GTR content and at fixed feeding rate (1 kg/h), the mixing torque is considerably higher when the rubber particles are grafted.

5.4 Conclusions

In this Chapter, the aim was to demonstrate that through the implementation of the proposed methodology in this research, it is possible to fabricate polystyrene-reinforced compounds by the addition of cross-linked rubber particles from recycled tires in the form of GTR. This methodology was designed to

integrate two processes, which successive combination has demonstrated to provide synergistic effects. These processes involve the free-radical polymerization of styrene in the presence of GTR by using a mix of peroxide initiators, and compounding of the resulting product in a twin-screw extruder. The grafting of styrene onto GTR ensures good interfacial adhesion between PS and GTR and compounding favors fine dispersion of GTR in the PS matrix.

This methodology was applied to fabricate three distinct composites having interesting mechanical properties. Thus, when adding 30 wt% and 50 wt% of GTR, the notched Charpy impact strength of neat polystyrene can be increased between 40 and 200%. Moreover, a composite containing 70 wt% of GTR displays a performance similar to that of a thermoplastic elastomer vulcanizate (TPV) and its strain at break can reach 120%.

At the beginning of this work, the composites specifications were defined in order to define targeted properties and characteristics (cf., Sect. 3.3.1). These involved a series of essential and useful needs. According to these latter, it is possible to stand the following conclusive remarks about the composites obtained:

- The composites are rich in GTR (30 to 70 wt%). This incentives the recycling of tire rubber and has a positive impact on the environment. The composites produced may be presented as granulates which can be easily processed by thermoforming in high-shear mixers (e.g. twin-screw extruder, microcompounder). Neither additional additives nor aromatic solvents were added to the formulations. In addition, some preliminary tests suggested that such composites can be reprocessed several times, e.g., via extrusion and injection molding, without a substantial decrease of their initial impact strength properties.
- With respect to the fabrication of the composites, GTR was used as received without neither purification with organic solvents nor cryogenic grinding. The styrene monomer was used without previous purification. Moreover, the grafting polymerization in a batch reactor was performed in air atmosphere. Only one or two compounding stages were required to get the desirable properties. The only source of waste generation was the gases containing VOCs and produced during the compounding stages. No chemical liquid wastes were produced. The costs required for raw materials pre-treatment (e.g. purification and cryogenic grinding) and multiple extrusions may be avoided. In general, the transformation process yield was above 95%, since by-products can be recycled to the process.

The parameters reported in the literature as influencing thermoplastics toughening were analyzed. The microstructure of the composites leading to effective polystyrene toughening were identified, described and quantified. These findings enhance our understanding of the different factors that dictate the ultimate mechanical properties of polystyrene-reinforced composites with GTR. In addition, this analysis may be transferable to systems involving different thermoplastics filled with GTR.

General conclusions and perspectives

Our vision with this thesis is to contribute to the research of sustainable alternatives to favor recycling of materials derived from end-of-life tires. One of them consists in using the recycled rubber material as form of ground particles or GTR to toughen thermoplastic polymers. Through toughening, the crosslinked rubber structure of GTR confers to the polymer a certain ductility, and thereby, the capability to better withstand mechanical stresses before failure. Toughness depends on the cohesion of the polymer-particle interface, polymer molar mass, rubber content, degree of dispersion (i.e. particle size) and spatial distribution of the rubber particles. At the same time, these factors depend themselves on the type of processes implemented for the elaboration of such composite materials.

In this perspective, the objective of this work was to use GTR as reinforcing agent to toughen brittle polymers such as polystyrene. This research is divided in three parts:

The first part is related to the study of the kinetics of the free-radical grafting polymerization of styrene onto GTR and the comprehension of the effects caused by the presence of these rubber particles. For this purpose, the course of the overall reaction was monitored by DSC. Sample preparation and measurement procedures implemented led to obtain repeatable measurements and reliable data coherent with theory. Therefore, one of the most significant contributions to emerge from this experimental study, is the validation of the DSC analysis as a valuable method to investigate the kinetics of polymerization systems in presence of GTR. Experimental results revealed that GTR affects both the initial rate of polymerization and the overall monomer conversion. The effects of the GTR content, initiator nature and concentration, GTR formulation and polymerization temperature were analyzed. The second major contribution is the identification of the series of phenomena displayed by the presence of GTR, which are associated to multiple chemical interactions occurring between the reactants and carbon black, additives and impurities contained in the formulation of GTR, as well as limitations in mass transfer due to its crosslinked structure itself. The current findings not only added substantially to our understanding of this polymerization system, but also led to provide to the literature the first values of the overall effective kinetic rate constant and activation energies by using two different-nature initiator agents.

The second part of this work presents a mechanistic modelling approach for the theoretical study of the kinetics of the free-radical polymerization of styrene. The kinetic model combines both the chemical and thermal initiation mechanisms. The reaction scheme involves the elementary reactions of initiation, propagation, termination and chain transfer. Parameter estimation was realized by fitting with the data of monomer conversion and average molecular weight from the series of experiments carried out by DSC and batch reactions. Model simulations show that the reaction mechanism and set of parameters proposed lead to predict with high accuracy the results obtained for the bulk and solution polymerizations over a wide range of temperature and initiator concentration. A relevant finding was

that DSC measurements provided reliable and valuable data leading to a more accurate estimation of model parameters. Concerning the grafting polymerization system in presence of GTR, once again, the DSC study was essential to identify the changes in the overall polymerization rate and the phenomena induced by the presence of GTR. These were considered through a series of elementary reactions added to the validated kinetic scheme of the styrene homopolymerization. Therefore, the reaction scheme proposed accounts for a triple initiation mechanism involving chemical, thermal and redox initiation, the formation of both grafted and free polymer chains, and inhibitory reactions.

Once the kinetics of the grafting polymerization reaction was explored and the influence of GTR in this system was elucidated, the attention was turned towards the development of composite materials based on polystyrene and GTR. Therefore, the third part of this work focused on a novel methodology to fabricate polystyrene-reinforced materials rich in GTR. Through the analysis of the relationships existing between the degree of dispersion and distribution of the rubber particles, mechanical properties and methods for composites elaboration, the methodology conceived combines two strategies with two different but complementary purposes:

- increase the interfacial adhesion between PS and GTR particles by grafting the polymer to the backbone of GTR through free-radical bulk polymerization, with a mix of peroxide initiator agents (BPO, DCP and DHBP) in a batch reactor,
- compounding the resulting product several times in a twin-screw extruder to favor fine dispersion, i.e. reduce the particle size and spatial distribution of GTR through the PS matrix.

The proposed methodology was applied by preparing three different materials containing 30, 50 and 70 wt% of GTR. Operating conditions were defined to promote high conversion and grafting efficiency. The effects of the GTR content on the polymer qualities were discussed. Polystyrene was effectively grafted onto GTR particles. It was corroborated that the polymerization rate is strongly inhibited and the final monomer conversion is reduced with increasing GTR loading. The presence of polymer chains with low molecular weight predominates. Subsequently, the microstructure and mechanical properties of the products obtained were followed after each extrusion. A first main conclusion of this experimental work is that the methodology proposed led to a satisfactory improvement of the notched Charpy impact strength of polystyrene by a factor of 2 by adding 50 wt% of GTR. The original size of GTR was reduced in more than two orders of magnitude after one extrusion passage. It was demonstrated that good interfacial adhesion between GTR and PS before and after compounding, as well as compounding temperature, were crucial to successfully reinforce PS. Depending on the GTR content, two polystyrene materials, having different mechanical behavior, were obtained by applying this methodology: impact resistant (containing 30 and 50 wt% of GTR) and thermoplastic elastomer vulcanized (with 70 wt% of GTR). These findings enhanced our understanding of the factors that dictate the ultimate mechanical properties of polystyrene-reinforced composites with GTR.

Perspectives of this research

The experimental study of the effect of GTR on the kinetics of the free-radical polymerization of styrene by DSC, needs to be further pursued. This will lead to determine the extent of the redox initiation and inhibition effects. In this work, an effort was made to calculate the overall inhibition constant, nevertheless, preliminary estimations do not lead to obtain consistent results and additional experimental data is required.

Parameter estimation of the kinetic model describing the free-radical bulk polymerization of styrene in the presence of GTR is a challenge to address in order to access to a better comprehension and description of this complex system. This model may help future researches in predicting and optimizing the polymerization conditions. By complementing with the experimental data from DSC analyses,

the approach proposed by Eghtesadi and McAuley [141], through the implementation of a mean square based statistical method, may be contemplated to rank and select the most estimable parameters, which could be further estimated by fitting with the DSC and batch reactions results.

To classify the polystyrene-reinforced composites obtained between the existent commercial categories of reinforced polystyrenes (e.g. HIPS and SBS), further work is required to compare the mechanical properties with those of commercial materials having similar polymer molar masses: M_n ranging between 2,00E+04 and 8,00E+04 g/mol, and M_w from 3,20E+04 to 1,70E+05 g/mol. Otherwise, it is possible to consider defining the operating conditions of the grafting polymerization onto GTR leading to synthesize *in-situ* polystyrene with higher molar mass and close to those of the commercial resins, for which M_n is usually up to 1E+05 g/mol.

Bibliography

- [1] A.B. Strong. *Fundamentals of composites manufacturing: materials, methods and applications*. 2nd ed. Dearborn, Mich: Society of Manufacturing Engineers, 2008.
- [2] K. Tarverdi. *Management, recycling and reuse of waste composites. Chapter 11. Improving the mechanical recycling and reuse of mixed plastics and polymer composites*. Elsevier, 2010.
- [3] I. Manas-Zloczower. *Mixing and compounding of polymers theory and practice*. 2nd. Munchen: Hanser, C., 2009.
- [4] F.C. Campbell. *Structural composite materials*. Materials Park, Ohio: ASM International, 2010.
- [5] European Tyre ETRMA and Rubber Manufacturers Association. “Annual Report 2017”. In: (2010).
- [6] M. Sienkiewicz et al. “Progress in used tyres management in the European Union: A review”. In: *Waste Management* 32.10 (Oct. 2012), pp. 1742–1751.
- [7] USTMA U.S. Tire Manufacturers Association. “2017 U.S. Scrap tire management summary (July 2018)”. In: (July 2017).
- [8] Modern Tire Dealer Magazin Jan 2018. “World leaders in new tires sales for the fiscal year 2017, in billions of U.S. dollars”. In: 1 (Jan. 2018).
- [9] U.S. Tire Manufacturers Association. “What’s In a Tire”. In: (May 2017).
- [10] S. Ramarad et al. “Waste tire rubber in polymer blends: A review on the evolution, properties and future”. In: *Progress in Materials Science* 72 (July 2015), pp. 100–140.
- [11] J. Karger-Kocsis, L. Mészáros, and T. Bárány. “Ground tyre rubber (GTR) in thermoplastics, thermosets, and rubbers”. In: *Journal of Materials Science* 48.1 (Jan. 2013), pp. 1–38.
- [12] OICA International Organization of Motor Vehicle Manufacturers. “Number of vehicles in use worldwide 2015 | Statistic”. In: *Statista* (2015).
- [13] Worldwide. Bryan Garnier and Co. “World Tires Demand”. In: *The Freedonia Group* (2018).
- [14] European Tyre ETRMA and Rubber Manufacturers Association. “The European Tyre Industry Facts and Figures, 2017 Edition”. In: (2010).
- [15] J.E. Mark, B. Erman, and F.R. Eirich. *Science and technology of rubber*. 1994.
- [16] P.A. Ciullo and N. Hewitt. *Compounding materials*. Norwich, NY: Elsevier, 1999, pp. 4–49.
- [17] M. Sienkiewicz et al. “Environmentally friendly polymer-rubber composites obtained from waste tyres: A review”. In: *Journal of Cleaner Production* 147 (Mar. 2017), pp. 560–571.
- [18] European Tyre ETRMA and Rubber Manufacturers Association. “End-of-life Tyre Report 2015”. In: (2010).
- [19] Filiale française de valorisation des pneus usagées Aliapur. “Research and Development Innovations”. In: *Rapport d'activité 2017, www.aliapur.fr* (2017).

- [20] Filiale française de valorisation des pneus usagées Aliapur. “Research and Development Innovations”. In: *Aliapur Web Site*, www.aliapur.fr (2018).
- [21] Recycling Research Institute. “Crumb Rubber Overview”. In: *Scrap Tire News*, www.scraptirenews.com (2018).
- [22] D. Dobrota and G. Dobrota. “An innovative method in the regeneration of waste rubber and the sustainable development”. In: *Journal of Cleaner Production* 172 (Jan. 2018), pp. 3591–3599.
- [23] M. Pittolo and R. P. Burford. “Rubber-crumb modified polystyrene”. In: *Journal of materials science* 21.5 (1986), pp. 1769–1774.
- [24] A. Guglielmotti, C. Lucignano, and F. Quadrini. “Plastics, Rubber and Composites. Production of rubber parts by tyre recycling without using virgin materials”. In: 41 (Feb. 2012), pp. 40–46.
- [25] Roll gom company. “Fabrication de roues en caoutchouc recyclé”. In: *Roll-gom Web Site*, www.rollgom.com/fr (2018).
- [26] S.K. De, A. Isayev, and K. Khait. *Rubber Recycling*. London: CRC Press, 2005.
- [27] A. Isayev. “Single and twin extruders with ultrasound horns for decrosslinking and devulcanization”. Pat. WO/2012/142562. Akron Ohio US The University of Akron 852 Cricket Circle. Oct. 2012.
- [28] S. Coiai et al. “Modification of Cross-Linked Rubber Particles by Free Radical Polymerization”. In: *Macromolecular Symposia* 234.1 (Feb. 2006), pp. 193–202.
- [29] S.H. Lee, M. Balasubramanian, and J.K. Kim. “Dynamic reaction inside co-rotating twin screw extruder. I. Truck tire model material/PP blends: Truck Tire Model Material/Polypropylene Blends”. In: *Journal of Applied Polymer Science* 106.5 (Dec. 2007), pp. 3193–3208.
- [30] D. Tuchman and S. L. Rosen. “The mechanical properties of plastics containing cryogenically ground tire”. In: *Journal of Elastomers & Plastics* 10.2 (Apr. 1978), pp. 115–128.
- [31] H. Yazdani et al. “Devulcanization of waste tires using a twin-screw extruder: The effects of processing conditions”. In: *Journal of Vinyl and Additive Technology* 17.1 (Mar. 2011), pp. 64–69.
- [32] G. Tao et al. “The effect of devulcanization level on mechanical properties of reclaimed rubber by thermal-mechanical shearing devulcanization”. In: *Journal of Applied Polymer Science* 129.5 (Sept. 2013), pp. 2598–2605.
- [33] B. Adhikari, D. De, and S. Maiti. “Reclamation and recycling of waste rubber”. In: *Progress in Polymer Science* 25.7 (Sept. 2000), pp. 909–948.
- [34] W. Feng and A.I. Isayev. “Continuous ultrasonic devulcanization of unfilled butyl rubber”. In: *Journal of Applied Polymer Science* 94.3 (Nov. 2014), pp. 1316–1325.
- [35] J. Yun et al. “Comparative analysis of ultrasonically devulcanized unfilled SBR, NR, and EPDM rubbers”. In: *Journal of Applied Polymer Science* 88.2 (Apr. 2003), pp. 434–441.
- [36] R. Sonnier et al. “Compatibilisation of polyethylene/ground tyre rubber blends by $\dot{\gamma}$ irradiation”. In: *Polymer Degradation and Stability* 91.10 (Oct. 2006), pp. 2375–2379.
- [37] R. Sonnier et al. “Polyethylene/ground tyre rubber blends: Influence of particle morphology and oxidation on mechanical properties”. In: *Polymer Testing* 26.2 (2007), pp. 274–281.
- [38] J.I. Kim, S.H. Ryu, and Y.W. Chang. “Mechanical and dynamic mechanical properties of waste rubber powder/HDPE composite”. In: *Journal of Applied Polymer Science* 77.12 (Sept. 2000), pp. 2595–2602.
- [39] R. Scaffaro et al. “Formulation, characterization and optimization of the processing condition of blends of recycled polyethylene and ground tyre rubber: Mechanical and rheological analysis”. In: *Polymer Degradation and Stability* 90.2 (Nov. 2005), pp. 281–287.

- [40] H. Ismail, M. Awang, and M.A. Hazizan. "Effect of waste tire dust (WTD) size on the mechanical and morphological properties of polypropylene/Waste tire dust (PP/WTD) blends". In: *Polymer-Plastics Technology and Engineering* 45.4 (May 2006), pp. 463–468.
- [41] X. Colom et al. "Structural and mechanical studies on modified reused tyres composites". In: *European Polymer Journal* 42.10 (Oct. 2006), pp. 2369–2378.
- [42] F. Cataldo, O. Ursini, and G. Angelini. "Surface oxidation of rubber crumb with ozone". In: *Polymer Degradation and Stability* 95.5 (May 2010), pp. 803–810.
- [43] A.A. Yehia et al. "Effect of chemically modified waste rubber powder as a filler in natural rubber vulcanizates". In: *Journal of Applied Polymer Science* 93.1 (July 2004), pp. 30–36.
- [44] X. Colom, F. Carrillo, and J. Canavate. "Composites reinforced with reused tyres: Surface oxidant treatment to improve the interfacial compatibility". In: *Composites Part A: Applied Science and Manufacturing* 38.1 (Jan. 2007), pp. 44–50.
- [45] J. Zhang et al. "Compatibility of waste rubber powder/polystyrene blends by the addition of styrene grafted styrene butadiene rubber copolymer: effect on morphology and properties". In: *Polymer Bulletin* 70.10 (June 2013), pp. 2829–2841.
- [46] P. Phinyocheep, F. H. Axtell, and T. Laosee. "Influence of compatibilizers on mechanical properties, crystallization, and morphology of polypropylene/scrap rubber dust blends". In: *Journal of Applied Polymer Science* 86.1 (Oct. 2002), pp. 148–159.
- [47] J.L. Zhang et al. "Graft polymerization of styrene onto waste rubber powder and surface characterization of graft copolymer". In: *Polymer Bulletin* 68.3 (Feb. 2012), pp. 789–801.
- [48] R. Sonnier et al. "Compatibilizing thermoplastic/ground tyre rubber powder blends: Efficiency and limits". In: *Polymer Testing* 27.7 (Oct. 2008), pp. 901–907.
- [49] Y.A. Aggour, A.S. Al-Shihri, and M.R. Bazzt. "Surface Modification of Waste Tire by Grafting with Styrene and Maleic Anhydride". In: *Open Journal of Polymer Chemistry* 02.2 (2012), pp. 70–76.
- [50] J. Saelao and P. Phinyocheep. "Influence of styrene on grafting efficiency of maleic anhydride onto natural rubber". In: *Journal of Applied Polymer Science* 95.1 (Jan. 2005), pp. 28–38.
- [51] P. Heim, O. De Linares, and Laure Hym. "Polystyrene et copolymères de styrene". In: *Techniques ingénieur Matières thermoplastiques : monographies* (July 2002).
- [52] N. Niessner and D. Wagner. *Practical guide to structures properties and applications of styrenic polymers*. London: Smithers Rapra, 2013.
- [53] Michel BIRON. "Propriétés des thermoplastiques. Tableaux comparatifs". In: *Techniques de l'ingénieur Matières thermoplastiques : monographies base documentaire : TIB147DUO.ref. article : am3306* (2014).
- [54] G. Gao et al. "Deformation mechanism of polystyrene toughened with sub-micrometer monodisperse rubber particles". In: *Polymer International* 55.11 (Nov. 2006), pp. 1215–1221.
- [55] N. Yu. "Study of the Kinetics of Free Radical Polymerization of Styrene in a Three Dimensional Network and Applications for Used Tire Recycling". PhD thesis. Nancy, France: University of Lorraine, Dec. 2015.
- [56] A. Brydon, G. M. Burnett, and G. G. Cameron. "Free-radical grafting of monomers to polydienes. I. Effect of reaction conditions on grafting of styrene to polybutadiene". In: *Journal of Polymer Science: Polymer Chemistry Edition* 11.12 (Dec. 1973), pp. 3255–3269.
- [57] D.S. Achilias, A.K. Nikolaidis, and G.P. Karayannidis. "PMMA/ organomodified montmorillonite nanocomposites prepared by in situ bulk polymerization". In: *Journal of Thermal Analysis and Calorimetry* 102.2 (Nov. 2010), pp. 451–460.
- [58] D.S. Achilias. "Investigation of the radical polymerization kinetics using DSC and mechanistic or isoconversional methods". In: *Journal of Thermal Analysis and Calorimetry* 116.3 (June 2014), pp. 1379–1386.

- [59] E.L. Rodriguez. "The effect of free radical initiators and fillers on the cure of unsaturated polyester resins". In: *Polymer Engineering and Science* 31.14 (July 1991), pp. 1022–1028.
- [60] R. Xiong. "Studies in polymer composites based on carbon containing pulverized rubber materials". PhD thesis. Chicago: Illinois Institute of Technology, July 2010.
- [61] O. Bera et al. "A new approach for the kinetic modeling of free radical bulk polymerization of styrene". In: *Polymer Journal* 43.10 (Oct. 2011), pp. 826–831.
- [62] F. L. Marten and A. E. Hamielec. "High-conversion diffusion-controlled polymerization of styrene. I". In: *Journal of Applied Polymer Science* 27.2 (Feb. 1982), pp. 489–505.
- [63] G.G. Odian. *Principles of polymerization*. 4th ed. Hoboken, N.J: Wiley-Interscience, 2004.
- [64] L.K. Tong and W.O. Kenyon. "Heats of polymerization. III. Styrene and substituted styrenes". In: *Journal of the American Chemical Society* 69.6 (June 1947), pp. 1402–1405.
- [65] G. Kraus, J.T. Gruver, and K.W. Rollmann. "Inhibition of polymerization by carbon blacks". In: *Journal of Polymer Science* 36.130 (Apr. 1959), pp. 564–565.
- [66] K. Ohkita et al. "The free radical polymerization of vinyl monomers in the presence of carbon black". In: *Carbon* 13.5 (1975), pp. 443–448.
- [67] S. Kiatkamjornwong and P. Pomsanam. "Synthesis and characterization of styrenic-based polymerized toner and its composite for electrophotographic printing". In: *Journal of Applied Polymer Science* 89.1 (July 2003), pp. 238–248.
- [68] ASTM E2253-16. "Standard Test Method for Temperature and Enthalpy Measurement Validation of Differential Scanning Calorimeters". In: *ASTM International* (2006).
- [69] K. Fujiki, N. Tsubokawa, and Y. Sone. "Radical grafting from carbon black. Graft polymerization of vinyl monomers initiated by Azo groups introduced onto carbon black surface". In: *Polymer Journal* 22.8 (Aug. 1990), pp. 661–670.
- [70] S. Hoppe. "Contribution à l'étude de deux procédés d'élaboration de matériaux composites présentant des propriétés d'absorption aux ondes hyperfréquences." PhD thesis. France: Institut National Polytechnique de Lorraine (INPL). Ecole Nationale Supérieure des Industries Chimiques, Feb. 1995.
- [71] L. R. Radovic. "Chemistry and physics of carbon". In: *Energy & Fuels* 15.2 (Mar. 2001), pp. 502–502.
- [72] "Initiators and Reactor Additives for Thermoplastics". In: (Jan. 2013). Posted at www.akzonobel.com.
- [73] N. Tsubokawa, K. Fujiki, and Y. Sone. "Radical grafting from carbon black. Graft polymerization of vinyl monomers initiated by peroxyester groups introduced onto carbon black surface". In: *Polymer Journal* 20.3 (Mar. 1988), pp. 213–220.
- [74] K. Ohkita, N. Tsubokawa, and E. Saitoh. "The competitive reactions of initiator fragments and growing polymer chains against the surface of carbon black". In: *Carbon* 16.1 (1978), pp. 41–45.
- [75] T. Alfrey and C. C. Price. "Relative reactivities in vinyl copolymerization". In: *Journal of Polymer Science* 2.1 (Feb. 1947), pp. 101–106.
- [76] S.T. Balke and A.E. Hamielec. "Bulk polymerization of methyl methacrylate". In: *Journal of Applied Polymer Science* 17.3 (Mar. 1973), pp. 905–949.
- [77] K. Ohkita et al. "Influence of oxygen-containing groups of carbon black on the thermal polymerization of styrene". In: *Nippon Gomu Kyokaishi* 49.12 (1976), pp. 900–907.
- [78] N. Sbirrazzuoli and S. Vyazovkin. "Learning about epoxy cure mechanisms from isoconversional analysis of DSC data". In: *Thermochimica Acta* 388.1-2 (June 2002), pp. 289–298.

- [79] V.N. Kondratiev. "Comprehensive chemical kinetics. Chain reactions". In: *Comprehensive chemical kinetics*. Vol. 2. Elsevier, 1969, pp. 81–188.
- [80] P.J. Flory. *Principles of polymer chemistry*. 19. print. Ithaca, NY: Cornell Univ. Press, 2006.
- [81] A. Coupard and C. G'Sell. *Génie mécanique des caoutchoucs et des élastomères thermoplastiques*. French. Nancy: Apollor, 1997.
- [82] R. N. Rothon and Rapra Technology Limited, eds. *Particulate-filled polymer composites*. 2nd ed. Shrewsbury, UK: Rapra Technology, 2003.
- [83] I.M. WARD. *Mechanical properties of solid polymers*. 1st Edition. Wiley, 1971.
- [84] C. B. Bucknall and D. R. Paul. "Notched impact behavior of polymer blends: Part 1: New model for particle size dependence". In: *Polymer* 50.23 (Nov. 2009), pp. 5539–5548.
- [85] C. B. Bucknall and D. R. Paul. "Notched impact behaviour of polymer blends: Part 2: Dependence of critical particle size on rubber particle volume fraction". In: *Polymer* 54.1 (Jan. 2013), pp. 320–329.
- [86] J. J. Huang, H. Keskkula, and D. R. Paul. "Comparison of the toughening behavior of nylon 6 versus an amorphous polyamide using various maleated elastomers". en. In: *Polymer* 47.2 (Jan. 2006), pp. 639–651.
- [87] S. Wu. "A generalized criterion for rubber toughening: The critical matrix ligament thickness". In: *Journal of Applied Polymer Science* 35.2 (Feb. 1988), pp. 549–561.
- [88] D. G. Gilbert and A. M. Donald. "Toughening mechanisms in high impact polystyrene". en. In: *Journal of Materials Science* 21.5 (May 1986), pp. 1819–1823.
- [89] Y. Okamoto et al. "Impact improvement mechanism of HIPS with bimodal distribution of rubber particle size". In: *Macromolecules* 24.20 (Sept. 1991), pp. 5639–5644.
- [90] X. Colom et al. "Effect of the particle size and acid pretreatments on compatibility and properties of recycled HDPE plastic bottles filled with ground tyre powder". In: *Journal of Applied Polymer Science* 112.4 (May 2009), pp. 1882–1890.
- [91] R. Mujal-Rosas et al. "Study on dielectric, thermal, and mechanical properties of the ethylene vinyl acetate reinforced with ground tire rubber". In: *Journal of Reinforced Plastics and Composites* 30.7 (Apr. 2011), pp. 581–592.
- [92] S. Tantayanon and S. Juikham. "Enhanced toughening of poly (propylene) with reclaimed-tire rubber". In: *Journal of applied polymer science* 91.1 (2004), pp. 510–515.
- [93] G. S. Ananthapadmanabha and V. Deshpande. "Influence of aspect ratio of fillers on the properties of acrylonitrile butadiene styrene composites". In: *Journal of Applied Polymer Science* 135.11 (Nov. 2017), p. 46023.
- [94] H. Wiebking. "Fillers in PVC a Review of the Basics". In: *Specialty Minerals Inc.* (Nov. 1998).
- [95] D. Raghavan, H. Huynh, and C. F. Ferraris. "Workability, mechanical properties, and chemical stability of a recycled tyre rubber-filled cementitious composite". In: *Journal of Materials Science* 33.7 (Apr. 1998), pp. 1745–1752.
- [96] D. G. Cook, A. Rudin, and A. Plumtree. "Fracture mechanics parameters for polystyrene under high speed impact". In: *Polymer Engineering and Science* 30.10 (May 1990), pp. 596–602.
- [97] J. L. White, H. Potente, and U. Berghaus. *Screw extrusion: science and technology*. Progress in polymer processing. Munich ; Cincinnati: Hanser, 2003.
- [98] S-P Rwei, I. Manas-Zloczower, and D. L. Feke. "Analysis of dispersion of carbon black in polymeric melts and its effect on compound properties". en. In: *Polymer Engineering and Science* 32.2 (Jan. 1992), pp. 130–135.
- [99] Y. Suetsugu. "State of Dispersion and Mechanical Properties Correlation in Small Particle Filled Polymer Composites". In: *International Polymer Processing* 5.3 (Sept. 1990), pp. 184–190.

- [100] Y. Wang and J. Huang. "Single screw extrusion compounding of particulate filled thermoplastics: State of dispersion and its influence on impact properties". In: *Journal of Applied Polymer Science* 60.11 (June 1996), pp. 1779–1791.
- [101] E. L. Cussler and G. D. Moggridge. *Chemical product design*. 2nd ed. Cambridge series in chemical engineering. Cambridge ; New York: Cambridge University Press, 2011.
- [102] Spraying Systems Co. "Automatic and air atomizing spray nozzles (Withdrawn 2006)". In: (2014). Posted at www.spraying.fr.
- [103] R. Reiner. *General Overview of the Compounding Process: Tasks, Selected Applications, and Process Zones*. Munich: Hanser, 2008, p. 354.
- [104] J. L. White. *Twin screw extrusion: technology and principles*. Munich ; New York : New York: Hanser Publishers ; Distributed in the U.S.A. and Canada by Oxford University Press, 1991, p. 295.
- [105] P. Andersen. *Mixing practices in Co-Rotating Twin Screw Extruders*. 2nd. München: Hanser, Carl, 2009, pp. 947–979.
- [106] Riyadh Al-Raoush and Apostolos Papadopoulos. "Representative elementary volume analysis of porous media using X-ray computed tomography". In: *Powder Technology* 200.1-2 (June 2010), pp. 69–77.
- [107] T. Kanit et al. "Determination of the size of the representative volume element for random composites: statistical and numerical approach". In: *International Journal of Solids and Structures* 40.13-14 (June 2003), pp. 3647–3679.
- [108] ASTM D1959-97. "Standard Test Method for Iodine Value of Drying Oils and Fatty Acids (Withdrawn 2006)". In: *ASTM International*, www.astm.org (1997).
- [109] ASTM D471-16a. "Standard Test Method for Rubber Property Effect of Liquids". In: *ASTM International*, www.astm.org (2016).
- [110] E. Di Giuseppe et al. "Lignocellulosic fiber breakage in a molten polymer. Part 2. Quantitative analysis of the breakage mechanisms during compounding". In: *Composites Part A: Applied Science and Manufacturing* 95 (Apr. 2017), pp. 31–39.
- [111] M. Takano and L.E. Nielsen. "The notch sensitivity of polymeric materials". In: *Journal of Applied Polymer Science* 20.8 (Aug. 1976), pp. 2193–2207.
- [112] J. D. Ferry. *Viscoelastic properties of polymers*. 3d ed. New York: Wiley, 1980.
- [113] M. A. Hallam, G. Pollard, and I. M. Ward. "Relationship between tensile strength and molecular weight of highly drawn polyethylenes". In: *Journal of Materials Science Letters* 6.8 (Aug. 1987), pp. 975–976.
- [114] J. R. Davis, ed. *Tensile testing*. 2. ed. Materials Park, Ohio: ASM International, 2004.
- [115] C. C. Liao et al. "Thermokinetics evaluation and simulations for the polymerization of styrene in the presence of various inhibitor concentrations". In: *Journal of Thermal Analysis and Calorimetry* 85.1 (July 2006), pp. 65–71.
- [116] A. W. Hui and A. E. Hamielec. "Thermal polymerization of styrene at high conversions and temperatures. An experimental study". In: *Journal of Applied Polymer Science* 16.3 (1972), pp. 749–769.
- [117] F. R. Mayo. "The dimerization of styrene". In: *Journal of the American Chemical Society* 90.5 (Feb. 1968), pp. 1289–1295.
- [118] F. R. Mayo. "Chain Transfer in the Polymerization of Styrene. VIII. Chain Transfer with Bromobenzene and Mechanism of Thermal Initiation¹". In: *Journal of the American Chemical Society* 75.24 (Dec. 1953), pp. 6133–6141.

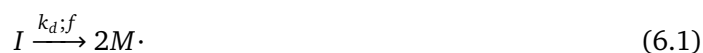
- [119] W. A. Pryor and J. H. Coco. "Computer Simulation of the Polymerization of Styrene. The Mechanism of Thermal Initiation and the Importance of Primary Radical Termination". In: *Macromolecules* 3.5 (Sept. 1970), pp. 500–508.
- [120] A. Husain and A. E. Hamielec. "Thermal polymerization of styrene". In: *Journal of Applied Polymer Science* 22.5 (1978), pp. 1207–1223.
- [121] D. S. Achilias and C. Kiparissides. "Development of a general mathematical framework for modeling diffusion-controlled free-radical polymerization reactions". In: *Macromolecules* 25.14 (July 1992), pp. 3739–3750.
- [122] N. Tefera, G. Weickert, and K. R. Westerterp. "Modeling of free radical polymerization up to high conversion. II. Development of a mathematical model". In: *Journal of Applied Polymer Science* 63.12 (Mar. 21, 1997), pp. 1663–1680.
- [123] G. A. O'neil, M. B. Wisnudel, and J. M. Torkelson. "Gel effect in free radical polymerization: model discrimination of its cause". In: *AIChE journal* 44.5 (1998), pp. 1226–1231.
- [124] C. Kotoulas et al. "A comprehensive kinetic model for the combined chemical and thermal polymerization of styrene up to high conversions". In: *Macromolecular Chemistry and Physics* 204.10 (June 2003), pp. 1305–1314.
- [125] J. D. Woloszyn and K. B. McAuley. "Application of Parameter Selection and Estimation Techniques in a Thermal Styrene Polymerization Model". In: *Macromolecular Reaction Engineering* 5.9-10 (Oct. 2011), pp. 453–466.
- [126] J. D. Woloszyn et al. "Parameter Selection and Estimation Techniques in a Styrene Polymerization Model". In: *Macromolecular Reaction Engineering* 7.7 (July 2013), pp. 293–310.
- [127] M. Buback et al. "Critically evaluated rate coefficients for free-radical polymerization, 1. Propagation rate coefficient for styrene". In: *Macromolecular Chemistry and Physics* 196.10 (1995), pp. 3267–3280.
- [128] S. Beuermann and M. Buback. "Rate coefficients of free-radical polymerization deduced from pulsed laser experiments". In: *Progress in Polymer Science* 27.2 (2002), pp. 191–254.
- [129] K. Horie, I. Mita, and H. Kambe. "Calorimetric investigation of polymerization reactions. I. Diffusion-controlled polymerization of methyl methacrylate and styrene". In: *Journal of Polymer Science Part A-1: Polymer Chemistry* 6.9 (1968), pp. 2663–2676.
- [130] K. Horie, I. Mita, and H. Kambe. "Calorimetric investigation of polymerization reactions. II. Copolymerization of diethyl fumarate with styrene". In: *Journal of Polymer Science Part A-1: Polymer Chemistry* 7.9 (Sept. 1969), pp. 2561–2573.
- [131] J. R. Ebdon and B. J. Hunt. "Study of the free-radical polymerization of styrene by differential scanning calorimetry". In: *Analytical Chemistry* 45.4 (Apr. 1973), pp. 804–806.
- [132] P. Manaresi, V. Passalacqua, and F. Pilati. "Kinetics of graft polymerization of styrene on cis-1,4-polybutadiene". In: *Polymer* 16.7 (July 1975), pp. 520–526.
- [133] N.-J. Huang and D. C. Sundberg. "Fundamental studies of grafting reactions in free radical copolymerization. IV. Grafting of styrene, acrylate, and methacrylate monomers onto vinylpolybutadiene using benzoyl peroxide and AIBN initiators in solution polymerization." In: *Journal of Polymer Science Part A: Polymer Chemistry* 33.15 (Nov. 15, 1995), pp. 2587–2603.
- [134] E. Mastan and S. Zhu. "Method of moments: A versatile tool for deterministic modeling of polymerization kinetics". In: *European Polymer Journal* 68 (2015), pp. 139–160.
- [135] R.C.M. Zabisky et al. "A kinetic model for olefin polymerization in high-pressure tubular reactors: a review and update". In: *Polymer* 33.11 (Jan. 1992), pp. 2243–2262.
- [136] J. Qin, W. Guo, and Z. Zhang. "A kinetic study on bulk thermal polymerization of styrene". In: *Polymer* 43.26 (2002), pp. 7521–7527.

- [137] J. Qin, W. Guo, and Z. Zhang. “Modeling of the bulk free radical polymerization up to high conversion—three stage polymerization model I. Model examination and apparent reaction rate constants”. In: *Polymer* 43.4 (2002), pp. 1163–1170.
- [138] Dimitris S. Achilias. “A Review of Modeling of Diffusion Controlled Polymerization Reactions”. In: *Macromolecular Theory and Simulations* 16.4 (May 25, 2007), pp. 319–347.
- [139] A. Keramopoulos and C. Kiparissides. “Development of a Comprehensive Model for Diffusion-Controlled Free-Radical Co-polymerization Reactions”. In: *Macromolecules* 35.10 (May 2002), pp. 4155–4166.
- [140] M. A. Villalobos, A. E. Hamielec, and P. E. Wood. “Bulk and suspension polymerization of styrene in the presence of n-pentane. An evaluation of monofunctional and bifunctional initiation”. In: *Journal of applied polymer science* 50.2 (1993), pp. 327–343.
- [141] Z. Eghtesadi and K. B. McAuley. “Mean Square Error Based Method for Parameter Ranking and Selection To Obtain Accurate Predictions at Specified Operating Conditions”. In: *Industrial & Engineering Chemistry Research* 53.14 (Apr. 9, 2014), pp. 6033–6046.
- [142] J. B. P. Soares and T. F. L. McKenna. *Polyolefin reaction engineering*. Weinheim: Wiley-VCH, 2012.
- [143] T. F. McKenna and J.B.P. Soares. “Single particle modelling for olefin polymerization on supported catalysts: A review and proposals for future developments”. In: *Chemical Engineering Science* 56.13 (July 2001), pp. 3931–3949.
- [144] M. Alkatheri. *Catalytic Olefin Polymerization: Modelling Of Heterogeneous Kinetics and Single-Particle Growth*. 2015.
- [145] V. Kanellopoulos et al. “Comprehensive Analysis of Single-Particle Growth in Heterogeneous Olefin Polymerization: The Random-Pore Polymeric Flow Model”. In: *Industrial & Engineering Chemistry Research* 43.17 (Aug. 2004), pp. 5166–5180.
- [146] J. A. Debling and W. H. Ray. “Heat and Mass Transfer Effects in Multistage Polymerization Processes: Impact Polypropylene”. In: *Industrial & Engineering Chemistry Research* 34.10 (Oct. 1995), pp. 3466–3480.
- [147] M. Hamba, G. C. Han-Adebekun, and W. H. Ray. “Kinetic study of gas phase olefin polymerization with a TiCl₄/MgCl₂ catalyst. II. Kinetic parameter estimation and model building”. In: *Journal of Polymer Science Part A: Polymer Chemistry* 35.10 (July 30, 1997), pp. 2075–2096.
- [148] H. W. McCormick, F. M. Brower, and L. Kin. “The effect of molecular weight distribution on the physical properties of polystyrene”. In: *Journal of Polymer Science* 39.135 (Sept. 1959), pp. 87–100.
- [149] C. B. Bucknall. *Impact Strength*. Dordrecht: Springer Netherlands, 1977, pp. 272–304.

Appendix 1

(Chapter 2, Sect. 2.3.3.1)

A typical, simplified free-radical polymerization kinetic scheme consists of a sequence of three steps, involving radical initiation (Eq. (6.1)), propagation (Eq. (6.2)) and termination (Eq. (6.4)) reactions. To this classical kinetic scheme, one can include a generalized inhibition reaction (Eq. (6.3)), when supporting indications or evidence exist. In the present work, Z designates in a generalized manner all those elements of GTR that act as inhibitor or retarder in the course of the polymerization.



where I , $MZ\cdot$ and P denote the initiator, deactivated radical and dead polymer, respectively. f is the initiator efficiency and k_d , k_p , k_z and k_t are the respective kinetic rate constants of the initiator decomposition, radical propagation, deactivation (i.e., by inhibitor) and termination (e.g., by combination or disproportionation) reactions. On the basis of the postulated kinetic scheme (Eq. (6.1)-(6.4)), and under the assumptions of constant radical concentration and the LCH, Eq. (6.5) can be derived (i.e., via direct integration of Eq. (2.2)) to express the variation of the monomer concentration (or equivalently monomer conversion) with respect to time :

$$-\ln(1-x) = k_p[M\cdot]t \quad (6.5)$$

In order to express the concentration of radicals, $M\cdot$, the QSSA can be applied to yield the following equation:

$$2fk_d[I] - 2k_t[M\cdot]^2 - k_z[M\cdot][Z] = 0 \quad (6.6)$$

Note that the reactivity of the radical $M_nZ\cdot$ has been considered too low to further promote polymerization. In addition, the decomposition rate constant, k_d , corresponds to the overall decomposition rate of the initiator, including thermal homolysis and eventual redox decomposition. From the above expression it can be seen that, when all terms are important, the final expression of $M_n\cdot$ will be a root of the quadratic algebraic equation who's generalized form is far from being simplified. In contrast, significant simplification can be achieved if one considers two extreme cases for the radical termination

mechanism. When radical termination takes place primarily by bi-radical termination (Eq. (6.4)), considering inhibition reactions (Eq. (6.3)) as negligible, the expression of $M_n \cdot$ is reduced to the commonly employed :

$$[M \cdot] = \left(f \frac{k_d}{k_t} [I] \right)^{1/2} \quad (6.7)$$

On the other hand, if the radical inhibition reactions (Eq. (6.4)) are considered as the dominant mechanism of radical termination, the following expression is obtained for $[M \cdot]$:

$$[M \cdot] = 2f \frac{k_d}{k_z} \frac{[I]}{[Z]} \quad (6.8)$$

Overall activation energy

To the typical case where inhibition reactions, considering an oversimplified general kinetic scheme (i.e., containing only the radical initiation, propagation and termination reactions) and under the assumptions of Long-Chain Hypothesis (LCH) and Quasi Steady-State Assumption (QSSA) for the polymer radicals [79], the polymerization rate R_p will be given by Eq. 2.2:

$$R_p = k_p [M \cdot] [M] = k_p [M] \left(\frac{R_i}{2k_t} \right)^{1/2} \quad (6.9)$$

$$R_i = 2f k_d [I] \quad (6.10)$$

$$R_p = k_p \left(\frac{k_d}{k_t} \right)^{1/2} \cdot (f [I])^{1/2} \cdot [M] \quad (6.11)$$

By expressing the rate constants as Arrhenius-type functions, in terms of the activation Energy E_a and the pre-exponential factor A_0 , as follows:

$$k = A_0 \cdot \exp\left(\frac{-E_a}{RT}\right) \quad (6.12)$$

The first term of the Eq. ?? can be expressed as:

$$\ln\left(k_p \left(\frac{k_d}{k_t}\right)^{1/2}\right) = \ln\left(A_p \left(\frac{A_d}{A_t}\right)^{1/2}\right) - \left(\frac{E_p + 0.5(E_d - E_t)}{RT}\right) \quad (6.13)$$

Where the last term of the Eq. 6.13 corresponds to the overall activation energy E_{eff} .

Appendix 2

(Chapter 4, Sect. 5.3.1.2)

The notched Charpy *IS* of each free-PS matrices, namely free-PS1, free-PS2 and free-PS3, was predicted by means of a correlation function between the notched Charpy *IS* of neat polystyrene and its molecular M_w . This function was determined by using values reported in the literature [96, 148], and experimental measurements carried out in this work. This procedure was adopted since no relevant data or correlations between the Charpy *IS* and M_w (close to those measured for the three distinct free-PS, i.e., M_w from 3,3E+04 to 5,15E+04 g/mol) was found in the literature.

The experimental measurements were performed on a series of impact specimens made of polystyrene having different M_w , but close to those measured for free-PS1, free-PS2 and free-PS3, after the first extrusion of their respective composites. Such polystyrene was prepared by solution polymerization in toluene, at the compositions and conditions presented in Sect. 3.7.2. The desired molecular weight were obtained by controlling the initiator concentration (BPO) and polymerization temperature.

A set of four solution polymerizations were performed in total. The molecular weight of the polystyrene obtained is shown in Table 6.1. Data are sorted by ascending molecular weight. Note that the most of the values sought for M_w (from 3,3E+04 to 5,15E+04 g/mol) are included in the range of values obtained.

Table 6.1 – *Molecular weight of polystyrene obtained by solution polymerization.*

No.	BPO/styrene (wt%)	Temp. (°C)	M_n (g/mol)	M_w (g/mol)	M_w/M_n
1	1.22	80	1,70E+04 ($\pm 5,2E+02$)	2,97E+04 ($\pm 2,9E+02$)	1,7 ($\pm 0,05$)
2	1.18	80	1,84E+04 ($\pm 5,1E+02$)	3,69E+04 ($\pm 3,2E+04$)	2,2 ($\pm 0,07$)
3	0.8	90	2,26E+04 ($\pm 1,2E+03$)	4,14E+04 ($\pm 3,1E+02$)	1,8 ($\pm 0,1$)
4	0.8	80	2,55E+04 ($\pm 1,4E+03$)	4,73E+04 ($\pm 4,8E+02$)	1,9 ($\pm 0,1$)

The impact specimens were fabricated by compression. These were tested without notch because they broke during notching due to their low molecular weight. The results of the unnotched Charpy *IS* are shown in Table 6.2.

The data used to predict the values of unnotched Charpy *IS* are illustrated in Figure 6.1. Note that the above experimental data (green dots), helped to determine the values of *IS* at the lower M_w values (dotted gray lines show the specific values of M_w sought). These were found to be in good agreement

Table 6.2 – Notched and unnotched Charpy IS of the polystyrene obtained by solution polymerization

No.	Unnotched Charpy IS (kJ/m ²)
1	0,63 (±0,04)
2	0,67 (±0,04)
3	0,71 (±0,03)
4	0,75 (±0,05)

with the lowest value reported in literature (black dots).

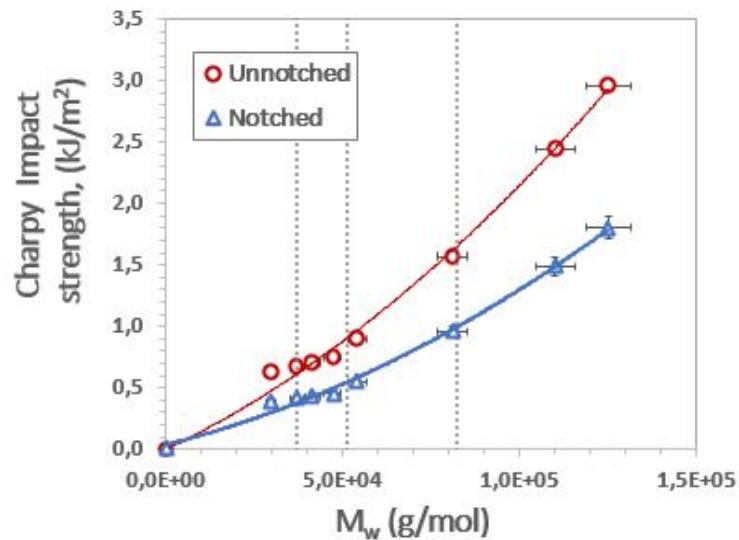


Figure 6.1 – Comparison of the unnotched and notched Charpy IS of polystyrene in function of M_w . Data produced in this work and literature values from [96, 148]. Dotted lines represent the specific values of M_w sought.

The function that predicted the best the data is indicated in the equation here below. The factor of r^2 value is equal to 0,995.

$$IS_{PS} \text{ (kJ/m}^2\text{)} = 8 \cdot 10^{-11} \cdot M_w^2 + 1 \cdot 10^{-5} \cdot M_w$$

Finally, to predict the values of notched Charpy IS, this equation was multiplied by a factor that quantifies the reduction of the impact resistance caused by the presence of the notch. This factor was calculated from direct measurements of the notched and unnotched Charpy IS of PS6, which resisted notching.

Table 6.3 – Notch sensibility of PS6. Variation of the Charpy IS when notching specimens for impact testing.

Charpy IS (kJ/m ²)		IS reduction by notching (%)
Unnotched	Notched	
5,16 (±0,06)	2,02 (±0,06)	60,86 (±0,06)

Table 6.3 shows that the impact resistance of PS6 decreases in about 61% when impact specimens are notched. In general, this value agrees well with differences reported in literature at similar testing conditions. However, the notch sensitivity can be either lower or higher since it largely depends on testing parameters, specimens manufacturing, etc. [111, 149]. Then, the correlation above is multiplied by a factor of 0,39.

The final values of unnotched and notched Charpy IS calculated for free-PS are shown in Table 6.4.

Table 6.4 – Predicted notched and unnotched Charpy IS of free-PS.

Polystyrene matrix	Charpy IS (kJ/m^2)	
	Unnotched	Notched
free-PS1	1,30 ($\pm 0,03$)	0,51 ($\pm 0,02$)
free-PS2	0,65 ($\pm 0,07$)	0,25 ($\pm 0,03$)
free-PS3	0,78 ($\pm 0,04$)	0,30 ($\pm 0,02$)

Résumé étendu en français (Extended abstract in French)

Introduction et contexte de cette recherche

L'industrie des produits en caoutchouc et des pneus affiche un développement et une croissance continus dans le monde entier. De la gomme à effacer aux chaussures et des vélos à l'aérospatiale, les produits en caoutchouc ont trouvé une grande variété d'applications dans notre vie quotidienne [5–7]. Le principal marché du caoutchouc est dominé par le secteur du transport et représente plus de 75% de la production mondiale principalement destinée à la fabrication de pneumatiques [5]. Les plus grands fabricants mondiaux de pneus sont établis aux États-Unis, à l'Union européenne (UE) et au Japon [8].

Le secteur automobile est le principal contributeur à l'accumulation dramatique de pneus usagés [5, 6, 10, 11]. Entre 2006 et 2015, le nombre de voitures particulières et de véhicules utilitaires en circulation dans le monde entier est passé de 926 600 à 1282 300 000 unités [12]. À la suite de cette activité, la production annuelle de pneus a atteint un taux de croissance annuel de plus de 20% au cours des six dernières années [13]. En 2016, plus de 285 millions de pneus (véhicules légers) ont été commercialisés dans l'UE, représentant 20% du marché mondial [14]. Une étude récente sur l'industrie mondiale des pneumatiques [13] a révélé que la demande mondiale de pneus automobiles tous types en 2019 est estimée à plus de 3,0 milliards unités dont un tiers est destiné au commerce des moteurs. Ces chiffres statistiques supposent que les véhicules et les marchés des pneus continuent de se développer à un rythme croissant. Par conséquent, une augmentation respective est observée pour les pneus post-consommation.

Au moment où les pneus sont démontés des véhicules pour être remplacés et jetés, ils génèrent plus de 17 millions de tonnes (1.4 milliard d'unités) de déchets chaque année et continuent d'augmenter de 2% par an [6]. Les anciennes méthodes d'élimination des pneus post-consommation reposaient sur l'enfouissement et le stockage, ce qui a conduit à des problèmes environnementaux et de santé publique majeurs, liés au risque d'incendie avec génération de gaz toxiques, prolifération de vecteurs (c.-à-d. transmission épidémique comme le paludisme, la dengue et chikungunya) et d'autres animaux nuisibles (c.-à-d. les rongeurs et les serpents). De plus, certains composants chimiques et métaux présents dans la formulation des pneus migrent dans les lixiviations entraînant également la pollution des sols. En effet, les pneus possèdent une structure technique qui les rend difficiles à retraiter et qui représente un défi pour leur réutilisation et leur recyclage [10, 11, 15].

Certaines régions ont en effet changé leurs politiques pour promouvoir un contrôle durable de certains déchets plastiques générés. C'est ainsi, par exemple, que les fabricants et importateurs des marchés des pneumatiques en caoutchouc ont développé des modèles de gestion exemplaires pour la récupération et le recyclage des pneumatiques post-consommation. Celles-ci ont conduit à de grands progrès

dans la résolution d'une partie des problèmes environnementaux causés par la suraccumulation de déchets plastiques.

Les pneus sont un assemblage complexe de composants et de propriétés, conçu pour combiner haute performance avec une longue durée de vie des produits et une capacité opérationnelle dans une large gamme d'environnements [15]. Les pneus post-consommation sont considérés comme une source importante de matières premières aux propriétés intéressantes. Ironiquement, du point de vue technique, ces qualités remarquables présentent aussi un énorme obstacle au recyclage et à la valorisation [6]. Les pneus sont essentiellement constitués d'un composite textile/acier/caoutchouc, dont la formulation varie en fonction du véhicule d'application envisagée [5, 9, 15].

La Figure 6.2 montre un exemple des matériaux utilisés dans les pneus pour véhicules légers et camions, qui peuvent contenir environ douze et vingt composants de formulation, respectivement [9, 10]. En général, les assemblages de pneus sont une combinaison de divers mélanges de caoutchouc, fibres de renforcement (c.-à-d. cordes d'acier et fibres polymères/textiles (c.-à-d. nylon, polyester, cellulose), des charges de caoutchouc et des additifs. Chacun de ces composants contribue individuellement et collectivement au service et à la performance du produit [15].

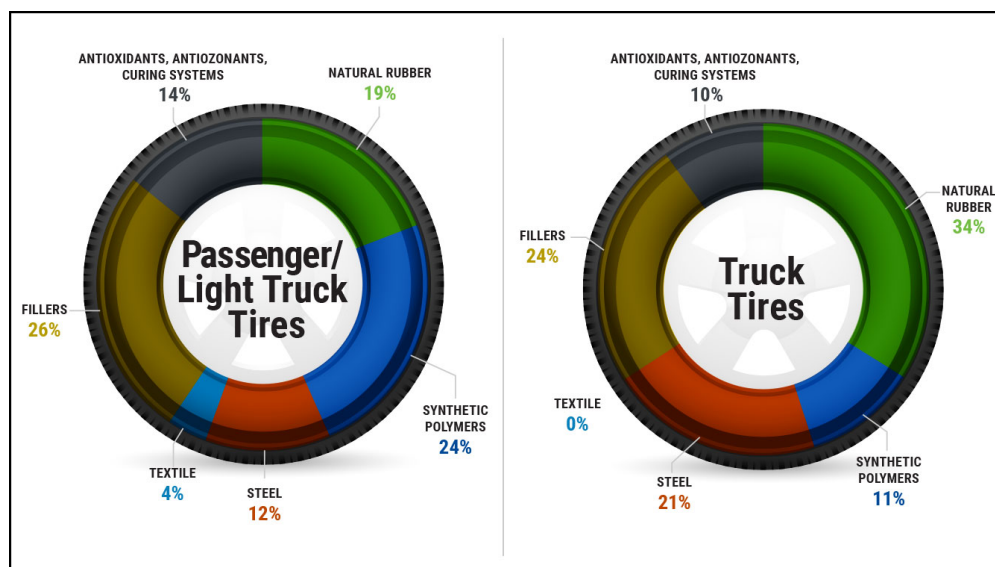


Figure 6.2 – Exemple de composition de pneus de tourisme/camionnette et de camion. Association des Fabricants de Pneus Américains (2017) [9].

La phase composite de caoutchouc représente environ 70% à 80% de la masse totale du pneu, et peut être créé à partir d'une grande variété de caoutchoucs naturels et synthétiques de haute qualité, d'agents de renforcement et additifs. L'ajout de charges comme le noir de carbone, l'argile et la silice amorphe renforcent les propriétés mécaniques des caoutchoucs et améliore leur résistance à l'usure et au roulement. Additifs tels que stabilisants et antioxydants sont également intégrés pour empêcher les effets de dégradation dus au vieillissement, à l'oxydation, à l'exposition à l'environnement, etc. [9, 16]. Enfin, la formulation est vulcanisée avec un système d'agents vulcanisant à base de soufre et de zinc, créant des ponts chimiques entre les chaînes élastomères pour former une structure de réseau réticulée tridimensionnelle renforcée [15]. En conséquence, le pneumatique obtenu est un composite élastique, insoluble, infusible et non biodégradable.

A la recherche de solutions durables pour valoriser les pneus en fin de vie, une alternative durable consiste à profiter des propriétés remarquables de la phase de caoutchouc vulcanisée et renforcée. Ainsi, après plusieurs étapes de broyage des pneus, il est tout à fait possible d'obtenir des granulés ou poudres

fines de caoutchouc, commercialement appelées poudrettes de caoutchouc couramment connues par leur sigles en anglais comme “GTR” ou “Ground Tire Rubber”.

Le GTR peut être utilisé pour développer une série de nouveaux produits aux applications pratiques au quotidien. De plus, la formulation de matériaux composites thermoplastiques par ajout de GTR est une option prometteuse pour encourager le recyclage et, en même temps, pour créer des matériaux aux propriétés mécaniques et à prix intéressants. En ce qui concerne les composites de polystyrène (PS) renforcés avec du GTR, les problèmes liés à l’incompatibilité interfaciale entre le GTR et le PS ont été partiellement surmontés via la stratégie de polymérisation par greffage. De plus, certaines conditions permettant d’optimiser la conversion des monomères, plus particulièrement la formation de chaînes de polystyrène greffées, ont été identifiées. Néanmoins, peu est connu sur l’effet du GTR dans la cinétique de ce système de polymérisation et, par exemple, on ne sait pas quels facteurs limitent la conversion du styrène.

D’autre part, la plupart des études ont atteint une légère augmentation de la résistance aux chocs et des propriétés de traction du PS en ajoutant de faibles quantités de GTR (généralement inférieures à 30% en poids). En fait, la recherche à ce jour a eu tendance à se concentrer uniquement sur l’amélioration de l’adhérence interfaciale entre le GTR et le PS en tant que facteur crucial pour la résistance aux chocs du polystyrène. Les connaissances actuelles sur les matériaux thermoplastiques chargés montrent que la résistance dépend fortement du degré de dispersion et de la distribution spatiale du GTR dans la matrice polymère. En particulier, le polystyrène peut être renforcé efficacement par l’addition de particules de caoutchouc de quelques microns de taille ou par la combinaison de particules de grande taille et inférieures au micromètre. Cela implique la nécessité de réduire la taille de particule d’origine du GTR de plus de deux ordres de grandeur. Néanmoins, ceci est difficile à réaliser par les techniques de broyage classiques en raison de la grande extensibilité et élasticité des particules de caoutchouc vulcanisé.

L’objectif de ce travail est de développer une nouvelle méthodologie pour renforcer les polymères cassants, comme le polystyrène, en utilisant le GTR comme agent de renforcement. Les matériaux doivent être riches en GTR dans le but de maximiser les taux de recyclage GTR. Cette méthodologie combine deux processus:

- polymérisation par greffage radicalaire du styrène sur GTR en utilisant un mélange d’initiateurs peroxydes, tels que BPO et DCP, dans un réacteur batch,
- ensuite, mélanger le produit obtenu dans une extrudeuse baxis. Ces processus consécutifs conduisent à assurer la bonne adhésion interfaciale entre PS et GTR et à favoriser une dispersion fine et une distribution spatiale du GTR à travers la matrice PS.

Polymérisation radicalaire de styrène présence de GTR

Dans un premier temps, une étude de la polymérisation en masse radicalaire du styrène en présence de GTR est menée en suivant le déroulement de la réaction par calorimétrie différentielle à balayage (DSC). Des conditions différentes en termes de température (85, 95 et 120 °C) et de composition, et deux initiateurs chimiques de nature différente, BPO et AMBN sont testées, afin d’aborder sélectivement le rôle de la présence de GTR au cours de la réaction de polymérisation.

La Figure 6.3 montre les effets de la présence de GTR sur le flux de chaleur DSC et la conversion de monomère de la polymérisation radicalaire en masse du styrène (ligne noire continue). On peut voir que l’addition de 30% en poids de GTR (pointillés bleus) et 50% (pointillés verts) affecte clairement à la fois la vitesse initiale de polymérisation et la conversion globale du monomère. Plus précisément, une augmentation de la teneur en GTR décale le pic exothermique maximal du thermogramme vers un

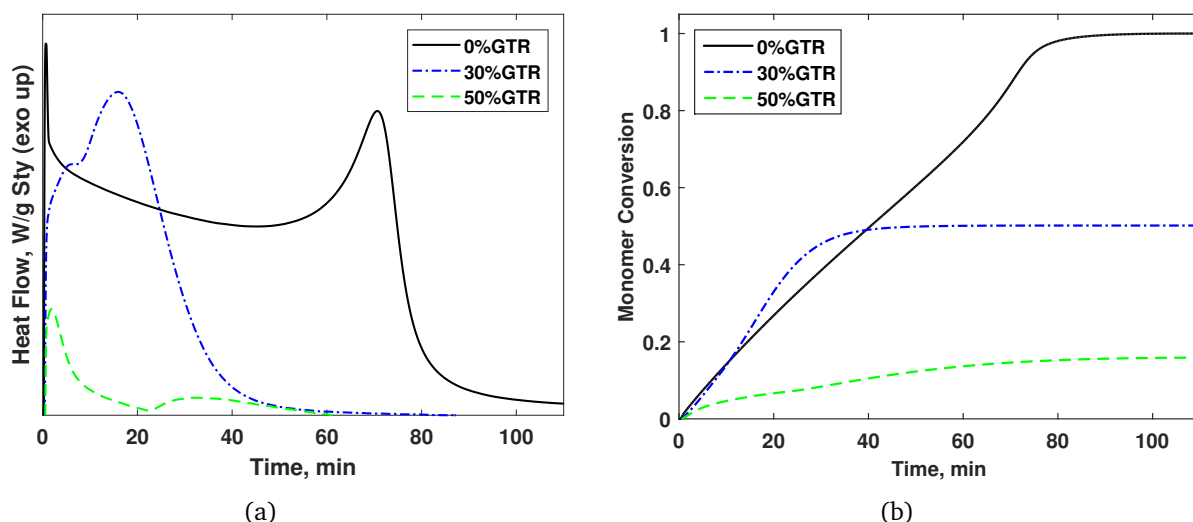


Figure 6.3 – Effet de la teneur en GTR sur l'évolution a) du flux thermique et b) de la conversion des monomères, lors de la polymérisation isotherme du styrène initiée par BPO en présence de particules de GTR. ($T=90\text{ °C}$; rapport BPO/St=4.6 % en poids).

temps de polymérisation inférieur. En même temps, la conversion ultime du monomère est également significativement réduite (cf. Fig. 6.3b).

Plusieurs études ont démontré que la polymérisation initiée par le peroxyde de monomères vinyliques était catalysée, inhibée et/ou retardée par la présence de noir de carbone [60, 65–67, 69, 70]. En fait, la surface du noir de carbone est principalement recouverte de groupes contenant de l'oxygène, tels que des structures carboxyle, des groupes phénoliques ou alcooliques hydroxyle, carbonyle et quinone. Au même temps, certains des atomes de carbone ont des valences non satisfaites, conduisant à une réactivité de transfert d'électrons élevée [71]. En conséquence, lorsque la polymérisation est initiée par un peroxyde organique, tel que le BPO, ces radicaux peuvent réagir avec les électrons non appariés pour donner naissance à de nouveaux sites actifs, auxquels les radicaux polymères primaires et en croissance entrent en compétition pour réagir. La réactivité des radicaux nouvellement formés n'est pas complètement inerte et peut donc subir d'autres réactions principalement avec des chaînes de propagation. D'autre part, il est bien connu que la combinaison de peroxydes avec des agents réducteurs est courante dans la production de radicaux à des taux raisonnables sur une large gamme de températures [63]. Par conséquent, lorsque le BPO entre en contact avec les nombreux groupes oxydes à la surface du noir de carbone, il subit une forte réaction redox [67]. La réaction de décomposition redox est favorisée à des températures relativement basses en raison de son énergie d'activation (c'est-à-dire 40-60 kJ/mol) qui est nettement inférieure à celle de la décomposition thermique (c'est-à-dire 120-150 kJ/mol) [63, 72].

Les résultats ont montré que, en général, l'addition de GTR présente un effet globalement négatif sur l'étendue finale de la réaction mais, en même temps, peut également avoir un impact positif ou négatif sur la vitesse de polymérisation. Ces effets peuvent être plus ou moins prononcés selon le type d'agent initiateur. Les écarts les plus importants ont été observés pour le système initié au peroxyde (c'est-à-dire avec le BPO), qui présentait une inhibition sévère qui augmentait avec la teneur en particules de caoutchouc et pouvait conduire à de très faibles conversions de monomères. Au contraire, la réaction initiée avec un composé azoïque (c'est-à-dire AMBN) a été modérément retardée et légèrement inhibée uniquement à des pourcentages de GTR élevés. Les effets observés ont été principalement attribués aux interactions chimiques induites par le noir de carbone, les additifs et les impuretés présents dans la formulation du GTR.

Une nouvelle méthodologie pour préparer des composites de polystyrène renforcés avec du GTR

Dans un deuxième temps, une nouvelle méthodologie est proposée pour améliorer les propriétés mécaniques du polystyrène par l'ajout de grandes quantités de particules de caoutchouc recyclé telles que le GTR. Le procédé présenté dans la Figure 6.4 combine deux étapes cruciales. Tout d'abord, la réaction de greffage du styrène sur la surface de GTR à l'aide des agents amorceurs peroxydes (BPO, DCP et DHBP). Ensuite, le produit de la polymérisation, GTR-greffé-PS, est mis en forme dans une extrudeuse bi-vis (en comparant deux profils de vis différents), une fois à haute température (180 à 200 °C) et puis, deux fois à basse température (90 à 100 °C).

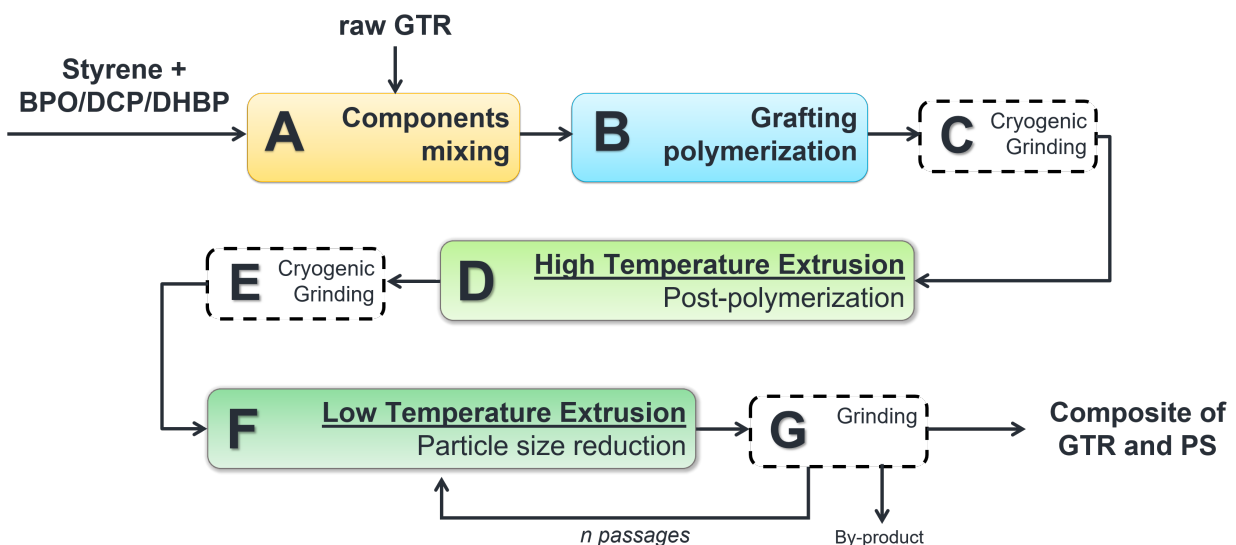


Figure 6.4 – Schéma des étapes du procédé implémenté

La Figure 6.5 compare les mesures de résistance aux chocs Charpy des composites de GTR-greffé-PS obtenus après 1, 2 et 3 extrusions, avec celles de la matrice de polystyrène pure. Ce qui ressort de cette figure c'est que la résistance aux chocs des deux composites contenant 30 % (30GTR-g-PS/f-PS1) et 50 % (50GTR-g-PS/f-PS2) en poids de GTR surpasse celui de leurs matrices de polystyrène respectives (f-PS1 et f-PS2). Cela suggère que la présence de particules de GTR-greffé-PS améliore efficacement la résistance aux chocs du PS, et elle semble augmenter avec la teneur GTR. Ainsi, lors de l'ajout de 30% et 50% en poids de GTR, la résistance au choc Charpy entaillée du polystyrène pur peut être augmentée entre 40 et 200%. Après la deuxième extrusion, il semble que la résistance des composites reste pratiquement inchangée.

Ensuite, un composite contenant 70% en poids de GTR a été préparé, cette fois-ci affichant des propriétés de traction intéressantes. La Figure 6.6 montre les courbes contrainte-déformation des éprouvettes de traction des composites obtenus après 1 et 2 étapes d'extrusion avec deux profils de vis différents. Les matériaux montrent une performance similaire à celle d'un vulcanisat élastomère thermoplastique (TPV) et sa déformation à la rupture peut atteindre entre 80 et 120%, ce qui est considérablement supérieur au 2.5 % de déformation mesuré pour la matrice polystyrène pure.

Un des objectifs de cette recherche était de démontrer que grâce à la mise en oeuvre de la méthodologie proposée, il est possible de fabriquer des composites renforcés de polystyrène par l'ajout de particules

de caoutchouc réticulé à partir de pneus recyclés sous forme de GTR. Cette méthodologie a été conçue pour intégrer deux processus, dont la combinaison successive a démontré fournir des effets synergiques.

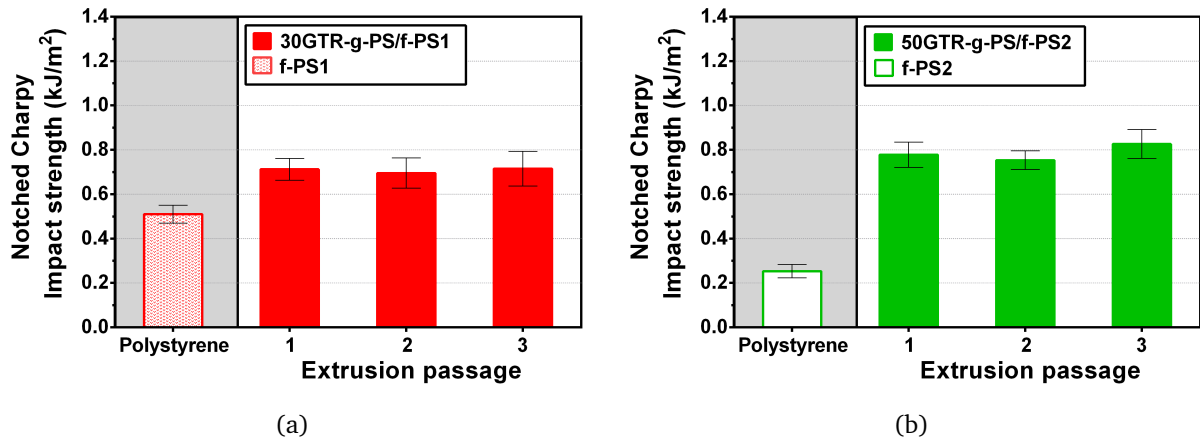


Figure 6.5 – Comparaison de la résistance aux chocs Charpy entre la matrice polystyrène et les composites après 1, 2 and 3 extrusions avec (a) 30% en poids de GTR (30GTR-g-PS/f-PS1) et (b) 50% en poids de GTR (50GTR-g-PS/f-PS2).

Ces procédés impliquent la polymérisation radicalaire du styrène en présence de GTR en utilisant un mélange d'initiateurs de peroxyde, et le mélange du produit résultant dans une extrudeuse bivis. Le greffage du styrène sur GTR assure une bonne adhérence interfaciale entre PS et GTR et le compoundage favorise une fine dispersion du GTR dans la matrice PS.

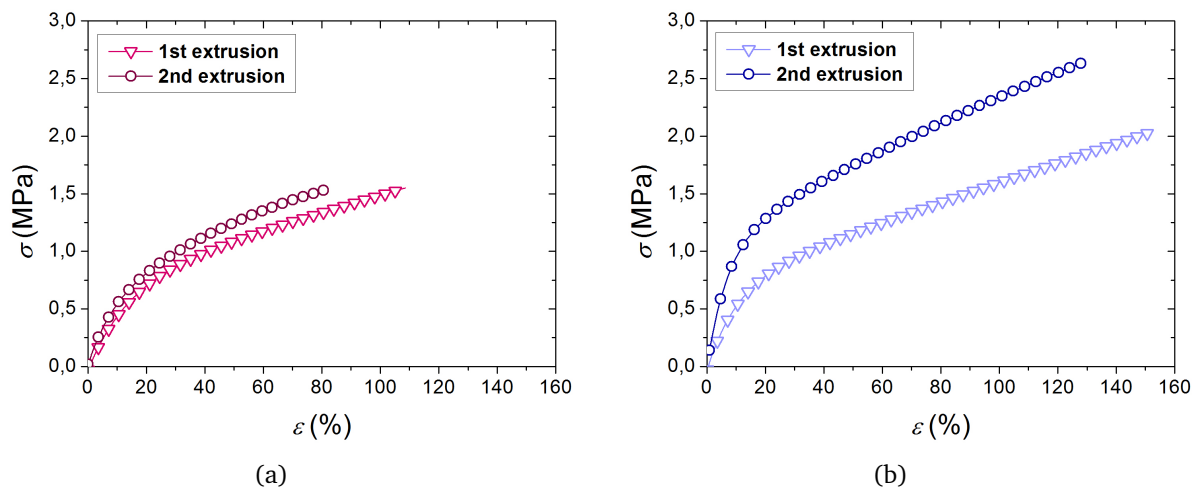


Figure 6.6 – Courbes contrainte-déformation des éprouvettes de traction des composites avec 70% de GTR en poids extrudés avec des profils de vis différents: (a) Profil 1 et (b) Profil 2.

Conclusions

Notre vision avec cette thèse est de contribuer à la recherche d'alternatives durables pour favoriser le recyclage des matériaux issus de pneus en fin de vie. L'un d'eux consiste à utiliser le caoutchouc recyclé sous forme de particules broyées ou de GTR pour renforcer les polymères thermoplastiques. Par ren-

forcement, la structure en caoutchouc réticulé du GTR confère au polymère une certaine ductilité, et par là, la capacité de mieux résister aux contraintes mécaniques avant rupture. La résistance dépend de la cohésion de l'interface polymère-particule, de la masse molaire du polymère, de la teneur en caoutchouc, du degré de dispersion (c'est-à-dire de la taille des particules) et de la distribution spatiale des particules de caoutchouc. Dans le même temps, ces facteurs dépendent eux-mêmes du type de procédés mis en oeuvre pour l'élaboration de tels matériaux composites.

La méthodologie proposée a été appliquée en préparant trois matériaux différents contenant 30, 50 et 70% en poids de GTR. Les conditions opératoires ont été définies pour favoriser une conversion et une efficacité de greffage élevées. Les effets de la teneur en GTR sur les qualités du polymère ont été discutés. Le polystyrène a été efficacement greffé sur des particules de GTR. Il a été corroboré que la vitesse de polymérisation est fortement inhibée et que la conversion finale du monomère est réduite avec l'augmentation de la charge de GTR. La présence de chaînes polymères de bas poids moléculaire prédomine. Par la suite, la microstructure et les propriétés mécaniques des produits obtenus ont été suivies après chaque extrusion. Une première conclusion principale de ce travail expérimental est que la méthodologie proposée a conduit à une amélioration satisfaisante de la résistance au choc Charpy entaillée du polystyrène d'un facteur 2 en ajoutant 50% en poids de GTR. La taille d'origine du GTR a été réduite de plus de deux ordres de grandeur après un passage d'extrusion. Il a été démontré qu'une bonne adhérence interfaciale entre le GTR et le PS avant et après le mélange, ainsi que la température de mélange, étaient cruciales pour renforcer avec succès le PS. En fonction de la teneur en GTR, deux matériaux en polystyrène, ayant un comportement mécanique différent, ont été obtenus en appliquant cette méthodologie: résistant aux chocs (contenant 30 et 50% en poids de GTR) et élastomère thermo-plastique vulcanisé (avec 70% en poids de GTR). Ces résultats ont amélioré notre compréhension des facteurs qui dictent les propriétés mécaniques ultimes des composites renforcés de polystyrène avec du GTR.

Nomenclature

Mechanical properties

Symbol	Designation	Units
\varnothing	Characteristic mean diameter of the particle	μm
ε_r	Elongation at break	%
IS	Impact strength	kJ/m^2
τ	Extrusion torque	Nm
σ_r	Ultimate strength	MPa
Φ	Volume fraction of particles	%
E	Young's modulus	MPa
σ_r	Yield strength	MPa
Stand. Dev.	Standard Deviation	

Kinetics

MW	Molecular weight of polystyrene	Kg/mol
MW_m	Molecular weight of styrene	Kg/mol
t	time	s
GE	Grafting efficiency	%
I	Initiator	$\text{mol} \cdot \text{L}^{-1}$
I_0	Initial initiator concentration	$\text{mol} \cdot \text{L}^{-1}$
PR	Primary radical	$\text{mol} \cdot \text{L}^{-1}$
M	Monomer	$\text{mol} \cdot \text{L}^{-1}$
AH	Diels-Alder adduct	$\text{mol} \cdot \text{L}^{-1}$
AR	1-Phenyltetraaryl radical	$\text{mol} \cdot \text{L}^{-1}$
MH	Styryl	$\text{mol} \cdot \text{L}^{-1}$
R_i	Monomer radical	$\text{mol} \cdot \text{L}^{-1}$
R_1	Monomer radical of size 1	$\text{mol} \cdot \text{L}^{-1}$
R_2	Monomer radical of size 2	$\text{mol} \cdot \text{L}^{-1}$
R_3	Monomer radical of size 3	$\text{mol} \cdot \text{L}^{-1}$
R_n	Monomer radical of size n	$\text{mol} \cdot \text{L}^{-1}$
R_{n+1}	Monomer radical of size n+1	$\text{mol} \cdot \text{L}^{-1}$
R_m	Monomer radical of size m	$\text{mol} \cdot \text{L}^{-1}$
D_3	Trimers	$\text{mol} \cdot \text{L}^{-1}$
D_m	dead polymer of size m	$\text{mol} \cdot \text{L}^{-1}$
D_n	dead polymer of size n	$\text{mol} \cdot \text{L}^{-1}$
D_{n+m}	dead polymer of size n+m	$\text{mol} \cdot \text{L}^{-1}$
D_{n-m}	dead polymer of size n-m	$\text{mol} \cdot \text{L}^{-1}$

Symbol	Designation	Units
G	GTR	$mol \cdot L^{-1}$
GPR	GTR radical	$mol \cdot L^{-1}$
GR_n	GTR-monomer radical of size n	$mol \cdot L^{-1}$
GR_{n+1}	GTR-monomer radical of size n+1	$mol \cdot L^{-1}$
CB	Carbon black	$mol \cdot L^{-1}$
GD_m	dead GTR-polymer of size m	$mol \cdot L^{-1}$
GD_n	dead GTR-polymer of size n	$mol \cdot L^{-1}$
GD_{n+m}	dead GTR-polymer of size n+m	$mol \cdot L^{-1}$
f_1	Chemical initiator efficiency	-
k_d	Initiator decomposition rate constant	s^{-1}
k_I	Chemical initiation reaction rate constant	$L \cdot mol^{-1} \cdot s^{-1}$
k_1	Styrene dimerization rate constant	$L \cdot mol^{-1} \cdot s^{-1}$
k_{-1}	Diels-Alder decomposition reaction rate constant	s^{-1}
k_2	Styrene-induced homolysis reaction rate constant	$L \cdot mol^{-1} \cdot s^{-1}$
k_A	Thermal initiation reaction rate constant	$L \cdot mol^{-1} \cdot s^{-1}$
k_B	Thermal initiation reaction rate constant	$L \cdot mol^{-1} \cdot s^{-1}$
k_C	Trimer rate constant	$L \cdot mol^{-1} \cdot s^{-1}$
k_p	Propagation rate constant	$L \cdot mol^{-1} \cdot s^{-1}$
k_{fm}	Chain transfer to monomer rate constant	$L \cdot mol^{-1} \cdot s^{-1}$
k_{fa}	Chain transfer to adduct rate constant	$L \cdot mol^{-1} \cdot s^{-1}$
k_{fp}	Chain transfer to polymer rate constant	$L \cdot mol^{-1} \cdot s^{-1}$
k_S	Scission of polymer chains rate constant	$L \cdot mol^{-1} \cdot s^{-1}$
k_{tc}	Termination by combination rate constant of free polymer	$L \cdot mol^{-1} \cdot s^{-1}$
k_{td}	Termination by disproportionation rate constant of free polymer	$L \cdot mol^{-1} \cdot s^{-1}$
k_{tpr}	Termination by primary radicals rate constant	$L \cdot mol^{-1} \cdot s^{-1}$
f_2	Initiation efficiency of radicals produced by redox	-
k_{dCB}	Redox decomposition rate constant	$L \cdot mol^{-1} \cdot s^{-1}$
k_{IG}	Primary radicals attack GTR initiation reaction rate constant	$L \cdot mol^{-1} \cdot s^{-1}$
k_{pG}	Propagation rate constant of graft polymer	$L \cdot mol^{-1} \cdot s^{-1}$
k_{fmG}	Chain transfer to monomer rate constant	$L \cdot mol^{-1} \cdot s^{-1}$
k_{fG}	Chain transfer to graft polymer rate constant	$L \cdot mol^{-1} \cdot s^{-1}$
k_{fCB}	Chain transfer to carbon black rate constant of free polymer	$L \cdot mol^{-1} \cdot s^{-1}$
k_{fCBG}	Chain transfer to carbon black rate constant of graft polymer	$L \cdot mol^{-1} \cdot s^{-1}$
k_{fAHG}	Chain transfer to adduct rate constant of graft polymer	$L \cdot mol^{-1} \cdot s^{-1}$
k_{SG}	Scission of grafted polymer chains rate constant	$L \cdot mol^{-1} \cdot s^{-1}$
k_{tcG}	Termination by combination rate constant of graft polymer	$L \cdot mol^{-1} \cdot s^{-1}$
k_{tdG}	Termination by disproportionation rate constant of graft polymer	$L \cdot mol^{-1} \cdot s^{-1}$

Symbol	Designation	Units
k_{tprG}	Termination by primary radicals rate constant graft polymer	$L \cdot mol^{-1} \cdot s^{-1}$
$\delta(n)$	Kronecker's δ function	-
$k_{t,seg}$	Effective-segmental diffusion-limited termination rate coefficient	$L \cdot mol^{-1} \cdot s^{-1}$
$\delta(c)$	Segmental diffusion parameter for styrene	$L \cdot g^{-1}$
C_p	Concentration of polymer in the system	$L \cdot L^{-1}$
K	Critical variable for the onset of the 2nd stage of diffusion control	$kg^{0.5} \cdot mol^{-0.5}$
T_{gp}	Glass transition temperature of polymer	K
T_{gm}	Glass transition temperature of monomer	K
A	Adjustable parameter for the onset of the 2nd stage	-
V_f	Total free volume	-
K_{cr}	Critical constant for the onset of the 2nd stage of diffusion control	$kg^{0.5} \cdot mol^{-0.5}$
A_{cr}	Pre-exponential factor of K_{cr}	$(g \cdot mol^{-1})^{0.5}$
$V_{f,cr}$	Free volume at the onset point of the 2nd stage of diffusion control	-
E_{cr}	Activation factor of K_{cr}	K^{-1}
R	Universal gas constant	$cal \cdot mol_{-1} \cdot K_{-1}$
α_m	Thermal expansion coefficient of monomer	K^{-1}
α_p	Thermal expansion coefficient of polymer	K^{-1}
V_m	Monomer volume	L
V_p	Polymer volume	L
V_t	Monomer plus polymer total volume	L
d_m	Monomer density	$g \cdot L^{-1}$
d_p	Polymer density	$g \cdot L^{-1}$
d_I	Initiator density	$g \cdot L^{-1}$
k_T	Effective translational diffusion-limited termination rate coefficient	$L \cdot mol^{-1} \cdot s^{-1}$
$Mwcr$	Weight-average molecular weight of dead polymer chains at the onset of the 2nd stage of diffusion control	$kg \cdot mol_{-1}$
n	Coefficient for translational diffusion-limited termination	$cal \cdot mol^{-1}$
N_{av}	Avogadro number	mol^{-1}
σ	Lennard-Jones diameter for a styrene molecule	m
δ	Root-mean-squared end to end distance per square root of the number of monomer units	$m \cdot num^{-0.5}$
jc	Number of monomer units between entanglements on a polymer chain	num
$k_{t,rd}$	Effective reactional diffusion-limited termination rate coefficient	$L \cdot mol^{-1} \cdot s^{-1}$
$k_{t,eff}$	Effective overall diffusion-limited termination rate coefficient	$L \cdot mol^{-1} \cdot s^{-1}$
$V_{f,crm}$	Free volume at the onset point of the 3rd stage of diffusion control	-
A_{crm}	Adjustable parameter for the onset of the 3rd stage	-
E_{crm}	Adjustable activation energy for the onset of 3rd stage	$cal \cdot mol^{-1}$

Symbol	Designation	Units
$k_{p,eff}$	Effective diffusion-limited propagation rate coefficient	$L \cdot mol^{-1} \cdot s^{-1}$
B	Adjustable parameter for 3rd stage	-
C_{rRatio}	Adjustable parameter for 4th stage	-
$V_{f,creff}$	Free volume at the onset point of the 4th stage of diffusion control	-
C	Adjustable parameter for the onset of 4th stage	-
f_{i0}	Efficiency factor for thermally induced radical initiation	-
$f_{i,eff}$	Effective diffusion-limited efficiency factor for thermally induced radical initiation	-
Subscripts		
I	Initiator	
m	Monomer	
P	Polymer	
t	Termination	
0	Initial conditions	

List of Figures

1.1	World's largest tire manufacturers in 2017	8
1.2	Example of composition of passenger/light truck tires and truck tires	9
1.3	Flow diagram process of post-consumer tires transformation for material recycling.	10
1.4	Flow diagram of used tires utilization in the most important manufacturer and trader regions and countries in the world	12
1.5	SEM micrographs displaying differences of GTR particles morphology after mechanical grinding process at two different temperature.	13
1.6	Exemples of products manufactured by using GTR.	14
1.7	Compatibilization strategies used for GTR modification	15
1.8	Schematic representation of devulcanized and reclaimed GTR product.	16
1.9	Styrene structure	19
1.10	HIPS structure	19
1.11	Schematic representation of blending GTR with commercial PS	20
1.12	A schematic representation of styrene polymerization in a single GTR particle.	21
2.1	Effect of the initiator type and temperature on a) heat flow and b) monomer conversion in function of time during isothermal free-radical bulk polymerization of styrene by using a ratio initiator to styrene of 4.6 wt%.	31
2.2	Replicate DSC thermograms of the free-radical polymerization of styrene in presence of GTR with AMBN initiator. (50 wt% of GTR, T= 90 °C ; AMBN/St=4.6 wt%).	33
2.3	Effect of the GTR content on the evolution of a) heat flow and b) monomer conversion, during the isothermal BPO-initiated polymerization of styrene in the presence of GTR particles. (T=90 °C ; ratio BPO/St=4.6 wt%).	34
2.4	Series of oxygen-containing groups that can be found on carbon black surfaces.	35
2.5	Effect of the GTR content on the evolution of monomer conversion during the isothermal AMBN-initiated radical polymerization of styrene, in the presence of GTR. (T=90°C ; ratio AMBN/St=4.6 wt%).	36
2.6	Styrene conversion vs time in presence of 30 wt% of untreated GTR and chloroform-treated GTR (pur-GTR) at 90°C . (BPO/St=4.6 wt%).	37
2.7	Influence of the GTR content on the final conversion of the BPO-initiated styrene polymerization at 90 °C for two different cases: BPO/St and BPO/(St+GTR) equal to 4.6 wt%.	38
2.8	Calculation of the a) overall kinetic constant k and b) effective activation energy E_{eff} for the BPO-initiated styrene polymerization, in the presence of GTR (30 wt%).	40
3.1	Example of typical stress-strain curves for standard polystyrene, HIPS and SBS bloc copolymers	46
3.2	Main parameters influencing toughness in thermoplastic composites reinforced with GTR	47

3.4	Notched Charpy impact strength of different commercial polystyrenes measured by Cook and Rudin 1990.	49
3.5	Dispersion and distribution mixing types of particles in polymers	50
3.6	Experimental procedure to prepare blends of GTR and PS with improved mechanical properties.	55
3.7	Absorption rate of styrene by both types of GTR.	56
3.8	Grafted-PS/ free-PS ratio (St-g/St-f) as the function of styrene conversion	58
3.9	Polymerization reactor set-up	59
3.10	Spraying nozzle	59
3.11	Appearance of the original GTR and product after grafting PS.	61
3.12	Following the mixing torque during styrene polymerization in presence of GTR in a batch reactor	61
3.13	Measurement of the temperature distribution through the batch reactor during styrene polymerization	62
3.14	Scheme of the system reactor-stirrer	62
3.15	Processing zones in a twin-screw extruder	63
3.16	Intermeshed screw elements	64
3.17	Screw profile used for compounding in the previous research	65
3.18	Gradual diminution of the size of GTR-g-PS particles after several extrusions. Results from the previous research.	65
3.19	Screw configuration used for preliminary tests.	67
3.20	Variation of the extrusion torque in function of the screw velocity for different feeding rates of raw GTR.	67
3.21	Schema of the implemented process steps	68
3.22	Experimental conditions tested	69
3.23	Soxhlet extraction	74
3.24	GTR titration for double-bonds quantification	75
3.25	Procedure for GTR and GTR-grafted-PS particles' separation	76
3.26	Charpy impact testing	79
3.27	Tensile strength testing	80
3.28	Stress-strain curve and tensile properties.	81
3.29	Molds and specimens for impact and strength testing.	83
3.30	Compression molding of polystyrene impact specimens	83
4.1	Predicted and DSC monitored monomer conversion (discret points) in function of time during the isothermal free-radical bulk polymerization of styrene by using a ratio BPO to styrene of 4.6 wt%	99
4.2	Predicted evolution of M_n and M_w of polystyrene during the isothermal free-radical bulk polymerization of styrene	100
4.3	Comparison of predictions and experimental measurements of the conversion history of the bulk polymerization of styrene at 90 °C initiated with BPO.	100
4.4	Model predictions and experimental measurements of the evolution of M_n and M_w of during the BPO initiated bulk polymerization of styrene at 90 °C	101
4.5	Predicted and experimental data of conversion evolution in time of the bulk polymerization of styrene at 120 °C and 150 °C initiated with BPO.	101
4.6	Predicted and experimental M_n and M_w of the bulk polymerization of styrene at 120 °C and 150 °C initiated with BPO.	102
4.7	Comparison between predicted evolution and experimental ultimate conversion of the free-radical solution polymerization of styrene in toluene	102
4.8	Predicted trends and experimental measurements of M_n and M_w of the polystyrene formed during the BPO initiated radical solution polymerization of styrene at 80 °C with different amount of BPO	103

4.9	Electron withdrawing groups in BPO (left) and electron release substituents in DCP (right)	106
5.1	Effect of GTR content on monomer conversion.	120
5.2	Effect of GTR content on x in function of t for polymerization systems containing 30 wt%, 50 wt% and 70 wt% GTR.	120
5.3	Morphology of GTR particles before grafting.	122
5.4	Morphologies of the GTR particles after modification via polystyrene grafting.	122
5.5	FTIR spectrum of GTR-grafted-PS particles from composites containing different amounts of GTR.	123
5.6	Effect of grafted-PS onto/into GTR on the thermal properties of the composites obtained.	124
5.7	Effect of the GTR content on the average molecular weight of free-PS.	125
5.8	Screw configurations tested.	128
5.9	Load cell responses during the impact events.	132
5.10	Comparison of the Charpy <i>IS</i> of polystyrene vs polystyrene composites after a single extrusion.	134
5.11	Fracture surfaces of impact specimens of the composites after a single extrusion.	135
5.12	Stress-strain curves of tensile specimens of composites with 50 wt% of equiv-GTR or raw GTR after a single extrusion	137
5.13	Fracture surfaces of tensile specimens of the composites.	138
5.14	Morphology of the particles contained in the composites before and after a single extrusion	138
5.15	Zoom of the morphology of 50GTR-g-PS particles before and after a single extrusion	139
5.16	Comparison of the PSD between raw GTR and 50GTR-g-PS particles after a single extrusion	139
5.17	Example of deconvolution of the PSD curve of 50GTR-g-PS particles	140
5.18	Comparison of the PSD of particles of raw GTR and particles of 50GTR and 50GTR-g-PS after a single extrusion	140
5.19	Comparison of the PSD of raw GTR particles and grafted ones of 30GTR-g-PS and 50GTR-g-PS.	141
5.20	Comparison of the Charpy <i>IS</i> between the polystyrene matrices and composites after 1, 2 and 3 extrusions	144
5.21	Fractured surfaces of impact specimens of the 50GTR-g-PS/f-PS2 composite after 1, 2 and 3 extrusions.	145
5.22	Stress-strain curves of tensile specimens of the composites after 1, 2 and 3 extrusions.	146
5.23	Fracture surfaces of tensile specimens of the 50GTR-g-PS/f-PS2 composite after 1, 2 and 3 extrusions.	147
5.24	Morphology of the 50GTR-g-PS particles before and after 1, 2 and 3 extrusions.	148
5.25	Comparison of the PSD of raw GTR with 30GTR-g-PS, 50GTR-g-PS and 50GTR particles.	149
5.26	Evolution of the notched Charpy <i>IS</i> after multiple extrusions of the 50GTR-g-PS/f-PS2 composite.	150
5.27	Comparison between notched and unnotched Charpy <i>IS</i> of impact specimens of the 50GTR-g-PS/f-PS2 composite.	151
5.28	Comparison of the Charpy <i>IS</i> of free-PS3 vs the 50GTR-g-PS/f-PS3 composite after 1, 2 and 3 extrusions with screw Profile-2.	154
5.29	Fracture surfaces of impact specimens of the 50GTR-g-PS/f-PS3 composite after 1, 2 and 3 extrusions with screw Profile-2.	155
5.30	Stress-strain curves of tensile specimens of the 50GTR-g-PS/f-PS3 composite extruded 1, 2 and 3 times with screw Profile-2	155
5.31	Fractured surfaces of tensile specimens of the 50GTR-g-PS/f-PS3 compound after 1, 2 and 3 extrusions with screw Profile-2.	156
5.32	Changes in the morphology of the 50GTR-g-PS particles before and after 1, 2 and 3 extrusions with screw Profile-2.	157
5.33	Comparison of the PSD of raw GTR with 50GTR-g-PS particles after 1, 2 and 3 extrusions with screw Profile-2.	158

5.34	Stress-strain curves of tensile specimens of the 70GTR-g-PS/f-PS4 and 70GTR/PS6 compounds after 1 and 2 extrusions with screw Profile-1.	161
5.35	Fractured surfaces of tensile specimens of the 70GTR-g-PS/f-PS4 and 70GTR/PS6 composites after 1 and 2 extrusions with screw Profile-1.	161
5.36	Stress-strain curves of tensile specimens of the 70GTR-g-PS/f-PS5 composite after 1 and 2 extrusions with screw Profile-2	162
5.37	Changes in the morphology of the 70GTR-g-PS particles dispersed in free-PS4 before and after 1 and 2 extrusions with screw Profile-1.	163
5.38	Comparison of the PSD of raw GTR with particles contained in the composites with 70 wt% of equiv-GTR or raw GTR after 1 and 2 extrusions.	165
6.1	Comparison of the unnotched and notched Charpy <i>IS</i> of polystyrene as a function of M_w	184
6.2	Exemple de composition de pneus de tourisme/camionnette et de pneus de camion	188
6.3	Effet de la teneur en GTR sur l'évolution a) du flux thermique et b) de la conversion des monomères, lors de la polymérisation isotherme du styrène initiée par BPO en présence de particules de GTR. (T=90 °C ; rapport BPO/St=4.6 % en poids).	190
6.4	Schéma des étapes du procédé implémenté	191
6.5	Comparaison de la résistance aux chocs Charpy entre la matrice polystyrène et les composites après 1, 2 and 3 extrusions	192
6.6	Courbes contrainte-déformation des éprouvettes de traction des composites avec 70% de GTR en poids extrudés avec des profils de vis différents	192

List of Tables

1.1	Example of GTR composition according to the tire category.	13
1.2	Physical and chemical methods explored to modify the surface of GTR.	17
1.3	Influence of some polymerization parameters on monomer conversion and grafting efficiency.	23
2.1	Compositions of the tested samples.	32
2.2	Reaction enthalpy and monomer conversion values of replicate measurements at T=90 °C and 50 wt% of GTR.	33
2.3	Calculated activation energy E_{eff} values.	41
3.1	Intrinsic and extrinsic parameters and their influence on toughness of composites based on GTR and thermoplastics	52
3.2	Comparison of the mechanical properties of GPPS and HIPS	53
3.3	Product specification for the preparation of GTR-reinforced polystyrene composites	54
3.4	Characteristics of the commercial GTR	55
3.5	Composition of GTR elastomers	56
3.6	Physical and mechanical properties of GPPS	56
3.7	Polymerization system composition proposed by Yu 2015	57
3.8	Polymerization reactor set-up: equipments and devices specifications	60
3.9	Setting and process parameters identified in the compounding process	64
3.10	Compounding conditions implemented by Yu 2015	65
3.11	Technical specifications of the twin-screw extruder.	66
3.12	Compounding conditions of the preliminary tests.	67
3.13	Conditions for components mixing.	69
3.14	Operating conditions for grafting polymerization.	70
3.15	Composition and operating conditions	70
3.16	Analytical techniques implemented for evaluating properties of the composites	73
3.17	Standard dimensions of impact specimens	78
3.18	Instrumented hammer specifications.	78
3.19	Standard dimensions of tensile specimens	80
3.20	Tensile testing conditions	81
3.21	Injection-molding conditions	82
4.1	Bulk polymerization conditions tested in the batch reactor of 1 L capacity	90
4.2	Bulk polymerization conditions tested in the batch reactor of 3 L capacity	91
4.3	Final estimated pre-exponential and activation energies used in styrene polymerization model.	98
4.4	Diffusion control parameters in styrene polymerization model.	99
4.5	Physical properties of styrene and polystyrene	99

4.6	Kinetic constant parameters involved in the grafting polymerization mechanism of styrene in presence of GTR.	112
4.7	Mole mean number of double bonds contained in the different types of elastomers present in GTR	113
4.8	Concentration of double-bonds present in GTR	114
5.1	Composition of the grafting polymerization systems tested.	119
5.2	Effect of GTR on <i>GE</i> of polymerization systems containing 50 wt% of GTR.	121
5.3	Characteristic vibrational bands of neat free-PS and raw GTR measured by FTIR.	124
5.4	Influence of the GTR content on the molecular weight and T_g of free-PS.	125
5.5	Compounding conditions	128
5.6	Set of composites extruded.	129
5.7	Average molecular weight of the polystyrene matrices.	130
5.8	Ultimate x and <i>GE</i> of polystyrene after a single extrusion at high temperature.	131
5.9	Molecular weight of free-PS in grafted composites after a single extrusion.	131
5.10	Notched and unnotched Charpy <i>IS</i> of the polystyrene matrices.	133
5.11	Improvement or deterioration percentages of the notched Charpy <i>IS</i> of the polystyrene matrices. Compounds after a single extrusion.	133
5.12	Tensile properties of the composites after a single extrusion.	137
5.13	Characteristic diameters of particles of raw GTR and particles of 50GTR and 50GTR-g-PS after a single extrusion	141
5.14	Characteristic diameters of raw GTR particles and 30GTR-g-PS and 50GTR-g-PS ones after a single extrusion.	141
5.15	Improvement or deterioration percentages of the notched Charpy <i>IS</i> of the polystyrene matrices. Compounds after a 1, 2 and 3 extrusions.	145
5.16	Tensile properties of the 50GTR-g-PS/f-PS2 and 50GTR/PS6 composites after 1, 2 and 3 extrusions.	146
5.17	Characteristic diameters of particles of 50GTR, 30GTR-g-PS and 50GTR-g-PS after 1, 2 and 3 extrusions	150
5.18	Ultimate x and <i>GE</i> of polystyrene after a single extrusion at high temperature with screw Profile-2.	153
5.19	Molecular weight of free-PS3 after a single extrusion of the 50GTR-g-PS/f-PS3 composite with screw Profile-2.	153
5.20	Comparison of the improvement of notched Charpy <i>IS</i> of polystyrene when changing the screw profile.	154
5.21	Effect of the screw profile on the tensile properties of the composite containing 50 wt% of equiv-GTR and extruded with screw Profile-2	156
5.22	Characteristic diameters of raw GTR and particles of 50GTR-g-PS after 1, 2 and 3 extrusions with screw Profile-2.	158
5.23	Ultimate x of polystyrene after a single extrusion of composites containing 70 wt% of equiv-GTR.	160
5.24	Molecular weight of free-PS4 and free-PS5 after a single extrusion.	160
5.25	Tensile properties of 70GTR/PS6, 70GTR-g-PS/f-PS4 and 70GTR-g-PS/f-PS5 composites after 1 and 2 extrusions.	163
5.26	Characteristic diameters of raw GTR and particles contained in the composites with 70 wt% of equiv-GTR or raw GTR after 1 and 2 extrusions.	164
6.1	Molecular weight of polystyrene obtained by solution polymerization.	183
6.2	Notched and unnotched Charpy <i>IS</i> of the polystyrene obtained by solution polymerization.	184
6.3	Notch sensibility of PS6. Variation of the Charpy <i>IS</i> when notching specimens for impact testing.	184
6.4	Predicted notched and unnotched Charpy <i>IS</i> of free-PS.	185

Effects of the presence of recycled tire powders of the radical polymerization of styrene and the properties of the resulting materials

Recycling of end-of-life tire-derived materials is considered a sustainable approach to managing the over-accumulation of these wastes worldwide. The rubber phase of these post-consumer tires is considered as a valuable source because it consists of a sulfur-crosslinked reinforced elastomer phase which displays interesting mechanical properties such as high extensibility and elasticity. One of the alternatives for used tire rubber recycling consists in grinding it into fine powders, commercially called ground tire rubber or GTR. The latter can be dispersed in thermoplastic polymers in order to improve some of their properties such as impact strength.

This work aims to use GTR as a reinforcing agent to toughen brittle polymers such as polystyrene (PS). It is composed of three parts. In the first part, the effect of the presence of GTR on the kinetics of the free-radical polymerization of styrene is studied by differential scanning calorimetry. During the polymerization of styrene in the presence of GTR, styrene is partly homopolymerized, leading to free PS, and partly grafted onto GTR, leading to PS grafted onto GTR (denoted as GTR-g-PS). Benzoyl peroxide, which is widely used to initiate the grafting polymerization of styrene onto GTR, and 2,2-azobis(2-methylbutyronitrile), are used as free radical initiators. In general, the presence of GTR shows a negative effect on the ultimate monomer conversion to polymer. Moreover, it may have a positive or negative impact on the rate of polymerization. These effects can be more or less pronounced, depending on the type of initiator used. In the second part of the work, a mechanistic model is developed to describe the free-radical polymerization of pure styrene in a batch reactor. The model allows predicting the evolution of the total monomer conversion and that of the average molecular weights of PS during the polymerization. The parameters of the model are estimated based on literature data and on experiments conducted under different conditions. The validity of the model is demonstrated via comparison with additional experimental data, generated through a series of DSC analyses as well as pilot-scale reactor runs. Subsequently, the same model is modified to take into account the reactions occurring in the presence of GTR. The third part of the work addresses the development of a new methodology combining two processes to prepare GTR toughened PS. These processes involve the free-radical polymerization of styrene in the presence of GTR and compounding of the resulting product in a twin-screw extruder. The grafting of styrene onto GTR ensures good interfacial adhesion between PS and GTR and compounding favors fine dispersion of GTR in the PS matrix. Results show that the notched Charpy impact strength of neat PS can be increased by a factor of 2 by adding 50 wt% of GTR. Moreover, a PS/GTR blend containing 70 wt% of GTR displays a performance similar to that of a thermoplastic elastomer vulcanizate (TPV) and its strain at break can reach 120%.

Keywords

Ground tire rubber, recycling, high impact polystyrene, polymerization kinetics, compounding, calorimetry, kinetic modeling.

Impacte de la présence de poudrettes de caoutchouc recyclé dans la cinétique de la polymérisation radicalaire de styrène et les propriétés des matériaux obtenus

Le recyclage des matériaux dérivés des pneus en fin de vie est considéré comme une approche durable de la gestion de la suraccumulation de ces déchets dans le monde. La phase caoutchouc de ces pneus post-consommation est considérée comme une source importante car elle consiste en une phase élastomère renforcée, réticulée au soufre, qui présente des propriétés mécaniques intéressantes, telles qu'une extensibilité et une élasticité élevées. L'une des alternatives pour le recyclage des caoutchoucs de pneus usagés consiste à les broyer en poudres fines, appelées dans le commerce poudrette de pneus usés, plus connu par ses sigles en anglais "GTR" (ground tire rubber). Ces dernières peuvent être dispersées dans des polymères thermoplastiques afin d'améliorer certaines de leurs propriétés telles que la résistance aux chocs.

Ce travail vise à utiliser le GTR comme agent de renforcement pour renforcer les polymères fragiles tels que le polystyrène (PS). Il est composé de trois parties. Dans la première partie, l'effet de la présence de GTR sur la cinétique de la polymérisation radicalaire du styrène est étudié par calorimétrie différentielle à balayage. Au cours de la polymérisation du styrène en présence de GTR, le styrène est partiellement homopolymérisé, conduisant à la formation de PS libre, et partiellement greffé sur le GTR, ce qui conduit à un PS greffé sur le GTR (noté GTR-g-PS). Le peroxyde de benzoyle, largement utilisé pour amorcer la polymérisation par greffage du styrène sur le GTR, et le 2,2-azobis (2-méthylbutyronitrile) sont utilisés comme amorceurs de radicaux libres. En général, la présence de GTR montre un effet négatif sur la conversion finale du monomère en polymère. De plus, cela peut avoir un impact positif ou négatif sur le taux de polymérisation. Ces effets peuvent être plus ou moins prononcés, en fonction du type d'amorceur utilisé. Dans la deuxième partie du travail, un modèle mécanistique est développé pour décrire la polymérisation radicalaire du styrène pur dans un réacteur discontinu. Le modèle permet de prédire l'évolution de la conversion totale du monomère et celle des masses molaires moyennes du PS lors de la polymérisation. Les paramètres du modèle sont estimés à partir de données de la littérature et d'expériences menées dans différentes conditions. La validité du modèle est démontrée par la comparaison avec des données expérimentales supplémentaires, générées par une série d'analyses DSC ainsi que par des essais dans un réacteur pilote. Subséquemment, le même modèle est modifié pour prendre en compte les réactions se produisant en présence de GTR. La troisième partie du travail porte sur le développement d'une nouvelle méthodologie combinant deux processus pour préparer un PS renforcé avec du GTR. Ces procédés impliquent la polymérisation radicalaire du styrène en présence de GTR et le mélange du produit résultant dans une extrudeuse bi-vis. Le greffage du styrène sur le GTR assure une bonne adhésion interfaciale entre PS et GTR et le compoundage favorise la dispersion fine du GTR dans la matrice de PS. Les résultats montrent que la résistance au choc Charpy (sur éprouvette entaillée) du PS pur peut être augmentée d'un facteur de 2 en ajoutant 50% en poids de GTR. En outre, un mélange PS/GTR contenant 70% en poids de GTR présente une performance similaire à celle d'un vulcanisat d'élastomère thermoplastique (TPV) et son élongation à la rupture peut atteindre 120%.

Mots-clés

Poudrette de pneus usagés, recyclage, polystyrène choc, cinétique de la polymérisation, compoundage, calorimétrie, modélisation de la cinétique.